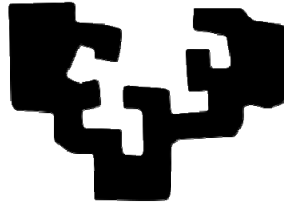


eman ta zabal zazu



Universidad
del País Vasco

Euskal Herriko
Unibertsitatea

Polymer-based electrolytes for all-solid-state lithium-sulfur batteries

Xabier Júdez López, 2019

*UNIVERSITY OF THE BASQUE COUNTRY
DEPARTMENT OF CHEMICAL ENGINEERING
FACULTY OF SCIENCE AND TECHNOLOGY. LEIOA*

Polymer-based electrolytes for all-solid-state lithium-sulfur batteries

PhD candidate	Xabier Júdez López
PhD supervisors	José Antonio González Marcos Lide M. Rodríguez Martínez
Date	October of 2019

*“Cuando estemos mal, acordaos de dónde
venimos y cuáles son nuestros valores”*

Manu García

ACKNOWLEDGEMENTS

Llegado el momento de concluir el trabajo de estos últimos años, no me gustaría terminar sin tomarme un respiro para agradecer como se merecen a todos aquellos que han me han apoyado. Me gustaría comenzar agradeciendo al Gobierno Vasco la financiación de esta tesis mediante las becas del programa predoctoral y al Departamento de Ingeniería Química los años de formación y por permitirme llevarla a cabo.

Me gustaría agradecer a José Antonio la primera oportunidad que me concedió allá por 2015 de empezar a trabajar con él, sus consejos y su orientación durante estos años consecutivos de trabajos de fin de grado, master y esta tesis doctoral. Que decir de Lide... gracias por la primera oportunidad, la enorme confianza que siempre has depositado en mí, y por tantos y tantos consejos profesionales, pero sobre todo, personales. Ez nuke, ezta, Aitor ahaztu nahiko hainbeste aholku, laguntza, eta nigatik egin duzun borrokaren ostean.

I would like to acknowledge 妹妹 (姐姐 in reality) and 张恒 (kind of 哥哥) for all the teaching, help, supervision, corrections, guiding, *etc.* in the daily work. Thank you Michel for all your valuable help, inspiration and kindness.

Gracias a todos mis compañeros de trabajo, grupo y línea por toda la ayuda y los buenos momentos (Aldalur *et al.*). Gracias a mi pareja de pádel por sacar el tiempo que no te sobra para corregir esta tesis. To Lixin por for being a *máquina*. A María, Begoña por darle un poco de ambiente desde el primer día al ala este del CIC y crear una zona donde compartir nuestras penurias. A todos los estudiantes de doctorado por el buen ambiente y la ayuda mutua. A María, de nuevo, por todos los momentos durante nuestras vidas paralelas, que (de momento) divergen. A Elena y demás personal administrativo y de mantenimiento por sacarme las castañas del fuego a menudo...

A mis amigos (cuadrilla *et al.*) por ayudarme a desconectar y relativizar.

A mis abuelos, tíos, primos, suegros, cuñados, concuñados y demás familia; pero en especial a los tres txikitos, por los momentos divertidos y su cariño, que tanto me ayudan a desconectar.

Por supuesto, a mis padres y hermana por apoyarme incondicionalmente y facilitarme enormemente este trabajo.

Idoiari, nola ez, egunero nire ondoan egoteagatik: Gasteiztik Txinaraino!

Ta zuretzat

Euskal Herriko gailurrak

zutik gaudenaren seinaleak

GORA ZUEK!

ABSTRACT

Among different “beyond lithium-ion” batteries, lithium-sulfur batteries are one of the most attractive alternatives, especially due to their high achievable gravimetric energy densities of over 400 Wh kg⁻¹. However, the several intrinsic limitations, *i.e.*, low conductivity of sulfur, shuttle effect or the challenging use of metallic lithium (Li⁰), still hinders their market deployment. The use of solid electrolytes will not only help to face those challenges, but, according to our models, will allow to increase achievable energy density values, especially with the use of lightweight solid polymer electrolytes (SPEs).

During this work, the first assembled all-solid-state lithium-sulfur battery (ASSLSB), based on the state of the art lithium bis(trifluoromethanesulfonyl)imide (LiTFSI)/poly(ethylene oxide) SPE electrolyte, showed a poor cyclability. The further study of the prepared coin cells allowed to identify the Li⁰/SPE interface as the critical point in the cell performance. Thus, different strategies for the stabilization of the cells were designed accordingly, including the use of additives, electrolyte fillers, alternative imide salts, and novel fluorine free salts.

The use of additives, both state of art lithium nitrate and novel lithium azide, generated a protective and highly conductive solid/electrolyte interface (SEI) passivation layer on the metallic electrode, highlighting the importance of Li⁰ protection, and the benefits of Li₃N SEI-building material. Later, the use of aluminum oxide electrolyte filler was demonstrated to improve the cell performance by means of reaction intermediates immobilization and the generation of an excellent quality SEI layer on Li⁰.

In a different approach, LiTFSI salt was substituted by lithium bis(fluorosulfonyl)imide (LiFSI) alternative, which generated a robust SEI on Li⁰, based on highly protective LiF, enabling the long-term cycling of the cell. However, its unstable nature against lithium polysulfides reduced cell capacity. Therefore, asymmetric lithium (fluorosulfonyl) (trifluoromethanesulfonyl) (LiFTFSI), which contains both functionalities of TFSI⁻ and FSI⁻ anions, was demonstrated to combine benefits from both salts, allowing stable cycling without sacrificing cell capacity. The last chapter, focused in the use of the novel fluorine-free lithium tricyanomethanide (LiTCM) salt, which would bring benefits in both environmental sustainability and reduction of costs. This novel salt generated a completely different fluorine-free SEI, and featured an excellent cell performance, which was upscaled to pouch cell size for the first time.

All these results demonstrate that the stability of the Li⁰ electrode is of paramount importance for the proper operation of SPE-based ASSLSBs. This thesis work has explored different alternative electrolyte recipes, and depicted in detail the working mechanism behind the observed improvements, obtaining notable improvements in cell performance.

LABURPENA

“Litio-ioitik haratagoko” bateria desberdinen artean, litio-sufrezko bateriak aukera erakargarrietako bat dira, lortu dezaketen energia grabimetrikoengatik bereziki, $> 400 \text{ Wh kg}^{-1}$. Alabaina, haien guztizko garapena eta komertzializazioa ez da lortu oraindik limitazio desberdinak dira eta: sufreakondu baxua, “*shuttle effect*” deritzona, edota litio metalikoaren (Li^0) erabilpenak dakartzen erronkak. Elektrolito solidoen erabilpenak ez lituzke limitazio hauek gainditzen lagunduko bakarrik, baizik eta, gure modeloen arabera, lortu daitekeen energia grabimetrikoa handitu ere, bereziki pisu baxuko polimerozko elektrolito solidoen (SPEs) bitartez.

Lan honen garapenean, lehendabiziko aldiaren montatutako egoera solido litio sufrezko bateriak (ASSLSBs), aurretik bibliografian erabilitako litio bis(trifluorometanosulfonil) imida (LiTFSI)/poli(etileno oxidoa) (PEO) materialetan oinarrituta, errendimendu eskasa lortu zuen. Bateriaren azterketa sakonago bati esker, Li^0/SPE interfazea identifikatu zen bateriaren elementu mugatzaile bezala. Hortaz, interfaze honen estabilizaziorako estrategia desberdinak disenainatu ziren: aditiboen erabilera, filler zeramikoaren erabilera, imida gatz desberdinen erabilera eta fluororik gabe gatz berrien erabilpena.

Aditiboen erabilerrari esker, bai litio nitrato komuna eta litio azida berria, Li^0 -an solido/elektrolito interfaze (SEI) geruza babesgarria bat sortzen lortu zen, bide batez Li^0 -aren babesaren garrantzia nabarmentzen, eta zehatzago, Li_3N SEI material eraikitzaileen onurak nabarmentzen. Gero, aluminio oxidoa elektrolito fillerraren eragina aztertu zen, eta baterien errendimendua hobeto zitekeela ikusi zen, disolbatutako erreakzio produktuak atxikitzeke ahalmenagatik eta haren eraginagatik Li^0 gaineko SEI geruzaren kalitatean.

Geroago, planteamendu desberdin batetan, LiTFSI gatz litio bis(florosulfonil)imida (LiFSI) gatzagatik ordezkatu zen. Gatz honek, SEI geruza babesle sendo bat lortzea ahalbidetu zuen, LiF materialean oinarrituta eta epe luzeko baterien jarduna ahalbidetuz. Hala ere, haren estabilitate ezak litio polisulfuroen aurrean bateriaren kapazitatea txikitzea eragin zuen. Hortaz, ikuspegi desberdin batetan, litio (fluorosulfonol) (trifluorometanosulfonil) (LiFTFSI) gatz asimetrikoa ikertu zen, aurreko bi gatz onurak bateratzeko gai frogatu zena, epe luzean jarduteko ahalmenarekin, baina kapazitate galerarik gabe. Azkenik, fluororik gabeko litio trizianometanida (LiTCM) gatz berria ikertu zen, jasangarritasunean eta kostuen murrizketan ekar ditzazkeen onurengatik. Gatz berri honekin errendimendu bikaina lortu zen, fluororik gabeko kimikan oinarritutako SEI berri batetan oinarrituta. Honek ere ahalbidetu zituen lehen ikerlanak pouch cell tamainan.

Emaitz hauek frogatu zuten Li^0 -aren estabilitatea ezinbestekoa dela SPE-tan oinarritutako ASSLSBs baterien errendimendurako. Tesi lan honek aukera desberdinak ikertu eta bakoitzaren mekanismoak zehaztasunez deskribatu ditu, baterien errendimenduan hobekutza nabarmenak lortuz.

RESUMEN

Introducción y motivación

El continuo desarrollo de sistemas de almacenamiento de energía más eficientes y competitivos es crucial para una completa transición hacia modelos energéticos más sostenibles. Existen diferentes métodos de almacenamiento energético, entre los que las baterías toman un interés especial debido a su portabilidad, lo que permite integrarlas en dispositivos electrónicos y en vehículos.

Las baterías son dispositivos de almacenamiento y conversión de energía basados en reacciones electroquímicas de reducción y oxidación (redox) en los electrodos de las celdas. A día de hoy, se han propuesto centenares de combinaciones funcionales de materiales para la su construcción, siendo hasta finales del siglo pasado la combinación Zn-MnO₂ la más común en baterías no recargables y Ni-Cd la más común en las recargables. Sin embargo, tras décadas de investigación, en las últimas décadas se ha avanzado significativamente con la propuesta y desarrollo de baterías recargables de ion de litio (Li-ion), basadas en la intercalación y desintercalación de iones de litio. Desde su comercialización en 1991, las baterías de Li-ion han dominado el mercado. Sin embargo, tras años de investigación y desarrollo, están muy cerca de alcanzar su rendimiento máximo, sin llegar a satisfacer aún las especificaciones necesarias para las aplicaciones más exigentes, como los vehículos eléctricos. Además, su coste es alto y su impacto medioambiental significativo.

Por ese motivo, en las últimas décadas, y en paralelo al desarrollo de baterías de Li-ion, diversas combinaciones de materiales alternativas han sido propuestas por la comunidad científica para mejorar aspectos como la densidad energética o el coste. Entre las diferentes alternativas, destacan las baterías formadas por un electrodo de litio y otro de azufre (Li-S). Estas baterías se basan en la sustitución de electrodos basados en óxidos complejos, en Li-ion, por los basados en azufre, residuo de la industria petroquímica y material no tóxico. Además, el azufre posee una capacidad teórica de 1675 mAh g⁻¹, hasta 10 veces superior a los óxidos empleados en baterías de Li-ion. Todo esto confiere a este sistema la posibilidad de alcanzar mayores niveles de almacenamiento energético por unidad de masa, *i.e.*, densidad energética, además a un coste previsiblemente menor.

Sin embargo, el completo desarrollo y comercialización de estas baterías se ha visto ralentizado por las diversas problemáticas que surgen debido al complejo mecanismo electroquímico en el que están basadas. Por un lado, el azufre es un pobre conductor de electrones, lo que penaliza la cinética de las reacciones redox, requiriendo el uso de materiales adicionales que permitan el correcto flujo de electrones. Por otro lado, en este sistema es necesario el uso de un electrodo de litio metálico (Li⁰), lo que trae consigo posibles problemas de estabilidad y seguridad, por la alta reactividad de este metal y su tendencia a formar estructuras

VIII

ramificadas durante su funcionamiento, denominadas dendritas, que pueden llegar a cortocircuitar las baterías. Finalmente, así como las baterías de Li-ion se basan en reacciones de intercalación relativamente simples, las baterías de Li-S se basan en la conversión del azufre (S_8) a sulfuro de litio (Li_2S) mediante una reacción de conversión multietapa en el que se generan varios compuestos altamente solubles, denominados polisulfuros de litio, cuya alta movilidad puede generar pérdidas de material activo en los electrodos, la reducción de la vida útil de las celdas, y reacciones indeseadas en el electrodo de litio, en el denominado “efecto lanzadera” o “efecto *shuttle*”.

No obstante, y pese a las limitaciones, debido a su enorme potencial diversos estudios se han centrado, en especial en la última década, en el desarrollo de baterías de Li-S. Estos estudios se han enfocado en la búsqueda de nuevos y mejorados elementos de la celda, tales como mejores estructuras carbonosas para un mejor confinamiento del azufre en el electrodo, electrolitos que reducen la solubilidad de polisulfuros o en una mejor protección del electrodo de Li^0 mediante el uso de aditivos o capas de protección. Muchos de estos estudios se centran en la extensión de la vida útil de estas baterías, lo que puede identificarse como la mayor limitación con respecto a las baterías de Li-ion.

Entre las diferentes estrategias estudiadas destaca el uso de electrolitos sólidos, por ser una estrategia en la que no se ha profundizado demasiado pero que puede ayudar a hacer frente a varias limitaciones inherentes de estas baterías. Los electrolitos sólidos pueden ser inorgánicos (también denominados cerámicos), poliméricos o composites (combinación de partículas cerámicas en una estructura polimérica). Los primeros presentan una alta conductividad de iones de litio (Li^+) a temperatura ambiente, pero su fragilidad hace que sea muy difícil aún preparar electrolitos con espesores lo suficientemente pequeños para alcanzar densidades energéticas competitivas. Los segundos, sin embargo, pese a presentar bajas conductividades a temperatura ambiente, son sencillos de manipular y es posible obtener electrolitos de espesores muy competitivos. Entre las diferentes opciones, destaca el uso de óxido de polietileno (PEO), por sus excelentes propiedades. Sin embargo, su baja conductividad a temperatura ambiente obliga a operar las baterías a temperaturas por encima de su punto de fusión, de unos 60-65°C. Por ello, el uso de composites pretende mejorar las conductividades mediante la inclusión de partículas cerámicas en la matriz polimérica. Además, se ha demostrado que estas partículas pueden afectar notablemente la estabilidad del electrodo de Li^0 .

Si se observa el estado del arte del uso de electrolitos sólidos en baterías de Li-S, se puede ver que los estudios basados en electrolitos poliméricos y cerámicos presentan aún resultados limitados, lo que sugiere un amplio margen de mejora. Además, destaca que el uso de composites puede mejorar el rendimiento en comparación con los electrolitos puramente poliméricos. Tras extraer datos de operación realistas de estos sistemas, fueron incluidos en un modelo desarrollado para el cálculo energético de la densidad energética alcanzable en función de una diversidad de parámetros. De los resultados de estas estimaciones se pueden

extraer diversas conclusiones. Por un lado, la alta densidad de los materiales cerámicos hace que sea necesario el uso de espesores de electrolitos mínimos, aún difíciles de alcanzar, para superar los valores actuales de las baterías de Li-ion. Por el contrario, la ligereza de los electrolitos poliméricos, o composites con bajo contenido de carga cerámica, y la posibilidad de alcanzar fácilmente espesores mínimos hace que sea viable alcanzar densidades energéticas superiores. Además, en comparación con las celdas basadas en electrolitos líquidos convencionales, la posibilidad de eliminar elementos inertes de la celda, como el separador o el aglutinante en el electrodo, hace que sea más sencillo obtener densidades energéticas superiores con el uso de electrolitos sólidos. El modelado de los sistemas permitió además fijar los parámetros para el desarrollo de la celda de referencia.

Por todo ello, por un lado, el uso de electrolitos sólidos puede ayudar a superar simultáneamente varias limitaciones inherentes a los sistemas de Li-S. Por otro lado, se concluyó que entre los electrolitos sólidos, los poliméricos o los composites con baja carga cerámica permiten alcanzar más sencillamente valores superiores de densidad energética. Por todo ello, el objetivo de esta tesis se ha fijado en el desarrollo de baterías de Li-S en estado sólido basadas en electrolitos poliméricos.

Desarrollo de la celda sólida de referencia y comprensión de la problemática

Durante los primeros ensayos, los resultados basados en celdas con el electrolito polimérico de referencia basado en PEO y la sal bis(trifluorometilsulfonyl)imida de litio (LiTFSI) no fueron satisfactorios. Pese a que la capacidad de descarga de la celda era satisfactoria, la respuesta de la celda a cargas rápidas era pobre y a su estabilidad se veía comprometida después de menos de 15 ciclos incluso en cargas lentas. Estos resultados coinciden con los previamente reportados para sistemas similares, pero ningún artículo detalla el mecanismo de fallo de la celda. Por eso, creímos necesario la comprensión de éste con el objetivo de diseñar estrategias de mejora acordes.

Para ello, la fabricación y propiedades de la membrana y su influencia en la celda fueron analizadas más detenidamente. La caracterización de las propiedades fisicoquímicas y electroquímicas de la membrana de LiTFSI/PEO mostró resultados adecuados en cuanto a las propiedades mecánicas de la membrana, su estabilidad térmica y electroquímica y en sus valores de conductividad en la temperatura de operación. Además, la presencia de polisulfuros disueltos en la membrana de PEO después del ciclado hizo necesario el estudio de compatibilidad, que mostró una alta estabilidad del anión de la sal LiTFSI frente a los polisulfuros, lo que es deseable para un ciclado estable de las baterías. Sin embargo, durante el estudio de la compatibilidad de la membrana con el electrodo de Li^0 se identificaron ciertas limitaciones. Las celdas basadas en la configuración simétrica de $\text{Li}^0 | \text{LiTFSI/PEO} | \text{Li}^0$ sólo pudieron operar establemente durante un tiempo muy

limitado, menor de 200 h, indicando una pobre compatibilidad de las membranas con el electrodo metálico.

Pese a no poder observar el litio directamente después del ciclado debido a las propiedades adhesivas del PEO por encima de su punto de fusión, la simulación del sistema fue llevada a cabo con el electrolito líquido equivalente 1,2-dimetoxietano (DME). El análisis de los depósitos de Li^0 en presencia de LiTFSI/DME mostró la existencia de diversas estructuras irregulares y dendríticas. Además, el análisis de éstos mediante espectroscopia de fotoelectrones emitidos por rayos X (XPS) mostró que la capa generada en la intercara Li^0 /electrolito (capa SEI), y que idealmente se espera que actúe como capa de protección, era de baja calidad, compuesta en su mayoría por productos de reducción del disolvente o por productos de reducción incompleta de la sal.

Con todo ello, se puede llegar a la conclusión de que la baja calidad de la capa SEI sobre el Li^0 es el elemento que limita el correcto funcionamiento de la celda. En el caso de la celda de Li-S, la presencia de polisulfuros disueltos en el electrolito polimérico y la pobre protección del Li^0 , expone el electrodo metálico al ataque de éstos, generando un consumo excesivo de electrones y por tanto, la sobrecarga de la celda y los consiguientes problemas de estabilidad. Por todo ello, este trabajo doctoral se centró en el estudio de diversas estrategias para modificar la composición del electrolitos poliméricos de referencia LiTFSI/PEO y mejorar así su compatibilidad con el Li^0 . Estas estrategias incluyen el uso de aditivos o inclusión de cargas cerámicas para obtener electrolitos composites. También se exploró la sustitución de la sal de referencia LiTFSI mediante el uso de sales alternativas que contengan el grupo imida o el uso de sales novedosas y libres de flúor.

Uso de aditivos

La primera estrategia se centró en el uso del uso de dos aditivos diferentes en la membrana de LiTFSI/PEO. Los aditivos estudiados fueron el LiNO_3 , el aditivo más común en las baterías de Li-S, y el LiN_3 , un nuevo aditivo nunca antes estudiado. Las membranas obtenidas tras la incorporación de los aditivos presentaron características ligeramente peores en ciertos aspectos, como en la estabilidad electroquímica o conductividad, siendo en todo caso aceptables para el uso en las condiciones de ciclado. Como punto más destacado, el uso de LiNO_3 y LiN_3 permitió casi duplicar y triplicar, respectivamente, el tiempo de ciclado de las celdas simétricas de Li^0 , lo que indica una mejora sustancial en la compatibilidad de la membrana con el electrodo metálico. Además se disminuyó la resistencia relacionada con la SEI, especialmente en el segundo caso.

Las imágenes de los depósitos de Li^0 en presencia de los aditivos mostraron estructuras más planas y homogéneas, con ausencia de dendritas. El análisis XPS de estos depósitos demostró la presencia de Li_3N , especie altamente protectora y conductora. Esto permitió deducir que mientras que el LiNO_3 generaba Li_3N y

otros productos menos conductores como el Li_2O , el LiN_3 se reducía generando Li_3N exclusivamente. El uso de ambos aditivos disminuyó la capacidad de descarga de la celda un 20%, pero mejoró notablemente la estabilidad gracias a la mejor protección del Li^0 , duplicando el número de ciclos de funcionamiento estable. Este trabajo supuso el uso por primera vez de aditivos en membranas de poliméricas para celdas de Li-S y la confirmación de que mediante la estabilización del electrodo metálico la ciclabilidad de la celda podía mejorarse notablemente.

Uso de cargas cerámicas

La siguiente estrategia se centró en el uso de pequeñas cantidades de cargas cerámicas en el electrolito. Para ello se seleccionó una carga cerámica activa, conductora de Li^+ , denominada *LiCGC* (siglas para *lithium ion conductive glass ceramic*), y una inactiva, Al_2O_3 . La carga activa se seleccionó por su alta conductividad y su estabilidad frente a la humedad y el oxígeno, permitiendo su manipulación en el exterior. La carga inactiva se seleccionó debido a su bajo coste, su estabilidad y su efecto en la pasivación del Li^0 . En ambos casos las partículas cerámicas fueron dispersadas homogéneamente en la matriz polimérica, pero no se obtuvo ninguna mejora en la conductividad, permitiendo concluir que las cargas como tal no mejoran la conductividad si no se atiende a otras propiedades tales como tamaño, forma u orientación. Sin embargo ambas cargas cerámicas afectaron significativamente la estabilidad del electrolito frente al Li^0 . Así como la alúmina mejoró notablemente la calidad de la SEI generada, permitiendo multiplicar por 6 el tiempo de ciclado de la celda simétrica de Li^0 , el LiCGC no sólo no mejoró la estabilidad, si no que la empeoró. Además, mientras que la Al_2O_3 demostró ser estable frente a los polisulfuros y ser capaz de retenerlos mediante interacciones dipolo-dipolo, el LiCGC resultó ser inestable, reaccionando con estos y litiándose, lo que genera el colapso de la estructura. Los resultados del LiCGC fueron confirmados mediante estudios bibliográficos coetáneos, que demostraron que la partícula cerámica sufría una reducción irreversible en contacto directo con el Li^0 o con los polisulfuros.

Con todo esto, al aplicar el electrolito de Al_2O_3 en la celda de Li-S, la estabilidad mejoró notablemente, permitiendo el ciclado en cargas rápidas, pero disminuyó la capacidad de descarga considerablemente. Sin embargo, esto es comprensible tras la caracterización previa, en la que quedó demostrado que la partícula cerámica del electrolito puede interaccionar fuertemente con los polisulfuros, lo que los inmovilizaría lejos del electrodo, impidiendo que ataquen el Li^0 , pero también su posterior reacción en el electrodo.

Con todo esto, y teniendo en cuenta el potencial de las mejoras observadas, el diseño de la celda se modificó. Por un lado, se añadió Al_2O_3 en el cátodo como reservorio de polisulfuros. Por otro lado, se añadió una membrana final con carga cerámica en contacto con el Li^0 para la estabilización de éste. Además, se añadió una membrana libre de carga en contacto con el electrodo de azufre, que permitiese

el libre movimiento de polisulfuros, evitando que queden anclados a partículas cerámicas y permitiendo su posterior uso. Esta nueva configuración permitió ciclar la celda establemente incluso en cargas rápidas, pero sin ninguna pérdida en la capacidad con respecto a la celda de referencia. En este capítulo se aplicó por primera vez el uso de membranas con doble función, pudiendo aprovechar las ventajas de la Al_2O_3 tanto en la estabilización del Li^0 como en su capacidad de retención de polisulfuros.

Uso de sales con grupos imida alternativas

Pese a que las estrategias previas enfocadas en la incorporación de aditivos o cargas cerámicas han dado buenos resultados, es necesario explorar una estrategia alternativa: la sustitución de la sal de referencia LiTFSI por otras con similar estructura.

La primera sal explorada fue la bis(fluorosulfonil)imida de litio (LiFSI). Las membranas preparadas con esta sal presentaron de nuevo propiedades más limitadas que las preparadas con LiTFSI, pero aceptables en las condiciones de operación. La mayor diferencia que mostraron estas membranas fue una mejor compatibilidad con el electrodo de Li^0 . El análisis de los depósitos de Li^0 generados en presencia de esta sal mostró estructuras planas y homogéneas, con ausencia de estructuras dendríticas. El análisis por XPS de estos depósitos desveló que la sal LiFSI tendía a reducirse completamente sobre la superficie del electrodo metálico, generando entre otros el material altamente protector LiF. Este hecho se debe a la mayor reactividad de los grupos terminales S–F de esta sal en comparación con los grupos C–F₃ del LiTFSI. Sin embargo, esta mayor reactividad también hace que la sal sea sensible al ataque de polisulfuros, lo que genera la degradación de la sal y el consumo indeseado de polisulfuros. Cuando la membrana LiFSI/PEO fue aplicada en la celda de Li-S, se obtuvieron excelentes resultados en términos de estabilidad de ciclado por la protección del electrodo metálico, llegando a obtener 1000 ciclos estables, pero con una pérdida de capacidad considerable respecto al sistema basado en LiTFSI, debido a la alta reactividad de la sal y el consumo de polisulfuros.

Por este motivo, se propuso el uso de la sal (trifluorometilsulfonil)(fluorosulfonil)imida de litio (LiFTFSI), que combina en su estructura molecular una mitad de la sal LiTFSI y la otra de la sal LiFSI. La membrana obtenida con esta sal presentó características fisicoquímicas y electroquímicas intermedias entre las anteriormente nombradas. Sin embargo, las celdas simétricas de Li^0 basadas en LiFTFSI fueron capaces de obtener tiempos de ciclado mejorados y el anión de esta sal mostró una reactividad reducida frente a los polisulfuros. Con todo esto, el ciclado de las celdas basadas en LiFTFSI/PEO mostró una respuesta estable a ciclos rápidos y la habilidad de mantener un ciclado estable durante 50 ciclos.

Con todo ello, mientras que los estudios muestran que las sales LiTFSI o LiFSI difícilmente pueden ser usadas como sales únicas, la sal LiFTFSI es una solución intermedia óptima, que combina la una protección suficiente del Li^0 y una estabilidad suficiente del anión. En líneas generales, este capítulo demuestra también la importancia de la sal del electrolito en el rendimiento de la celda, tanto en la estabilidad como en la capacidad de ésta.

Uso de sales sin flúor

La química del flúor es costosa económica y medioambientalmente. Por ello se propuso finalmente el uso de una sal novedosa sin flúor, la sal tricitanometanida de litio (LiTCM). De nuevo, se obtuvieron membranas con propiedades adecuadas, incluso mejoradas en ciertos aspectos, como la selectividad a la conducción de Li^+ y su conductividad.

Esta sal destaca por la ausencia total de flúor, por lo que cabe esperar la química de la capa SEI generada sobre el Li^0 sea totalmente diferente a los sistemas previos, basados, por ejemplo, en LiF. Las celdas simétricas de Li^0 basadas en LiTCM/PEO mostraron un ciclado mejorado con respecto a las basadas en LiTFSI, en términos de tiempo de ciclado, y sobre todo, en una reducción de la resistencia de la celda. El análisis XPS de estas celdas mostró una capa SEI formada por el material altamente conductor Li_3N y por estructuras complejas basadas en $\text{C}=\text{N}$, lo que conferirían a la capa SEI unas cualidades únicas en términos de conductividad y estabilidad estructural. Las celdas de Li-S basadas en esta sal mostraron una estabilidad mejorada respecto a las de referencia, pero sobretudo una excelente respuesta en términos de capacidad a cargas rápidas, con pérdidas de solo un 9 % al disminuir el tiempo de carga de 10 a 5 h.

Debido a los buenos resultados, los resultados fueron escalados de celdas de tamaño de botón a celdas pouch, de un tamaño unas 15 veces superior. Los resultados en términos de capacidad fueron similares en ambos tamaños, pero la estabilidad se vio comprometida. Sin embargo, el aumento del tamaño del electrodo de Li^0 fue identificado como la etapa limitante en este proceso. Por eso, las futuras etapas de este trabajo se van a centrar en una mayor atención a la estabilidad de este electrodo. Para ello se estudiará la combinación de técnicas estudiadas durante este trabajo, como la combinación de sales que permita una capa SEI que combine LiF y Li_3N ; o el recubrimiento de los electrodos mediante la incorporación de capas nanométricas de Al_2O_3 mediante pulverización con iones.

En definitiva, este trabajo ha explorado diferentes conceptos que han mejorado notablemente la estabilidad y el rendimiento de las baterías poliméricas de Li-S, mediante la selección de materiales, su testeo y la comprensión de su mecanismo de actuación, finalizando con el posterior desarrollo del concepto. Los resultados reportados se encuentran entre los más destacables de la bibliografía.

LIST OF ABBREVIATIONS

ASSLSB= All-solid-state lithium-sulfur battery

CE= Coulombic efficiency

DFT= Density functional theory

DME= 1,2-dimethoxyethane

DSC= Differential scanning calorimetry

EIS= Electrochemical impedance spectroscopy

GB= Glove box

ISE= Inorganic solid electrolyte

LAGP= $\text{Li}_{1+x}\text{Ge}_{2-x}\text{Al}_x(\text{PO}_4)_3$

LATP= $\text{Li}_{1+x}\text{Ti}_{2-x}\text{Al}_x(\text{PO}_4)_3$

LE= Liquid electrolyte

LFP= LiFePO_4

Li⁰= Metallic lithium

Li⁺= Lithium ion

LIB= Lithium-ion battery

LICGC= Lithium-ion conducting glass ceramic

LiFSI= Lithium bis(fluorosulfonyl)imide

LiFTFSI= Lithium (fluorosulfonyl) (trifluoromethanesulfonyl) imide

Li-IC= Lithium-intercalation cathode

LSB= Lithium-sulfur battery

LiTFSI= Lithium bis(trifluoromethanesulfonyl) imide

LiTCM= Lithium tricyanomethanide

NaSICON= sodium super ionic conductor

NCA= $\text{LiNi}_x\text{Co}_y\text{Al}_z$

NIB= Sodium-ion batteries

NMC= $\text{LiNi}_x\text{Mn}_y\text{Co}_z\text{O}_2$

PEO= Poly(ethylene oxide)

TGA= Thermogravimetric analysis

SCE= Solid composite electrolyte

SEI= Solid/electrolyte interphase

SEM= Scanning electron microscopy

SPE= Solid polymer electrolyte

RT= Room temperature

SS= Stainless steel

XPS= X-ray photoelectron spectroscopy

XRD= X-ray diffraction

INDEX

1	INTRODUCTION AND OBJECTIVES	1
2	MODELING ENERGY DENSITY AND REFERENCE CELL SYSTEM DEFINITION.....	51
3	ELECTROLYTE ADDITIVES	75
4	ELECTROLYTE FILLERS.....	91
5	ALTERNATIVE IMIDE-CONTAINING SALTS..	115
6	FLUORINE-FREE SALTS	145
7	GENERAL OVERVIEW.....	169
8	CONCLUSIVE REMARKS	179
	APPENDIX.....	183

Chapter 1:

Introduction and objectives

In this chapter, the importance of energy storage is highlighted, and different battery technologies are described. Among the different presented “beyond Li-ion batteries”, lithium-sulfur batteries stand out for their high achievable gravimetric energy densities. The specific issues for lithium-sulfur batteries are described in this section, together with the possible solutions and the definition of the objective of the thesis.

INDEX

1	INTRODUCTION AND OBJECTIVES	5
1.1	IMPORTANCE OF ENERGY STORAGE	5
1.2	BATTERIES	5
1.3	BEYOND LI-ION	11
1.3.1	Alternative metals.....	11
1.3.2	Li-intercalation cathode batteries.....	12
1.3.3	Li-air batteries	13
1.3.4	Li-organic batteries	14
1.3.5	Li-S batteries.....	15
1.4	DEEPER INTO LI-S BATTERIES	16
1.4.1	Working principle of Li-S batteries.....	16
1.4.2	Challenges in Li-S batteries.....	21
1.4.3	Strategies to overcome limitations	23
1.4.3.1	Strategies in the positive electrode.....	24
1.4.3.2	Strategies in the negative electrode	26
1.4.3.3	Strategies in the electrolyte	26
1.4.4	Solid-state Li-S batteries.....	30
1.4.4.1	Inorganic solid electrolytes	30
1.4.4.2	Solid Polymer electrolytes.....	31
1.4.4.3	Solid composite electrolytes.....	32
1.4.4.4	State of Art study in all-solid-state Li-S batteries	33
1.5	IDENTIFIED POTENTIAL RESEARCH AREAS	41
1.6	OBJECTIVES OF THE THESIS.....	41
1.7	REFERENCES	43

1 INTRODUCTION AND OBJECTIVES

1.1 IMPORTANCE OF ENERGY STORAGE

The technological revolution of the past few centuries has been powered by combustion reaction of fossil fuels, whose future supply will be limited and whose emission caused severe disturbances in global climate and living beings, such as greenhouse effect or air pollution.¹⁻³ By 2050, the expansion of human population is expected to reach 9 billion people and predictions show that if renewable energy systems are not rapidly scaled up, the fossil fuels consumption will continue growing exponentially.⁴

Therefore, the development of a sustainable energy model is of paramount need. Its development involve three major challenges: i) energy saving, ii) efficiency improvement in energy production, and iii) the replacement of fossil fuels by various sources of renewable energies.⁵ However, the deployment of renewable energy sources, such as wind, solar or hydroelectric, is limited by their intermittent or seasonal availability.

In this regard, large-scale energy storage could accumulate the energy produced in peak periods of wind, sun or rain and introduce it gradually in the electrical grid. Grid-energy storage could be done in several ways, such as air compression, pumped-storage hydroelectricity, gravitational potential energy storage, or by batteries.⁶ Among all the options, batteries are the only ones that can also help to electrify the transport sector, whose energy consumption can represent up to 30% of total energy consumption in developed countries,^{7,8} enabling the replacement of fossil fuels by renewable energies.

Thus, the continuous development of more efficient and competitive batteries is nowadays crucial for a complete transition from conventional energy model to more sustainable one. Furthermore, batteries have been also crucial in human development by powering a wide variety of portable electronics, from laptop computers and cameras to microchips or pacemakers.

1.2 BATTERIES

Batteries are electrochemical energy conversion and storage devices that are able to convert electrical energy into electrochemical energy and storage it under a chemical form. This technique lies in the fact that both electrical and chemical energy share the same carrier, the electron (e^-).⁹

Systems for electrochemical energy storage and conversion include batteries, supercapacitors and fuel cells. Although the energy conversion and storage mechanism are different in each system, all share common features: they consist

of two electrodes at different potential in contact with and separated by an electrolyte. In all the cases reactions take place at the electrodes, while electrolyte acts only as ion conductor and generated or consumed e^- travel around an external circuit. While batteries and supercapacitors are considered closed systems, in which electrodes are the charge transfer mediums and contain active materials; fuel cells are open systems where electrodes are just the charge transfer media, and the active compounds that will undergo electrochemical reactions are fed from outside the cell.

Finally, the difference between batteries and supercapacitors relies on the type of conversion reaction. While in batteries the energy is stored or delivered via reduction/oxidation (*i.e.*, redox) reactions, the working principle of supercapacitors lies on the orientation of electrolyte ions at the electrode/electrolyte interface, where the so-called electrical double layer is formed and released, resulting in a parallel movement of e^- .¹⁰ **Figure 1.1** summarizes the working principles of the three electrochemical systems at discharging state.

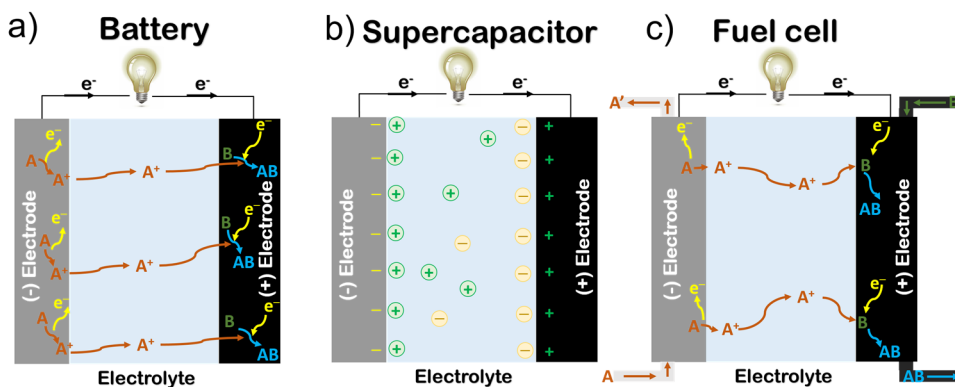


Figure 1.1. Schematic representation of electrochemical energy storage and conversion devices, including a) batteries, b) supercaps and c) fuel cells. A' in the fuel cell scheme represents the unreacted A fuel.

The different working principle confers different properties and applications to each system. Batteries have found, by far, the most application sectors and have established a very strong market position.¹⁰ Capacitors are not able to store as much energy per volume or mass unit as batteries, but their extremely fast charges and discharges and extended lifespan makes them suitable for applications where instantaneous and high power response is needed, such as in grid power buffers, motor starters, or braking energy recovery systems in electric vehicles.¹¹ In contrast, fuel cells are still in development stage and are searching for a “killer application” that allows their penetration into the market. In the future, fuel cells and capacitors will probably find the most promising markets in some specific

sectors that nowadays use batteries, but where their properties allows them to provide more suitable performances.¹⁰

Deeper into batteries, based on the definition given by Linden and Reddy in the fourth edition of “Linden’s Handbook of Batteries”,¹² a primary battery is a device that converts the chemical energy contained in its active material into electric energy by means of an electrochemical redox reaction. In the case of secondary batteries, also known as “rechargeable batteries” the battery can be charged reversibly. While the term “battery” is often used, the basic electrochemical unit is called “cell”. A battery consist on one or more cells connected in series or parallel. The cell consist of three major elements,¹³ including:

- **Anode:** electrode that gives up e^- to the external circuit and it is oxidized during the discharge.
- **Cathode:** electrode which accepts e^- from the external circuit and it is reduced during the discharge.
- **Electrolyte:** the medium for transfer of charge, as ions, between anode and cathode.

This classification can be confusing, because the electrodes named as “anode” and “cathode” must shift depending if the cell is discharging or charging. For this reason, it is more appropriate to name them as negative and positive electrode, based on their electric potential values. However, according to the vast majority of the published works, the term “anode” refers to the negative electrode and the term “cathode” to the positive electrode.

Cell operation of a battery is shown in **Figure 1.2**. During the discharge (**Figure 1.2a**), when both electrodes are connected by means of an external device, negative electrode material (represented as A) is oxidized (A^+) and e^- flow through the external load to the positive electrode, where e^- are accepted and positive electrode material (B^+) is reduced (B). During the charge (**Figure 1.2b**), the current flow is reversed and oxidation takes place now at the positive electrode. Then, e^- move in the opposite direction thought the external circuit and are accepted by the negative electrode material.

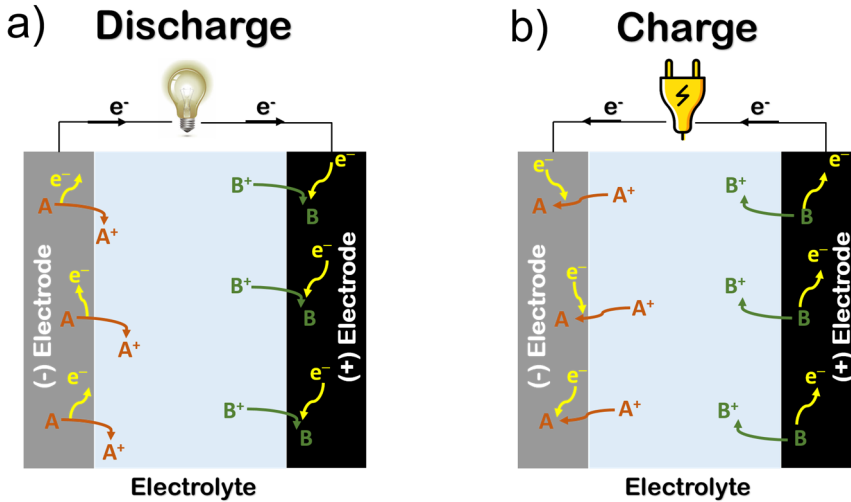


Figure 1.2. Electrochemical operation of a cell during a) discharge and b) charge.

The electric charge stored in a battery is measured by means of capacity. The units of capacity are Coulomb ($1C = 1As$) or more typically Ampere hour ($1Ah = 3600As = 3600C$). The theoretical capacity that an electroactive material provides or store can be calculated according to Faraday's law, and it is directly associated with the quantity of e^- the material will deliver per unit of mass.

$$C_g = \frac{n_e \cdot F}{M_w} \quad (1.1)$$

Where C_g is the gravimetric capacity, n_e is the amount of transferred e^- per redox reaction, F is Faraday's constant and M_w is the molar mass of the structural unit. However, in reality, full capacity from a material is rarely obtained due to several operation limitations such as energy losses due to internal resistance, component degradation or the presence of side-reactions.

Usually, the cells cannot deliver as much capacity during the discharge as it is provided in the charge (or reverse in some cases), due to energy loss in several undesired processes. Herein, *Coulombic efficiency* (CE) term is used to measure the ratio of discharge and charge capacity obtained during the cell cycling, as defined by following equation, where $C_{discharge}$ is the capacity obtained during the discharge and C_{charge} is the capacity provided during the charge. The value is usually given as a percentage.

$$CE = \frac{C_{discharge}}{C_{charge}} \quad (1.2)$$

The current at which a battery is either charged or discharged is measured by intensity. The unit of intensity is Ampere (A). In research, the cycling current is usually converted to C -rate, defined as follows:

$$C - rate = \frac{i_{applied}}{i_{1h}} \quad (1.3)$$

Where $i_{applied}$ is the applied current and i_{1h} is the necessary current to charge/discharge the cell in 1h. For example, a C -rate of 0.1C, means 10 hours for complete charge or discharge.

The cell voltage will be determined by the potential difference between both electrodes, and it is measured in Volts (V). The two electrodes have different chemical potentials, which are dictated by the chemistry that occurs in each of them.¹⁴ Finally, to calculate the energy of a cell, E_{cell} (Wh) its voltage and capacity are multiplied:

$$E_{cell} = C_{cell} \cdot V_{cell} \quad (1.4)$$

However, usually the voltage of a cell is not constant during the whole charge/discharge process. In that case, the capacity value should be integrated in the whole range of voltage values.

$$E_{cell} = \int_0^{C_{cell}} V_{cell} dC \quad (1.5)$$

Nevertheless, this calculation is not common, so an average voltage is usually defined for the calculation. Finally, the electric power of a cell, P_{cell} , (W) is the rate at which electrical energy could be transferred. It can be obtained by the division of the energy of the cell by the charge/discharge time, t .

$$P_{cell} = \frac{C_{cell}}{t} \quad (1.6)$$

It is worth mentioning, that some of these parameters are usually studied in gravimetric or volumetric terms, such as gravimetric capacity, or gravimetric and volumetric energy and power. This strategy enables the comparison of storage ability of different materials and systems.

To increase the energy of a battery or cell we can tune both voltage and capacity. Hundreds of electrochemical couples were proposed during the nineteenth and early twentieth centuries, being Zn-MnO₂ the most common primary battery and lead-acid and Ni-Cd the most common secondary ones.¹⁴ However, the intensive research work has led to the development and commercialization of higher

performance and sustainability batteries in the last decades, *i.e.*, nickel-metal hydride (Ni-MH) and Li-ion batteries (LIBs). Each type of battery has different inherent properties which, in some cases, makes them suitable for specific applications. For example, while lead-acid batteries have very limited specific energies around 35 Wh kg^{-1} , their fast kinetics allow them to provide fast discharges, and thus high gravimetric power, making them the most common batteries for starting, lighting and ignition in cars.¹⁵

Nowadays, battery market is dominated by LIBs despite a significant quota of primary alkaline Zn-MnO₂ and secondary Ni-MH systems.¹⁵ The LIBs, firstly commercialized by Sony in 1991, lies in lithium ion (Li⁺) exchange between graphite anode and a layered oxide cathode (Li_{1-x}T^MO₂, being T^M a transition metal, usually Co), based on the “rocking-chair” mechanism proposed by our colleague Prof. Armand.¹⁶ **Figure 1.3** shows schematically the working principle of LIB batteries. During the charge, the Li⁺ deintercalates from the layered oxide material in the positive electrode, releasing e⁻. While the Li⁺ travel to the negative electrode through the ion conductive electrolyte, the e⁻ move through an external circuit with the help of an external energy source. Once in the negative electrode, Li⁺ reunite again with the e⁻ and intercalate into the carbonaceous structure. In contrast, during the discharge, the process occurs in the opposite direction, but with a spontaneous e⁻ flow from negative to positive electrode. In LIBs the same ion, Li⁺, participates at both electrodes, being reversibly inserted and extracted, lying on the so called “rocking-chair” principle.

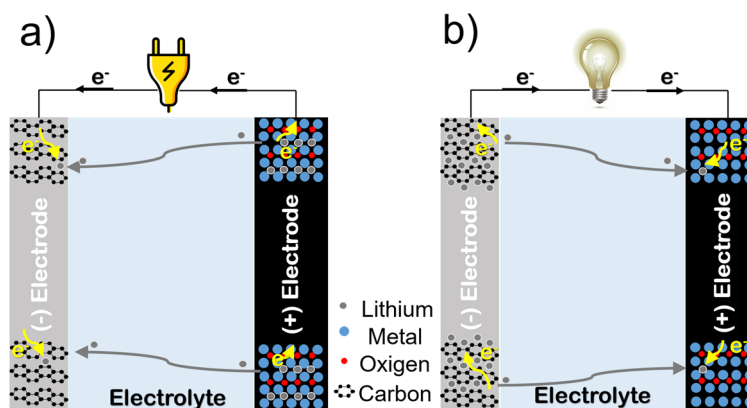


Figure 1.3. Schematic representation of a) charge and b) discharge mechanism in a generic Li-ion battery.

Initially, the energy storage ability of the LIBs (150 Wh kg^{-1}), was up to three times higher than those of previous alkaline systems, and made them specially suitable for portable electronics, which resulted in their first commercialization and billions of units sold by now.^{2,14} However, after several years of development

the performance of LIBs seems close to their practical limits, while they cannot fully satisfy the needs of modern portable electronics or electric vehicles. Nowadays, many researchers still work in the development of higher performance LIB-based systems with the study of new alternatives. For example, by the implementation of novel high-capacity materials, prepared by chemical substitution of cobalt by manganese, nickel or lithium (e.g., Li-rich $\text{LiNi}_x\text{Mn}_y\text{Co}_z\text{O}_2$, NMC) it is possible to double the practical capacity of the active materials.¹⁷ Other alternative strategies focus on the implementation of solid electrolytes that allow the use of pure metallic lithium (Li^0) as negative electrode which, according to our viability calculations, could improve over the 30% gravimetric energy density of the batteries.

The limited room for improvement, along with other factors such as safety concerns, environmental impact and high cost of rare metals such as Ni or Co, have motivated the parallel search of a new generation of post LIBs, which will be presented in the following section.

1.3 BEYOND LI-ION

In the last decades, several efforts have been devoted to the search of alternative battery systems, which could overcome actual limitations of LIBs and/or could palliate environmental, safety or high-cost concerns. Strategies have mainly focused on the substitution of Li^+ by alternative alkali or alkali earth metals, such as sodium (Na-ion batteries), potassium (K-ion batteries) or magnesium (Mg-ion batteries); or the use of novel conversion positive electrodes, such as oxygen (Li- O_2 /air batteries), sulfur (Li-S batteries) or organic compounds (Li-organic batteries). Furthermore, the combination of several strategies is also possible, as proved by the reports on Na-S or Mg-air batteries.^{18,19} However, for simplicity, this section will only briefly describe the most extensively studied and developed “beyond LIB” systems.

1.3.1 Alternative metals

Calculations shown that at an average of 5% year growth rate in lithium mining reserves, a severe shortage will be encountered in less than 65 years. Together with these possible raw material shortage, the uneven distribution of lithium reserves may generate political conflicts, casting shadows on future sustainability of lithium market.²⁰ Therefore, batteries based on alternative intercalation metals have been widely explored.

Na-ion battery (NIB) started to be investigated in early 1980s, but the research decreased significantly after the successful commercialization of first LIB in 1991. However, with the predicted rise of energy storage market, the interest in this

battery systems has risen again due to the abundance and low cost of sodium derivatives.²¹ Among different alkaline metals, sodium is the one that ideally would require less technological efforts in a transition from lithium to sodium.²⁰ Moreover, based on wide availability (4th most abundant element in earth crust) and low cost of sodium (≈ 150 \$/ton Na_2CO_3 vs. ≈ 5000 \$/ton Li_2CO_3), NIBs have the potential for meeting large scale grid energy storage needs, and may become competitive to LIB in other specific markets.²²

Although sodium is the most widely studied and developed alternative, other alkaline and alkaline earth metals have been explored by academia and industry. For example, potassium, is a relatively abundant element which can also be refined with much lower cost than lithium-based materials. K/K^+ offers a lower reduction potential compared to Na/Na^+ , allowing K-ion batteries to operate at higher voltage, and thus, could compete with NIBs in terms of energy density, and specially power density.^{23–27}

Zn, extensively used in commercial primary batteries, *e.g.*, Zn-MnO₂ batteries, is another example of studied materials for secondary batteries, due to its low cost, natural abundance and high energy density.²⁸ The use of Zn²⁺ energy carrier is attractive due to its good compatibility with a wide variety of electrolytes and the possibility to deliver reasonably high specific energy when paired with some electrode materials, particularly, in aqueous electrolytes.²⁹ However, critical knowledge is still missing for designing adequate negative electrode materials for reversible hosting Zn²⁺ and its application in rechargeable devices.²⁸

1.3.2 Li-intercalation cathode batteries

Before deepening into more disrupting technologies, Li-intercalation cathode (Li-IC) batteries should be addressed. Motivated by the nearly 10 times higher theoretical capacity in respect to graphite and the lowest reported reduction potential of Li^0 (-3.04 V vs. standard hydrogen electrode), the substitution of conventional graphite negative electrodes by Li^0 , and its direct pairing with previously mentioned intercalation metal oxides in the positive electrode, *i.e.*, NMC, LiFePO_4 (LFP), $\text{LiNi}_x\text{Co}_y\text{Al}_z$ (NCA), has the potential to improve the energy density significantly. After falling into oblivion for several decades because of safety concerns and after years of development of graphite-based negative electrodes, the use of Li^0 is now “ready for revival”, due to the development of novel investigation tools and nanotechnology based solutions.³⁰ Nowadays, Li^0 is considered the “holy-grail” of batteries due to its extremely high capacity, low molecular weight and possessing the lowest negative reduction potential.³¹

However, the use of liquid electrolytes along with pure Li^0 electrodes is yet considered challenging and potentially dangerous, so the coupling of Li^0 with solid electrolytes has drawn considerable attention from both academia and industry

sectors. The suitability of this technology has been demonstrated by the massive deployment of Bolloré Bluecar in several cities world-wide, based on Li^0 |polymer electrolyte|LFP battery configuration.³² A perspective article, presenting an in-depth analysis of the attainable energy density, overall safety and cost on all-solid-state Li-IC batteries was published by our group,³³ discussing the existing approaches from literature towards the claimed energy density and safety improvements. Possible solutions to the remaining challenges and new directions were also given, aiming at designing practical and high performance batteries. The article included **Figure 1.4**, where the achievable energy densities for different battery technologies are compared.

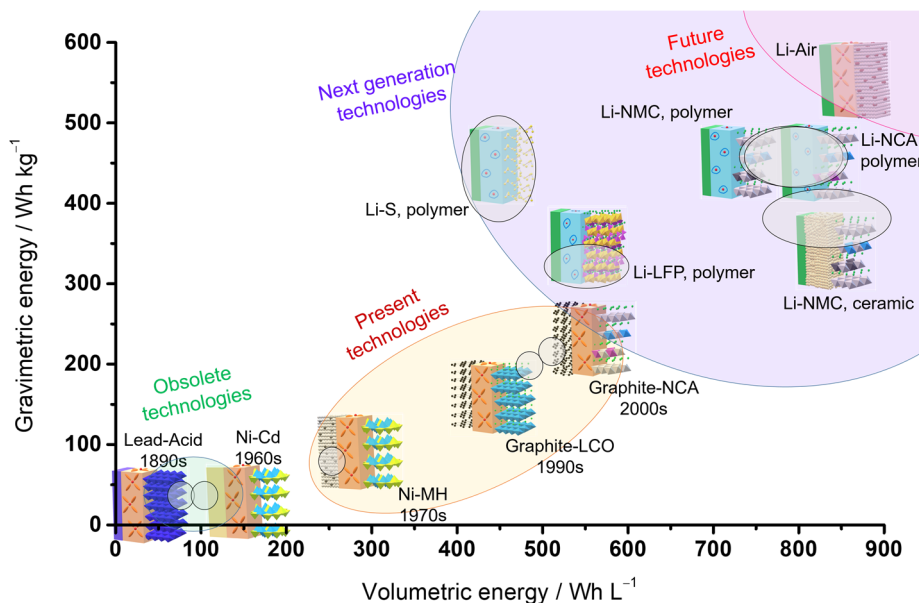


Figure 1.4. Overview of the evolution of technologies and the role of all-solid-state Li-IC batteries.

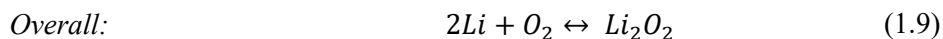
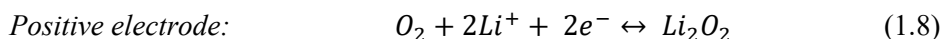
Other battery technologies, still maintain Li^0 negative electrode, but substituting intercalation materials in the positive electrode by other conversion materials or electroactive organic materials, as depicted in further points.

1.3.3 Li-air batteries

Rechargeable Li-air batteries have attracted increasing attention due to their ultrahigh theoretical energy densities of 3458 Wh kg^{-1} and reported values up to 2000 Wh kg^{-1} at cell level, which have even surpassed the practical value of gasoline, 1700 Wh kg^{-1} . Furthermore, if an external O_2 supply is considered and its mass is excluded, the theoretical energy can reach superlative values of 11428 Wh kg^{-1} .³⁴ This battery system, often called Li- O_2 battery, is based on the

following electrochemical reactions of Li^0 and O_2 in aprotic electrolytes:

Table 1.1. Reaction mechanism of Li-air batteries.³⁴



This system could be considered the most promising ‘beyond Li-ion’ rechargeable battery technology. However, its impact is still limited due to the technical difficulties, including the achievement of high energy densities at acceptable cycle-life, large overpotential and significant volume changes upon cycling, instability of the Li^0 electrode, effect of impurities in the O_2 -supply, uncontrolled precipitation and dissolution of the discharge products, and limited kinetics and mass transfer.^{34,35}

1.3.4 Li-organic batteries

Organic batteries comprising redox-active organic materials, usually polymers, have emerged as promising candidates in the pursuit of electrochemical energy storage systems with high-performance, low cost, and environmental benignancy, due to the use of abundant, environmentally-friendly and biocompatible organic materials. Organic compounds offer a versatile platform for tailoring the physicochemical and electrochemical properties of electrode materials (*e.g.*, solubility, redox potential and specific capacity). Therefore, several redox-active organic molecules have been proposed. One inherent property of this material family is its structural flexibility due to the attachment of redox-active moieties to polymer backbones, enabling the construction of electrodes with superior flexibility and processability, which are imperative features for wearable technologies.

The electrochemical behavior of organic materials is based on simple redox reactions, instead of complex intercalation mechanism, where sluggish transformation of lattice limits reaction kinetics.¹³ For that reason, some organic-based batteries, specially radical polymer based batteries, show impressive rate performance, with no capacity decay up to rates of 10C and almost 50 % capacity retention at 300C, which corresponds to charge and discharge times of 12 s.³⁶

Finally, even most of the published studies pair organic redox-active materials with Li^0 electrodes, structural flexibility of organic materials enables the reversible storage of other metal-ions rather than Li^+ for the same active material,^{37–42} allowing the use of alternative highly abundant and accessible metal electrodes. A detailed work was published by our group, aiming to provide insights on the

material design and cell engineering for building competitive and high-energy density organic materials.⁴³ **Figure 1.5** shows the table of contents picture of the article.

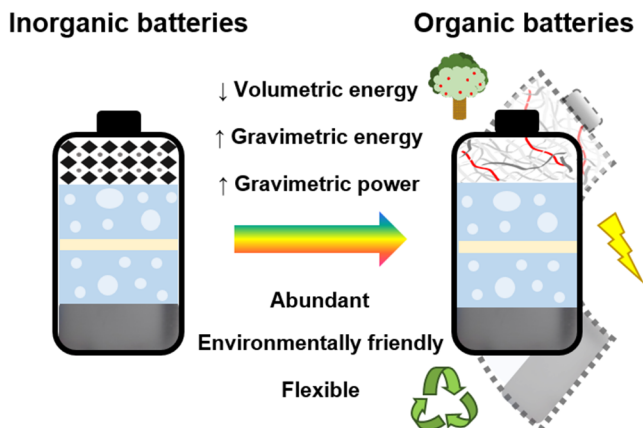


Figure 1.5. Schematic representation of the benefits of the substitution of conventional intercalation cathodes by redox-active organic materials. Reprinted with permission from ref. 43. Copyright 2019 Americal Chemical Society.

1.3.5 Li-S batteries

Li-S batteries (LSBs) are usually composed of a sulfur-based positive electrode, Li^+ conductive electrolyte and, a Li^0 negative electrode. Elemental sulfur, S_8 , is the most commonly employed electroactive material, due to its high theoretical capacity of 1675 mAh g^{-1} at an average voltage of $2.1 \text{ V vs. Li/Li}^+$, which leads to theoretical energy densities of 2500 Wh kg^{-1} and reported energy density of up to $400 \text{ Wh}^{-1} \text{ kg}$ at cell level.^{44,45} The working principle of LSBs lies on the following overall reaction:



However, this battery chemistry still presents many challenges due to various limitations that yet hinder their market-scale deployment, such as electronic insulating behavior of sulfur, the stability and capacity retention issues related to the generation of soluble intermediate products, and the instability of Li^0 upon cycling.

Driven by their particularly high gravimetric energy, this battery system is suitable to replace LIBs in weight-crucial applications, *e.g.*, electrical vehicles, drones or high-altitude pseudo-satellites. Nowadays, Oxis Energy (United Kingdom) and Sion Power (United States) have been the first two private companies that develop LSBs including research and manufacturing activities. Remarkably, Airbus

Defence and Space, in collaboration with Sion Power, achieved a world-record flight of more than 14 days without refueling or landing in 2015 with the Zephyr High Altitude Pseudo-Satellite, which was powered by solar energy during the day and 350 Wh kg⁻¹ LSBs during the night.^{46,47} At the same time, Oxis Energy also joint Airbus Defence and Space, aiming at the development of Li-S technology for space applications.⁴⁸

Due to its high specific energy, low cost and the environmental friendliness of sulfur, LSBs have attracted enormous attention in the last years. Therefore, this PhD thesis has been focused in LSBs. The following sections will depict in detail the properties, opportunities, challenges and the actual status of the Li-S batteries.

1.4 DEEPER INTO LI-S BATTERIES

1.4.1 Working principle of Li-S batteries

The working principle of LSBs lies on the reversible electrochemical conversion reaction of S₈ and Li⁰. Li⁰ is considered the ‘holy-grail’ of the batteries, for its lowest reduction potential, low molecular weight and impressive theoretical capacity of 3861 mAh g⁻¹.³¹ S₈ is also considered a very promising electroactive material due to its high capacity (1675 mAh g⁻¹, S₈ hosts up to 16 e⁻), moderate average voltage of 2.1 V vs. Li/Li⁺, environmental benignancy, abundance and low cost.

Sulfur, mostly in the form of sulfur containing minerals, is the 16th most abundant element in the lithosphere. S₈ was firstly recognized as a valuable chemical agent as far back as 1600 B.C.E. by Egyptians to bleach cotton fabric. Nowadays, it is present in several areas such as petroleum refining, mining, pulp and paper processing, rubber production and construction, and it is consumed in commodities as sulfuric acid, antimicrobial agents or chemical dyes.⁴⁹

Remarkably, from the chemical engineering point of view, abundant S₈ is obtained in the desulfurization processes in oil refineries, whose aim is to decrease the sulfur content in commercial fossil fuels below < 10 ppm to meet environmental restrictions, in order to avoid SO_x generation during fuel combustion process.^{50,51}

Regardless the bad reputation of S₈, it should be considered as a non-toxic substance. It is not considered as irritant, mutagen or carcinogenic agent, and even a chronic exposure will not have any negative effects. Its bad reputation comes from its by-products. At high temperatures sulfur may burn to produce SO₂, extremely irritating, or may react to produce H₂S, toxic and explosive. However, under moderate temperatures and pressures, sulfur is stable and non-reactive.⁵² Notably, in the refineries, the generated sulfur is commonly stored in open-air above-ground facilities, in powder or brick form, as shown in **Figure 1.6**.

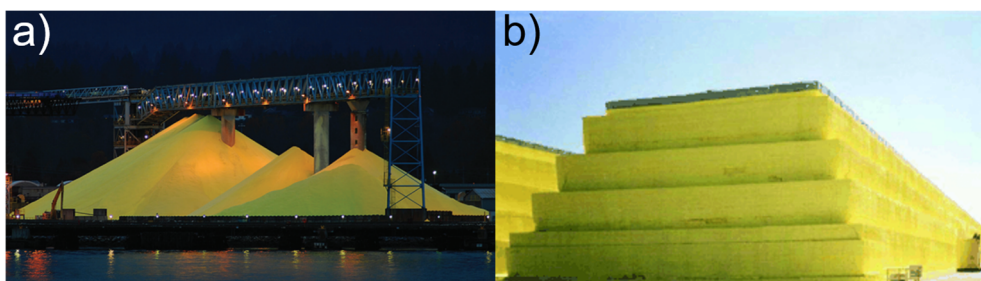
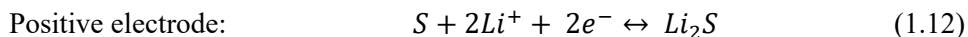


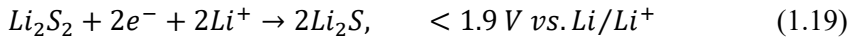
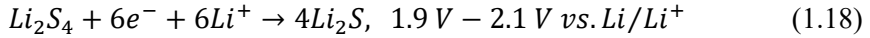
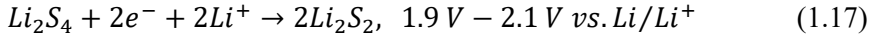
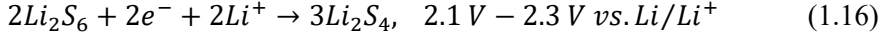
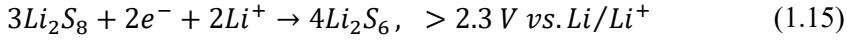
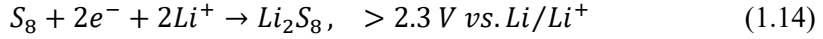
Figure 1.6. Examples of above-ground a) sulfur powder and b) sulfur bricks storage sites resulting from desulfuration of petroleum via Claus process. Reproduced from ref.⁵³ (Copyright 2019 Nature Publishing Group) and ref. 54 (Copyright 2019 Wiley-VCH) with permission.

Back to electrochemistry, LSBs are usually composed of a S_8 -based composite positive electrode, Li^+ conductive electrolyte and a Li^0 negative electrode. The electrochemistry could be summarized into the following reversible reactions.

Table 1.2. Simplified reaction mechanism in Li-S batteries.



Contrary to LIBs, after cell assembling the positive electrode of the LSBs is already delithiated, *i.e.*, in charge state. The most remarkable complexity in LSBs is that, in reality, reaction (1.12) is not a straight and single step-reaction, but a multistep reduction reaction, where several intermediate reaction products, *i.e.*, lithium polysulfides [Li_2S_x ($1 \leq x \leq 8$), LiPSs] are generated. These discharge reactions have been widely studied and the model stated by Moy *et al.*⁵⁵ and depicted in **Table 1.3** is the commonly accepted mechanism:

Table 1.3. Extended discharge mechanism in LSBs.

Consequently, discharge profile in LSBs shows three-steps profile, with an upper plateau at $> 2.3 \text{ V vs. Li/Li}^+$ [reactions (1.14)-(1.15)], sloping region about $2.1\text{-}2.3 \text{ V vs. Li/Li}^+$ [reaction (1.16)] and a low plateau at $< 2.1 \text{ V vs. Li/Li}^+$ [reactions (1.17)-(1.19)]. However, discharge and charge mechanism, and thus, voltage profile, are highly dependent on electrode and electrolyte composition, electronic and ionic conductivity, internal cell resistance or discharge/charge rate, so it is not possible to propose a general model that works in every single case. In contrast, the charge process has not yet been studied and understood in such detail due to the overlapping of simultaneous reactions. **Figure 1.7a** shows the schematic representation of a cell during discharge and charge. **Figure 1.7b** shows the voltage profile of a LSB during the discharge, where the three regions are highlighted, and their initial and final intermediate products are presented.

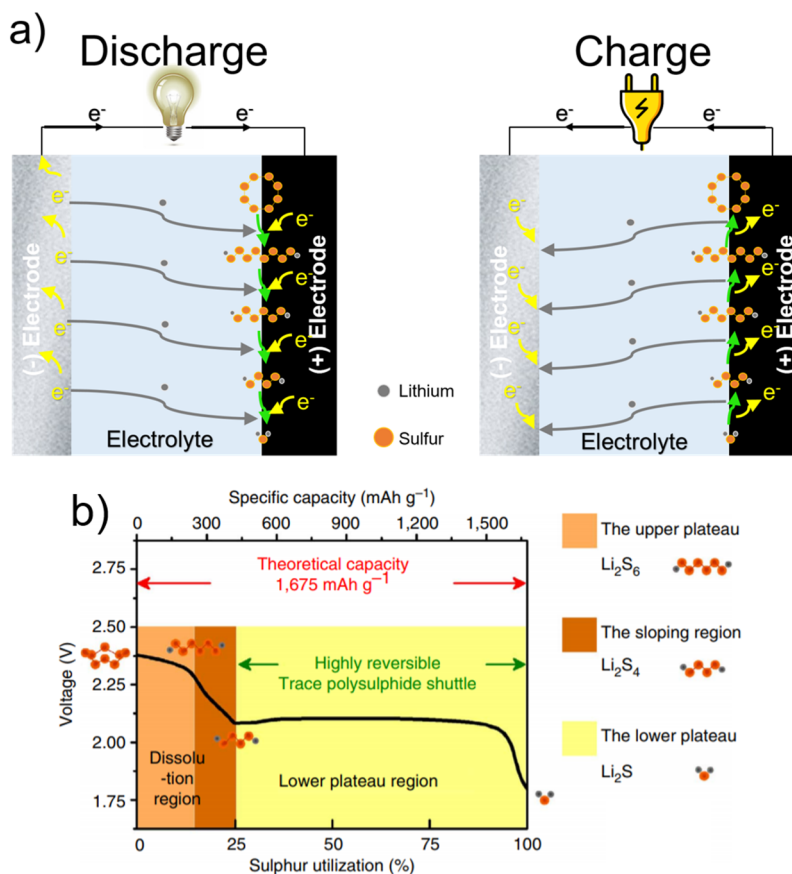


Figure 1.7. Schematic representation of a) discharge and b) charge reactions in Li-S batteries. c) Voltage profile of Li-S during discharge, with the three differentiated steps and their initial and final LiPS species. Reproduced from ref. 56 with permission. Copyright 2019 Nature Publishing group.

It is important to mention at this point that long chain LiPSs, Li_2S_x ($x \geq 4$) are highly soluble in common organic liquid electrolytes, and therefore they can diffuse through the cathode structure and electrolyte due to concentration and potential gradients, generating active mass loss in the positive electrode and parasitic reactions in the negative one, in the so-called “LiPS shuttle effect”. This issue will be further discussed in detail in section 1.4.2.

Regarding the practical development of LSBs, the use of pure S_8 electrodes is not possible, due to its electronically insulating nature. Therefore, sulfur needs to be surrounded by an extent electronic conducting carbon structure that can ensure a proper e^- transfer to the particle surface. Moreover, this carbon matrix also plays an important role to accommodate up to 80 v.l.% expansion of the electroactive material, maintaining a proper structural integrity, avoiding collapse or lack of

contact with electroactive materials.⁵⁷

Furthermore, a binder is needed to attach the electrode components to the current collector and to ensure the structural integrity of the cathode. The most common binder in LSBs, as well as in LIBs, is polyvinylidene fluoride (PVDF). The current collector works as a substrate support for the positive electrode material and distributes currents homogeneously over its surface, acting as connection between electrode and external circuits.⁵⁸ Aluminum foil is the most common choice as positive electrode current collector due to its low cost, high conductivity, and stability in the working voltage range.

Regarding the electrolyte, conventional carbonate solvents, such as ethylene carbonate or dimethyl carbonate, employed in LIBs, along with typical LiPF_6 salt are reactive to LiPS species. Thus, the mixture of lithium bis(trifluoromethanesulfonyl) imide (LiTFSI) salt in a mixture of linear 1,2-dimethoxyethane (DME) and cyclic 1,3-dioxolane (DOL) ether solvents are the most employed solvents in Li-S batteries due to their better compatibility with LiPS species.^{59,60} LiTFSI salt presents a good stability against LiPS and the highly delocalized charge distribution in TFSI⁻ anion leads to a sufficient solubility of LiTFSI in ether solvents, and consequently high Li^+ conductivity.⁶¹ DOL has the ability to form insoluble, flexible and Li^+ conductive surface films of dioxolane oligomer on Li^0 surface, which helps to protect Li^0 integrity during morphology and volume changes while cycling.⁶² These interfacial films are usually known as solid-electrolyte interface (SEI) layers. On the contrary, DME provides high LiPS solubility, necessary for appropriate reaction kinetics, and decreases electrolyte viscosity.⁶⁰ Finally, the LiNO_3 additive also allows the formation of a robust passivation SEI layer on Li^0 , which is believed to be composed mainly of Li_xNO_y species, as well as Li_2O , LiNO_2 and Li_3N .^{63,64} This passivation layer suppresses, to some extent, undesired reaction with soluble LiPS; and has also been reported to catalyze the conversion of highly soluble LiPS to S_8 . A physical barrier is needed to avoid direct contact between electrodes and thus, short circuit. This element is called separator and must possess a good electrolyte wettability and enough mechanical resistance to stay intact while cycling. Commercially available polypropylene/polyethylene (PP/PE) combined separator from Celgard[®] is commonly used in LSBs.

Another important component of LSBs is the negative electrode, and self-standing Li^0 is the most common choice. Li^0 is very reactive to moisture, especially to humidity, so all the handling and battery assembly must be carried out in an argon atmosphere glove box or in humidity free dry rooms. Once in operation, the Li^0 is very reactive to the electrolyte, electrolyte salts or additives, and thus, several reaction products can be found on its surface. Some reaction products, such as LiF or Li_3N are desirable and can generate compact, protective and highly Li^+ conductive SEI films, which can help to passivate Li^0 and protect it from further undesirable reactions.

Finally, regarding the cell packaging, commercial batteries are commercialized in various shapes, including coin cell, cylindrical or prismatic battery casings. However, in the case of research-level, coin cells are the most common choice for their simplicity, low cost, and small size. Small size allows cell testing material amount as low as few milligrams. In coin cell format, the cell components are stacked and closed under pressure. Another option is the use of larger size pouch cells, which is commonly used during first steps of the upscaling process. In pouch cells, one or multiple layers can be stacked together and sealed under vacuum in a low-cost case bag. However, the necessary amount of materials to build a pouch cell may be more than 10 times higher than that of the coin cells, so it is usually used only after an initial optimization process at coin cell level. **Figure 1.8** shows the schematic representation of coin cell and pouch cell.

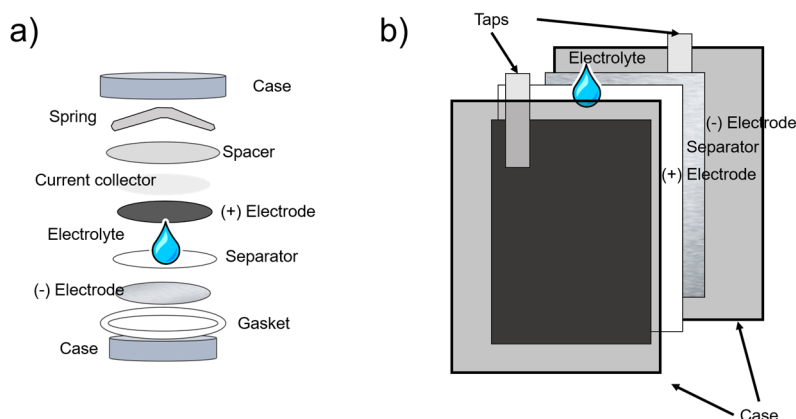


Figure 1.8. Schematic representation of common cell packaging for battery study at lab-scale for a) coin cell and b) pouch cell using liquid electrolyte.

1.4.2 Challenges in Li-S batteries

Despite its enormous potential as high energy density batteries, the practical application and full commercialization of LSBs has been hindered by several technical challenges:

- Low electronic conductivity of sulfur and final discharge product Li_2S ($\sim 30 \text{ S cm}^{-1}$) formed during cycling, along with their structural and morphological changes (80 vol.% expansion) during the discharge and charge, results in unstable electrochemical contact within positive electrode. These issues result in lower utilization of active material, poor cycle life and low storage efficiency.⁶⁵ This forces to decrease the amount of active material in the positive electrode limiting active material loadings to values usually lower than 70 wt.%.

- LSBs can today achieve energy density values as high as 350 kWh kg^{-1} , but the low electronic conductivity of the aforementioned electroactive materials and the sluggish redox kinetic of the formation/breakdown of the S–S bond limits their performance at high cycling rates, and thus, limits their application in high-power crucial applications.⁶⁶
- Cell component degradation is a common problem in batteries due to the presence of organic electrolytes, metallic electrodes and soluble reaction intermediates. These result in side reactions, self-discharge, or corrosion of cell components, such as current collector. In LSBs the chemical environment is especially harsh due to the presence of highly reactive LiPSs.⁶⁶
- The use of Li^0 in the negative electrode generates stability and safety challenges. Li^0 is unstable in contact with organic electrolytes and may sometimes react to generate undesired and highly resistive reaction products, *i.e.*, mossy/dead Li^0 . On the other hand, during cycling, Li^+ are continuously plated and stripped into and from the negative electrode. The non-uniform Li^+ deposition while charging, or the presence of nucleation points will generate ramified Li^0 microstructures that grow beyond the anode surface, *i.e.*, lithium dendrites. These dendrites will deteriorate battery life due to an increasingly exposed Li^0 surface, decrease negative electrode capacity, and may finally pierce the separator and grow up to the positive electrode, short circuiting the cell, which may lead to thermal collapse of the cell.
- Finally, as mentioned previously, high order LiPSs are highly soluble in common organic solvents (*e.g.*, Li_2S_8 possesses a 6 M solubility in DME/DOL)⁶⁷. LiPSs are easily dissolved in the electrolyte and diffuse through the electrolyte driven by concentration and potential gradients. During the charge, this long-chain LiPSs can reach the negative electrode and be reduced to shorter species, consuming e^- and Li^+ undesirably. If the newly generated LiPSs are still soluble, they can diffuse back to the cathode and get oxidized in the following charge; but if they are reduced to low order insoluble Li_2S , these will irreversibly deposit on the Li^0 surface, poisoning and passivating it. This process, called “LiPS shuttle-effect” contributes to active material loss in the positive electrode, corrosion and passivation of Li^0 in the negative electrode, low Coulombic efficiency or inability to charge the cell, self-discharge and increased cell resistance.^{65,66} However, LiPS solubility is considered a “double-edge sword”. Apart from the well-known negative effects from LiPS shuttling, their dissolution from the bulk sulfur brings a positive effect enhancing the electrochemical utilization of the electronically insulating S_8 .⁶⁸ Thus, it is believed that LiPS solubility should be promoted as long as they can be confined in the positive electrode area.

In conclusion, LSBs have a strong potential to substitute LIBs in applications where gravimetric energy density plays a critical role. However, due to a complex

multi-step chemistry and the presence of insulating or overactive compounds, researchers are still facing many challenges (as summarized in **Figure 1.9**) and are far from exploiting all the benefits from this battery system.

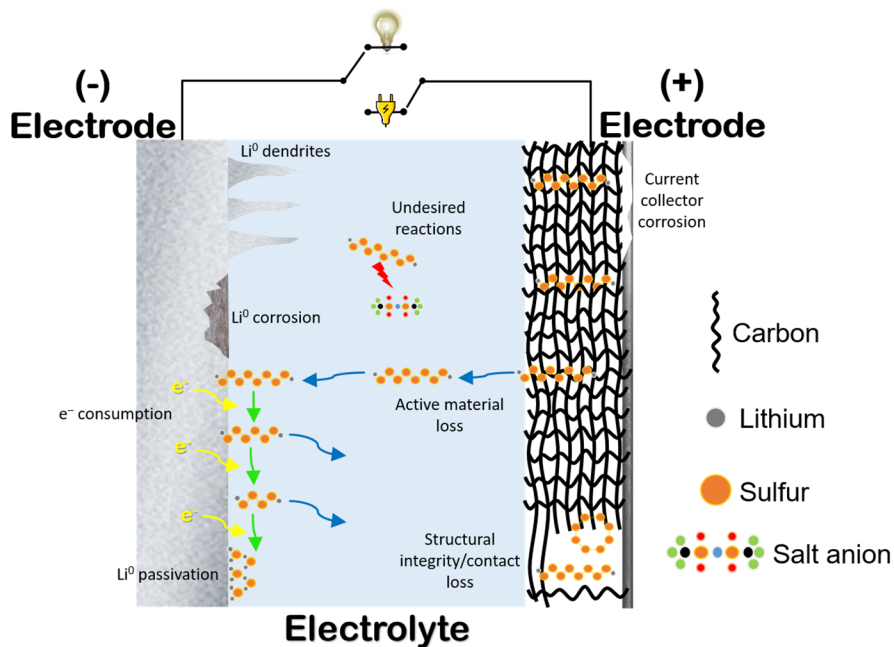


Figure 1.9. Schematic representation of the electrochemical, chemical and degradation mechanisms in LSBs.

1.4.3 Strategies to overcome limitations

Despite the challenges, the research in the last decade has brought enormous advances in the development of LSBs, and the considerable room for improvement continuously attracts interest from several research groups and companies, with a continuously growing number of publications in the decade of 2010s, as seen in **Figure 1.10**. It is also remarkable that while in 2010 Li-S related studies represented less than 0.5% of the total of battery researches, in 2018 they represented a 5%, a significant quota in battery research field.

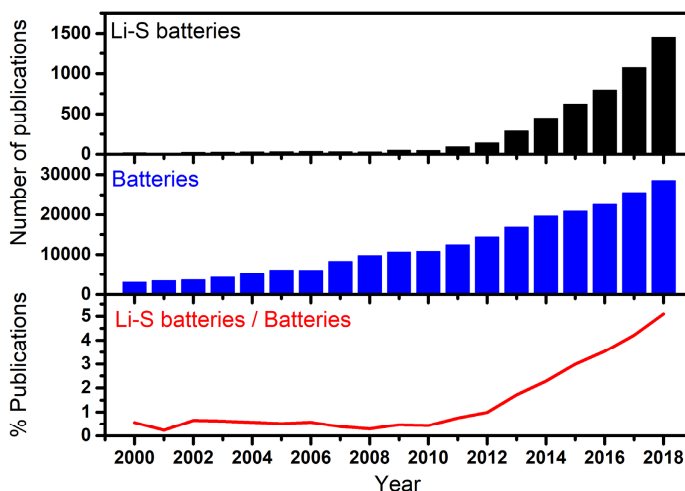


Figure 1.10. Evolution of the total number of publications in LSBs (upper part) and in batteries (medium part); and the percentage of Li-S related studies ones over the total. Data were obtained from Scopus database with the keywords “lithium sulfur batteries” and “batteries”.

Up to date, several strategies have been implemented in every single element of LSBs to deal with its challenging limitations. For simplicity, those strategies will be divided into three groups, *i.e.*, strategies in the positive electrode, in the negative electrode and in the electrolyte. However, most of these strategies are transversal and have impact in overall cell performance.

1.4.3.1 Strategies in the positive electrode

The multicomponent positive electrode offers several possibilities to tune its components with the aim of improve battery properties. One of the most studied options is the use of different carbons. Numerous and various carbon substrates have been developed, such as microporous, mesoporous and hierarchical porous carbon, carbon black, hollow carbon spheres, carbon nanotubes and nanofibers. In these studies, the carbon possesses at least one of the following specific functions for improving cycling performance: i) containing or immobilizing active material, ii) trapping the dissolved LiPSs, iii) accelerating e^- transport and iv) absorbing or channeling the liquid electrolyte.⁶⁵ At the same time, many of these papers focus on an optimized sulfur encapsulation into the carbon structures by optimum mechanical mixing processes by heat treatments (*i.e.*, melting diffusion or sulfur vaporization) or by solution-based synthesis. A better encapsulation will facilitate sulfur/carbon contact and decrease sulfur particle size, improving conversion and enabling faster kinetics.^{57,65}

Another component that has been studied in depth is the binder. Due to the limited e^- conductivity of S and Li_2S , as well as the presence of LiPSs, the introduction of functional binders can be of great interest. Functional binders could be tailored to increase the electronic conductivity and/or their LiPS absorption capability (*i.e.*, polarity), acting even as an electro catalytic activity centers.⁶⁹ Several functional binders that improve the performance of LSBs can be found in the literature, such as, reduced graphene oxide/polyacrylic acid,⁷⁰ Li^+ -Nafion/Polyvinylpyrrolidone@nano-silica,⁷¹ or polyethylenimine/poly(ethylene glycol) diglycidyl ether cross-linked polymers.⁷²

Regarding electroactive material, the most popular choice is cyclic S_8 , due to its low cost and superior capacity. Nevertheless, there are several works that propose alternative organic structures that contain electroactive disulfide bonds (S–S) or thioether functional groups (C–S–C) in, *i.e.*, organosulfurs. Among all, the so-called sulfur copolymers stand out, which are polymeric structures that contain long ($-\text{S}_n-$) chains, with sulfur contents as high as 80-90 wt.% in respect to the total of the organic structure. The use of organosulfur enables yet high discharge capacities, a better electronic conductivity of the whole active material and a diminished shuttle effect due to an improved chemical and physical active material confinement.^{49,73}

Another alternative strategy focuses in the substitution of S_8 by LiPSs as starting active material. For example, Manthiram *et al.* reported some works where Li_2S_6 solutions were incorporated to carbonaceous structures. In that case, it is important to insulate LiPSs in positive electrode area, so LiPS-impermeable ceramic membranes were incorporated in contact with positive electrode, along with another conventional polypropylene or glass fiber separator.^{74–76} Other studies employ solid Li_2S as starting material. Li_2S is a Li-rich material, enabling its pairing with Li^0 -free negative electrodes, where Li^+ can be lithiated/delithiated while charging and discharging, in the so-called “Sulfur Lithium-ion” batteries. This strategy enables the use of high capacity S–S redox bond without the necessity of using of a Li^0 electrode.^{77–81}

Positive electrode additives, additional components with a maximum of 5-10% concentration, in either weight or volume, are considered a simple and effective approach to improve battery performance. Among others, transition metal oxides or complex oxides have been intensively studied due to the ability to reversibly absorb hydrophilic polysulfides.⁸² For example, anatase- TiO_2 , rutile- TiO_2 , Cr_2O_3 , ZnO , V_2O and RuO_2 have been demonstrated to effectively suppress LiPS diffusion and shuttle effect in absence on LiNO_3 .^{83,84}

Even it is the least studied component compared to the others in the positive electrode, the current collector plays a crucial role. At high current densities it may not be able to transfer satisfactorily e^- to the cathode due to contact limitations between current collector and electrode laminate, and its stability maybe

compromised under corrosive elements such as organic solvents.⁵⁸ Some research works used carbon coated current collectors to both improve contact and protect the aluminum from corrosion, while other studies demonstrated the suitability of substituting aluminum current collector by 3D porous carbonaceous current collector or nickel foam with satisfactory results.^{58,85}

1.4.3.2 Strategies in the negative electrode

During the initial years of LSB development, significant progress has been made towards the study of the positive electrodes, as demonstrated in the previous section. In contrast, negative electrode, which is directly involved in shuttle effect, has been often overlooked. Lately, the necessity of stable negative electrode for stable cycling has been increasingly addressed.⁸⁶ Li^0 is the preferred electrode material for the negative electrode in LSBs, but apart from the common challenges related to use of Li^0 , its use in LSBs becomes more complicated due to the presence of soluble reaction intermediates, which generates a more dynamic SEI than in conventional LIBs.⁸⁶

SEI layer plays a critical role in the Li^0 protection. Some studies generate *ex-situ* coating on Li^0 before cycling, *e.g.*, by the addition of a 0.8 μm Al foil on Li^0 surface by pressure and cured under temperature.⁸⁷ A thin protective Li-Al alloy layer can be generated, which lowers charge transfer resistance, decreases polarization and improves rate capability.

Our colleagues at CIC Energigune⁸⁸ demonstrated the suitability of both *in-situ* and *ex-situ* techniques to generate a conductive Li_3N layers on the top of Li^0 and cycled them in LSBs. *In-situ* technique was based on the addition of azidotrimethylsilate $[(\text{CH}_3)_3\text{SiN}_3]$ electrolyte additive, while *ex-situ* technique deposited a layer of 95% Li_3N over the Li^0 by drop coating.

On the other hand, Li^0 can be completely substituted. For example, some alloys allow a reversible lithiation and delithiation process and are believed to be more stable than bare Li^0 with a very competitive capacity. For example, Si can offer a very high theoretical capacity of 4200 mAh g^{-1} during lithiation and after galvanostatic lithiation it can be paired with a sulfur containing positive electrode.⁸⁹ Carbon-based negative electrode have also demonstrated a good cycling stability compared to Li^0 due to the stable SEI formed on its surface.^{90,91}

1.4.3.3 Strategies in the electrolyte

Contrary to positive electrode, where hundreds of different recipes and combinations can be found, the LiTFSI in DME/DOL + LiNO_3 electrolyte is used in the vast majority of the research performed worldwide. Some works introduce variations to the traditional recipe with positive effects. For example, the use of

lithium bis(fluorosulfonyl imide) (LiFSI) as a single or dual-salt has been demonstrated to contribute to the formation of a high quality SEI layer, and thus, to obtain an improved protection of Li^0 .^{92,93}

Replacing conventional electrolytes by ionic liquid is another appealing strategy to improve LSB performance. Room temperature ionic liquid electrolytes, *e.g.*, N-methyl-N-propylpiperidinium bis(trifluoromethanesulfonyl) imide, have been associated to current collector corrosion inhibitors, high quality SEI precursor in Li^0 based batteries, as well as LiPS solubility diminishers.^{94,95}

Regarding additives, as mentioned in section 1.4.1, LiNO_3 is the most common electrolyte additive for LSBs, especially due to its ability to protect Li^0 . However, the layers generated by LiNO_3 are believed to grow indefinitely with the continuous consumption of the additive.⁹⁶ Jia *et al.*⁹⁷ proposed the use of KNO_3 to exploit the synergetic effect of K^+ and NO_3^- . While the NO_3^- can generate the abovementioned layer, K^+ , with a more positive reduction potential than Li/Li^+ will be deposited in its metallic form on the growing Li^0 , slowing down the growth of dendrites. Other additives have also been proven to form a suitable SEI on Li^0 allowing a stable LSB cycling, such as, P_2S_5 ,⁹⁸ controlled trace amounts of water,⁹⁹ LiI ⁷⁹, or biphenyl-4,4'-dithiol.¹⁰⁰

In comparison to the SEI layer on Li^0 anode, there has been much less research on positive electrode film-forming electrolyte additives. However, the fundamental challenges originating from the cathode in LSBs are of great importance and deserve more attention. Regarding protection of the positive electrode, for example, the recently mentioned LiI additive reported by Wu *et al.*,⁷⁹ created a smooth and uniform protective coating of polymer like films on the surface of cathode particles, after the induced polymerization of DME.

Redox mediators, whose aim is to improve the utilization of active materials and the kinetics of the systems, are another kind of electrolyte additives. Redox mediators are reversible redox couples that experience an oxidation/reduction process at the electrode surface and diffuse later to the active material, promoting its redox activity. Most of the redox mediations in LSBs aimed the enhancement of Li_2S utilization. For example Aurbach *et al.*¹⁰¹ demonstrated the tremendous impact of the addition of various metallocenes and LiI on the promotion of Li_2S oxidation to higher order LiPS species.

Other electrolyte additives for LSBs aim to limit self-discharge,¹⁰² act as flame retardants,¹⁰³ or act as hydrofluoric acid scavengers to enable the use of LiPF_6 salt.¹⁰⁴ However, a more detailed discussion of electrolyte additives for LSBs, along with additives for Li-IC and Li-air batteries were included in our review publication.¹⁰⁵

From the previous analysis it can be concluded that LSBs are complex electrochemical devices that need adequate strategies to overcome their inherent

challenges. **Figure 1.11** summarizes the different mentioned strategies and the corresponding challenges they allow to overcome. This figure gives an idea of the complexity of LSBs and of the transversality of the applied strategies. For example, certain strategies that can confine LiPSs in the positive electrode, will help to enhance the negative electrode stability by avoiding its poisoning.

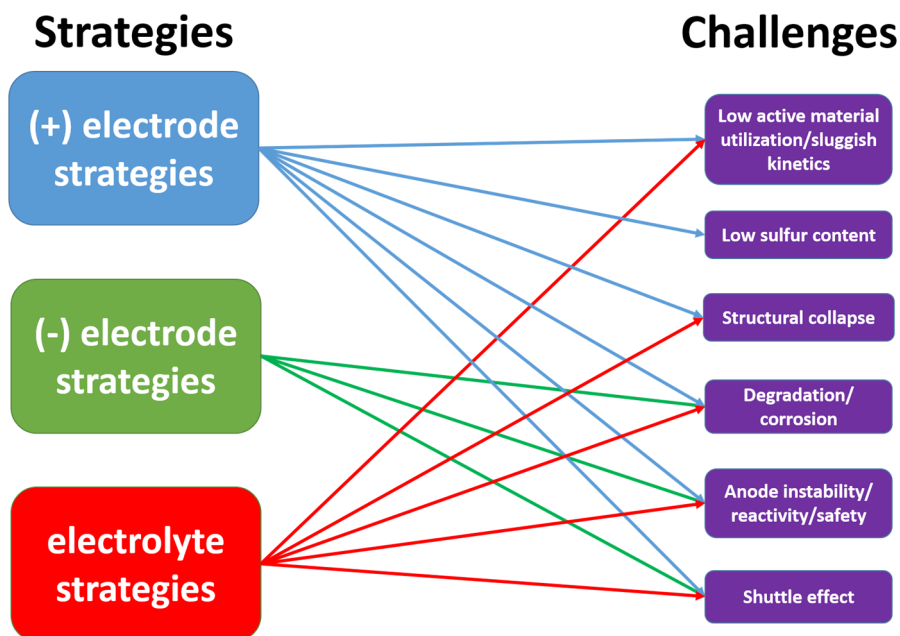


Figure 1.11. Different possible strategies in each cell compartment and the corresponding challenges that could be overcome.

At this point, the replacement of liquid electrolytes by solid-state electrolytes emerges as a promising alternative, which could address simultaneously the most challenging limitations of LSBs, with a special focus on safety and diminished LiPS solubility. Furthermore, a recent work by Offer *et al.*¹⁰⁶ synthesized the challenges faced by the LSBs technology and the activities pursued by the research community to solve them. It was shown that the research community mostly focused on the positive electrode development (**Figure 1.12**), while a balanced and multidisciplinary combination of approaches is highly required. These authors pointed out some research areas that are being understudied but are key or the development of LSB technology. Among others, polymer/solid state electrolyte or negative electrode coating/SEI (strictly related to electrolyte) were highlighted. Therefore, the study of all-solid-state electrolytes for LSBs is not only a promising approach, but a niche topic with plenty of room for development.

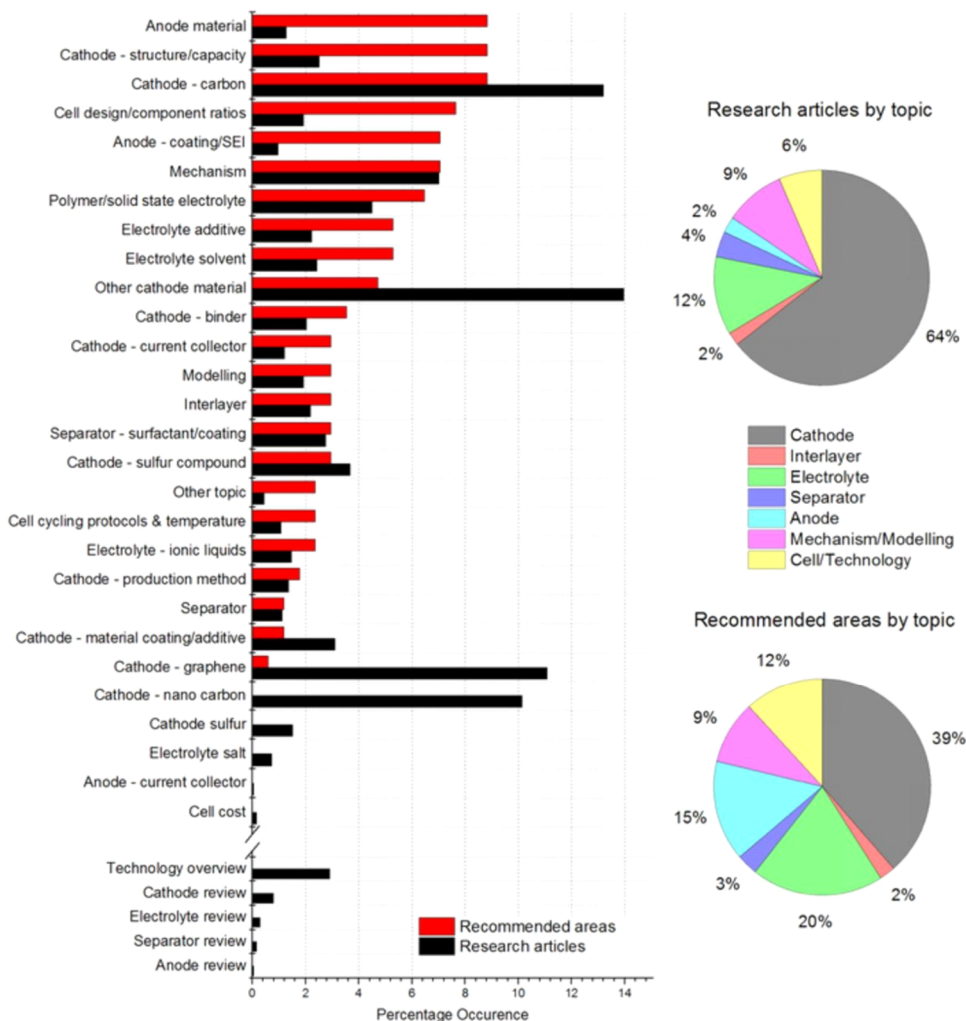


Figure 1.12. Comparison of the topics addressed in research articles vs. the recommended topic split that has been suggested in related review articles. Reproduced from ref. 106 with permission. Copyright 2019 The Electrochemical Society.

Hence, the following point will present an overview of properties and the current status of all-solid-state electrolytes for LSBs, in order to identify the most common configurations, parameters, limitations and possible areas of improvement.

1.4.4 Solid-state Li-S batteries

Organic solvents used in conventional liquid electrolytes are highly flammable and its pairing with Li^0 may arise safety concerns. To replace these battery components, solid-state Li^+ conductors, *i.e.*, solid electrolytes, have emerged as promising alternatives, enabling the development of safe all-solid-state lithium-sulfur batteries (ASSLSBs). Solid electrolytes enable the building up of intrinsically safer and more environmentally friendly batteries, due to the elimination of volatile organic solvents, their relatively high Li^0 -compatibility, and dendrite suppression. Specifically in ASSLSBs, solid electrolytes offer lower LiPS solubility or even total impermeability, which hinders or completely eliminates their diffusion and, thus, the shuttle effect. Solid electrolytes can be divided into three groups: inorganic solid electrolytes (ISE), solid polymer electrolytes (SPE), and solid composite electrolytes (SCE), the combination of the previous two. In the following points, ASSLSBs with these three different type of electrolyte will be discussed in detail.

1.4.4.1 Inorganic solid electrolytes

Faraday, Hittorf, and Gaugain found in the 19th century some inorganic solid materials with an abnormal enhancement of electrical conductivity with temperature that could not be interpreted as arising in electronic conductivity, which was later ascribed to a yet unknown ionic conductivity. The late 19th and initial 20th centuries brought the discovery and mechanistic understanding of some inorganic electrolytes such as ZrO_2 by Nernst and Schottky, or several other electrolytes suitable for fuel cells by Baur and Priess. At the end of 1960s, some novel inorganic solid electrolytes were obtained via innovative synthesis strategies and attracted much attention due to their high ionic conductivity and potential application in batteries.¹⁰⁷

To date, several kinds of inorganic materials have been proposed as potential candidates for Li^0 based batteries, *e.g.*, garnets, sulfides, Li-adapted sodium superionic conductors, Li superionic conductors, *etc.*^{108,109} ISE electrolytes, either glassy or crystalline ceramic materials, possess high Li^+ conductivity at room temperature (RT) and Li^+ transference number (t_{Li^+} , selectivity to Li^+) close to 1.¹¹⁰ Bulk conductivity values comparable with liquid electrolytes (LEs) have been already reported for ISE. For example, Kamaya *et al.*¹¹¹ reported a $\text{Li}_{10}\text{GeP}_2\text{S}_{12}$ LISICON-type crystalline sulfide electrolyte with a conductivity of $1.2 \times 10^{-2} \text{ S cm}^{-1}$ at RT. However, their inherent rigidity and fragility, a poor solid-solid interfacial contact between ISE and electrodes and difficulty for large scale processability still hinders its large-scale application. Moreover, ISEs possess more dense structures compared to LEs, and while the density of a DME-DOL based electrolyte is around 1.13 g cm^{-3} , the density of ceramic may vary from 1.90

g cm^{-3} in $\text{Li}_2\text{S-P}_2\text{S}_5$ glassy electrolyte,¹¹² or 2.92 for $\text{Li}_{1+x}\text{Ti}_{2-x}\text{Al}_x(\text{PO}_4)_3$ (LATP),¹¹³ to values as high as 5.15 for $\text{Li}_{6.55}\text{Ga}_{0.15}\text{La}_3\text{Zr}_2\text{O}_{12}$ for garnet materials.¹¹⁴ This, along with the difficulty to prepare thin ceramic layer with competitive thickness of few tens of microns, generates an exaggerated weight contribution of the ceramic electrolyte, penalizing overall energy density of the cell.

Regarding LSBs, ISE can mitigate the dendrite growth due to their high mechanical modulus and present negligible LiPS solubility. Several works have already proven the suitability of some ISE as LiPS impermeable layers interlayers, such as LATP,¹¹⁵ or $\text{Li}_{1+x}\text{Ge}_{2-x}\text{Al}_x(\text{PO}_4)_3$ (LAGP)¹¹⁶ materials. However, $\text{Li}_2\text{S-P}_2\text{S}_5$ combined glassy sulfide electrolyte is the most common choice in ISE-based ASSLSBs, due to its good compatibility, high conductivity, and decent electrode/electrolyte contact at RT.

1.4.4.2 Solid Polymer electrolytes

The discovery of solid polymer electrolytes (SPEs) dates back four decades ago when Wright *et al.*^{117,118} reported the conductivity in complexes formed by NaI and NaSCN salts and PEO. In 1979, Prof. Armand *et al.*¹¹⁹ proposed the application of SPEs for the development of all-solid-state Li-IC batteries.

SPEs presents appealing properties such as low cost, inherent safety, easy processing and manipulation, and flexibility. However their main limitation is their low conductivity, and acceptable conductivity values ($> 10^{-4} \text{ S cm}^{-1}$) have not yet been achieved at RT. In these Li^+ conducting electrolytes, lithium salts with low dissociation energy are dissolved in high molecular weight polymer matrices containing high concentration of Lewis base groups such as ether ($-\text{O}-$), carbonyl ($-\text{C}=\text{O}$) and cyano ($-\text{C}\equiv\text{N}$), and thus, high donor number, which serve as ligands for coordinating Li^+ of the dissolved salt.

Among all the investigated polymer materials for SPE, polyethylene oxide (PEO) has received special attention and extensive research due to its easy fabrication, low cost, good mechanical properties, electrochemical stability, high chain flexibility and its high solvation power.^{120,121} PEO has properly spaced ether solvating units which confers high solvation ability and allow the formation of favored Li salt/PEO complex, providing sufficient concentration of Li^+ . It also presents high chain flexibility, allowing rapid ion transport.¹²² However, the main drawback of PEO-based SPEs is its low ionic conductivity at RT ($< 10^{-5} \text{ S cm}^{-1}$) caused by the semi-crystalline nature of PEO matrix below its melting point (65°C).

Regarding LSBs, SPE electrolytes can offer good electrochemical stability against Li^0 and diminished dendrite formation, while offering a limited LiPS solubility. Therefore, the use of SPEs is an attractive, safe, easy and low cost solution to face most critical limitations of this technology.

In order to study the viability of the use of all-solid-state electrolytes in LSBs in terms of energy density of the cell, a model developed by Dr. Otaegui was adapted by our colleague Dr. Li in 2016.¹²³ The calculations showed for the first time that i) the cells based on thin solid electrolyte can feature improved gravimetric energy densities in comparison with liquid electrolyte based ones, and that ii) the high density of the ISEs may penalize energy density values, but the use of lightweight SPEs may allow to reach unprecedented gravimetric energy density values.

1.4.4.3 Solid composite electrolytes

In response to the intrinsic limitations of pure SPE and ISE, their combination, *i.e.*, solid composite electrolytes (SCEs), are becoming an increasingly appealing choice for the development of all-solid-state batteries. A composite electrolyte consists of the mixture of an inert (inactive, no Li^+ conductive) or Li^+ conducting inorganic ceramic (active, Li^+ conductive), and an organic polymer matrix. This configuration can take advantage of the synergetic effect either of high ionic conductivity at low temperatures from inorganic phase; and interfacial properties, improved mechanical stability, and good interfacial contact inherited from the organic matrix. The improved conductivity can be derived from ceramic phase when it is active, or from interfacial interactions between the fillers and the polymer when inactive, such as increased chain mobility, or lowered polymer crystallinity.

Since the first study published by Weston and Steele¹²⁴ in 1982 focusing on the effect in the conductivity of different Al_2O_3 amounts in a PEO matrix, many efforts have been devoted towards the development of composite electrolytes. The mechanism behind the conductivity improvement in inactive filler composite electrolytes compared to that of pure polymer electrolytes has not yet been completely understood, but it is usually attributed to different phenomena, occurring simultaneously. One suggested mechanism is that ceramic fillers act as plasticizers, preventing polymer chain reorganization, decreasing crystallinity and enhancing Li^+ mobility through the amorphous phases.^{125,126} In the case of composite electrolytes with fillers having high dielectric constants and Lewis base surface groups, interactions between filler and polymer polar groups will increase electrolyte salt dissociation, which will in turn increase the availability of free Li^+ in the electrolyte, ultimately leading to an increased t_{Li^+} and ionic conductivity.^{127,128} For active fillers, a proposed mechanism is that Li^+ will hop in a sequential manner replacing nearby vacancies generated in highly conductive and uninterrupted ion pathways in interface layers between polymer and ceramic particles.^{127,129}

A more detailed study for composite electrolytes can be found in a specific book chapter devoted to solid electrolytes for future Li-IC batteries written by our group.¹³⁰

1.4.4.4 State of Art study in all-solid-state Li-S batteries

This section presents an in-depth State of Art study ASSLSBs with the aim of identifying common parameters and main weaknesses and strengths of actual systems. **Table 1.4** summarizes the most remarkable publications in ASSLSBs within the different abovementioned electrolyte families, along with detailed information about electrode composition, electrolyte formulation, performance, *etc.* It also presents some representative liquid electrolyte-based LSB research results for comparison.

It is noticeable that the initial articles in LSBs never reported areal active material loading, but the most recent ones do. This is related to the fact that LSBs research is advancing towards real application research. For the study of the performance of an active material it is important to mention the material performance per mass unit, *i.e.*, gravimetric capacity (mAh g^{-1}), but also the content of material per surface unit (g cm^{-2}). This will allow the complete study of the material, combining how it behaves and how much material there is, based on areal capacity (mAh cm^{-2} , the product of the combination of the previous two terms).

Table 1.4. State of Art of Li-S cells with various types of electrolytes from literature. The list of references is included in the section 1 in the Appendix.

Positive electrode		Negative electrode	Electrolyte		Cycle performance			Reference	
Composition / wt.%	S loading / mg cm ⁻²		Composition, wt.%	σ / mS cm ⁻¹	Discharge capacity / mAh g _{Sulfur} ^{-1*}	T / °C	Rate	Year	Ref.
Inorganic solid electrolyte									
S@Cu (38) / AB (5) / SE (57). AM: 23	N/A	Li/In	80Li ₂ S-20P ₂ S ₅	5 (25 °C)	660 (1 st) vs. 650 (20 th); CuS	25	64 μ A cm ⁻²	2003	S1
S (27) / Cu (21.4) / AB (1.6) / SE (50)	N/A	Li _{4,4} Ge	60Li ₂ S-40SiS ₂	0.2 (25 °C)	1000 (1 st) vs. 1100 (5 th)	25	64 μ A cm ⁻²	2004	S2
Li ₂ S@Cu (38) / AB (5) / SE (57). AM: 18	N/A	In	80Li ₂ S-20P ₂ S ₅	5 (25 °C)	500 (1 st) vs. 340 (20 th); based on Cu-Li ₂ S	25	64 μ A cm ⁻²	2008	S3
S (25) / AB (25) / SE (50)	N/A	Li _{0,61} Al	Li _{3,25} Ge _{0,25} P _{0,7} ₅ S ₄	2.2 (25 °C)	1500 (1 st) vs. 900 (10 th)	25	13 μ A cm ⁻²	2008	S4
Li ₂ S (15) / AB (15) / SE (70)	≈ 5	In	0.01Li ₃ PO ₄ -0.63Li ₂ S-0.36SiS ₂	1.5 (30 °C)	900 (1 st) vs. 750 (20 th); Li ₂ S	30	0.01C	2010	S5
S (25) / AB (25) / SE (50)	N/A	Li/In	80Li ₂ S-20P ₂ S ₅	5 (25 °C)	1200 (1 st) vs. 996 (200 th)	25	64 μ A cm ⁻²	2011	S6
Li ₃ PS ₉ (60) / C (30) / PVC (10)	0.15-0.36	Li/Ni	Li ₃ PS ₄	0.1 (60 °C)	1400 (1 st) vs. 1200 (300 th); S	60	15 μ A cm ⁻²	2013	S7
S (15) / MC (35) / SE (50). AM: N/A	N/A	Li _{0,61} Al	Li _{3,25} Ge _{0,25} P _{0,7} ₅ S ₄	2.2 (25 °C)	1600 (1 st) vs. 700 (30 th)	25	13 μ A cm ⁻²	2013	S8
S (50) / KB (10) / SE (40)	N/A	Li _{0,79} In	60Li ₂ S-40P ₂ S ₅	0.02 (25 °C)	1300 (1 st) vs. 1300 (50 th)	25	1.3 mA cm ⁻²	2014	S9
S@KB@Maxso rb (50) / SE (50)	≈3	Li	LiBH ₄	N.A.	1140 (1 st) vs. 730 (45 th)	120	0.05C	2014	S10
S (30) / CNF (10) / SE (60)	0.75	Li	75Li ₂ S-25P ₂ S ₅	0.1 (30 °C)	1600 (1 st) vs. 1400 (10 th)	30	0.05C	2015	S11
Li ₂ S(36)/ C (18) / Li ₆ PS ₅ Cl (6)/ 80Li ₂ S-20P ₂ S ₅ (40).	3.6	Li-In	80Li ₂ S-20P ₂ S ₅	1.3 (25 °C)	≈800 (1 st) vs. 830 (60 th), Li ₂ S	25	0.03C	2016	S12
rGO@S (30) + AB (20)+ Li ₁₀ GeP ₂ S ₁₂ (50). AM: 11-14	0.4-0.5	Li	Li ₁₀ GeP ₂ S ₁₂ // 75 Li ₂ S-24 P ₂ S ₅ -1 P ₂ O ₅	N.A.	900 (1 st) vs. 830 (750 th).	60	1C	2017	S13
S@CR (30) / SE (70). AM: 9	0.57	Li-In	Li _{10,05} Ge _{1,05} P _{1,95} S ₁₂	1 (25 °C)	1500 (1 st) vs. 1500 (50 th).	25	0.5C	2018	S14
S@CNT (N/A) / MC (N/A) / SE (60). AM: 25	1.1	Li-In	78Li ₂ S-22P ₂ S ₅	1 (25 °C)	1140 (1 st) vs. 1140 (400 th).	25	0.1C	2018	S15
Li ₂ S (30) / SE (60) / VGCF (10)	N/A	In	70Li ₂ S-30P ₂ S ₅ + 2 Ni ₂ P	2.2 (25 °C)	429 (1 st) vs. 454 (20 th).	25	64 μ A cm ⁻²	2018	S16

FeS ₂ (30) / S (30) / C (40)	1-5	Li	LiI-Pi ₃ PS ₄	1 (25 °C)	1200 (5 th) vs. 1200 (20 th) [1 mg cm ⁻²], FeS ₂ +S	20	0.05C	2018	S17
SeS ₂ (40) / Li ₃ PS ₄ (40) / AB (20)	1.6 - 15	Li	Li _{10.05} Ge _{1.05} P _{0.1} . ₉₅ S ₁₂ - Li ₃ PS ₄	0.2 (25 °C)	1000 (1 st) vs. 1000 (50 th) [1.6 mg cm ⁻²]	60	0.25C	2019	S18
Solid polymer electrolytes									
S (50) / C (16) / SE (34)	N/A	Li	PEO / LiTFSI	0.5 (90 °C)	722 (1 st) vs. 70 (20 th)	90	0.1 mA cm ⁻²	2000	S19
S (50) / AB (15) / SE (35)	N/A	Li	PEO / LiTf	0.08 (90 °C)	1200 (1 st) vs. 200 (10 th)	90	C/17	2002	S20
S (50) / AB (30) / SE (20)	N/A	Li	PEO / LiTf	N/A	1484 (1 st) vs. 800 (10 th)	90	0.125 mA cm ⁻²	2004	S21
S (N/A) / C (N/A) / PEO (N/A)	N/A	Li	PEO / LiBF ₄	0.05 (80 °C)	1200 (1 st) vs. 250 (10 th)	80	70 μA cm ⁻²	2007	S22
CMK3@S (65) / SP (10) / SE (20) / PVdF (5). AM: 45	1	Li	PEO / LiTnFSI	0.1 (60 °C)	450 (6 th) vs. 450 (200 th)	60	0.2C	2016	S23
			PEO / LiTFSI	N/A	600 (6 th) vs. 300 (200 th)				
S@C@PANI (80) / CB (10) / SE (10). AM: 30	0.8	Li	PEO / LiTFSI	0.2 (60 °C)	1350 (6 th) vs. 600 (40 th)	100	0.3C	2017	S24
C@S (80) / AB (10) / PVDF (10). AM= 52	0.6-1	Li	PEO / LiClO ₄	≈ 0.48 (60 °C)	600 (1 st) vs. 600 (30 th).	60	0.1C	2018	S25
Composite polymer electrolyte									
S (50) / AB (15) / SE (35)	N/A	Li	PEO / LiTf + 15 Ti _n O _{2n+1}	0.1 (90 °C)	1675 (1 st) vs. 500 (10 th)	90	C/17	2002	S20
S@PEO (80) / AB (10) / PVDF (10). AM= 24	N/A	Li	PEO / LiTFSI + 10 γ-LiAlO ₂	N.A.	452 (1 st) vs. 184 (50 th); electrode,	75	0.1 mA cm ⁻²	2005	S26
S (N/A) / AB (N/A) / PEO (N/A)	N. A.	Li	PEO / LiBF ₄ + 10 Al ₂ O ₃	0.3 (80 °C)	1600 (1 st) vs. 40 (10 th)	80	70 μA cm ⁻²	2007	S22
S@C (80) / SP (10) / PVdF (10). AM= 40	N/A	Li	PEO / LiTf + 10 S-ZrO ₂ + Li ₂ S	0.1 (70 °C)	900 (1 st)	90	0.018C	2010	S27
			PEO / LiTf + 10 S-ZrO ₂ + Li ₂ S	0.1 (70 °C)	450 (4 th) vs. 450 (50 th), Li ₂ S	70			
S@OMC (60) / AB (20) / PEO (20). AM= 40	N/A	Li	PEO / LiTFSI + 10 SiO ₂	0.5 (70 °C)	1266 (1 st) vs. 823 (25 th)	70	0.1 mA cm ⁻²	2011	S28
S@C@PANI (80) / CB (10) /	0.8	Li	PEO / LiTFSI + 6.5 MIL-53(Al)	N.A.	640 (200 th) vs. 558 (1000 th)	60	0.5C	2015	S29

SE (10). AM=34										
S@C@PANI (80) / CB (10) / SE (10). AM=30	0.8	Li	PEO / LiTFSI + 10 HNT	1.34 (60 °C)	800 (1 st), 745 (100 th)	25	0.1C	2017	S24	
S (60) / SP (30) / PAA (10)	0.7	Li	PEO / LiTFSI + 10 MIL-53(Al) + carbón interlayer	0.6 (80 °C)	1450 (1 st) vs. 792 (50 th);	80	0.5C	2017	S30	
S@Li ₇ La ₃ Zr ₂ O ₁₃ @C (80) / CB (10) / SE(10). AM= 61-64	0.6	Li	PEO / LiClO ₄ + 18.6 vl.% Li ₇ La ₃ Zr ₂ O ₁₃	0.1 (40 °C)	900 (1 st) vs. 900 (200 th).	37	0.1 mA cm ⁻²	2017	S31	
C@S (80) / AB (10) / PVDF (10). AM= 52	0.6-1	Li	PEO / LiClO ₄ ALD Al ₂ O ₃ on LATP PEO / LiClO ₄	≈ 0.7 (60 °C)	1035 (1 st) vs. 823 (100 th).	60	0.1C	2018	S25	
S@CNF / PEO + LiTFSI. AM=N/A	1.27	Li	PEO + Li _{0.33} La _{0.557} TiO ₃	0.23 (25 °C)	390 (1 st) vs. 415 (50 th).	RT	0.05C	2019	S32	

Representative liquid electrolytes

S@NG (92) / PVdF (8). AM=60	0.8	Li	1 M LiTFSI in DME/DOL + 1 LiNO ₃ + 0.2 M Li ₂ S ₈	N/A	802 (1 st) vs. 350 (2000 th)	25	2C	2014	S33
S@HCS (80) / MWCNT (10) / PTFE (10). AM= 53	1.6-1.8	Si-C	1 M LiTFSI in DME/DOL + 0.25 M LiNO ₃	N/A	765 (1 st) vs. 400 (1400 th)		0.5C	2014	S34
P(S-DVB) (60) / CB (30) / PEO (10). AM= 48	2	Li	1 M LiTFSI in DME/DOL + 2 wt.% LiNO ₃	N/A	1000 (1 st) vs. 700 (500 th)	25	0.25C	2016	S35
S@GA@PPY. AM=73	6	Li	1 M LiTFSI in DME/DOL + 0.1 M LiNO ₃	N/A	986 (1 st) vs. 687 (100 th)	N/A	0.5C	2016	S36
S@Fe ₂ O ₃ (80) / CB (10) / PTFE (10). AM= 48	1	Li	1 M LiTFSI in DME/DOL + 0.5 LiNO ₃	N/A	600 (1 st) vs. 400 (1000 th)	25	5C	2017	S37
Li ₂ S@Ni-P-S@GC (60) / CB (20) / PVdF (20). AM=36	5.2	Li	1 M LiTFSI in DME/DOL + 0.1 M LiNO ₃	N/A	700 (1 st) vs. 600 (300 th)	25	0.5C	2017	S38
S@GO@PAM AM (80) / CB (15) / PVdF (10). AM= 61	2	Li	1 M LiTFSI in DME/DOL + 2 wt.% LiNO ₃	N/A	727 (1 st) vs. 698 (500 th)	25	1C	2017	S39
S@N-GO/CNT@SPA NI (60) / CB (30) / PTFE (10). AM= 46.5	1-1.6	Li	1 M LiTFSI in DME/DOL + 0.3 M LiNO ₃	N/A	680 (1 st) vs. 483 (450 th)	25	4.5C	2017	S40
S@G (80) / MWCNT (10) / PVdF (10). AM=N/A	3.1	Li	1 M LiTFSI in DME/DOL + 2 wt.% LiNO ₃	N/A	650 (1 st) vs. 503 (2000 th)	RT	1C	2017	S41

S@G@HPC. AM= 67	3.6	Li	1 M LiTFSI in DME/DOL + 0.1 M LiNO ₃	N/A	793 (1 st) vs. 694 (2000 th)	N/A	0.5C	2017	S42
S@PRC@Ni (80) / CB (10) / PVdF (10). AM= 64	2	Li	1 M LiTFSI in DME/DOL + 1 wt.% LiNO ₃	N/A	1257 (1 st) vs. 851 (500 th)	N/A	0.2	2018	S43

*Discharge capacities referred to sulfur mass, unless specified

^a The abbreviations are listed as below: AB (acetylene black), ALD (atomic layer deposition), AM (active material), C (carbon), CB (carbon black), CMK-3 (CMK-3 carbon), CNF (carbon nanofiber), CNT (carbon nanotubes), CR (carbon replica), DEC (diethylene carbonate), DMC (dimethyl carbonate), EC (ethylene carbonate), G (graphene), GA (graphene aerogel), GC (graphene cage), HCS (hollow carbon spheres), HNT (halloysite nanotube), HPC (hierarchical porous carbon), KB (ketjen black), LiTf (lithium trifluoromethanesulfonate), LiTFSI (lithium bis(trifluorosulfonyl) imide), LiTNFSI (lithium (trifluoromethanesulfonyl) (n-nonafluorobutanesulfonyl) imide), MC (mesoporous carbon), MIL-53(Al) (metal-organic framework), MWCNT (multi-walled carbon nanotubes), N-CA (nitrogen-doped carbyne), Ni-P-S (nickel phosphosulfides), NG (nitrogen-doped graphene), N-GO/CNT (functionalized graphene oxide carbon nanotubes framework), OMC (ordered mesoporous carbon), PAA (polyacrylic acid), PANI (polyaniline), PAMAM (poly(amidoamine)), PEO (poly(ethylene oxide)), PPY (polypyrrole), PRC (puffed rice derived carbon), P(S-DVB) (poly (sulfur divinylbenzene)), PTFE (polytetrafluoroethylene), PVC (poly(vinyl chloride)), PVDF (polyvilydene fluoride), rGO (reduced graphene oxide), S (sulfur) / SE (solid electrolyte), SP (super P), SPANI (sulfonated polyaniline) , UMC (ultra-microporous carbon), VGCF (vapor grown carbon fiber).

Several conclusions can be drawn from the state of art revision. Regarding ISE, sulfide based electrolytes, *i.e.*, $(\text{Li}_2\text{S})_x\text{-(P}_2\text{S}_5)_y$ or similar, are the most common choice due to their good compatibility with LiPSs, high conductivity at RT, low density, relatively high ductility and possibility for cold-pressing preparation route. However, due to the difficulty to obtain thin electrolytes, most of the studies still report excessive electrolyte thicknesses, up to 1000 μm . Thus, these ISE-based ASSLSBs usually present poor rate capabilities and high overpotential between the charge and discharge, derived from high resistance of the electrolyte. The discharge/charge profile of LSBs with ISEs is quite different from the ones with LEs. The exact sulfur reduction reaction mechanism in ISEs still remains unclear. It is ambiguous if the absence of common upper-plateau, sloping region and low plateau regions is due to the direct S_8 to Li_2S solid-solid conversion or due to the high internal resistance of the cell. It is also remarkable that in order to improve cell stability, many studies substitute pure Li^0 negative electrodes by alloys, such as Li-In or Li-Al, which decreases the overall cell voltage.

Regarding SPE, only PEO-based electrolytes show acceptable results amid tested materials. It must be pointed out that apart from the work presented by Zhou *et al.*¹³¹ in 2016, in which they implemented a novel salt, the cyclability of the cells was limited. Some of the studies report at the same time the addition of active or inactive fillers to achieve improved performance. The main drawback of PEO-based electrolytes is the low conductivity at RT and the requirement to cycle the cells above the melting point of the electrolyte, usually 60-70 $^\circ\text{C}$. SCE-based ASSLSBs, on the contrary, show improved performance due to the influence of the ceramic particles. Even if most of the works still need to cycle at temperatures above the melting point of PEO, some recent research reports that the presence of the filler can improve electrolyte conductivity and enables cell cycling at lower temperature.

Figure 1.13 shows an analysis of key parameters for the different electrolyte families. **Figure 1.13a** shows active material percentage in the positive electrode for different electrolyte systems. In general, ASSLSBs yet report lower active material percentage than their liquid counterparts. In contrast to LE-based cells, where Li^+ transport to the sulfur particles is ensured by the wetting DME/DOL electrolyte, a considerable fraction of solid electrolyte needs to be included in positive electrode formulation to ensure Li^+ transport pathway. This electrolyte, often called catholyte, also acts as a binder in the positive electrodes of SPE-based and CPE-based solid-state-batteries. In ISE-based solid-state-batteries electrolyte is usually pressed along with other electrode component, generating a self-standing electrode.

Furthermore, **Figure 1.13b** shows that while LE based cells present active material loadings in the range of 1.5–6 mg cm^{-2} , solid electrolyte cells rarely report values

higher than 1.5 mg cm^{-2} (except for some very recent ISE-based works). This limitation can be ascribed to the challenging solid-solid contact of sulfur and other electrode components, *i.e.*, conductive carbon and catholyte. Therefore, it is usually necessary to increase a considerable amount of conductive carbon and catholyte to ensure a reasonable e^- conductivity, which leads to reduced active material content.

Figure 1.13c and **d** display the initial discharge capacity in gravimetric and areal terms (when available) for different electrolyte families. Initial gravimetric capacities of the cells based on all-solid-state electrolyte family show comparable value compared to LE. However, in terms of areal discharge capacities, only ISE can compete with the value of LE-based cells.

Moreover, ASSLSBs yet show shorter lifespan and rarely report over 150 cycles (**Figure 1.13e** and **f**, end of life capacity *vs.* cycle). This could be ascribed to the more challenging intrinsic mechanisms. In the absence of liquid electrolyte, the proper solubility of the reaction intermediates and the necessary Li^+ conduction through positive electrode to the surface of electroactive materials is hindered. These results demonstrate that the performance of ASSLSBs is not satisfactory yet, but there is still large opportunities for disruptive advances in the field.

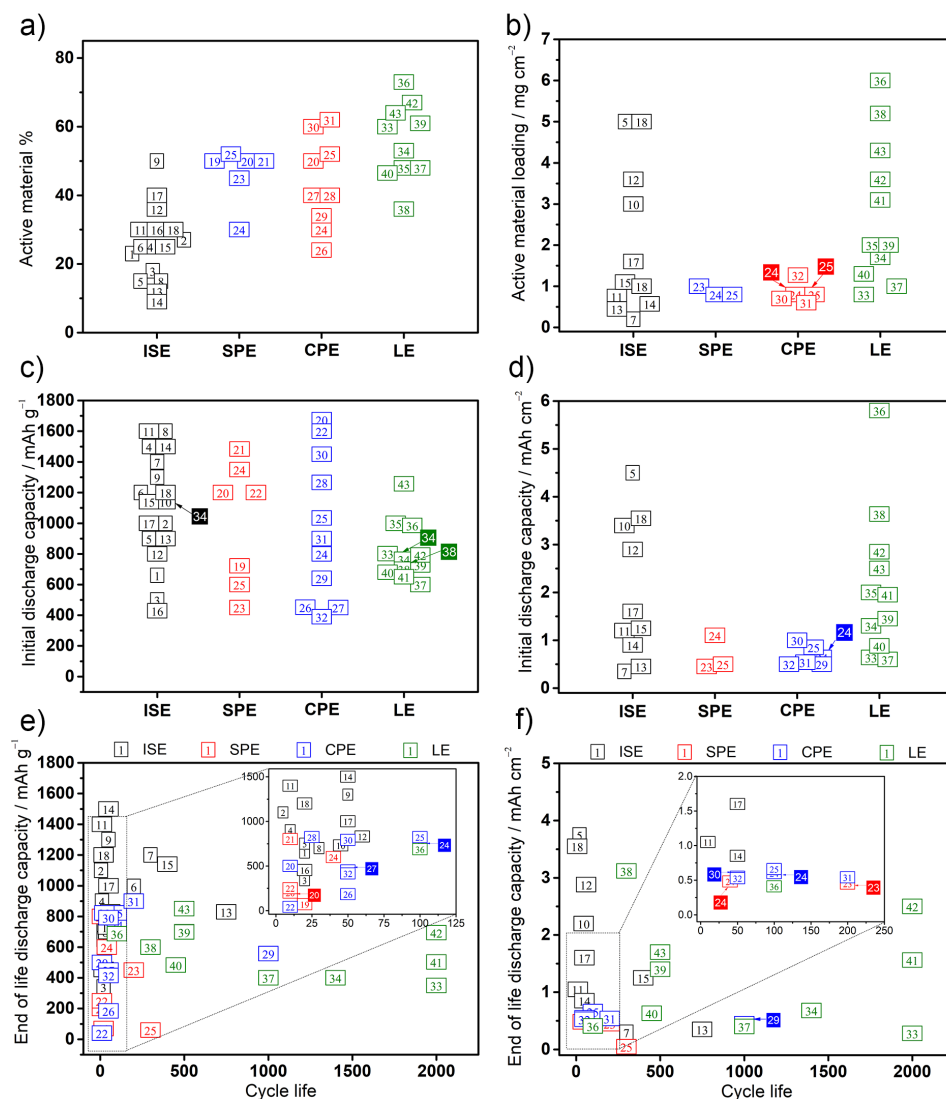


Figure 1.13. Study of different cell parameters with various kinds of electrolytes. a) Active material content in the positive electrode vs. type of electrolyte; b) active material loading in the positive electrode vs. type of electrolyte; initial discharge capacity vs. electrolyte in c) gravimetric terms and d) areal terms; end of life discharge capacity vs. cycle life for different kind of electrolytes in e) gravimetric terms and f) areal terms. Numbers refer to references in State of Art study.

1.5 IDENTIFIED POTENTIAL RESEARCH AREAS

The development of more efficient and competitive batteries is crucial for a complete transition to more sustainable energy models. Among different “beyond Li-ion” batteries, LSBs are one of the most attractive alternatives, especially for applications where high gravimetric energy density is crucial and working rates are moderate, such as high altitude pseudo-satellites. Even if some knowledge gained in decades of development of LIBs can be transferred to the development of LSBs, the different chemical environment often requires seeking for specific cell components, such as the replacement of conventional electrolytes and salts, or the use of additives.

LSBs have remarkable benefits compared to LIBs, such as the suppression of heavy-metals and the use of low cost S_8 , or the achievable high gravimetric energy density, but also present several challenges due their complex and multistep chemistry.

The use of solid electrolytes can simultaneously help to face several challenges of LSBs, such as the shuttle effect, dendrite growth, and the stability of the metallic negative electrode; while can also help to increase achievable energy density values. However, it is still a quite unexplored topic. Furthermore, previous calculations show that by using solid electrolytes, especially lightweight SPEs, high gravimetric energy density values can be achieved. The work to be done in this field is broad and several opportunities for breakthroughs and disruptive advances are envisaged.

1.6 OBJECTIVES OF THE THESIS

Accordingly, this thesis will focus in the development of SPE-based ASSLSBs. At the beginning of this Thesis, the research activity in SPEs for ASSLSBs was scarce and incipient. Therefore, looking at the potential advantages in achievable performance, the main focus of this work is the exploration of SPE systems that will significantly improve LSB performance in terms of energy density and lifetime.

The exploratory character of this work aims at achieving breakthroughs in performance and for that reason, several approaches are attempted, always focused on lightweight SPE and a basic positive electrode. This is done for achieving real appreciation of negative electrode/electrolyte operation. The main objective is to find materials combinations that produce significant improvements with respect the existing State of Art and provide a potential viable solution for ASSLSBs. For that purpose, the following points are identified as the main concrete objectives in the development of this work:

- Adaptation of the above-mentioned energy density calculation model to a more

realistic and updated properties to determine the viability of ASSLBs. This model will allow to identify viable cell parameters and targeted performance required for achieving competitive systems.

- The development of the reference system based on commercial materials to understand fabrication issues and set the grounds of this work. In this particular case, PEO-based SPE electrolyte is chosen as the most common material. The performance of this reference is still far from satisfactory, so the failure mechanisms need to be identified and depicted in detail in order to design appropriate realistic strategies to overcome these limitations and increase the lifespan of the cell. This work allowed the identification of electrolyte components as key factors that affect lifetime and performance of the battery. Among these components, additives, salts and fillers were identified as niche areas for breakthrough research to obtain quantitative advances in overall cell performance.
- The study of additives in the electrolyte for stabilizing cell performance. For that purpose, state-of-art LiNO_3 and novel LiN_3 were included in the electrolyte recipe and their effect is analyzed in detail.
- The study of Li^+ conductive glassy ceramic and aluminum oxide ceramic filler addition to the electrolyte and their effect in cell performance.
- The substitution of LiTFSI reference salt by alternative imide containing salts, *i.e.*, LiFSI and novel lithium (fluorosulfonyl)(trifluoromethanesulfonyl) imide salt, and the understanding of their effect on the cell performance.
- The substitution of LiTFSI salt by a fluorine-free alternative. Lithium tricyanomethanide (LiTCM) is studied and its role in the cell will be depicted, with special attention to its fluorine-free chemistry.
- The final objective will be the initial upscaling of the most promising electrolyte configuration from coin cell to pouch cell and the performance analysis including potential further improvements.

Therefore, the initial chapter will adapt the model developed by Dr. Otaegui and Dr. Li to study the viability of the proposed systems and allow to establish targeted parameters for competitive cell development. Later, the chapter will focus on the development of reference cell and the understanding of the cell failure mechanism. Once the problematics are defined, following chapters will focus on the use of alternative electrolyte options, including the use of novel additives, electrolyte fillers, alternative imide salts, and novel fluorine-free salts. Finally, all the results will be discussed and put into perspective in the general overview section.

1.7 REFERENCES

- (1) McGlade, C.; Ekins, P. The Geographical Distribution of Fossil Fuels Unused When Limiting Global Warming to 2°C. *Nature* **2015**, *517* (7533), 187–190.
- (2) Tarascon, J.-M.; Armand, M. Issues and Challenges Facing Rechargeable Lithium Batteries. *Nature* **2001**, *414* (6861), 359–367.
- (3) Bernstein, J. A.; Alexis, N.; Barnes, C.; Bernstein, I. L.; Bernstein, J. A.; Nel, A.; Peden, D.; Diaz-Sanchez, D.; Tarlo, S. M.; Williams, P. B. Health Effects of Air Pollution. *J. Allergy Clin. Immunol.* **2004**, *114* (5), 1116–1123.
- (4) Wagner, L.; Ross, I.; Foster, J.; Hankamer, B. Trading off Global Fuel Supply, CO₂ Emissions and Sustainable Development. *PLoS One* **2016**, *11* (3), 1–17.
- (5) Lund, H. Renewable Energy Strategies for Sustainable Development. *Energy* **2007**, *32* (6), 912–919.
- (6) Dunn, B.; Kamath, H.; Tarascon, J.-M. Electrical Energy Storage for the Grid: A Battery of Choices. *Science* (80-.). **2011**, *334* (6058), 928–935.
- (7) Pérez-Lombard, L.; Ortiz, J.; Pout, C. A Review on Buildings Energy Consumption Information. *Energy Build.* **2008**, *40* (3), 394–398.
- (8) U.S Energy Information Administration. Energy Use for Transportation https://www.eia.gov/energyexplained/?page=us_energy_transportation#tab1 (accessed Apr 16, 2019).
- (9) RS2E. Electrochemical energy storage: simple definition <https://www.energie-rs2e.com/en/articleblog/electrochemical-energy-storage-simple-definition> (accessed Apr 16, 2019).
- (10) Winter, M.; Brodd, R. J. What Are Batteries, Fuel Cells, and Supercapacitors? *Chem. Rev.* **2004**, *104* (10), 4245–4269.
- (11) Herrera, V.; Milo, A.; Gaztañaga, H.; Etxeberria-Otadui, I.; Villarreal, I.; Camblong, H. Adaptive Energy Management Strategy and Optimal Sizing Applied on a Battery-Supercapacitor Based Tramway. *Appl. Energy* **2016**, *169*, 831–845.
- (12) Reddy, T. B.; Linden, D. *Linden's Handbook of Batteries*, 4th ed.; McGraw-Hill, 2011.
- (13) Muench, S.; Wild, A.; Friebe, C.; Häupler, B.; Janoschka, T.; Schubert, U. S. Polymer-Based Organic Batteries. *Chem. Rev.* **2016**, *116* (16), 9438–9484.
- (14) Armand, M.; Tarascon, J.-M. Building Better Batteries. *Nature* **2008**, *451* (7179), 652–657.
- (15) Palacín, M. R. Recent Advances in Rechargeable Battery Materials: A Chemist's Perspective. *Chem. Soc. Rev.* **2009**, *38* (9), 2565–2575.
- (16) Armand, M. Intercalation Electrodes. In *Materials for Advanced Batteries*; Springer US, 1980; pp 145–161.
- (17) Rozier, P.; Tarascon, J. M. Review—Li-Rich Layered Oxide Cathodes for Next-Generation Li-Ion Batteries: Chances and Challenges. *J. Electrochem. Soc.* **2015**, *162* (14), A2490–A2499.
- (18) Li, C.-S.; Sun, Y.; Gebert, F.; Chou, S.-L. Current Progress on Rechargeable Magnesium-Air Battery. *Adv. Energy Mater.* **2017**, *7* (24), 1700869.
- (19) Adelhelm, P.; Hartmann, P.; Bender, C. L.; Busche, M.; Eufinger, C.; Janek, J. From Lithium to Sodium: Cell Chemistry of Room Temperature Sodium–Air and Sodium–Sulfur Batteries. *Beilstein J. Nanotechnol.* **2015**, *6* (1), 1016–1055.

- (20) Chen, L.; Fiore, M.; Wang, J. E.; Ruffo, R.; Kim, D.-K.; Longoni, G. Readiness Level of Sodium-Ion Battery Technology: A Materials Review. *Adv. Sustain. Syst.* **2018**, *2* (3), 1700153.
- (21) Li, Y.; Lu, Y.; Zhao, C.; Hu, Y. S.; Titirici, M. M.; Li, H.; Huang, X.; Chen, L. Recent Advances of Electrode Materials for Low-Cost Sodium-Ion Batteries towards Practical Application for Grid Energy Storage. *Energy Storage Mater.* **2017**, *7* (January), 130–151.
- (22) Slater, M. D.; Kim, D.; Lee, E.; Johnson, C. S. Sodium-Ion Batteries. *Adv. Funct. Mater.* **2013**, *23* (8), 947–958.
- (23) Ong, S. P.; Chevrier, V. L.; Hautier, G.; Jain, A.; Moore, C.; Kim, S.; Ma, X.; Ceder, G. Voltage, Stability and Diffusion Barrier Differences between Sodium-Ion and Lithium-Ion Intercalation Materials. *Energy Environ. Sci.* **2011**, *4* (9), 3680–3688.
- (24) Sagane, F.; Abe, T.; Iriyama, Y.; Ogumi, Z. Li⁺ and Na⁺ Transfer through Interfaces between Inorganic Solid Electrolytes and Polymer or Liquid Electrolytes. *J. Power Sources* **2005**, *146* (1–2), 749–752.
- (25) Komaba, S.; Hasegawa, T.; Dahbi, M.; Kubota, K. Potassium Intercalation into Graphite to Realize High-Voltage/High-Power Potassium-Ion Batteries and Potassium-Ion Capacitors. *Electrochem. commun.* **2015**, *60*, 172–175.
- (26) Leonard, D. P.; Wei, Z.; Chen, G.; Du, F.; Ji, X. Water-in-Salt Electrolyte for Potassium-Ion Batteries. *ACS Energy Lett.* **2018**, *3* (2), 373–374.
- (27) Jiang, L.; Lu, Y.; Zhao, C.; Liu, L.; Zhang, J.; Zhang, Q.; Shen, X.; Zhao, J.; Yu, X.; Li, H.; et al. Building Aqueous K-Ion Batteries for Energy Storage. *Nat. Energy* **2019**, *4* (6), 495–503.
- (28) Cheng, Y.; Luo, L.; Zhong, L.; Chen, J.; Li, B.; Wang, W.; Mao, S. X.; Wang, C.; Sprenkle, V. L.; Li, G.; et al. Highly Reversible Zinc-Ion Intercalation into Chevrel Phase Mo₆S₈ Nanocubes and Applications for Advanced Zinc-Ion Batteries. *ACS Appl. Mater. Interfaces* **2016**, *8* (22), 13673–13677.
- (29) Xu, C.; Li, B.; Du, H.; Kang, F. Energetic Zinc Ion Chemistry: The Rechargeable Zinc Ion Battery. *Angew. Chemie - Int. Ed.* **2012**, *51* (4), 933–935.
- (30) Lin, D.; Liu, Y.; Cui, Y. Reviving the Lithium Metal Anode for High-Energy Batteries. *Nat. Nanotechnol.* **2017**, *12* (3), 194–206.
- (31) Cheng, X. B.; Zhang, Q. Dendrite-Free Lithium Metal Anodes: Stable Solid Electrolyte Interphases for High-Efficiency Batteries. *J. Mater. Chem. A* **2015**, *3* (14), 7207–7209.
- (32) Bolloré, G. Bluecar <https://www.bluecar.fr/> (accessed May 9, 2019).
- (33) Judez, X.; Eshetu, G. G.; Li, C.; Rodriguez-Martinez, L. M.; Zhang, H.; Armand, M. Opportunities for Rechargeable Solid-State Batteries Based on Li-Intercalation Cathodes. *Joule* **2018**, *2* (11), 2208–2224.
- (34) Ma, Z.; Yuan, X.; Li, L.; Ma, Z. F.; Wilkinson, D. P.; Zhang, L.; Zhang, J. A Review of Cathode Materials and Structures for Rechargeable Lithium-Air Batteries. *Energy Environ. Sci.* **2015**, *8* (8), 2144–2198.
- (35) Christensen, J.; Albertus, P.; Sanchez-Carrera, R. S.; Lohmann, T.; Kozinsky, B.; Liedtke, R.; Ahmed, J.; Kojic, A. A Critical Review of Li/Air Batteries. *J. Electrochem. Soc.* **2011**, *159* (2), R1–R30.
- (36) Cheng, Y. Y.; Li, C. C.; Lee, J. T. Electrochemical Behavior of Organic Radical Polymer Cathodes in Organic Radical Batteries with N-Butyl-N-Methylpyrrolidinium Bis(Trifluoromethylsulfonyl)Imide Ionic Liquid

- Electrolytes. *Electrochim. Acta* **2012**, *66*, 332–339.
- (37) Song, Z.; Zhan, H.; Zhou, Y. Anthraquinone Based Polymer as High Performance Cathode Material for Rechargeable Lithium Batteries. *Chem. Commun.* **2009**, No. 4, 448–450.
- (38) Deng, W.; Liang, X.; Wu, X.; Qian, J.; Cao, Y.; Ai, X.; Feng, J.; Yang, H. A Low Cost, All-Organic Na-Ion Battery Based on Polymeric Cathode and Anode. *Sci. Rep.* **2013**, *3* (1), 2671.
- (39) Jian, Z.; Liang, Y.; Pérez, I. A. R.; Yao, Y.; Ji, X. Poly(Anthraquinonyl Sulfide) Cathode for Potassium-Ion Batteries. *Electrochem. commun.* **2016**, *71*, 5–8.
- (40) Han, X.; Chang, C.; Yuan, L.; Sun, T.; Sun, J. Aromatic Carbonyl Derivative Polymers as High-Performance Li-Ion Storage Materials. *Adv. Mater.* **2007**, *19* (12), 1616–1621.
- (41) Luo, W.; Allen, M.; Raju, V.; Ji, X. An Organic Pigment as a High-Performance Cathode for Sodium-Ion Batteries. *Adv. Energy Mater.* **2014**, *4* (15), 1400554.
- (42) Chen, Y.; Luo, W.; Carter, M.; Zhou, L.; Dai, J.; Fu, K.; Lacey, S.; Li, T.; Wan, J.; Han, X.; et al. Organic Electrode for Non-Aqueous Potassium-Ion Batteries. *Nano Energy* **2015**, *18*, 205–211.
- (43) Judez, X.; Qiao, L.; Armand, M.; Zhang, H. Energy Density Assessment of Organic Batteries. *ACS Appl. Energy Mater.* **2019**, *2* (6), 4008–4015.
- (44) Manthiram, A.; Chung, S. H.; Zu, C. Lithium-Sulfur Batteries: Progress and Prospects. *Adv. Mater.* **2015**, *27* (12), 1980–2006.
- (45) Xu, R.; Yue, J.; Liu, S.; Tu, J.; Han, F.; Liu, P.; Wang, C. Cathode-Supported All-Solid-State Lithium-Sulfur Batteries with High Cell-Level Energy Density. *ACS Energy Lett.* **2019**, *4* (5), 1073–1079.
- (46) Sion Power to provide enhanced Li-S batteries to Airbus Defence and Space for new Zephyr HAPS; 350 Wh/kg
<https://www.greencarcongress.com/2015/06/20150611-sion.html> (accessed May 13, 2019).
- (47) Bassett, S. Airbus Zephyr – Using Lithium Sulfur Batteries to Revolutionise Communications. In *Lithium Sulfur: Mechanisms, Modelling & Materials*; 2017.
- (48) Energy, O. OXIS Energy Technology Launches into Space Project
<https://oxisenergy.com/oxis-energy-technology-launches-into-space-project/> (accessed May 13, 2019).
- (49) Griebel, J. J.; Glass, R. S.; Char, K.; Pyun, J. Polymerizations with Elemental Sulfur: A Novel Route to High Sulfur Content Polymers for Sustainability, Energy and Defense. *Prog. Polym. Sci.* **2016**, *58*, 90–125.
- (50) Demirbas, A.; Alidrisi, H.; Balubaid, M. A. API Gravity, Sulfur Content, and Desulfurization of Crude Oil. *Pet. Sci. Technol.* **2015**, *33* (1), 93–101.
- (51) Babich IV; Moulijn JA. Science and Technology of Novel Processes for Deep Desulfurization of Oil Refinery Streams : A Review Q. *Fuel* **2003**, *82*, 607–631.
- (52) Teck. Sulphur Safety Data Sheet. **2015**, 1–6.
- (53) Chung, W. J.; Griebel, J. J.; Kim, E. T.; Yoon, H.; Simmonds, A. G.; Ji, H. J.; Dirlam, P. T.; Glass, R. S.; Wie, J. J.; Nguyen, N. A.; et al. The Use of Elemental Sulfur as an Alternative Feedstock for Polymeric Materials. *Nat. Chem.* **2013**, *5* (6), 518–524.
- (54) Chung, W. J.; Simmonds, A. G.; Griebel, J. J.; Kim, E. T.; Suh, H. S.; Shim, I. B.; Glass, R. S.; Loy, D. A.; Theato, P.; Sung, Y. E.; et al. Elemental Sulfur as a Reactive Medium for Gold Nanoparticles and Nanocomposite Materials. *Angew.*

- Chemie - Int. Ed.* **2011**, *50* (48), 11409–11412.
- (55) Moy, D.; Manivannan, A.; Narayanan, S. R. Direct Measurement of Polysulfide Shuttle Current: A Window into Understanding the Performance of Lithium-Sulfur Cells. *J. Electrochem. Soc.* **2014**, *162* (1), A1–A7.
- (56) Su, Y. S.; Fu, Y.; Cochell, T.; Manthiram, A. A Strategic Approach to Recharging Lithium-Sulphur Batteries for Long Cycle Life. *Nat. Commun.* **2013**, *4*, 1–8.
- (57) Borchardt, L.; Oschatz, M.; Kaskel, S. Carbon Materials for Lithium Sulfur Batteries-Ten Critical Questions. *Chem. - A Eur. J.* **2016**, *22* (22), 7324–7351.
- (58) Peng, H. J.; Xu, W. T.; Zhu, L.; Wang, D. W.; Huang, J. Q.; Cheng, X. B.; Yuan, Z.; Wei, F.; Zhang, Q. 3D Carbonaceous Current Collectors: The Origin of Enhanced Cycling Stability for High-Sulfur-Loading Lithium-Sulfur Batteries. *Adv. Funct. Mater.* **2016**, *26* (35), 6351–6358.
- (59) Yim, T.; Park, M. S.; Yu, J. S.; Kim, K.; Im, K. Y.; Kim, J. H.; Jeong, G.; Jo, Y. N.; Woo, S. G.; Kang, K. S.; et al. Effect of Chemical Reactivity of Polysulfide toward Carbonate-Based Electrolyte on the Electrochemical Performance of Li-S Batteries. *Electrochim. Acta* **2013**, *107*, 454–460.
- (60) Zhang, S. S. Liquid Electrolyte Lithium/Sulfur Battery: Fundamental Chemistry, Problems, and Solutions. *J. Power Sources* **2013**, *231*, 153–162.
- (61) Xu, K. Nonaqueous Liquid Electrolytes for Lithium-Based Rechargeable Batteries. *Chem. Rev.* **2004**, *104* (10), 4303–4418.
- (62) Aurbach, D. Review of Selected Electrode-Solution Interactions Which Determine the Performance of Li and Li Ion Batteries. *J. Power Sources* **2000**, *89* (2), 206–218.
- (63) Aurbach, D.; Pollak, E.; Elazari, R.; Salitra, G.; Kelley, C. S.; Affinito, J. On the Surface Chemical Aspects of Very High Energy Density, Rechargeable Li-Sulfur Batteries. *J. Electrochem. Soc.* **2009**, *156* (8), A694.
- (64) Jaumann, T.; Balach, J.; Klose, M.; Oswald, S.; Eckert, J.; Giebeler, L. Role of 1,3-Dioxolane and LiNO₃ Addition on the Long Term Stability of Nanostructured Silicon/Carbon Anodes for Rechargeable Lithium Batteries. *J. Electrochem. Soc.* **2016**, *163* (3), A557–A564.
- (65) Manthiram, A.; Fu, Y.; Chung, S.-H.; Zu, C.; Su, Y.-S. Rechargeable Lithium-Sulfur Batteries. *Chem. Rev.* **2014**, *114* (23), 11751–11787.
- (66) Wild, M.; O'Neill, L.; Zhang, T.; Purkayastha, R.; Minton, G.; Marinescu, M.; Offer, G. J. Lithium Sulfur Batteries, a Mechanistic Review. *Energy Environ. Sci.* **2015**, *8* (12), 3477–3494.
- (67) Pan, H.; Wei, X.; Henderson, W. A.; Shao, Y.; Chen, J.; Bhattacharya, P.; Xiao, J.; Liu, J. On the Way Toward Understanding Solution Chemistry of Lithium Polysulfides for High Energy Li-S Redox Flow Batteries. *Adv. Energy Mater.* **2015**, *5* (16), 1–7.
- (68) Yu, X.; Manthiram, A. Electrode-Electrolyte Interfaces in Lithium-Sulfur Batteries with Liquid or Inorganic Solid Electrolytes. *Acc. Chem. Res.* **2017**, *50* (11), 2653–2660.
- (69) Qi, Q.; Lv, X.; Lv, W.; Yang, Q.-H. Multifunctional Binder Designs for Lithium-Sulfur Batteries. *J. Energy Chem.* **2019**, *39*, 88–100.
- (70) Xu, G.; Yan, Q. bo; Kushima, A.; Zhang, X.; Pan, J.; Li, J. Conductive Graphene Oxide-Polyacrylic Acid (GOPAA) Binder for Lithium-Sulfur Battery. *Nano Energy* **2017**, *31* (December 2016), 568–574.

- (71) Li, G.; Cai, W.; Liu, B.; Li, Z. A Multi Functional Binder with Lithium Ion Conductive Polymer and Polysulfide Absorbents to Improve Cycleability of Lithium-Sulfur Batteries. *J. Power Sources* **2015**, *294*, 187–192.
- (72) Chen, W.; Lei, T.; Qian, T.; Lv, W.; He, W.; Wu, C.; Liu, X.; Liu, J.; Chen, B.; Yan, C.; et al. A New Hydrophilic Binder Enabling Strongly Anchoring Polysulfides for High-Performance Sulfur Electrodes in Lithium-Sulfur Battery. *Adv. Energy Mater.* **2018**, *8* (12), 1–8.
- (73) Griebel, J. J.; Glass, R. S.; Char, K.; Pyun, J. Polymerizations with Elemental Sulfur: A Novel Route to High Sulfur Content Polymers for Sustainability, Energy and Defense. *Progress in Polymer Science*. Elsevier Ltd 2016, pp 90–125.
- (74) Yu, X.; Bi, Z.; Zhao, F.; Manthiram, A. Hybrid Lithium-Sulfur Batteries with a Solid Electrolyte Membrane and Lithium Polysulfide Catholyte. *ACS Appl. Mater. Interfaces* **2015**, *7* (30), 16625–16631.
- (75) Xu, H.; Wang, S.; Manthiram, A. Hybrid Lithium-Sulfur Batteries with an Advanced Gel Cathode and Stabilized Lithium-Metal Anode. *Adv. Energy Mater.* **2018**, *8* (23), 1–6.
- (76) Yu, X.; Bi, Z.; Zhao, F.; Manthiram, A. Polysulfide-Shuttle Control in Lithium-Sulfur Batteries with a Chemically/Electrochemically Compatible NaSICON-Type Solid Electrolyte. *Adv. Energy Mater.* **2016**, *6* (24).
- (77) Waluš, S.; Barchasz, C.; Bouchet, R.; Martin, J. F.; Leprêtre, J. C.; Alloin, F. Non-Woven Carbon Paper as Current Collector for Li-Ion/Li₂S System: Understanding of the First Charge Mechanism. *Electrochim. Acta* **2015**, *180*, 178–186.
- (78) Pan, H.; Han, K. S.; Vijayakumar, M.; Xiao, J.; Cao, R.; Chen, J.; Zhang, J.; Mueller, K. T.; Shao, Y.; Liu, J. Ammonium Additives to Dissolve Lithium Sulfide through Hydrogen Binding for High-Energy Lithium-Sulfur Batteries. *ACS Applied Materials and Interfaces*. 2017, pp 4290–4295.
- (79) Wu, F.; Lee, J. T.; Nitta, N.; Kim, H.; Borodin, O.; Yushin, G. Lithium Iodide as a Promising Electrolyte Additive for Lithium-Sulfur Batteries: Mechanisms of Performance Enhancement. *Adv. Mater.* **2015**, *27* (1), 101–108.
- (80) Zu, C.; Klein, M.; Manthiram, A. Activated Li₂S as a High-Performance Cathode for Rechargeable Lithium–Sulfur Batteries. *J. Phys. Chem. Lett.* **2014**, *5* (22), 3986–3991.
- (81) Klein, M. J.; Dolocan, A.; Zu, C.; Manthiram, A. An Effective Lithium Sulfide Encapsulation Strategy for Stable Lithium–Sulfur Batteries. *Adv. Energy Mater.* **2017**, *7* (20), 1–9.
- (82) Gu, X.; Lai, C. Recent Development of Metal Compound Applications in Lithium–Sulphur Batteries. *J. Mater. Res.* **2018**, *33* (1), 16–31.
- (83) Ding, N.; Zhou, L.; Zhou, C.; Geng, D.; Yang, J.; Chien, S. W.; Liu, Z.; Ng, M.-F.; Yu, A.; Hor, T. S. A.; et al. Building Better Lithium-Sulfur Batteries: From LiNO₃ to Solid Oxide Catalyst. *Sci. Rep.* **2016**, *6* (1), 33154.
- (84) Kim, M.-S.; Shin, E. S.; Kim, J.-S.; Cho, W. Il; Oh, S. H. The Effect of V₂O₅/C Additive on the Suppression of Polysulfide Dissolution in Li-Sulfur Batteries. *J. Electroceramics* **2014**, *33* (3–4), 142–148.
- (85) Chung, S. H.; Manthiram, A. Lithium-Sulfur Batteries with Superior Cycle Stability by Employing Porous Current Collectors. *Electrochim. Acta* **2013**, *107*, 569–576.

- (86) Cao, R.; Xu, W.; Lv, D.; Xiao, J.; Zhang, J. G. Anodes for Rechargeable Lithium-Sulfur Batteries. *Adv. Energy Mater.* **2015**, *5* (16), 1–23.
- (87) Kim, H.; Lee, J. T.; Lee, D. C.; Oschatz, M.; Cho, W. Il; Kaskel, S.; Yushin, G. Enhancing Performance of Li-S Cells Using a Li-Al Alloy Anode Coating. *Electrochem. commun.* **2013**, *36*, 38–41.
- (88) Baloch, M.; Shanmukaraj, D.; Bondarchuk, O.; Bekaert, E.; Rojo, T.; Armand, M. Variations on Li₃N Protective Coating Using Ex-Situ and in-Situ Techniques for Li^o in Sulphur Batteries. *Energy Storage Mater.* **2017**, *9* (January), 141–149.
- (89) Elazari, R.; Salitra, G.; Gershinshy, G.; Garsuch, A.; Panchenko, A.; Aurbach, D. Rechargeable Lithiated Silicon-Sulfur (SLS) Battery Prototypes. *Electrochem. commun.* **2012**, *14* (1), 21–24.
- (90) Zheng, S.; Chen, Y.; Xu, Y.; Yi, F.; Zhu, Y.; Liu, Y.; Yang, J.; Wang, C. In Situ Formed Lithium Sulfide/Microporous Carbon Cathodes for Lithium-Ion Batteries. *ACS Nano* **2013**, *7* (12), 10995–11003.
- (91) Verma, P.; Maire, P.; Novák, P. A Review of the Features and Analyses of the Solid Electrolyte Interphase in Li-Ion Batteries. *Electrochim. Acta* **2010**, *55* (22), 6332–6341.
- (92) Miao, R.; Yang, J.; Feng, X.; Jia, H.; Wang, J.; Nuli, Y. Novel Dual-Salts Electrolyte Solution for Dendrite-Free Lithium-Metal Based Rechargeable Batteries with High Cycle Reversibility. *J. Power Sources* **2014**, *271*, 291–297.
- (93) Kim, H.; Wu, F.; Lee, J. T.; Nitta, N.; Lin, H.-T.; Oschatz, M.; Cho, W. Il; Kaskel, S.; Borodin, O.; Yushin, G. In Situ Formation of Protective Coatings on Sulfur Cathodes in Lithium Batteries with LiFSI-Based Organic Electrolytes. *Adv. Energy Mater.* **2015**, *5* (6), 1401792.
- (94) Basile, A.; Bhatt, A. I.; O'Mullane, A. P. Stabilizing Lithium Metal Using Ionic Liquids for Long-Lived Batteries. *Nat. Commun.* **2016**, *7*, 1–11.
- (95) Wang, L.; Liu, J.; Yuan, S.; Wang, Y.; Xia, Y. To Mitigate Self-Discharge of Lithium-Sulfur Batteries by Optimizing Ionic Liquid Electrolytes. *Energy Environ. Sci.* **2016**, *9* (1), 224–231.
- (96) Zhang, S. S. Role of LiNO₃ in Rechargeable Lithium/Sulfur Battery. *Electrochim. Acta* **2012**, *70*, 344–348.
- (97) Jia, W.; Fan, C.; Wang, L.; Wang, Q.; Zhao, M.; Zhou, A.; Li, J. Extremely Accessible Potassium Nitrate (KNO₃) as the Highly Efficient Electrolyte Additive in Lithium Battery. *ACS Appl. Mater. Interfaces* **2016**, *8* (24), 15399–15405.
- (98) Lin, Z.; Liu, Z.; Fu, W.; Dudney, N. J.; Liang, C. Phosphorous Pentasulfide as a Novel Additive for High-Performance Lithium-Sulfur Batteries. *Adv. Funct. Mater.* **2013**, *23* (8), 1064–1069.
- (99) Wu, H.-L.; Haasch, R. T.; Perdue, B. R.; Apblett, C. A.; Gewirth, A. A. The Effect of Water-Containing Electrolyte on Lithium-Sulfur Batteries. *J. Power Sources* **2017**, *369*, 50–56.
- (100) Wu, H. L.; Shin, M.; Liu, Y. M.; See, K. A.; Gewirth, A. A. Thiol-Based Electrolyte Additives for High-Performance Lithium-Sulfur Batteries. *Nano Energy* **2017**, *32* (November 2016), 50–58.
- (101) Meini, S.; Elazari, R.; Rosenman, A.; Garsuch, A.; Aurbach, D. The Use of Redox Mediators for Enhancing Utilization of Li₂S Cathodes for Advanced Li-S Battery Systems. *J. Phys. Chem. Lett.* **2014**, *5* (5), 915–918.
- (102) Azimi, N.; Xue, Z.; Rago, N. D.; Takoudis, C.; Gordin, M. L.; Song, J.; Wang,

- D.; Zhang, Z. Fluorinated Electrolytes for Li-S Battery: Suppressing the Self-Discharge with an Electrolyte Containing Fluoroether Solvent. *J. Electrochem. Soc.* **2014**, *162* (1), A64–A68.
- (103) Jia, H.; Wang, J.; Lin, F.; Monroe, C. W.; Yang, J.; Nuli, Y. TPPi as a Flame Retardant for Rechargeable Lithium Batteries with Sulfur Composite Cathodes. *Chem. Commun.* **2014**, *50* (53), 7011–7013.
- (104) Yim, T.; Kang, K. S.; Yu, J. S.; Kim, K. J.; Park, M. S.; Woo, S. G.; Jeong, G.; Jo, Y. N.; Im, K. Y.; Kim, J. H.; et al. Effect of Acid Scavengers on Electrochemical Performance of Lithium-Sulfur Batteries: Functional Additives for Utilization of LiPF₆. *Jpn. J. Appl. Phys.* **2014**, *53* (8 SPEC. ISSUE 3).
- (105) Zhang, H.; Eshetu, G. G.; Judez, X.; Li, C.; Rodriguez-Martínez, L. M.; Armand, M. Electrolyte Additives for Lithium Metal Anodes and Rechargeable Lithium Metal Batteries: Progresses and Perspectives. *Angew. Chemie Int. Ed.* **2018**, *57*, 2–28.
- (106) Cleaver, T.; Kovacic, P.; Marinescu, M.; Zhang, T.; Offer, G. Perspective—Commercializing Lithium Sulfur Batteries: Are We Doing the Right Research? *J. Electrochem. Soc.* **2018**, *165* (1), A6029–A6033.
- (107) Gao, J.; Zhao, Y. S.; Shi, S. Q.; Li, H. Lithium-Ion Transport in Inorganic Solid State Electrolyte. *Chinese Phys. B* **2015**, *25* (1).
- (108) Zhao, N.; Khokhar, W.; Bi, Z.; Shi, C.; Guo, X.; Fan, L.-Z.; Nan, C.-W. Solid Garnet Batteries. *Joule* **2019**, *3* (5), 1190–1199.
- (109) Zheng, F.; Kotobuki, M.; Song, S.; Lai, M. O.; Lu, L. Review on Solid Electrolytes for All-Solid-State Lithium-Ion Batteries. *J. Power Sources* **2018**, *389* (April), 198–213.
- (110) Bachman, J. C.; Muy, S.; Grimaud, A.; Chang, H. H.; Pour, N.; Lux, S. F.; Paschos, O.; Maglia, F.; Lupart, S.; Lamp, P.; et al. Inorganic Solid-State Electrolytes for Lithium Batteries: Mechanisms and Properties Governing Ion Conduction. *Chem. Rev.* **2016**, *116* (1), 140–162.
- (111) Kamaya, N.; Homma, K.; Yamakawa, Y.; Hirayama, M.; Kanno, R.; Yonemura, M.; Kamiyama, T.; Kato, Y.; Hama, S.; Kawamoto, K.; et al. A Lithium Superionic Conductor. *Nat. Mater.* **2011**, *10* (9), 682–686.
- (112) SAKUDA, A.; HAYASHI, A.; TAKIGAWA, Y.; HIGASHI, K.; TATSUMISAGO, M. Evaluation of Elastic Modulus of Li₂S-P₂S₅ Glassy Solid Electrolyte by Ultrasonic Sound Velocity Measurement and Compression Test. *J. Ceram. Soc. Japan* **2013**, *121* (1419), 946–949.
- (113) Duluard, S.; Paillassa, A.; Puech, L.; Vinatier, P.; Turq, V.; Rozier, P.; Lenormand, P.; Taberna, P. L.; Simon, P.; Ansart, F. Lithium Conducting Solid Electrolyte Li_{1.3}Al_{0.3}Ti_{1.7}(PO₄)₃ Obtained via Solution Chemistry. *J. Eur. Ceram. Soc.* **2013**, *33* (6), 1145–1153.
- (114) Weller, J. M.; Whetten, J. A.; Chan, C. K. Synthesis of Fine Cubic Li₇La₃Zr₂O₁₂ Powders in Molten LiCl–KCl Eutectic and Facile Densification by Reversal of Li + /H + Exchange. *ACS Appl. Energy Mater.* **2018**, *1* (2), 552–560.
- (115) Wang, L.; Wang, Y.; Xia, Y. A High Performance Lithium-Ion Sulfur Battery Based on a Li₂S Cathode Using a Dual-Phase Electrolyte. *Energy Environ. Sci.* **2015**, *8* (5), 1551–1558.
- (116) Gu, S.; Huang, X.; Wang, Q.; Jin, J.; Wang, Q.; Wen, Z.; Qian, R. A Hybrid Electrolyte for Long-Life Semi-Solid-State Lithium Sulfur Batteries. *J. Mater. Chem. A* **2017**, *5* (27), 13971–13975.

- (117) Fenton, D. E.; Parker, J. M.; Wright, P. V. Complexes of Alkali Metal Ions with Poly(Ethylene Oxide). *Polymer (Guildf)*. **1973**, *14* (11), 589.
- (118) Wright, P. V. Electrical Conductivity in Ionic Complexes of Poly(Ethylene Oxide). *Br. Polym. J.* **1975**, *7* (5), 319–327.
- (119) Armand, M.; Chabagno, J. M.; Duclot, M. J. Polyethers as Solid Electrolytes. In Fast Ion Transp. Solids: Electrodes Electrolytes. In *Proceedings International Conference*; 1979; pp 131–136.
- (120) Arya, A.; Sharma, A. L. Insights into the Use of Polyethylene Oxide in Energy Storage/Conversion Devices: A Critical Review. *J. Phys. D. Appl. Phys.* **2017**, *50* (44), 443002.
- (121) Xue, Z.; He, D.; Xie, X. Poly(Ethylene Oxide)-Based Electrolytes for Lithium-Ion Batteries. *J. Mater. Chem. A* **2015**, *3* (38), 19218–19253.
- (122) Armand, M. Polymer Electrolytes. *Annu. Rev. Mater. Sci.* **1986**, *16*, 245–261.
- (123) Li, C.; Zhang, H.; Otaegui, L.; Singh, G.; Armand, M.; Rodriguez-Martinez, L. M. Estimation of Energy Density of Li-S Batteries with Liquid and Solid Electrolytes. *J. Power Sources* **2016**, *326*, 1–5.
- (124) Weston, J. E.; Steele, B. C. H. Effects of Inert Fillers on the Mechanical and Electrochemical Properties of Lithium Salt-Poly(Ethylene Oxide) Polymer Electrolytes. *Solid State Ionics* **1982**, *7* (1), 75–79.
- (125) Croce, F.; Appetecchi, G. B.; Persi, L.; Scrosati, B. Nanocomposite Polymer Electrolytes for Lithium Batteries. *Nature* **1998**, *394* (6692), 456–458.
- (126) Buvana, P.; Vishista, K.; Shanmukaraj, D.; Murugan, R. Lithium Garnet Oxide Dispersed Polymer Composite Membrane for Rechargeable Lithium Batteries. *Ionics (Kiel)*. **2017**, *23* (3), 541–548.
- (127) Yang, T.; Zheng, J.; Cheng, Q.; Hu, Y. Y.; Chan, C. K. Composite Polymer Electrolytes with Li₇La₃Zr₂O₁₂ Garnet-Type Nanowires as Ceramic Fillers: Mechanism of Conductivity Enhancement and Role of Doping and Morphology. *ACS Appl. Mater. Interfaces* **2017**, *9* (26), 21773–21780.
- (128) Golodnitsky, D.; Strauss, E.; Peled, E.; Greenbaum, S. Review—On Order and Disorder in Polymer Electrolytes. *J. Electrochem. Soc.* **2015**, *162* (14), A2551–A2566.
- (129) Liu, W.; Liu, N.; Sun, J.; Hsu, P. C.; Li, Y.; Lee, H. W.; Cui, Y. Ionic Conductivity Enhancement of Polymer Electrolytes with Ceramic Nanowire Fillers. *Nano Lett.* **2015**, *15* (4), 2740–2745.
- (130) Eshetu, G. G.; Judez, X.; Li, C.; Martinez-Ibañez, M.; Sánchez-Diez, E.; Rodriguez-Martinez, L. M.; Zhang, H.; Armand, M. CHAPTER 4. Solid Electrolytes for Lithium Metal and Future Lithium-Ion Batteries. In *Future Lithium-ion Batteries*; Royal Society of Chemistry: Cambridge, 2019; Vol. 2019-Janua, pp 72–101.
- (131) Ma, Q.; Qi, X.; Tong, B.; Zheng, Y.; Feng, W.; Nie, J.; Hu, Y.-S.; Li, H.; Huang, X.; Chen, L.; et al. Novel Li[(CF₃SO₂)_n(C₄F₉SO₂)_N]-Based Polymer Electrolytes for Solid-State Lithium Batteries with Superior Electrochemical Performance. *ACS Appl. Mater. Interfaces* **2016**, *8* (43), 29705–29712.

Chapter 2:

Modeling energy density and reference cell system definition

This chapter will start modelling the achievable energy density values of all-solid-state lithium-sulfur batteries with different electrolytes. Based on the obtained results, the parameters for the reference cell will be fixed and the first cells will be assembled. The performance of the first cells presented a poor stability, so the failure mechanism is studied in order to propose alternative electrolyte compositions accordingly.

INDEX

2	MODELING ENERGY DENSITY AND REFERENCE CELL SYSTEM DEFINITION.....	55
2.1	MODELLING ENERGY DENSITY	55
2.1.1	Basis of the model.....	55
2.1.2	Parameters for modelling	59
2.1.3	Results discussion and targeted parameters determination	60
2.2	REFERENCE CELL DEVELOPMENT	64
2.2.1	Failure analysis	65
2.2.1.1	Physicochemical and electrochemical characterization	66
2.2.1.2	Salt stability against LiPSs	68
2.2.1.3	Electrolyte behavior with the Li ⁰ electrode	69
2.3	DISCUSSION	72
2.4	CONCLUSIONS	73
2.5	REFERENCES	74

2 MODELING ENERGY DENSITY AND REFERENCE CELL SYSTEM DEFINITION

As stated in the Introduction, the aim of this thesis is the development of all-solid-state lithium-sulfur batteries (ASSLSBs), with great focus on poly(ethylene) oxide (PEO) polymer-based solid polymer electrolytes (SPEs), due to their potential benefits in terms of achievable gravimetric energy density values. This chapter initially corresponds to the adaptation of the previous energy density estimation models performed at CIC Energigune, in order to confirm the previous results and to identify viable parameters for the reference SPE-based ASSLSB cell development. After the first tests, the work will focus in the understanding of the failure mechanisms of the developed cell, with the aim of identifying key strategies for electrolyte development.

2.1 MODELLING ENERGY DENSITY

To study the influence of the implementation of all-solid-state electrolytes in ASSLSBs at energy density level, the previously mentioned model by our colleague Dr. Li will be adapted. For the present work of this Thesis, the model was completed and implemented in Scilab software, a free open-source numerically-oriented programming language, with the aim at extending its use and adapting easily the parameters to several technologies. Furthermore, the initial calculations by Dr. Li *et al.*¹ were based on parameters yet difficult to be achieved. Therefore, in order to confirm the benefits of solid electrolytes in more realistic conditions, some parameters will be adapted to the present values gathered from the on State of Art section of the previous chapter.

The further point will explain in detail the basis of the model and parameters for calculation will be fixed later. Finally, results will be discussed and targeted parameters will be determined.

2.1.1 Basis of the model

As mentioned at the Introduction, the energy of a cell is the product of delivered capacity (C_{cell}) multiplied by the average voltage (V_{cell}) at which that capacity is delivered. In order to calculate gravimetric, E_{cell}^g , or volumetric energy densities, E_{cell}^v , at cell level, the total energy value should be divided by total cell mass, m_{cell} , or total cell volume, v_{cell} , respectively:

$$E_{cell}^g = \frac{C_{cell} \cdot V_{cell}}{m_{cell}} \quad (2.1)$$

$$E_{cell}^v = \frac{C_{cell} \cdot V_{cell}}{v_{cell}} \quad (2.2)$$

However, to enable the calculation with available data, it must be performed in areal terms. Cell capacity can be expressed in areal terms, *i.e.*, areal capacity, C_{cell}^a , and so can be the mass, m_{cell}^a . On the contrary, voltage is an intensive property, independent from the mass or volume. Thus, gravimetric energy can be calculated as follows:

$$E_{cell}^g = \frac{C_{cell}^a \cdot V_{cell}}{m_{cell}^a} \quad (2.3)$$

In the case of volumetric energy, volume can be also expressed in areal terms, v_{cell}^a :

$$E_{cell}^g = \frac{C_{cell}^a \cdot V_{cell}}{v_{cell}^a} \quad (2.4)$$

In order to estimate both gravimetric and volumetric energy densities, an areal capacity value (a parameter that is often reported in battery studies) will be proposed and m_{cell}^a and v_{cell}^a will be calculated accordingly. V_{cell} value will only depend on the chemistry of the cell and it is a well-known parameter for different chemistries. m_{cell}^a will be calculated by the sum of mass of every single component of the cell, *i.e.*, current collector (m_{cc}^a), positive electrode (m_{pe}^a), separator (m_{sep}^a), electrolyte (m_{elec}^a) and negative electrode (m_{ne}^a). In this case, the calculation will be at cell level, and will not take into account the cell casing mass and volume, as it will be strongly dependent of the battery type, *e.g.*, coin cell, cylindrical, prismatic; and will be considered similar for all the studied systems. Furthermore, the aim of these calculation is to study the effect of some parameters rather than giving absolute values. m_{cell}^a can be calculated by the sum of cell components:

$$m_{cell}^a = m_{cc}^a + m_{pe}^a + m_{sep}^a + m_{elec}^a + m_{ne}^a \quad (2.5)$$

Current collector and separator mass will be independent to the areal capacity value, and their properties will be taken from commercial aluminum current collector and poly(propylene)/poly(ethylene) Celgard[®] separator.

The mass of the remaining components will be calculated based on the given areal capacity value. m_{pe}^a will be obtained from sulfur areal mass (m_s^a) and its contribution to the total mass, represented by sulfur content or fraction, f_s .

$$m_{pe}^a = \frac{m_s^a}{f_s} \quad (2.6)$$

f_s value will be set based on state-of-art studies. m_s^a can be calculated based on gravimetric capacity of the active material (C_s^g , another variable whose value will be fixed based on literature) and C_{cell}^a . Sulfur is the only electroactive material that contributes to the capacity of the cell, so C_{cell}^a could be also called C_s^a .

$$m_s^a = \frac{C_{cell}^a}{C_s^g} = \frac{C_s^a}{C_s^g} \quad (2.7)$$

Regarding the negative electrode, the mass will be calculated taking into account the ratio of capacity between negative and positive electrodes, *i.e.*, negative/positive electrode capacity ratio, *N/P* ratio. In the case of commercial lithium ion batteries (LIBs) this value is close to unity, with an excess of 5-10% at most. However, in lithium sulfur batteries (LSBs), where a pure lithium metal (Li^0) negative electrode is used, an excess of at least 3 is needed for a stable cycling. m_{ne}^a will be calculated based on *N/P* ratio and the gravimetric capacity of the Li^0 , C_{Li}^g , whose theoretical value is 3861 mAh g⁻¹:

$$m_{ne}^a = \frac{C_{cell}^a \cdot N/P}{C_{Li}^g} \quad (2.8)$$

Finally, the mass of electrolyte will be calculated depending on its nature. For liquid electrolytes, the mass of the electrolyte will be calculated based on the commonly used electrolyte volume to sulfur mass ratio, *E/S* ratio. This ratio is defined by electrolyte volume to sulfur mass. Finally, calculated electrolyte volume will be converted to mass by density value, ρ_{elec} .

$$m_{elec}^a = m_s^a \cdot E/S \cdot \rho_{elec} \quad (2.9)$$

In the case of solid electrolytes, the calculation should be different. In liquid systems, electrolyte amount needs to be increased when the active material is increased to ensure a proper cathode wettability and electrochemical performance, and therefore, is represented by *E/S* ratio. However, in solid electrolytes, the catholyte, *i.e.*, electrolyte present in the cathode, should be integrated in the cathode preparation step. In the case of solid polymer electrolyte (SPE)-based cells, the catholyte will simultaneously act as electrolyte in the cathode and as a binder in the cathode. In the case of inorganic solid electrolyte (ISE)-based cells, the inorganic particles will act only as electrolyte, and the use of binder will not be necessary, since the positive electrodes are prepared by pellet pressing. Therefore, in solid-electrolyte based cells, while the active material content is increased, the

catholyte amount will increase proportionally, but the electrolyte amount (only dependent on its thickness) will be kept constant.

In other words, while in liquid-electrolyte based cells an increasing liquid electrolyte amount should be introduced to ensure proper wettability when active material amount is increased, in solid systems the electrolyte amount is independent to active material loading, because a proportional amount of catholyte is already being included in the positive electrode.

Thus, in solid systems, electrolyte mass will be calculated just based on electrolyte thickness, t_{elec} , and its density, ρ_{elec} . In reality, solid electrolyte membranes are not completely compact so the porosity value, ε_{elec} , could be applied for correction.

$$m_{elec}^a = t_{elec} \cdot \rho_{elec} \cdot (1 - \varepsilon_{elec}) \quad (2.10)$$

It should be noted that in solid systems, the electrolyte acts also as a physical barrier to avoid direct contact between electrodes, so the addition of an extra separator is not necessary.

In the case of volumetric energy the total cell volume will be calculated as the sum of individual component volume.

$$v_{cell}^a = v_{cc}^a + v_{pe}^a + v_{sep}^a + v_{elec}^a + v_{ne}^a \quad (2.11)$$

Here, the current collector and separator volume are again independent and constant. Areal volume of any component, v_i^a , is, essentially its thickness. Again, the thickness of the commercially available aluminum current collector and separator is known. In the case of the positive electrode, the total areal volume will be the sum of sulfur, v_s^a , conductive carbon, v_c^a , and binder volumes, v_b^a , corrected again by the porosity of the cathode, $\varepsilon_{cathode}$. The volume contribution of carbon, v_c^a , and binder, v_b^a , will be calculated by their mass fraction (f_c and f_b) in the electrode and their density

$$v_{pe}^a = \frac{(v_s^a + v_c^a + v_b^a)}{(1 - \varepsilon_{cathode})} = \frac{\left(\frac{m_s^a}{f_s} + m_s^a \frac{f_c}{f_s} \frac{1}{\rho_c} + m_s^a \frac{f_b}{f_s} \frac{1}{\rho_b}\right)}{(1 - \varepsilon_{cathode})} \quad (2.12)$$

In the case of the negative electrode, the calculation will be similar to Eq. (2.8), but including Li^0 density term, ρ^{Li} .

$$v_{ne}^a = \frac{C_{cell}^a \cdot N/P}{C_{Li}^g \cdot \rho_{Li}} \quad (2.13)$$

Again, the volume of the electrolyte will be calculated in a different way for liquid

and solid systems. In the case of the liquid system, the electrolyte will fill the pores of the separator and positive electrode, so we can consider that it will not increase the total volume of the cell. In the case of solid electrolytes, it will be directly determined by the thickness.

Scilab codes can be found in the section 2 of the Appendix.

2.1.2 Parameters for modelling

A set of necessary cell parameters for energy density calculations have been extracted from the state-of-art study and are displayed in **Table 2.1**.

Table 2.1. Properties of the electrodes and the different electrolyte systems for the calculations.

Parameters	Solid electrolyte configuration	Liquid electrolyte	
Positive electrode	Active material / wt.%	40	60
	Active material utilization / mAh g ⁻¹	1000	1000
	Active material density / g cm ⁻³	1.96	1.96
	Working voltage / V	2.10	2.10
	Binder / wt.%	45	10
	Binder density / g cm ⁻³	1.90/5.15/1.20/x	1.78
	Carbon / wt.%	15	30
	Carbon density / g cm ⁻³	2.20	2.20
	Cathode porosity / %	0/0/20/20	10
	Current collector mass / mg cm ⁻²	2.70	2.70
Current collector thickness / μm	10	10	
Electrolyte	Separator mass / mg cm ⁻²	N/A	1.20
	Separator thickness / μm	N/A	25
	Electrolyte / Active material ratio (E/AM) (μL mg ⁻¹)	N/A	3-10
	Electrolyte thickness / μm	30-100	N/A
	Electrolyte density / g cm ⁻³	1.90/5.15/1.20/x	1.13
Electrolyte porosity / %	0/0/20/20	N/A	
Negative electrode	Negative / positive electrode capacity ratio	3	3
	Active material / wt.%	100	100
	Active material utilization / mAh g ⁻¹	3861	3861

The values separated by slash refer to glassy-inorganic solid electrolyte / garnet-inorganic solid electrolyte / solid polymer electrolyte / solid composite electrolyte. Variable *x* will be calculated according to the filler content in SCE.

Contrary to the previous publication, some parameters were adjusted based on State of Art values for a more realistic modelling. For example, the sulfur percentage was initially fixed always in 75 wt.%, but an adaptation to 40 wt.% in solid cells and to 60 wt.% in liquid ones is proposed for more realistic approach. The binder percentage, *i.e.*, catholyte, has been increased to 45 wt.% for solid configurations, to ensure a proper lithium ion (Li⁺) conduction in the positive electrode.

Furthermore, among solid electrolytes, a lower density glassy-ISE has been included for a more fair comparison, and the possibility to simulate cells based on solid composite electrolytes has been included.

Calculations for different electrolyte families include low density ISE (glassy-ISE, *e.g.*, $\text{Li}_2\text{S-P}_2\text{S}_5$), high density ISE (garnet-ISE, *e.g.*, $\text{Li}_{6.55}\text{Ga}_{0.15}\text{La}_3\text{Zr}_2\text{O}_{12}$), polymer electrolytes (SPE, *i.e.* PEO-based membranes) and composite electrolytes (SCE, *e.g.*, PEO matrix + $\text{Li}_{6.55}\text{Ga}_{0.15}\text{La}_3\text{Zr}_2\text{O}_{12}$ filler); along with the representative liquid electrolyte, *i.e.*, 1M LiTFSI in DME/DOL + 0.1 M LiNO_3 , for comparison.

All in all, this model will study the viability of solid electrolyte implementation in ASSLSBs in realistic operation conditions, based on a set of parameters such as electrolyte type or thickness, and will permit to set targeted performances.

2.1.3 Results discussion and targeted parameters determination

Estimations of energy density at cell level were done based on the amount and type of electrolyte. **Figure 2.1** shows the influence of areal capacity and various types of electrolytes in the values of energy density. The electrolyte quantity is represented by electrolyte thickness in solid electrolytes and by electrolyte/active material (E/AM , ml g_s^{-1}) ratio in liquid electrolytes (LEs). For comparison, a reference value of 250 Wh kg^{-1} and 700 Wh L^{-1} , was included as reference for LIBs. This value was obtained by the use of the same model in a previous work.²

Figure 2.1a demonstrates that, in our conditions, solid electrolyte-based LSBs can surpass gravimetric energy density values of LIBs, but could hardly compete in terms of volumetric energy, due to the low density of sulfur compared to materials employed in LIBs. In contrast to solid electrolytes, **Figure 2.1b** indicates that, in the conditions of the simulation, for LEs based cells, improved gravimetric energy densities would be only obtained in limited cases, *i.e.*, very high areal capacity or very low E/AM ratios. Additionally, it would not be possible to achieve superior volumetric energy values.

Some of the values from the first figures have been taken and represented in two dimensions. **Figure 2.1c** shows the importance of reducing the electrolyte thickness and density in ASSLSBs, and prove that both can critically penalize the energy density. For example, at 2 mAh cm^{-2} , doubling electrolyte thickness from 50 to 100 μm will decrease gravimetric energy density by 27% in SPE-based cells, and by 43% in ISE-garnet based cells. Regarding the density, while in an ASSLSB based on a 30-50 μm SPE, a cell with an areal capacity of 1-1.4 mAh cm^{-2} would surpass the energy density values of the reference LIB, for garnet electrolytes with the same thickness, values of 3-5 mAh cm^{-2} would be needed. In practical terms, SPE with competitive thicknesses of 50 μm or below can be obtained by low cost solvent casting and hot pressing techniques. However, it is still challenging to

obtain competitive thicknesses below 100-200 μm for ISE, due to the difficulty to process these materials owing to its brittle behavior.

For LEs cells, **Figure 2.1d** shows, that according to our estimations, E/AM values should necessarily be minimized to values around 3 or lower to be able to compete with LIBs. This is very challenging, since liquid electrolyte must soak the positive electrode and separator sufficiently. In contrast, in SPE thickness values of 50 μm or below are easily achievable.

Even if these results prove that both liquid-based and solid-based LSBs can surpass gravimetric energy density values of actual LIB batteries, the use of solid electrolytes seems more favorable in this aspect. When comparing SPE and LE electrolytes, the use of SPE seems to have more room to attain higher gravimetric energy density values. One of the reasons for this improvement is that while in positive electrodes for liquid-based cells binder and LE need to be added separately, in electrodes for solid state cells both functions are fulfilled simultaneously by the catholyte. The other reason is that while an inert separator is needed to avoid direct contact between electrodes in liquid cells, in solid cells the electrolyte itself acts as Li^+ conductive membrane and physical barrier between the electrodes, simultaneously. Therefore, even if positive electrodes for all-solid-state batteries may include lower amount of active material (40 wt.% vs. 65 wt.%), this is compensated by the substantial reduction of inert cell components, leading ultimately to improved energy densities.

In conclusion, this calculations confirm that by the use of all-solid-state electrolytes, especially low density SPEs, it is viable achieving high gravimetric energy densities that can remarkably surpass the values of LIBs. Additionally, the electrode composition based on 40 wt.% sulfur and 45 wt.% catholyte is validated, as energy densities values superior to those of LIBs can be achieved with this configuration. Furthermore, the thickness of the SPE membranes will be fixed to a maximum of 50 μm . With these conditions, we can also set a targeted performance of 1.2 mAh cm^{-2} for our ASSLSBs cells.

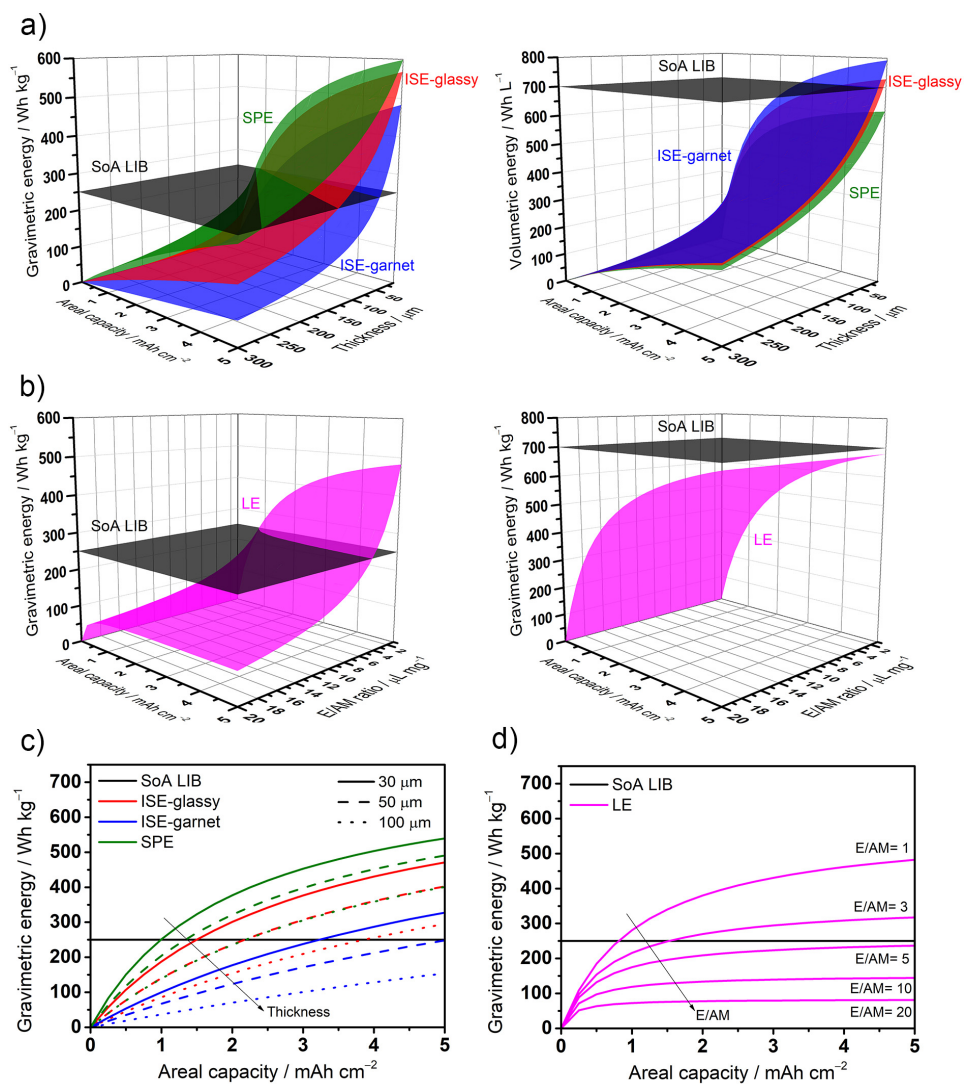


Figure 2.1. Estimated gravimetric (left) and volumetric (right) energy densities of LSBs for different electrolytes families, including a) different types of solid electrolytes and b) liquid electrolyte at different areal capacities and electrolyte amounts. Effect of the amount of electrolyte in gravimetric energy density, including c) the dependence of electrolyte thickness in solid cells and d) E/AM ratio in liquid cells. Values for state of art LIB were included as reference.

The previous figures show that the use of solid electrolytes, especially low density SPEs, can be beneficial for the improvement of gravimetric energy density. However, as highlighted in the State of Art study in the previous chapter, ceramic fillers are usually added to SPEs, in order to obtain solid composite electrolytes (SCEs) that allow improved cell cycling.

As mentioned before, the density of some materials used as fillers can be very high, e.g., $\text{Li}_{6.55}\text{Ga}_{0.15}\text{La}_3\text{Zr}_2\text{O}_{12}$, thus, their contribution to the electrolyte weight can be excessive. Hence, it is important to study the effect of the filler amount in the energy density of the system. **Figure 2.2** shows the effect in gravimetric energy of $\text{Li}_{6.55}\text{Ga}_{0.15}\text{La}_3\text{Zr}_2\text{O}_{12}$ filler content in a 50 μm thickness PEO-based SCE. Calculations shows that low filler contents will not penalize significantly the gravimetric energy of the cell. However, the addition of filler contents as high as 20 vl.% at the electrolyte can decrease by 20% the value of energy density at 2 mAh cm^{-2} .

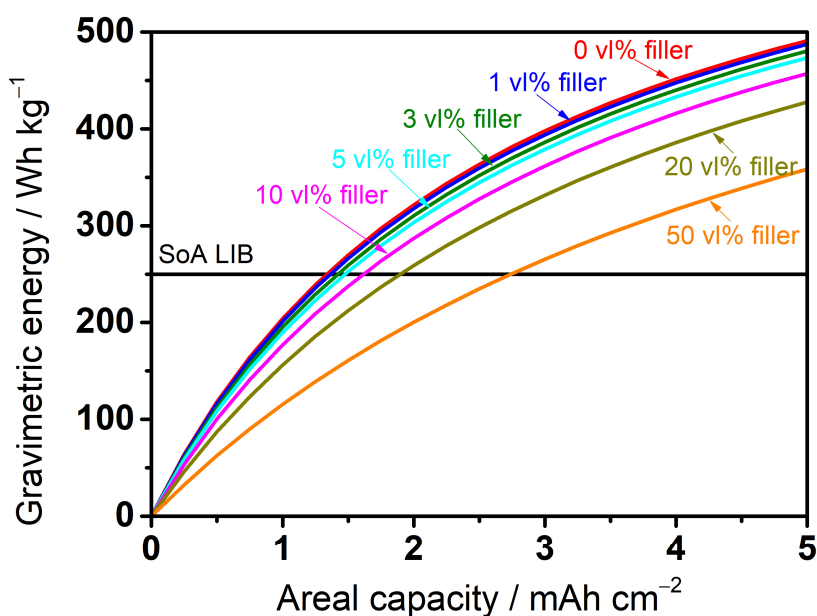


Figure 2.2. Influence of filler amount, quantified in volume percentage, in energy density for composite solid electrolyte cell, based on a 50 μm thickness polymer electrolyte and a $\text{Li}_{6.55}\text{Ga}_{0.15}\text{La}_3\text{Zr}_2\text{O}_{12}$ filler. Values for state of art LIB were included as reference.

These calculations highlight the importance of the use of lightweight electrolytes for achieving high energy density values. Accordingly, the addition of moderate quantities of high density ceramic materials as fillers must be well justified by remarkable improvements on battery performance.

In conclusion, apart from the previously mentioned benefits from ASSLSBs, such as safety and stability improvement, the use of solid-electrolytes can also boost the gravimetric energy density of LSBs. Especially, the use of SPEs and low filler content SCEs are a very appealing strategies due to their low density, flexibility and easy processability, which allows obtaining electrolytes with competitive thickness and low weight. Moreover, the proposed electrode recipe is validated

and the maximum electrolyte thickness has been fixed to 50 μm . A targeted cell performance of 1.2 mAh cm^{-2} has been fixed.

During the work of this Thesis further calculations on different parameters effect in gravimetric energy density and an in-depth State of Art study of ASSLSBs was published in a short review publication.³

2.2 REFERENCE CELL DEVELOPMENT

Based on State of Art studies and the studies of viability in the previous point, our first ASSLSBs will be based on SPE electrolytes. For the preparation of the PEO-based SPE, the most ordinary procedures were searched in literature (see State of Art section in Introduction chapter). The most commonly used lithium bis(trifluorosulfonyl)imide (LiTFSI) salt was selected, for its good compatibility in LSBs and due to the fact that its weakly coordinated anion confers it a high solubility in the PEO matrix. The LiTFSI/PEO salt molar ratio was fixed at 1/20. After different trials, the membranes were prepared by solvent-casting method and the thickness of the membranes by fixed to 50 μm by hot-pressing. All the finally defined and used experimental details can be found in the section 3 in the Appendix.

On the other hand, the sulfur content in the positive electrode was fixed to 40 wt.% and the content of the binder, *i.e.*, catholyte, was fixed to 45 wt.%. The remaining fraction was filled by Ketjen Black conductive carbon. At this point we must point out that a non-optimized positive electrode has been used, in order to emphasize the effect of the electrolyte in the cell cycling. A commercial Li^0 disc of 500 μm was used as negative electrode

Figure 2.3a shows a schematic representation of the prepared coin cell. The cell was cycled at 70 $^{\circ}\text{C}$, above the melting point of PEO, to obtain sufficient ionic conductivity from the SPEs. The cycling performance of the first assembled cell is shown in **Figure 2.3b**. Cell cycling at different rates are displayed, showing a high discharge capacity [*c.a.* 800 mAh g^{-1} (0.80 mAh cm^{-2}) at 0.05C and 420 mAh g^{-1} (0.42 mAh cm^{-2}) at 0.5C] but poor stability, in line with the previously reported works (State of Art section). Batteries show poor response at 0.2C rate or higher, with pronounced overcharge and low Coulombic efficiency. Discharge/charge profiles in **Figure 2.3c** present well defined discharge curves, but in contrast, overcharge and voltage fluctuation at high rates of 0.2C and 0.5C. Even at slower rates of 0.1C, the stability of the cell is compromised after 15 cycles, as seen by Coulombic efficiency decay (**Figure 2.3d**).

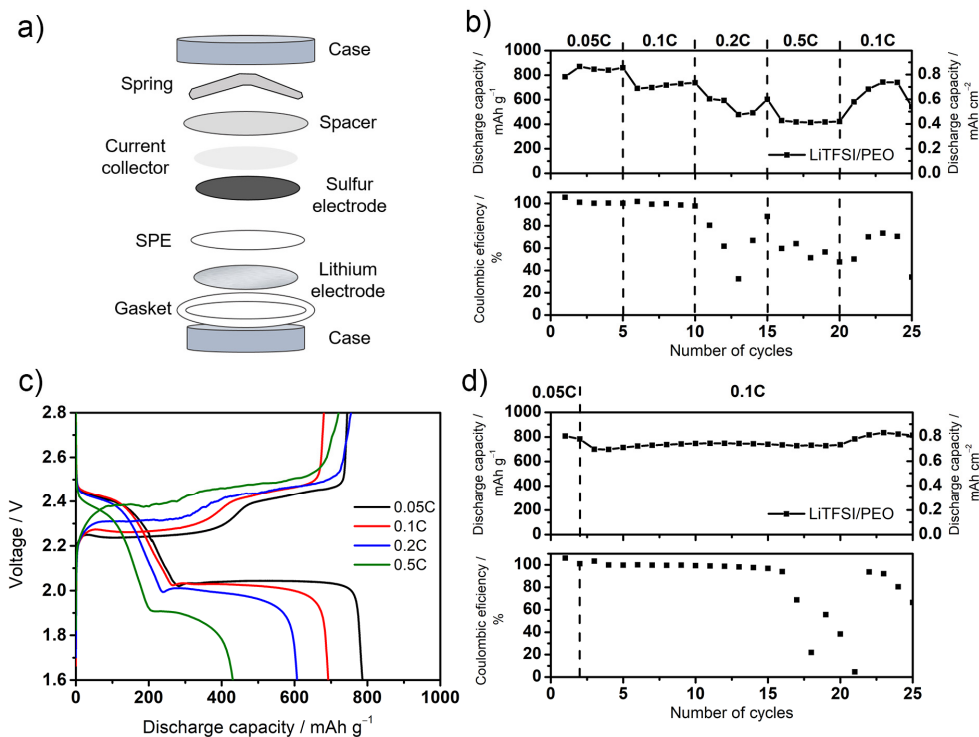


Figure 2.3. a) Schematic representation of the built SPE-based ASSLSBs. b) Rate capability and c) corresponding discharge/charge profiles for the first cycle of each discharge rate. d) Cell performance at 0.1C, after two initial cycles at 0.05C. All the cells were tested at 70 °C.

At this point, the LiTFSI/PEO-based ASSLSBs battery does not feature acceptable performance due to the abrupt Coulombic efficiency decay at high discharge/charge rates, *i.e.*, 0.2C and 0.5C, or after some cycles at lower rate of 0.1C. To solve these issues and to be able to propose alternative strategies, failure mechanism needs to be understood. Issues with LiTFSI/PEO membranes in ASSLSBs have also been reported in other studies, but the failure mechanism has not been depicted in detail before.⁴⁻⁶

2.2.1 Failure analysis

To fully understand the failure mechanisms of the assembled cells, a full set of characterizations were done to study different aspects of the prepared LiTFSI/PEO electrolyte. Those characterizations include the study of the physicochemical and electrochemical properties of the bare membrane, with the aim of identifying any possible limiting feature; the study of electrolyte salt stability against lithium polysulfides (LiPS), in order to detect possible degradation reactions; and the study

of the electrolyte behavior with the high reactive lithium electrode, to identify possible compatibility issues.

2.2.1.1 Physicochemical and electrochemical characterization

Figure 2.4 shows the physicochemical and electrochemical properties of the prepared LiTFSI/PEO membrane. **Figure 2.4a** describes a homogeneous self-standing 16 mm diameter translucent membrane. **Figure 2.4b** presents X-ray diffraction (XRD) spectra of the bare PEO, pristine LiTFSI salt and LiTFSI/PEO membrane at room temperature (RT). The membrane only shows characteristic diffraction peak that belong to the crystalline phase of the pure PEO at $2\theta = 19^\circ$ and 23° , and there is no peak from pristine LiTFSI, indicating the full salt solvation in PEO matrix and no presence of salt precipitate, as desired. The presence of typical diffraction peaks for neat PEO in the membrane suggests the existence of highly crystalline phase in the electrolytes at room temperature.

Electrochemical stability test on **Figure 2.4c** shows that the membrane features mild current responses related to PEO at above 3.8 V vs. Li/Li⁺. Later, the current intensifies at voltages above 5-5.5 V vs. Li/Li⁺, which is related to anion oxidation. However, as long as our cell voltage is limited to 2.8 V vs. Li/Li⁺ during charge, it can be discarded that the cell overcharge is related to membrane oxidation. Thermogravimetric analysis (TGA) of LiTFSI/PEO membrane (**Figure 2.4d**) shows a degradation temperature, *i.e.*, temperature for 95 wt.% weight loss, at 380 °C, which is well above our operation temperature of 70 °C, discarding as well any thermal stability issue.

Differential scanning calorimetry (DSC) in **Figure 2.4e** studies the phase transition dependence of the LiTFSI/PEO membrane with the temperature. Most remarkably, melting point (T_m) of the membrane is determined at 62 °C. Based on the melting enthalpy (ΔH_m) of our sample, and comparing the value with the value for the pure crystalline PEO (196 J g^{-1}),⁷ the crystalline fraction of our sample is determined to be 42%. The presence of a highly crystalline phase in the PEO membrane below T_m is again confirmed, as before by XRD. Finally, Arrhenius plot of conductivity in **Figure 2.4e** shows two different linear tendencies before and after the 60 °C, confirming the location of the T_m around 60 °C. The membrane shows a conductivity of $6.61 \times 10^{-4} \text{ S cm}^{-1}$ at operating temperature of 70 °C, which is considered sufficient for a proper battery operation.

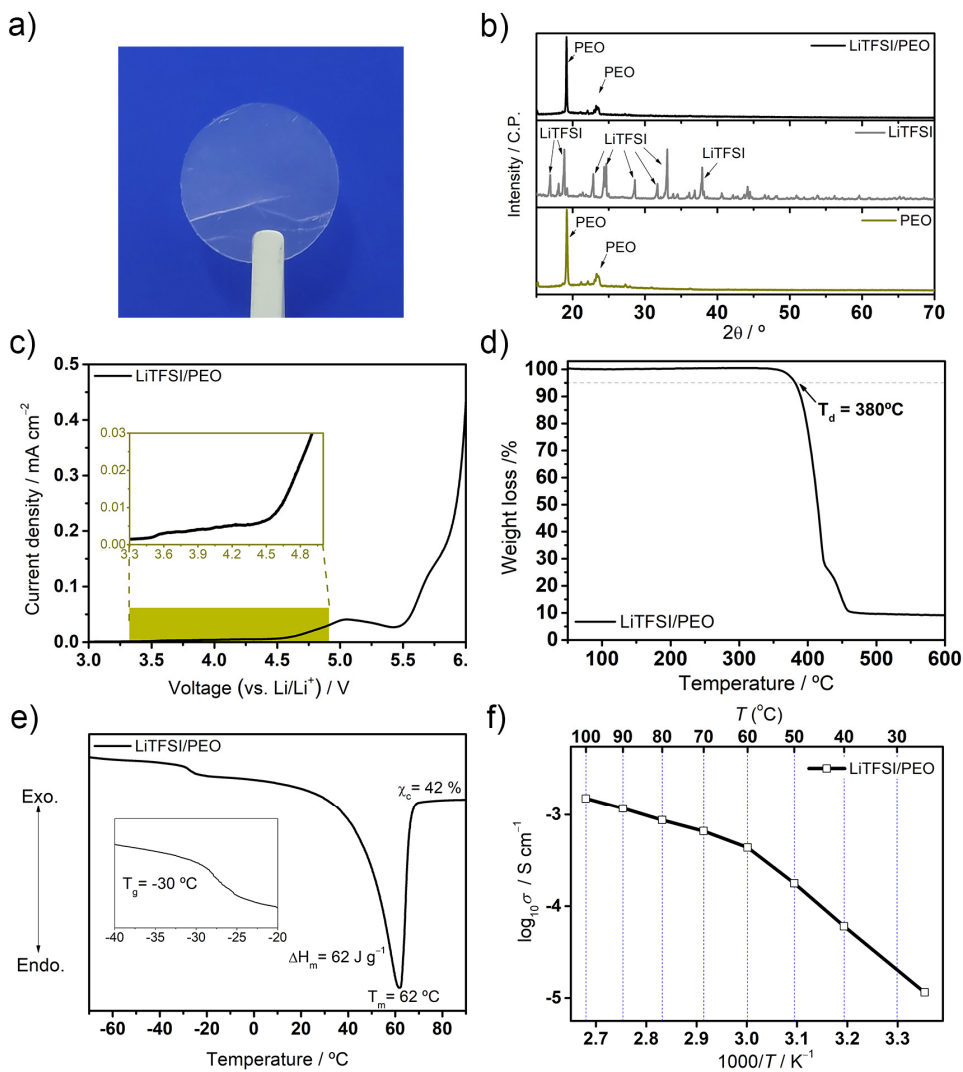


Figure 2.4. Physicochemical and electrochemical properties of LiTFSI/PEO membrane. a) XRD patterns of the pristine PEO, LiTFSI salt, and LiTFSI/PEO membrane. Inset figure shows the optical picture of the prepared membrane. b) Anodic stability test at 70°C , c) TGA traces, and d) Arrhenius plot of conductivity (DSC trace in the inset) of the LiTFSI/PEO membrane. T_d , T_g , T_m , ΔH_m and χ_c refer to degradation, glass transition and melting temperatures, melting enthalpy and crystallinity fraction, respectively.

All the characterized physicochemical and electrochemical properties do not indicate any limitation for ASSLSB battery operation, so the cell failure cannot be ascribed yet to any of the studied properties. Accordingly, the following steps will focus on the compatibility of the LiTFSI/PEO membrane with other ASSLSB cell components, *i.e.*, lithium polysulfides (LiPs) and the Li^0 electrode.

2.2.1.2 Salt stability against LiPSs

Contrary to Li-intercalation batteries, where there is no active material presence out of the positive electrode, LiPS diffusion and shuttle effect is a continuously reported issue in LSBs. At the end of the life of the cell, a visual *post-mortem* analysis was done. For that purpose, the cell was opened and observed to check the possible presence of LiPS in the electrolyte. Optical image in **Figure 2.5a** clearly shows a dark red coloration in the membrane border after cycling, indicating that even SPE may have lower LiPS solubility than liquid electrolytes, these intermediate species are still present in the electrolyte media. This fact has also been recently reported by other groups. For example, Wan et al.⁸ tracked *in-situ* the movement of LiPS in the LiTFSI/PEO electrolyte by optical microscope imaging and further supported by X-ray photoelectron spectroscopy (XPS) and Raman analyses. Another work by Zaghbi and co-workers⁹ studied PEO-based ASSLSBs batteries with *in-situ* scanning electron microscope (SEM) and ultraviolet–visible absorption spectroscopy (UV-VIS), showing clearly that LiPSs were dissolved into the SPE.

This highly reactive agents can irreversibly react with electrolyte salt anion and decompose it, generating degradation issues. Thus, LiTFSI salt compatibility with LiPSs is studied in **Figure 2.5b** and **Figure 2.5c**. 1 M LiTFSI/DME solution was prepared and Li₂S₆ (200:1 LiTFSI:LiPS molar ratio) was added. The color of the final solution was compared to a salt-free DME + LiPS solution (**Figure 2.5b**). Apparently, no color change was observed while both solutions show greenish coloration. The absence of color change was objectively confirmed by UV-VIS measurement in **Figure 2.5c**, and indicates that there is no reaction between the TFSI⁻ anion and the LiPSs. Therefore, cell failure issues cannot be related to this anion instability against reaction intermediates.

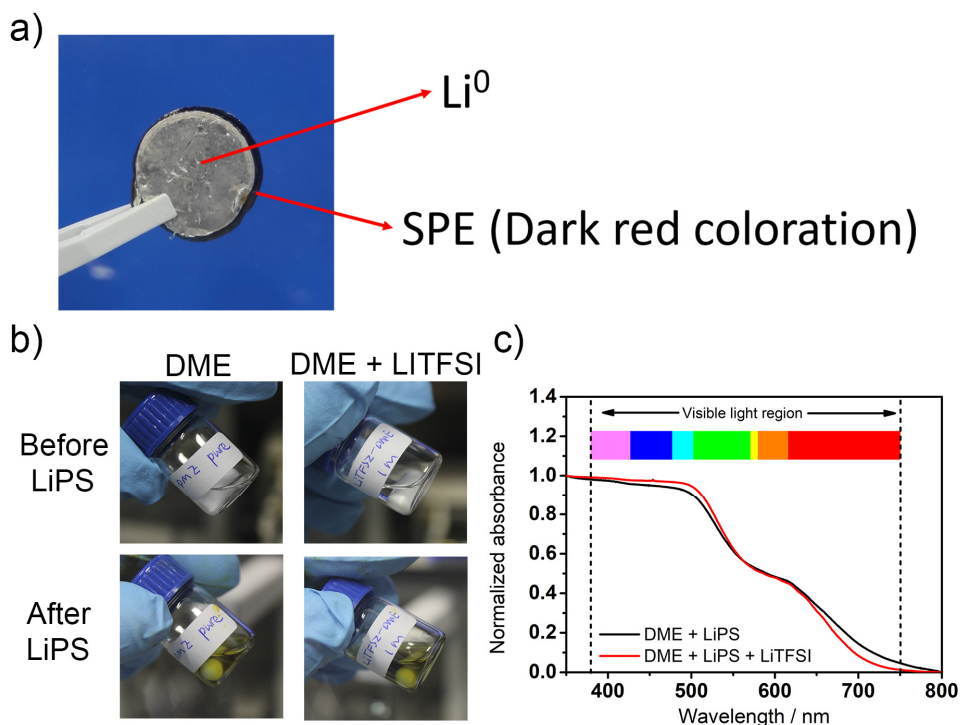


Figure 2.5. Stability of salt anion against LiPS species. a) Optical image of the ASSLSBs cell after failure. b) Appearance of and blank DME and 1 M LiTFSI/DME solution before and after the addition of the LiPS solution (200:1, LiTFSI:LiPS molar ratio) at room temperature. b) Normalized UV-vis absorption spectra of the LiPS-added solutions after 60 h of contact.

2.2.1.3 Electrolyte behavior with the Li⁰ electrode

The use of Li⁰ as negative electrode brings clear beneficial effects in terms of energy density. However, it presents limitations in terms of high reactivity against other cell components, and its ramified deposition may result in lithium dendrites, bringing stability and safety issues. Therefore, it is essential to study membrane stability against Li⁰.

Figure 2.6 presents the electrochemical behavior of metallic electrode in contact with the LiTFSI/PEO electrolyte. **Figure 2.6a** shows galvanostatic cycling of Li⁰ | LiTFSI/PEO | Li⁰ symmetric cells at 0.1 mA cm⁻² for 2 h semicycles at 70 °C. In this test, Li⁺ is stripped from one electrode and plated in the opposite electrode. After 2h, the direction of the current will change, and Li⁺ movement will be reversed. In our system, the voltage response with time demonstrates a stable cell operation at the beginning, which is an indicative of favorable compatibility.

However, after less than 200 h, the cell faces a voltage decay due to a Li^0 dendrite induced short circuit, which is a limited time for real battery performance. Furthermore, before a complete failure related to dendrite induced short-circuit, voltage profile shows some erratic cycles, which are indicative of unstable cycling. Usually, a poor Li^0 /electrolyte compatibility is related to a poor solid/electrolyte interface (SEI) layer, which is formed by reduction products of electrolyte and salt on the metallic surface. It is now generally accepted that the SEI is essential for the successful operation of lithium-based batteries, and its quality is a key factor that determines safety, performance and cycle life on the battery.¹⁰

The direct *post-mortem* study of the formed SEI on Li^0 surface after the cycling in SPE-based cells is not possible due to the strong adhesive properties of the molten PEO-based electrolytes after cycling at 70 °C, which impedes the separation between Li^0 electrode and SPE without any surface damage. Several attempts and methods were tried in order to analyze this system with no further success. Owing to these difficulties, 1,2-dimethoxyethane (DME) was selected as an archetype liquid electrolyte due to its analogous chemical structure to PEO and its ability to dissolve LiTFSI. Hence this strategy was used to analyze the quality of the SEI between Li^0 and electrolyte in presence of LiTFSI salt. **Figure 2.6b** shows SEM pictures of the Li^0 deposits onto Cu foil in the presence of LiTFSI/DME electrolytes after galvanostatic cycling at 0.1 mA cm⁻² for 20 h in a single direction. SEM figures shows non-uniform Li^0 deposits and several needle-like dendritic structures.

XPS data was harvested from the outmost SEI surface of the deposits (**Figure 2.6c**) and the data was fitted and analyzed by Dr. Zhang. Those results show some interesting properties. For example, C1s spectra show peaks at ≈ 288 eV and ≈ 286 eV which are characteristic from C–O containing species, *i.e.*, CH_3O – (R_1C –O) and $\text{H}_2\text{C}=\text{HC}$ –O– CH_3 (R_2C –O), resulting from the electrochemical reduction of DME.¹¹ N1s spectra shows a single peak belonging to unreacted salt and no presence of the other possible reduction products such as Li_3N . Finally, F1s spectra shows that the signal corresponding to the highly protective and desired LiF, which is derived from salt reduction, is weaker than that of species with $-\text{CF}_3$ ending that are related to unreacted salt remainings. These measurements indicate that the SEI is mainly formed by electrolyte reduction products, and that the desirable SEI products that could be obtained by salt reduction, *e.g.*, Li_3N and LiF, are scarce. This can be attributed, once again, to the high stability of the TFSI⁻ anion.

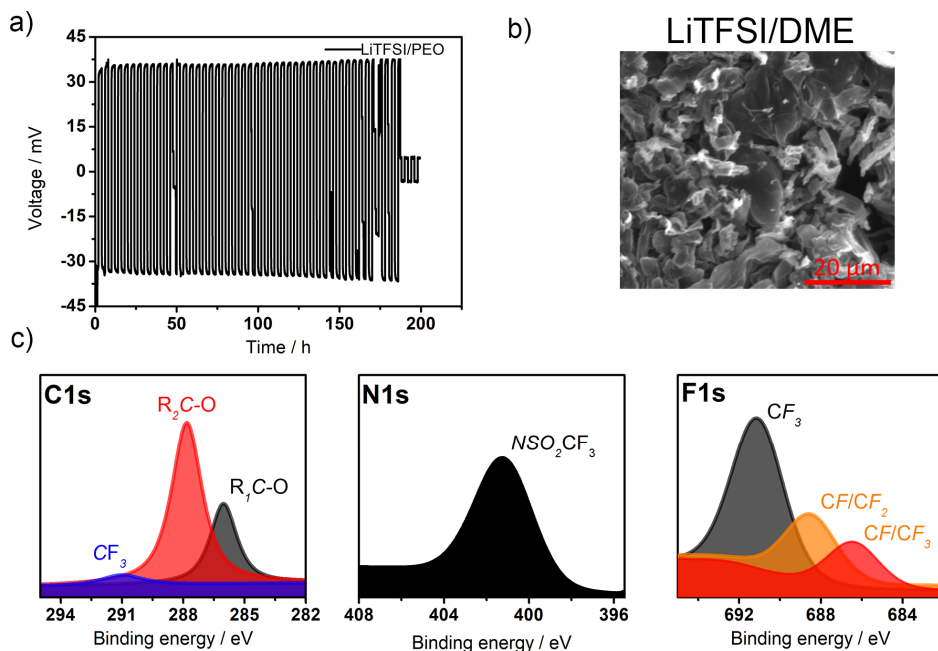


Figure 2.6. Electrochemical behavior of the Li^0 electrode in the as-prepared electrolytes. a) Galvanostatic cycling of $\text{Li}^0 \mid \text{LiTFSI/PEO} \mid \text{Li}^0$ symmetric cells at 0.1 mA cm^{-2} and 2 h semicycles at $70 \text{ }^\circ\text{C}$. b) SEM images and c) XPS spectra of Li^0 deposited onto Cu foil substrates ($\text{Li}^0 \mid \text{LiTFSI/DME} \mid \text{Cu}$ cells) at 0.1 mA cm^{-2} during 20 h at room temperature. $\text{R}_1\text{C-O}$ and $\text{R}_2\text{C-O}$ refer to $\text{CH}_3\text{O-}$ and $\text{H}_2\text{C=HC-O-CH}_3$.

These results prove that the decomposition of LiTFSI containing electrolytes will generate a poor quality SEI layer, mainly dominated by solvent electrolyte reduction products. This SEI layer will not be able to properly passivate the surface of the metal, which can finally result in Li^0 electrode failure due to formation of mossy or dendritic lithium. Furthermore, the presence of soluble LiPSs in the electrolytes makes Li^0 protection especially critical in LSBs due to the reduction reaction of LiPSs on its surface, leading to electrode poisoning and consume of e^- during cell charge, generating overcharge in the so called “polysulfide shuttle effect”. In short, the poor SEI and Li/electrolyte interface is the main reason for the cell failure of the LSBs with LiTFSI/PEO electrolyte. This hypothesis is in good agreement with the performance observed in $\text{Li}^0 \mid \text{LiTFSI/PEO} \mid \text{S}$ cathode full cells described previously.

2.3 DISCUSSION

The calculations based on our viability model show the use of solid-electrolytes in ASSLSBs, especially SPEs and low filler content SCEs, allow the achievement of superior gravimetric energy densities in comparison to LIBs. Furthermore, the modelling has also allowed to verify the proposed electrode recipe, to fix the maximum electrolyte thickness and to set targeted cell performance in 1.2 mAh cm^{-2} .

The first prepared reference cell, based on LiTFSI/PEO electrolyte, shows a poor cyclability, with an instable response to fast charges, or a prompt failure after 15 cycles at low charges. This results are in line with previously reported studies in the State of Art section, which show poor cell performance for SPEs in general and for LiTFSI/PEO electrolytes in particular. Even if in one specific case, the recent study from Ma *et al.*⁶ a more stable cycling is reported for a similar LiTFSI/PEO electrolyte, the delivered discharge capacity is lower than that of our system, which results in diminished LiPS generation, and the cathode recipe is more optimized, which can help to improve their retention. This will finally lead to a diminished shuttle effect.

In order to identify the failure mechanisms of our system, different characterization of the membranes and their components were carried out. Physicochemical and electrochemical characterization of the membrane showed adequate properties for cell cycling. The reactivity test did not reveal any evidence of undesired side reactions, but, LiPS presence in the membrane was identified after cycling.

Furthermore, the study of the LiTFSI/PEO membrane compatibility with Li^0 electrode revealed their poor compatibility. Therefore, the cell failure is undoubtedly related to a poor Li^0 /SPE compatibility, which forms a low quality SEI layer on the metallic negative electrode. During discharge, soluble LiPS intermediates are generated in the positive electrode, which can be dissolved in the electrolyte and diffuse to the negative electrode. During charge, those soluble intermediates will react with the ineffectively protected Li^0 and consume an excess of e^- , leading to cell overcharge. The cell failure mechanism is schematically represented in **Figure 2.7**.

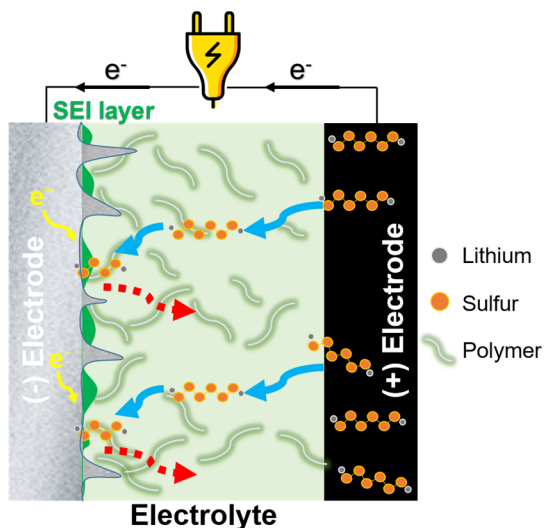


Figure 2.7. Schematic representation of the failure mechanism in LiTFSI/PEO electrolyte containing ASSLSB.

2.4 CONCLUSIONS

The energy density modelling allowed to confirm that by the use SPEs, ASSLSBs have the potential to obtain superior gravimetric energy density values in comparison with LIBs. Furthermore, the calculations allowed to verify cell parameters and set targeted performances.

After the assembly of the first LiTFSI/PEO-based ASSLSBs reference cell, it can be concluded that the system delivers poor performance due to the poor quality of the Li^0/SPE interface, which finally leads to shuttle-effect related overcharge. Thus, the search of disruptive advances in alternative electrolyte composition will be the motivation of the thesis.

This work will explore different strategies to overcome these limitations using various electrolyte additives, electrolyte fillers, alternative imide-containing salts and novel fluorine-free salts that allow successful ASSLSBs operation. These different strategies will be respectively divided into different chapters.

2.5 REFERENCES

- (1) Li, C.; Zhang, H.; Otaegui, L.; Singh, G.; Armand, M.; Rodriguez-Martinez, L. M. Estimation of Energy Density of Li-S Batteries with Liquid and Solid Electrolytes. *J. Power Sources* **2016**, *326*, 1–5.
- (2) Judez, X.; Eshetu, G. G.; Li, C.; Rodriguez-Martinez, L. M.; Zhang, H.; Armand, M. Opportunities for Rechargeable Solid-State Batteries Based on Li-Intercalation Cathodes. *Joule* **2018**, *2* (11), 2208–2224.
- (3) Judez, X.; Zhang, H.; Li, C.; Eshetu, G. G.; González-Marcos, J. A.; Armand, M.; Rodriguez-Martinez, L. M. Review—Solid Electrolytes for Safe and High Energy Density Lithium-Sulfur Batteries: Promises and Challenges. *J. Electrochem. Soc.* **2018**, *165* (1), A6008–A6016.
- (4) Marmorstein, D.; Yu, T. .; Striebel, K. .; McLarnon, F. .; Hou, J.; Cairns, E. . Electrochemical Performance of Lithium/Sulfur Cells with Three Different Polymer Electrolytes. *J. Power Sources* **2000**, *89* (2), 219–226.
- (5) Lin, Y.; Wang, X.; Liu, J.; Miller, J. D. Natural Halloysite Nano-Clay Electrolyte for Advanced All-Solid-State Lithium-Sulfur Batteries. *Nano Energy* **2017**, *31* (July 2016), 478–485.
- (6) Ma, Q.; Qi, X.; Tong, B.; Zheng, Y.; Feng, W.; Nie, J.; Hu, Y.-S.; Li, H.; Huang, X.; Chen, L.; et al. Novel Li[(CF₃SO₂)(n-C₄F₉SO₂)_n]-Based Polymer Electrolytes for Solid-State Lithium Batteries with Superior Electrochemical Performance. *ACS Appl. Mater. Interfaces* **2016**, *8* (43), 29705–29712.
- (7) Zardalidis, G.; Mars, J.; Allgaier, J.; Mezger, M.; Richter, D.; Floudas, G. Influence of Chain Topology on Polymer Crystallization: Poly(Ethylene Oxide) (PEO) Rings vs. Linear Chains. *Soft Matter* **2016**, *12* (39), 8124–8134.
- (8) Song, Y.-X.; Shi, Y.; Wan, J.; Lang, S.-Y.; Hu, X.-C.; Yan, H.-J.; Liu, B.; Guo, Y.-G.; Wen, R.; Wan, L.-J. Direct Tracking of the Polysulfide Shuttling and Interfacial Evolution in All-Solid-State Lithium–Sulfur Batteries: A Degradation Mechanism Study. *Energy Environ. Sci.* **2019**, *12* (8), 2496–2506.
- (9) Marceau, H.; Kim, C.-S.; Paoella, A.; Ladouceur, S.; Lagacé, M.; Chaker, M.; Vijh, A.; Guerfi, A.; Julien, C. M.; Mauger, A.; et al. In Operando Scanning Electron Microscopy and Ultraviolet–Visible Spectroscopy Studies of Lithium/Sulfur Cells Using All Solid-State Polymer Electrolyte. *J. Power Sources* **2016**, *319*, 247–254.
- (10) Peled, E.; Menkin, S. Review—SEI: Past, Present and Future. *J. Electrochem. Soc.* **2017**, *164* (7), A1703–A1719.
- (11) Aurbach, D. Identification of Surface Films Formed on Lithium in Dimethoxyethane and Tetrahydrofuran Solutions. *J. Electrochem. Soc.* **1988**, *135* (8), 1863.

Chapter 3:

Electrolyte additives

The present chapter explores for the first time the implementation of electrolyte additives into solid polymer electrolytes, in order to improve the cycling stability of our all-solid-state battery. Two additives are explored, including state-of-art LiNO_3 , and the newly proposed LiN_3 , which brings improved metallic lithium/electrolyte interfacial stability due to the generation of a highly protective and conductive Li_3N -based protective layer on the metallic electrode. The use of both additives enable a more stable and longer cell cycling, which highlights the importance on lithium protection.

INDEX

3	ELECTROLYTE ADDITIVES	79
3.1	PHYSICOCHEMICAL AND ELECTROCHEMICAL PROPERTIES	80
3.2	ELECTROCHEMICAL BEHAVIOR WITH Li^0	82
3.3	ELECTROCHEMICAL PERFORMANCE	86
3.4	DISCUSSION	87
3.5	CONCLUSIVE REMARKS	88
3.6	REFERENCES	88

3 ELECTROLYTE ADDITIVES

The use of electrolyte additives (additional elements in <5-10 % concentration, either in mass or volume) are one of the most enabling, cost effective and versatile strategies to improve cell performance. Additives can be tailored to tackle specific issues of lithium-sulfur batteries (LSBs). For example, regarding to limitations on the positive electrode, several electrolyte additives have been proposed to improve Li_2S utilization,¹⁻³ to act as redox mediators,⁴⁻⁶ or to form protective layers on it.^{1,7} Regarding general battery performance, a wide variety of electrolyte additives can effectively limit self-discharge,⁸⁻¹⁰ or act as flame-retardants.¹¹⁻¹³

Previous chapter highlighted that in order to develop a solid polymer electrolyte (SPE)-based all-solid-state lithium-sulfur batteries (ASSLSBs), the protection of metallic lithium (Li^0) electrode is of paramount importance to avoid early cell failure. The properties of the solid/electrolyte interface (SEI) layer on negative electrode/electrolyte interface play a vital role in dictating overall performance and stability, and its nature is highly dependent on a number of parameters, such as precycling conditions, composition of the native passivation layer, electrolyte impurities, electrolyte salts, or the presence of additives. Among all these factors, selection of additives is one of the most enabling and versatile approaches to boost the properties of Li^0 /electrolyte interface. A good additive for forming SEI films on Li^0 electrode should fulfil the following requirements: i) possess preferential reactions with Li^0 compared to other electrolyte components, ii) generate decomposition products that feature high ionic conductivity and remain stable towards other battery components, iii) generate a homogeneous coverage on Li^0 (it is essential that equivalent volume of SEI building materials is larger than the metallic anode itself).¹⁴

Among all additives, the use of LiNO_3 in LSBs clearly stands out after its recommendation by Aurbach et al.,¹⁵ which set a precedent in electrolyte recipe formulation. On the negative electrode side, the reduction of LiNO_3 leads mainly to the electrode protection by the formation of Li_xNO_y species,¹⁵ but can also lead to the formation of other products such as Li_2O or NO_2 radical,^{16,17}. However, the generated film has been proven to grow indefinitely with the continuous consumption of the additive,¹⁸ and oxidize sulfide species, which in some cases can form insoluble Li_xSO_y species.¹⁵ Thus, even if the use of LiNO_3 is effective, alternative additives have been widely investigated, *e.g.*, P_2S_5 sulfide has been identified to form a passivation layer on Li^0 , with the major product being conductive Li_3PS_4 ;¹⁹ controlled trace amounts of water have been demonstrated to generate LiOH rich SEI films;²⁰ or the presence of LiI yielded a very smooth surface on negative electrode without dendrites or Li_2S presence after cycling.¹

Among different SEI forming products, polycrystalline Li_3N is considered as a highly desired SEI-building candidate to protect Li^0 due to its high conductivity, *i.e.*, $6 \times 10^{-3} \text{ S cm}^{-1}$ at 25°C for a single-crystal, and superior stability against Li^0 .²¹ Furthermore, one of the requirements for a good SEI-building material is to have a higher equivalent volume compared to Li^0 ($12.99 \text{ cm}^3 \text{ mol}^{-1}$).¹⁴ In this regard, Li_3N ($26.8 \text{ cm}^3 \text{ mol}^{-1}$) is preferable than other desired SEI products, *e.g.*, LiF ($9.8 \text{ cm}^3 \text{ mol}^{-1}$). Different routes have been proposed to obtain Li_3N on the surface of negative Li^0 electrodes. Wu *et al.*²² obtained it by direct controlled reaction of Li^0 and N_2 gas. Baloch *et al.*²³ proposed a different approach with the use of azidotrimethylsilane $[(\text{CH}_3)_3\text{SiN}_3]$ electrolyte additive for an *in-situ* Li_3N layer formation.

This chapter will focus on the in the addition of 2 wt.% of two different electrolyte additives to the SPE membranes, with the aim of stabilizing negative electrode operation and allowing the stable cycling of SPE-based ASSLSBs. Apart from studying the effect of conventional LiNO_3 additive, never studied before in SPE-based ASSLSBs, lithium azide (LiN_3), a novel Li_3N forming additive, is proposed and its working mechanism is studied in detail. This novel work provides for the first time the study of additive addition to SPE for ASSLSBs. Firstly, the physicochemical and electrochemical properties of the prepared membranes and their compatibility with Li^0 will be studied, with due attention to the effect of the additives. Then, those membranes will be implemented in ASSLSBs, and the role and working mechanism of the additives will be studied.

3.1 PHYSICOCHEMICAL AND ELECTROCHEMICAL PROPERTIES

To prepare SPE membranes, 2 wt.% of the additive was added to the electrolyte slurry, and the membrane was obtained again by solvent casting method, following the procedures described in the section 3 in the Appendix. **Figure 3.1a** shows that after the addition of the additives translucent and self-standing membranes are obtained, which indicates that the presence of the additive does not affect mechanical properties of the membrane. The X-ray diffraction (XRD) patterns of the bare poly(ethylene oxide) PEO, pristine LiTFSI salt, LiNO_3 and LiN_3 additives, and additive containing membranes are shown in **Figure 3.1b**. Both additive containing membranes present only characteristic diffraction peaks that belong to the crystalline phase of the pure PEO at $2\theta = 19^\circ$ and 23° , and no peak from pristine LiTFSI or additives was observed, indicating their full solvation in PEO, as desired.

The sweep voltammetry test for LiNO_3 -added electrolyte in **Figure 3.1c** shows typical behavior for a PEO-based membrane, with an initial PEO oxidation starting at $3.8 \text{ V vs. Li/Li}^+$, and a further strong oxidation related to TFSI⁻ salt anion at

5-5.5 V vs. Li/Li^+ . This proved that the addition of the additive does not remarkably affect membrane resistance to oxidation. In contrast, LiN_3 containing membrane present a mild oxidation peak at around 3.7 V vs. Li/Li^+ . However, in global, the anodic stability of this membrane is not remarkably affected by the presence of LiN_3 . Thermal stability is neither affected by the addition of the additives, as shown by TGA traces in **Figure 3.1d**, that displays an unchanged degradation temperature, T_g , after the addition of the additives.

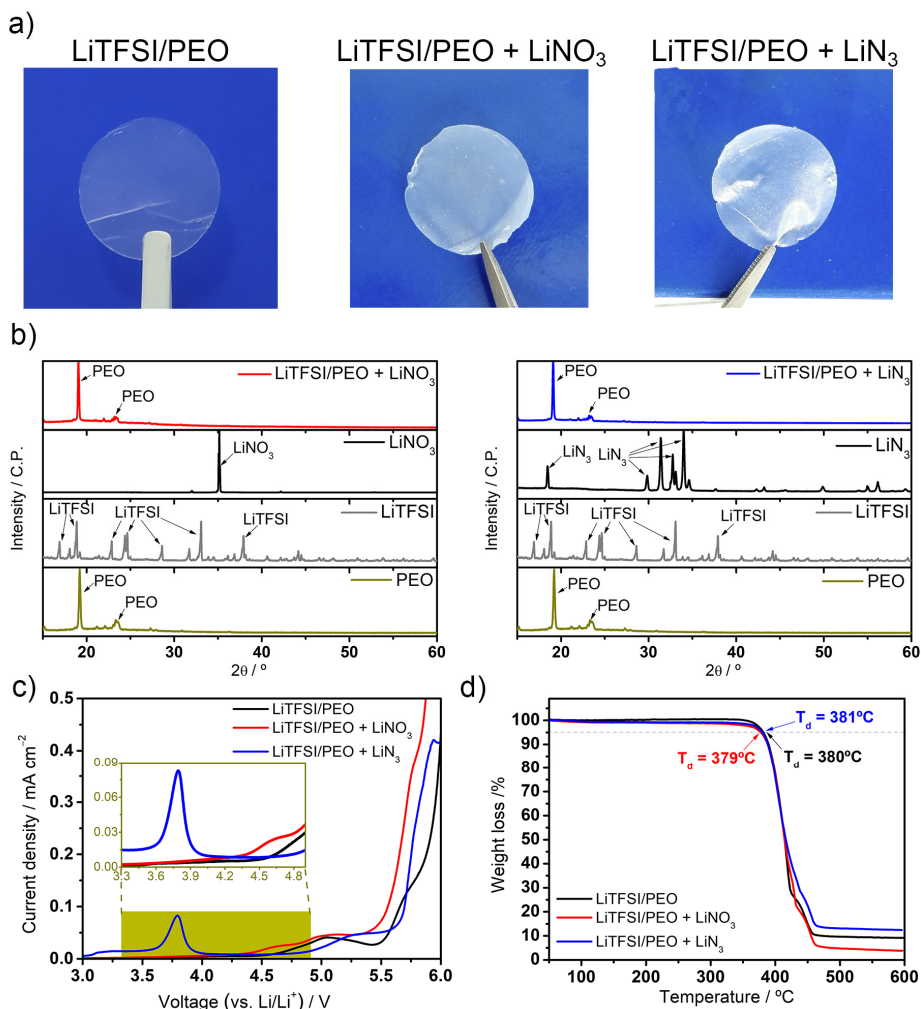


Figure 3.1. Physicochemical and electrochemical properties of LiTFSI/PEO reference and additive containing membranes. a) Optical images, b) XRD patterns, c) anodic stabilities at 70 $^\circ\text{C}$, and d) TGA traces.

Figure 3.2a shows differential scanning calorimetry (DSC) traces of the membranes, which show similar thermal transition for the additive-free and additive-containing membranes. The additive containing membranes have a similar glass transition temperature (T_g), and melting point (T_m), and slightly decreased melting enthalpy (ΔH_m) and crystallinity (χ_c). This is in good agreement with conductivity values of **Figure 3.2b**, with not remarkably affected conductivity values after the addition of both additives. The minor reduction in conductivity can be ascribed to hindered PEO chain mobility in the presence of additives. The conductivity is again acceptable above T_m , reaching in any case values above 10^{-4} S cm^{-1} .

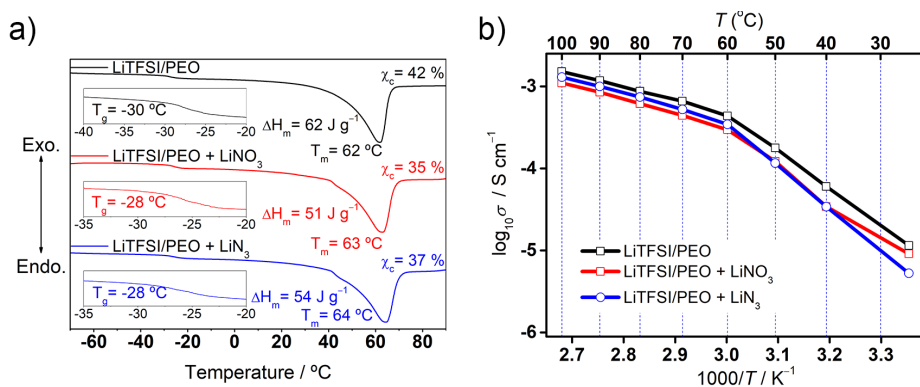


Figure 3.2. Physicochemical and electrochemical properties of LiTFSI/PEO reference and additive containing membranes. a) DSC traces and b) Arrhenius plots of ionic conductivity. T_d , T_g , T_m , ΔH_m and χ_c refer to degradation, glass transition and melting temperatures, melting enthalpy and crystallinity fraction, respectively.

In conclusion, additives have been completely solvated in PEO matrix and self-standing membranes have been obtained. Those membranes possess similar thermal and electrochemical properties compared to reference additive free membrane, and none of the properties have been compromised after the inclusion of the additives.

3.2 ELECTROCHEMICAL BEHAVIOR WITH Li^0

As demonstrated in the previous chapter, the compatibility of the SPE with Li^0 electrode is of paramount importance for the stable cycling of ASSLSBs. **Figure 3.3** studies the electrochemical behavior of the Li^0 electrode in contact with the additive containing electrolytes. **Figure 3.3a** shows galvanostatic cycling of $\text{Li}^0 | \text{SPE} | \text{Li}^0$ cells, at 0.1 mA h cm^{-2} and 2 h semicycles. While the reference LiTFSI/PEO faces a dendrite induced short circuit after less than 200 h of Li^+ plating and stripping, LiNO_3 added membrane can operate for almost 300 h.

Remarkably, LiN_3 containing membrane can operate for around 450 h, before the excessively low voltage of the cell indicates a possible short circuit. The improvement of the operation time is related to the better quality and mechanical stability of the SEI layer. The addition of both additives does not only increase the cycling life of the plating/stripping test, but also reduces the voltage hysteresis compared to blank electrolytes, which according to Ohm's law indicates a decrease on the total resistance of the symmetric cell. This is related to a decreased interfacial resistance due to higher conductivity of the reduced components in the SEI layer.

Unfortunately, the direct *post-mortem* analysis of the SEI layer formed on the top of Li^0 is again not possible in SPE based system, so 1,2-dimethoxyethane (DME) has been used as archetype electrolyte. **Figure 3.3b** indicates that the galvanostatic cycling of the cells with liquid electrolytes at 25 °C display the same tendency as SPE based ones, *i.e.*, extended cycle life and reduced overpotential. Remarkably, LiN_3 -containing cell shows again the lowest overpotential. **Figure 3.3c** includes scanning electron microscopy (SEM) images and X-ray photoelectron spectroscopy (XPS) spectra of the Li^0 deposits on Cu foil after 20 h of galvanostatic test at 25 °C for the reference DME-based electrolyte and for the additive added electrolytes. Both additives have a remarkable effect on Li^0 morphology. While reference electrolyte shows several needle-like structures, additive-added electrolytes, especially LiN_3 -added electrolyte possess flat, uniform and smooth structures, indicating the presence of homogeneous Li^0 deposits and of a robust SEI layer.

In order to deepen into the SEI study, the XPS analysis of the outermost surface of the Li^0 deposits was performed. The F1s spectra of the samples shows for all the systems two peaks corresponding to LiF and $-\text{CF}_3$, the first coming from the final salt reduction products, and the latest coming from residual LiTFSI salt or from its initial reduction products, such as $\text{Li}_2\text{NSO}_2\text{CF}_3$.²⁴ From the intensity of the peaks, it is surprising that LiNO_3 added electrolyte contains more LiF than LiN_3 added one. The fact that LiNO_3 promotes salt reduction needs to be further studied to draw a conclusion. However, the most distinguishing feature comes from the N1s spectra, where the effect of the additives is strongly evidenced. While the reference LiTFSI/DME only shows a single peak related residual LiTFSI or its reduction derivatives, the additive containing electrolytes show additional peaks. In LiNO_3 containing electrolyte, the dominant peak is assigned to R_2NO^- oxygen containing species, with an important presence of Li_3N product. On the contrary, in LiN_3 added electrolyte, Li_3N is found to be the most predominant SEI species. As stated in the introduction, Li_3N is highly conductive and hence desired SEI forming product, and the use of LiN_3 additive has been effectively proven to provide a high quality SEI with such desired product as dominant species.

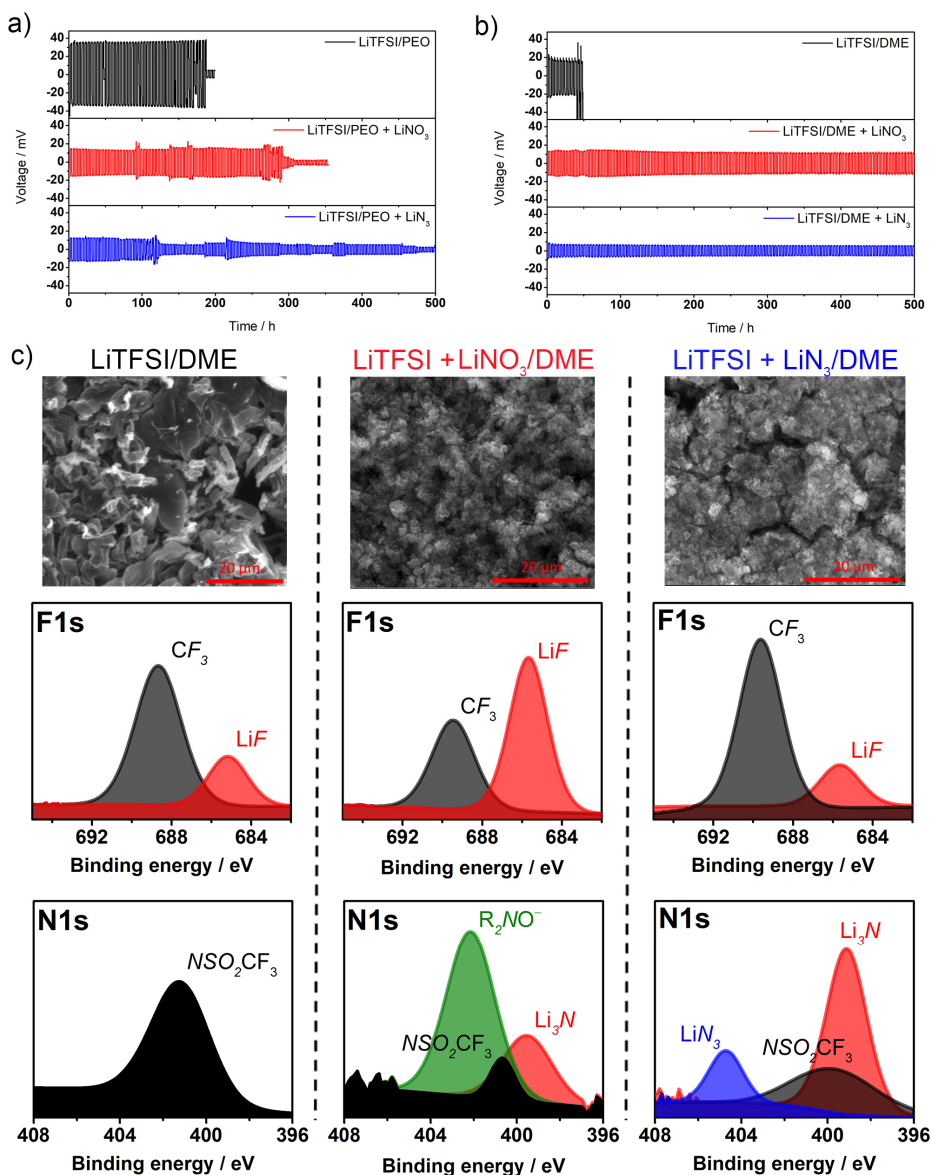
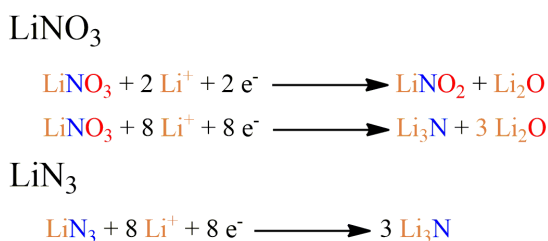


Figure 3.3. Electrochemical behavior of Li^0 electrode in the as-prepared electrolytes. a) Galvanostatic cycling of $\text{Li}^0|\text{SPE}|\text{Li}^0$ symmetric cells at 0.1 mA cm^{-2} and 2 h semicycles at 70 °C. b) Galvanostatic cycling of $\text{Li}^0|\text{DME}+\text{LiTFSI}+\text{additive}|\text{Li}^0$ symmetric cells at 0.1 mA cm^{-2} and 2 h semicycles at 25 °C. c) Optical and SEM images of Li^0 deposited onto

Cu substrates ($\text{Li}^0|\text{DME}+\text{SALT}|\text{Cu foil}$) at 0.1 mA cm^{-2} during 20 h at $25 \text{ }^\circ\text{C}$, and their corresponding XPS spectra. R_2 refers to organic moieties.

In order to shed light on the interaction between the salts and the additives with the Li^0 , chemical simulation of neat LiTFSI, LiNO_3 and Li_3N were carried out in collaboration with Dr. Eshetu. For that purpose, solutions of byphenyl radical anion (*ca.*, $0.4 \text{ V vs. Li/Li}^+$) and byphenyl radical di-anion (*ca.*, 0 V vs. Li/Li^+) were prepared in tetrahydrofuran solvent, by tuning byphenyl: Li^0 ratio. By changing the amount of byphenyl radicals to additives, reduction reactions involving different e^- amount can be simulated. When a reaction occurs, it can be confirmed by color change in solution. While LiNO_3 can easily get reduced at $0.4 \text{ V vs. Li/Li}^+$, Li_3N can only get reduced at potentials close to 0 V vs. Li/Li^+ , both via $8 e^-$ reduction. Therefore, we propose the following reaction mechanism:



Scheme 3.1. Proposed reactions mechanism between the additives and the Li^0 negative electrode.

According to this, the reduction of LiN_3 leads to Li_3N as unique product, while the reduction of LiNO_3 finally leads to Li_3N and much less conductive Li_2O ($<10^{-7} \text{ S cm}^{-1}$ at $25 \text{ }^\circ\text{C}$).²⁵ This explains the improved performance and lower overpotential of LiN_3 containing cells during the galvanostatic cycling symmetric cells.

Remarkably, during cell operation in Li^0 -based batteries, while additives get reduced on Li^0 surface, they can be oxidized as well on positive electrode surface during charge at sufficient cell voltage. As proven in **Figure 3.1c**, LiN_3 can be oxidized at above $3.7 \text{ V vs. Li/Li}^+$. Oxidation of LiN_3 additive on the positive electrode would lead to the formation of N_2 , which would later migrate to the anode side, reacting with Li^0 and generating further Li_3N . Due to the upper limited voltage, this will not happen in LSBs, but can occur when Li^0 is paired with intercalation materials, *e.g.*, LiCoO_2 or $\text{LiNi}_x\text{Mn}_y\text{Co}_z\text{O}_2$.

3.3 ELECTROCHEMICAL PERFORMANCE

Finally, due to the significant effect of the additives in Li^0 stabilization, the feasibility of conventional LiNO_3 and LiN_3 to improve the cell stability in SPE-based ASSLSBs has been studied. **Figure 3.4a** shows discharge capacity and Coulombic efficiency for the reference cell and the cells containing additives. The addition of either LiNO_3 or LiN_3 decreases delivered capacity from 700 mAh g^{-1} of the reference cell to $550\text{-}570 \text{ mAh g}^{-1}$ for the additive containing cells at 0.1C . However both cells show no capacity fade for at least 30 cycles. More remarkably, the Coulombic efficiency values are clearly improved, enabling stable cycling with efficiency values close to 100% for about 30 cycles, thanks to an effective Li^0 protection. **Figure 3.4b** displays discharge/charge profiles for the LiN_3 added ASSLSB. It shows stable profiles with the absence of overcharge for the 1st and 10th cycles. 30th cycle shows some mild overcharge (Coulombic efficiency values of *ca.* 90%), but in contrast to reference cell, it does not show abrupt charge capacity increase, which enables stable cycling and avoids a fast cell failure.

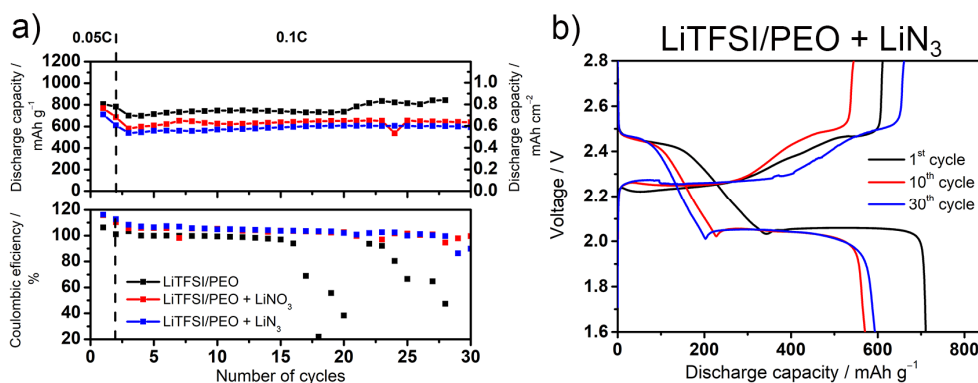


Figure 3.4. a) Discharge capacity and Coulombic efficiency of $\text{Li}^0|\text{SPE}$ (LiTFSI/PEO without and with LiNO_3 or LiN_3)|S electrode at a constant rate of 0.1C , after two initial cycles at 0.05C . b) Discharge/charge profiles of $\text{Li}^0|\text{LiTFSI/PEO} + \text{LiN}_3|\text{S}$ cell during 1st, 10th, and 30th cycles. All the measurements were done at 70°C .

The feasibility of conventional LiNO_3 and novel LiN_3 electrolyte additives has been proven for the stabilization of SPE-based ASSLSBs, both showing similar performance, and enabling doubling cell lifespan, with absence of overcharge during 30 cycles. This work proves for the first time the suitability of additive addition to SPEs in order to improve cycling stability of ASSLSBs.

3.4 DISCUSSION

Additive containing membranes were successfully obtained, with regard to the full solvation of the additives and the conservation of the self-standing properties. Characterizations revealed that the additive did not affect remarkably the physicochemical and electrochemical properties of the membrane. In contrast, the main influence of the additives was identified to be on the composition of the SEI layer on the Li^0 . The presence of both additives allowed to extend the cycle life of the symmetric Li^0 cells and reduced cell resistance, indicating a more favorable SEI formation. This SEI was found by XPS to consist of Li_3N in the case of LiN_3 , and of Li_3N and other oxygen containing groups in presence of LiNO_3 .

This improved quality of the SEI enabled more stable ASSLSB cycling. Even if the delivered discharge capacity of the cells was decreased around 20% after the addition of either additives, the additive presence allowed 30 stable cycles with Coulombic efficiency values close to 100%.

This work studied the implementation of additives in SPE membranes for ASSLSBs for the first time. The obtained results show a more stable performance compared to previous works, with especial attention to the flat evolution of Coulombic efficiency values, showing no presence of severe efficiency drops, in contrast to the reference cell and other publications (see **Table 3.1**).

Table 3.1. Comparison of the results of the present chapter and the previous works. The reference number refers to State of Art section. LiTf refers to lithium trifluoromethanesulfonate.

Ref.	Electrolyte recipe	Cycle life	End of life capacity / mAh g^{-1}	Coulombic efficiency evolution
S19	LiTFSI/PEO	20	70	No info.
S20	LiTf/PEO	10	200	No info.
S24	LiTFSI/PEO	40	600	No info
S25	LiClO_4 /PEO	30	600	Dramatic early drop
Our reference	LiTFSI/PEO	15	740	Dramatic drop
This work	LiTFSI/PEO + LiNO_3	<u>30</u>	570	<u>Flat evolution around 100%</u>
This work	LiTFSI/PEO + Li_3N	<u>30</u>	550	<u>Flat evolution around 100%</u>

However, the State of Art analysis also suggests that the performance of the cell could be further improved by the use of solid composite electrolytes. Thus, this option will be explored in the next chapter.

3.5 CONCLUSIVE REMARKS

In conclusion, this work sets a precedent in the incorporation of additives to SPEs for ASSLSBs. The use of electrolyte additives has been demonstrated to be a simple, viable and effective approach to circumvent the stability problems related to Li^0/SPE interfacial compatibility, by the generation of protective SEI with more desirable properties. Furthermore, the work in this chapter confirms the hypothesis of the former one, *i.e.*, the Li^0/SPE interface plays a pivotal role in ASSLSBs performance, and its stabilization will allow extending the lifespan of the cell.

On the one hand, conventional LiNO_3 electrolyte additive has been successfully implemented for the first time in SPE-based ASSLSBs, enabling the stabilization of the Li^0 electrode. On the other hand, Li_3N has been identified for the first time as a novel electrolyte additive for ASSLSBs. Even if the cells based on either additive feature a similar performance, enabling the ASSLSB cycling with high Coulombic efficiency by the formation of a uniform and dendrite-free SEI, the SEI in presence of the latter additive is richer in highly conductive and high molar volume Li_3N . Despite the fact that the delivered cell capacity decreased a 20% in the presence both additives, the doubling of cell lifetime outweighs this loss. This work was published by our group.²⁶

3.6 REFERENCES

- (1) Wu, F.; Lee, J. T.; Nitta, N.; Kim, H.; Borodin, O.; Yushin, G. Lithium Iodide as a Promising Electrolyte Additive for Lithium-Sulfur Batteries: Mechanisms of Performance Enhancement. *Adv. Mater.* **2015**, *27* (1), 101–108.
- (2) Zu, C.; Klein, M.; Manthiram, A. Activated Li_2S as a High-Performance Cathode for Rechargeable Lithium–Sulfur Batteries. *J. Phys. Chem. Lett.* **2014**, *5* (22), 3986–3991.
- (3) Pan, H.; Han, K. S.; Vijayakumar, M.; Xiao, J.; Cao, R.; Chen, J.; Zhang, J.; Mueller, K. T.; Shao, Y.; Liu, J. Ammonium Additives to Dissolve Lithium Sulfide through Hydrogen Binding for High-Energy Lithium–Sulfur Batteries. *ACS Appl. Mater. Interfaces* **2017**, *9* (5), 4290–4295.
- (4) Meini, S.; Elazari, R.; Rosenman, A.; Garsuch, A.; Aurbach, D. The Use of Redox Mediators for Enhancing Utilization of Li_2S Cathodes for Advanced Li-S Battery Systems. *J. Phys. Chem. Lett.* **2014**, *5* (5), 915–918.
- (5) Hernández, G.; Lago, N.; Shanmukaraj, D.; Armand, M.; Mecerreyes, D. Polyimide-Polyether Binders–Diminishing the Carbon Content in Lithium–Sulfur Batteries. *Mater. Today Energy* **2017**, *6*, 264–270.
- (6) Liu, M.; Ren, Y. X.; Jiang, H. R.; Luo, C.; Kang, F. Y.; Zhao, T. S. An Efficient

- Li₂S-Based Lithium-Ion Sulfur Battery Realized by a Bifunctional Electrolyte Additive. *Nano Energy* **2017**, *40* (August), 240–247.
- (7) Wu, F.; Thieme, S.; Ramanujapuram, A.; Zhao, E.; Weller, C.; Althues, H.; Kaskel, S.; Borodin, O.; Yushin, G. Toward In-Situ Protected Sulfur Cathodes by Using Lithium Bromide and Pre-Charge. *Nano Energy* **2017**, *40* (August), 170–179.
- (8) Azimi, N.; Xue, Z.; Rago, N. D.; Takoudis, C.; Gordin, M. L.; Song, J.; Wang, D.; Zhang, Z. Fluorinated Electrolytes for Li-S Battery: Suppressing the Self-Discharge with an Electrolyte Containing Fluoroether Solvent. *J. Electrochem. Soc.* **2015**, *162* (1), A64–A68.
- (9) Lacey, M. J.; Yalamanchili, A.; Maibach, J.; Tengstedt, C.; Edström, K.; Brandell, D. The Li–S Battery: An Investigation of Redox Shuttle and Self-Discharge Behaviour with LiNO₃-Containing Electrolytes. *RSC Adv.* **2016**, *6* (5), 3632–3641.
- (10) Kazazi, M.; Vaezi, M. R.; Kazemzadeh, A. Improving the Self-Discharge Behavior of Sulfur-Polypyrrole Cathode Material by LiNO₃ Electrolyte Additive. *Ionics (Kiel)*. **2014**, *20* (9), 1291–1300.
- (11) Jia, H.; Wang, J.; Lin, F.; Monroe, C. W.; Yang, J.; NuLi, Y. TPPi as a Flame Retardant for Rechargeable Lithium Batteries with Sulfur Composite Cathodes. *Chem. Commun.* **2014**, *50* (53), 7011–7013.
- (12) Wang, J.; Lin, F.; Jia, H.; Yang, J.; Monroe, C. W.; NuLi, Y. Towards a Safe Lithium-Sulfur Battery with a Flame-Inhibiting Electrolyte and a Sulfur-Based Composite Cathode. *Angew. Chemie Int. Ed.* **2014**, *53* (38), 10099–10104.
- (13) Lin, F.; Wang, J.; Jia, H.; Monroe, C. W.; Yang, J.; NuLi, Y. Nonflammable Electrolyte for Rechargeable Lithium Battery with Sulfur Based Composite Cathode Materials. *J. Power Sources* **2013**, *223*, 18–22.
- (14) Peled, E.; Menkin, S. Review—SEI: Past, Present and Future. *J. Electrochem. Soc.* **2017**, *164* (7), A1703–A1719.
- (15) Aurbach, D.; Pollak, E.; Elazari, R.; Salitra, G.; Kelley, C. S.; Affinito, J. On the Surface Chemical Aspects of Very High Energy Density, Rechargeable Li–Sulfur Batteries. *J. Electrochem. Soc.* **2009**, *156* (8), A694.
- (16) Jaumann, T.; Balach, J.; Klose, M.; Oswald, S.; Eckert, J.; Giebeler, L. Role of 1,3-Dioxolane and LiNO₃ Addition on the Long Term Stability of Nanostructured Silicon/Carbon Anodes for Rechargeable Lithium Batteries. *J. Electrochem. Soc.* **2016**, *163* (3), A557–A564.
- (17) Etacheri, V.; Geiger, U.; Gofer, Y.; Roberts, G. A.; Stefan, I. C.; Fasching, R.; Aurbach, D. Exceptional Electrochemical Performance of Si-Nanowires in 1,3-Dioxolane Solutions: A Surface Chemical Investigation. *Langmuir* **2012**, *28* (14), 6175–6184.
- (18) Zhang, S. S. Role of LiNO₃ in Rechargeable Lithium/Sulfur Battery. *Electrochim. Acta* **2012**, *70*, 344–348.
- (19) Lin, Z.; Liu, Z.; Fu, W.; Dudney, N. J.; Liang, C. Phosphorous Pentasulfide as a Novel Additive for High-Performance Lithium-Sulfur Batteries. *Adv. Funct. Mater.* **2013**, *23* (8), 1064–1069.
- (20) Wu, H.-L.; Haasch, R. T.; Perdue, B. R.; Apblett, C. A.; Gewirth, A. A. The Effect of Water-Containing Electrolyte on Lithium-Sulfur Batteries. *J. Power Sources* **2017**, *369*, 50–56.
- (21) Zhu, Y.; He, X.; Mo, Y. Strategies Based on Nitride Materials Chemistry to

- Stabilize Li Metal Anode. *Adv. Sci.* **2017**, *4* (8), 1600517.
- (22) Ma, G.; Wen, Z.; Wu, M.; Shen, C.; Wang, Q.; Jin, J.; Wu, X. A Lithium Anode Protection Guided Highly-Stable Lithium-Sulfur Battery. *Chem. Commun.* **2014**, *50* (91), 14209–14212.
- (23) Baloch, M.; Shanmukaraj, D.; Bondarchuk, O.; Bekaert, E.; Rojo, T.; Armand, M. Variations on Li₃N Protective Coating Using Ex-Situ and in-Situ Techniques for Li^o in Sulphur Batteries. *Energy Storage Mater.* **2017**, *9* (January), 141–149.
- (24) Eshetu, G. G.; Diemant, T.; Grugeon, S.; Behm, R. J.; Laruelle, S.; Armand, M.; Passerini, S. In-Depth Interfacial Chemistry and Reactivity Focused Investigation of Lithium–Imide- and Lithium–Imidazole-Based Electrolytes. *ACS Appl. Mater. Interfaces* **2016**, *8* (25), 16087–16100.
- (25) Ito, Y.; Miyauchi, K.; Oi, T. Ionic Conductivity of Li₂O-B₂O₃ Thin Films. *J. Non. Cryst. Solids* **1983**, *57* (3), 389–400.
- (26) Eshetu, G. G.; Judez, X.; Li, C.; Bondarchuk, O.; Rodriguez-Martinez, L. M.; Zhang, H.; Armand, M. Lithium Azide as an Electrolyte Additive for All-Solid-State Lithium-Sulfur Batteries. *Angew. Chemie Int. Ed.* **2017**, *56* (48), 15368–15372.

Chapter 4:

Electrolyte fillers

In this chapter the addition of a small amount of two electrolyte fillers is studied, including a lithium ion conducting glass (LICGC) and Al_2O_3 . The desired improvement in conductivity was not achieved, but a strong effect of the filler in lithium/polymer electrolyte compatibility was witnessed. LICGC featured a high reactivity against metallic lithium and lithium polysulfides, hindering its application in lithium-sulfur batteries. In contrast, Al_2O_3 was demonstrated to improve interfacial properties of the lithium and to strongly interact with lithium polysulfides, while maintaining its structural integrity. The proper understating of the mechanism of this filler in our batteries will allow to assemble cells with optimized properties in terms of cell capacity and stability.

INDEX

4	ELECTROLYTE FILLERS.....	95
4.1	PHYSICOCHEMICAL AND ELECTROCHEMICAL PROPERTIES.....	97
4.2	ELECTROCHEMICAL BEHAVIOR WITH THE Li^0 ELECTRODE	101
4.3	FILLER INTERACTION WITH LIPS.....	102
4.4	ELECTROCHEMICAL PERFORMANCE.....	104
4.5	NOVEL CELL DESIGN	106
4.6	DISCUSSION.....	108
4.7	CONCLUSIVE REMARKS	110
4.8	REFERENCES	111

4 ELECTROLYTE FILLERS

The aim of this chapter will be the stabilization of the cell without sacrificing cell capacity. Therefore, in a different approach, this chapter will explore the addition of electrolyte fillers to the electrolyte and its impact in the cell performance. Contrary to additives, which are present in solvated form in the electrolyte, electrolyte fillers will remain untouched in the polymer structure. For that purpose, the use of two different ceramic fillers will be studied.

Solid polymer electrolytes (SPEs) feature several attractive properties like low-cost, safety, easy processing and manipulation, and flexibility. However decent conductivities that allow battery operation at room temperature (RT) have not been yet achieved. On the contrary, inorganic solid electrolytes (ISEs) possess high conductivities at RT, but their application is yet limited by their inherent rigidity, fragility and poor interfacial contact. In response to the intrinsic limitations of both pure systems, their combination, *i.e.*, embedding ISE particles in a polymer matrix to obtain solid composite electrolytes (SCEs), have become an appealing choice. The main purpose of this combination is to take advantage of structural integrity, flexibility and good interfacial contact of SPE phase, and high ionic conductivity of ISE phase.

After the first study published by Weston and Steele¹ in 1982 on the effect in conductivity of different Al₂O₃ filler amounts in a poly(ethylene oxide) (PEO) matrix, several works have focused in the development of SCE. Ceramic fillers can be divided into two groups: active fillers, *i.e.*, those that have mobile lithium ions (Li⁺) in their structure and, thus, can conduct Li⁺; and inactive fillers, that do not contain Li⁺ and cannot transport it, but provide surface active properties that contribute to improve the performance.

Though some research activity for SCEs shows remarkable conductivity improvements compared to filler free counterparts,²⁻⁶ some others do not observe improvements or remarkable changes after the addition of the fillers.⁷⁻⁹ Therefore, it has been recently concluded that the simple addition of ceramic phase may not always improve conductivity. Several parameters, such as particle composition, concentration, size, shape, orientation, or surface functionality will dictate the interaction between polymer matrix and inorganic phase, and must be optimized to obtain the desired improvements. For example, Cui *et al.*³ showed that particle geometry could have a huge effect on conductivity. In that study, the conductivity obtained after the addition of one-dimensional Li_{0.33}La_{0.557}TiO₃ (LLTO) ceramic particles to polyacrylonitrile membranes was 2 orders of magnitude superior to the value obtained with spherical LLTO-added electrolytes. This improvement was attributed to the fast ion transport on the particle surface, whose area is clearly higher in nanowire fillers due to their higher aspect ratio.

However, conductivity is not always improved in all the reported literature. Thus, some studies diverted the attention to the effect of the fillers in the improvement of other properties, such as interfacial compatibility.^{8,10–12} For example, Zagórski *et al.*¹² combined $\text{Li}_{6.55}\text{Ga}_{0.15}\text{La}_3\text{Zr}_2\text{O}_{12}$ microparticles with LiTFSI/PEO membrane to obtain a SCE. Authors proved that while the total Li^+ conductivity was governed by the polymer phase, the addition of the ceramic particles played a significant role in the stabilization of the metallic lithium (Li^0)/electrolyte interface. In this regard, in a parallel study to the present thesis work, we were able to prepare SCE membranes by simple mechanical mixing with the addition of nanometric Al_2O_3 to LiTFSI/PEO and lithium bis(fluorosulfonyl) imide (LiFSI)/PEO membranes. The addition of these nanofillers remarkably improved chemical and electrochemical compatibility of the electrolyte with the membrane, allowing remarkably longer operation time in Li^0 plating and stripping tests. Particularly, LiFSI/PEO + Al_2O_3 cells showed excellent results, and enabled Li|SCE|LiFePO₄ cell cycling for 50 cycles with an excellent capacity retention. This work was published by our group.¹³

Regarding lithium sulfur batteries (LSBs), as shown in the state-of-art research section in the Introduction chapter, SCE-based all-solid-state lithium sulfur batteries (ASSLSBs) performance improved in comparison to the filler-free SPE-based systems. Some research groups reported improvements in conductivity,^{14–18} but their beneficial effect in cell performance is usually also related the improvement of Li^0 /electrolyte interface properties,^{14,16,17,19–21} or lithium polysulfide (LiPS) retention by means of a physical barrier.^{18,22}

This chapter will study the effect of two ceramic fillers in the reference LiTFSI/PEO membrane, including one passive filler and one active filler. Regarding the passive filler, 5 nanometer size $\gamma\text{-Al}_2\text{O}_3$ was selected due to its low cost, commercial availability, stability against moisture and its excellent compatibility with Li^0 . Within the active filler, commercial 400 nm particle size Li-ion conductive glass ceramic (LiCGC) from Ohara INC. will be studied. The exact composition of this material is unknown, but it is obtained after the mixture and thermal treatment of Li_2O , Al_2O_3 , SiO_2 , P_2O_5 , TiO_2 and GeO_2 .²³ Therefore, a Li-adapted sodium super ionic conductor (NaSICON) structure will be the final product, with an intermediate behavior between the well-studied $\text{Li}_{1+x}\text{Ti}_{2-x}\text{Al}_x(\text{PO}_4)_3$ (LATP) and $\text{Li}_{1+x}\text{Ge}_{2-x}\text{Al}_x(\text{PO}_4)_3$ (LAGP) materials. The use of this filler is interesting due to its high conductivity at RT ($> 10^{-3}$ S cm^{-1}), but specially because, in contrast to several active fillers, it is stable against moisture and can be safely handled in air.²³ The smallest commercially available particle size was chosen for both cases, and its content was set to 3 v1.% after an optimization in the development of the abovementioned work from our group.

Initially, the physicochemical and electrochemical properties of the prepared SCEs will be studied, with special attention to the effect of the fillers and their interaction with cell components. Then, those membranes will be tested in ASSLSBs, and the role of the filler will be discussed in detail.

4.1 PHYSICOCHEMICAL AND ELECTROCHEMICAL PROPERTIES

Membranes were again prepared by solvent-casting method in combination with filler dispersion in the membrane slurry by ball-milling method (experimental details are given in the section 3 of the Appendix). The optical images of the obtained membranes are presented in **Figure 4.1a**. These SCE membranes are self-standing and do not show visible particle agglomerates. In order to determine filler dispersion in the membrane, scanning electron microscopy (SEM) images of the obtained SCEs are shown in **Figure 4.1b**. For the LiCGC-added membrane, images show homogeneous particle dispersion. In contrast, for the Al_2O_3 -added membrane, the images show some cloud-like areas with higher filler concentration. This is related to the small particle size of the filler and its higher surface tension, which results in easier particle agglomeration. Nevertheless, filler dispersion is homogeneous in general.

X-ray diffraction (XRD) patterns of both SCE membranes are shown in **Figure 4.1c**. The absence of salt related peaks in the membrane, indicate again its full solvation in the PEO matrix. Both SCEs show peaks coming from the ceramic phase. While LiCGC related peaks are sharp and representative, those corresponding to the Al_2O_3 composite membrane are wide and weak due to its low structural crystallinity. These peaks fit with the original peaks of the pristine ceramics, indicating that the filler remains unreacted in the polymer matrix after membrane preparation process, as desired.

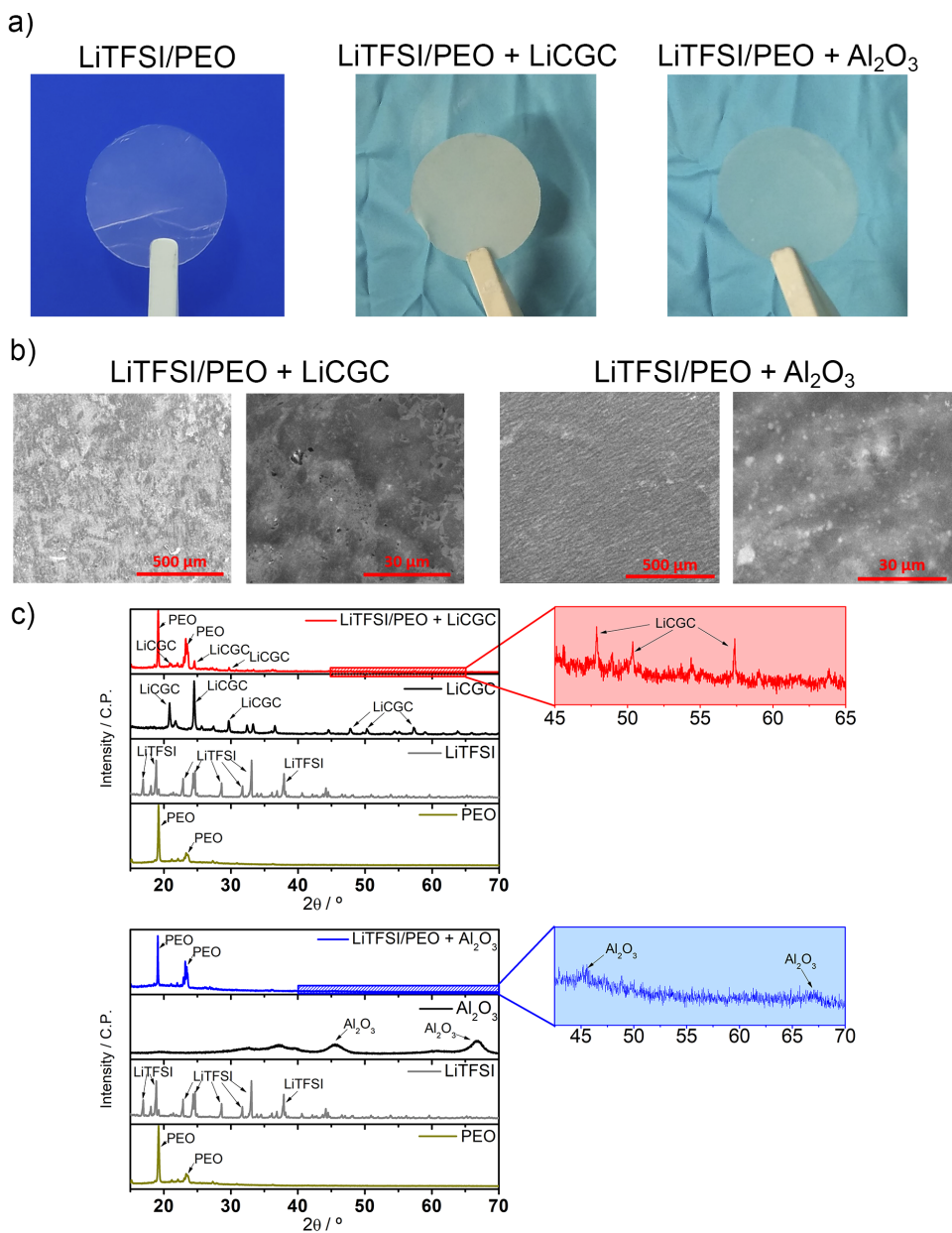


Figure 4.1. Physicochemical properties of the prepared membranes. a) Optical images of the reference LiTFSI/PEO SPE, and LiCGC or Al₂O₃ added SCEs. b) SEM images and c) XRD patterns of the SCEs.

The electrochemical and thermal stability of the obtained SCEs were studied by linear sweep voltammetry and thermogravimetric analysis (TGA) in **Figure 4.2**.

Regarding anodic stability, **Figure 4.2a** demonstrates that the addition of the fillers does not remarkably affect resistance to oxidation, with a mild oxidation current at 3.8 V vs. Li/Li^+ related to PEO and more abrupt currents starting from 5.0-5.5 V vs. Li/Li^+ , related to anion oxidation. **Figure 4.2b** presents also similar thermal stability, dictated again by LiTFSI/PEO phase and with no material loss at operating temperature of 70 °C or below.

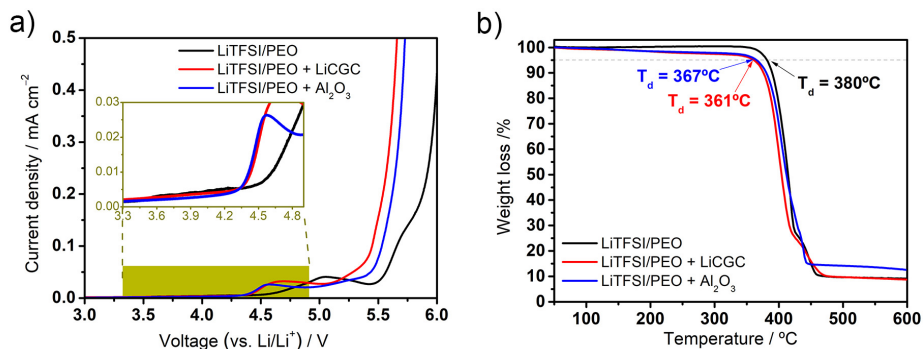


Figure 4.2. Stability studies of the reference LiTFSI/PEO SPE and the LiCGC or Al₂O₃ added SCE. a) Anodic stabilities at 70 °C and b) TGA traces.

The phase transition behavior and conductivity of the SCEs are presented in **Figure 4.3**. Differential scanning calorimetry (DSC) traces in **Figure 4.3a** show slightly decreased melting point for SCEs in comparison with filler-free SPE. However, all membranes feature similar crystallinity, so there is no evidence that filler addition is affecting remarkably thermal transition behavior. This is in agreement with conductivity measurements in **Figure 4.3b**, where the fillers do not feature increased ionic conductivity and there are still two clear independent tendencies before and after the melting point. The conductivity of the SCEs decreased after filler addition, but in contrast the addition of filler has a clear beneficial effect in Li^+ transport selectivity, *i.e.*, transference number (t_{Li^+}). While LiTFSI/PEO reference features a t_{Li^+} value of 0.15, LiCGC-containing SCE membrane has a value of 0.27 and Al₂O₃-containing one a value of 0.26 (**Figure 4.3c**). This improvement in cation transport selectivity has been already ascribed to interactions between filler, polymer chains and the salt, which can increase the dissociation of the latest,^{2,24,25} promote local relaxation and segmental motion of the polymer,²⁶ or form Li^+ -ceramic-polymer complexes that create preferential Li^+ transport routes.¹⁰ An increased t_{Li^+} value will decrease concentration-gradient-induced polarization of the electrolyte, reducing voltage losses, internal impedance and undesired side reactions of the cell.²⁷ Furthermore, even if the total ionic conductivity of the SCEs is lower than in reference the SPE, the higher transport selectivity comparable Li^+ conductivity to the reference filler-free membrane (**Figure 4.3d**).

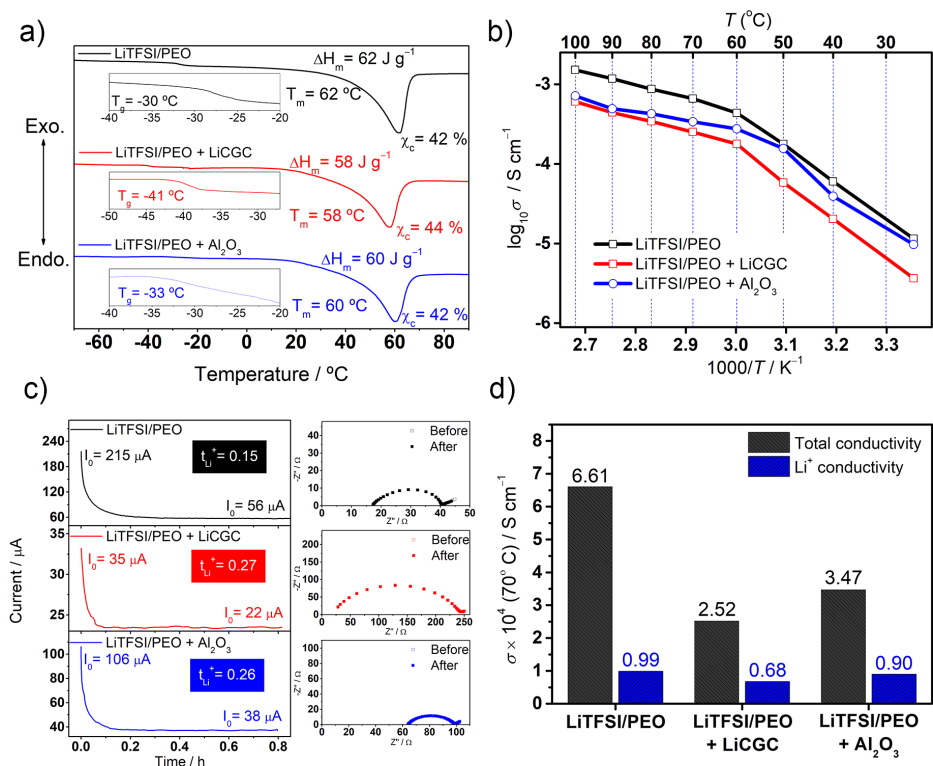


Figure 4.3. Physicochemical and electrochemical properties of LiTFSI/PEO reference SPE and LiCGC or Al₂O₃ containing SCEs. a) DSC traces; b) Arrhenius plots of ionic conductivity; c) Chronoamperometry test under 10 mV polarization at 70 °C, and electrochemical impedance spectroscopy measurements before and after the test for t_{Li^+} measurement; and d) Li^+ conductivity at 70 °C. T_d , T_g , T_m , ΔH_m and χ_c refer to degradation, glass transition and melting temperatures, melting enthalpy and cristallinity fraction, respectively.

In summary, all the above results suggest that the addition of the filler does not have a remarkable effect in physicochemical and electrochemical properties of the membranes. With our configuration, the addition of either active or inactive fillers did not result in an improvement of the conductivity or the modification of the thermal transition properties. The improvement of Li^+ transport selectivity was the most salient feature.

4.2 ELECTROCHEMICAL BEHAVIOR WITH THE Li⁰ ELECTRODE

As mentioned at the beginning of this chapter, the addition of a filler to a SPE can affect the quality of the Li⁰/electrolyte interface. Accordingly, it is necessary to study the interfacial compatibility of the prepared SCE with the metallic negative electrode. For that purpose, the galvanostatic cycling study of symmetric Li⁰|SCE|Li⁰ at 0.1 mA cm⁻² for 2 h semicycles was performed at 70 °C, and compared with reference SPE-based cell (**Figure 4.4a**). In the case of LiCGC containing SCE, poor cyclability is obtained for the symmetric cell, with an operation time that does not even reach 100 h, which is even less than the reference LiTFSI/PEO. This indicates that the ceramic filler has a negative effect on the quality of the solid/electrolyte interphase (SEI) layer on the Li⁰ surface. At this point, a more in-depth state of the art research was carried out focusing in the LiCGC/Li⁰ compatibility. The results shed some light in this point, due to the fact that some studies had already reported that LATP and LAGP had limited electrochemical stability windows. For LATP, it was reported that below 2.4 V vs. Li/Li⁺ the Ti⁴⁺ can easily get reduced.^{28,29} Indirectly, other research related to LAGP material confirmed this fact.^{30,31} Thus, it is not surprising that LiCGC filler, which contains Ti⁴⁺, will not be stable in direct contact with Li⁰ and its structural integrity will be compromised.

On the contrary, a great improvement was achieved after the addition of Al₂O₃. Stable cycling was obtained during 1200 h, over 6 times longer compared to reference filler-free SPE. This strongly evidences the contribution of this filler to the generation of a robust and excellent quality SEI layer. This improvement has been ascribed to different beneficial effects of this filler, such as passivation of the Li⁰ electrode (minimized exposed area to the polymer), impurity scavenging properties (removing residual traces of H₂O and O₂ impurities that can react and accelerate deterioration of Li⁰ and native SEI layer), the better penetration resistance (enhanced yield stress and elongation of the membrane) as an obstacle to dendrites formation or the increasing in t_{Li^+} , which could decrease anion mobility and concentration polarization.^{11,32,33}

Finally, the behavior of each of the cells is schematically represented in **Figure 4.4b**. The reference LiTFSI/PEO was described previously in Chapter 2 to form a poor quality SEI layer. Regarding, LiCGC, previous reports proved that ceramic filler is not stable in contact with Li⁰ and we have confirmed that in its presence the generated SEI layer is even of lower quality than the filler-free SPE. On the contrary, the effect of Al₂O₃ on SEI quality is outstanding, and the formed SEI allows symmetric cell cycling for over six-fold operation time compared to the cell with the reference SPE.

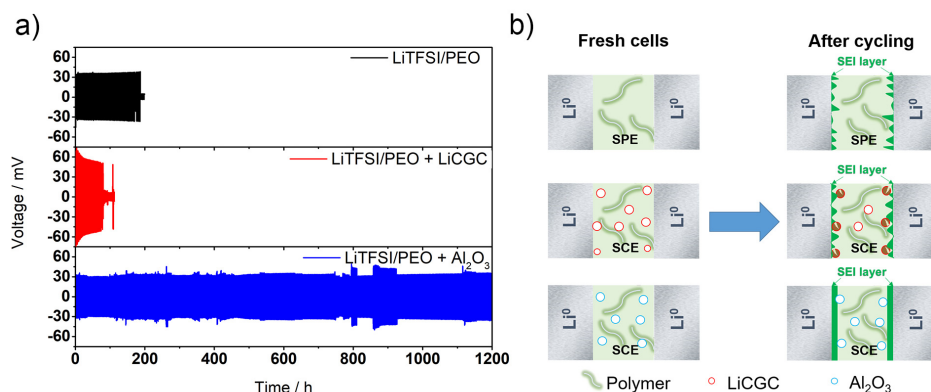


Figure 4.4. Electrochemical behavior of Li⁰ electrode in the as-prepared electrolytes. a) Galvanostatic cycling of Li⁰|SPE or SCE|Li⁰ symmetric cells at 0.1 mA cm⁻² and 2 h semicycles at 70 °C. b) Schematic representation of the cell behavior in presence of the different electrolytes.

This study demonstrates that low content of fillers as low as 3 vl.% can have a strong effect on the Li⁰/electrolyte interface quality.

4.3 FILLER INTERACTION WITH LiPS

Contrary to lithium-intercalation batteries, where the active material remains confined in the positive electrode area, in LSBs, intermediate discharge products, *i.e.*, LiPSs, can be dissolved into the electrolyte, as demonstrated in the previous chapter. Thus, it is important to study the compatibility of the filler with LiPS. For that purpose, solutions of 25 mM Li₂S₆ in DME were prepared. Later, 3 vl.% filler was added to the solutions and the mixtures were magnetically stirred for 1h. Later, solution was centrifuged to separate solid and liquid phases. Upper part of **Figure 4.5a** shows initial LiPS solution, the LiCGC added solution and the remaining liquid solution. After the addition of LiCGC powder, the solution clearly changes its color, losing the characteristic coloration related to LiPS, which indicates their complete reaction. On the other hand, the white color LiCGC powder shifts to grey, presumably due to a decomposition reaction. Coetaneously to this work, a study from Manthiram *et al.*²⁹ deepened in the understanding of the interaction between LATP and LiPSs. The study discovered that in contact with LiPSs, LATP gets lithiated and the Ti⁴⁺ of the structure gets reduced to Ti³⁺, generating changes in size and the anisotropic expansion of the structure, weakening the connection of the crystals and generating small cracks in the ceramic. At the same time, the authors proved that in presence of liquid electrolyte, Li₂CO₃ could be formed in the particle surface, which would increase interfacial resistance and impede the Li⁺ transport. One strategy to improve the stability of this NaSICON structure against

LiPS is the substitution of titanium by more stable germanium, generating the so-called LAGP. Even when our LiCGC contains germanium, there is still titanium present, which can be easily reduced by Li^0 . To analyze the possible structural changes, **Figure 4.5b** shows XRD spectra and photo (inset) of the LiCGC powder before and after the contact with LiPS. In agreement with the mentioned work, the XRD spectra of the LiCGC after LiPS contact shows an additional peak at $2\theta = 23^\circ$, indicated by an asterisk, corresponding with $\text{Li}_3\text{Ti}_{1.7}\text{Al}_{0.3}(\text{PO}_4)_3$, which is formed after the lithiation of conventional LATP, *i.e.*, $\text{Li}_{1.3}\text{Ti}_{1.7}\text{Al}_{0.3}(\text{PO}_4)_3$. Additional studies confirmed this issue.³⁴

In the case of Al_2O_3 (bottom part of **Figure 4.5a**), the shade of the solution changes from dark brownish/reddish to colorless, demonstrating the strong interaction of the ceramic particle with the LiPS, while the color of the solid powder changed to orange. The studies of the recovered solid phase by XRD in **Figure 4.5b** prove that Al_2O_3 in contact with LiPSs shows exactly the same pattern as the pristine one, proving that the ceramic particles were not reacted. Therefore, the color change to light orangish is just an indicative of the presence of LiPS on its surface. These results show that Al_2O_3 has a strong ability to absorb LiPS from the media, while maintaining its structural integrity during the process. This is in agreement with the previous literature, where different metal oxides, *e.g.*, MnO_2 ,³⁵ V_2O_5 ,³⁶ Nb_2O_5 ,³⁷ have been demonstrated to strongly absorb LiPS while keeping structural integrity, via dipole-dipole interaction between polar oxides and polar LiPSs. Even if other metal oxides, such as, Nb_2O_5 ³⁷ or RuO_2 ,³⁸ have proven to be stronger LiPS absorbers, Al_2O_3 has a unique balanced function between LiPS adsorption and Li^0 stabilization properties, apart from being one of the most cost competitive options.

In conclusion, LiCGC was proven to feature stability issues related to the fact that Ti^{4+} can be reduced to Ti^{3+} either electrochemically in contact with Li^0 , or chemically by contact with LiPS. This will generate a poor Li^0/SCE compatibility and LiPS consumption. On the other hand, Al_2O_3 has excellent compatibility with the metallic electrode and the ability to maintain structural integrity even after a strong interaction with LiPS.

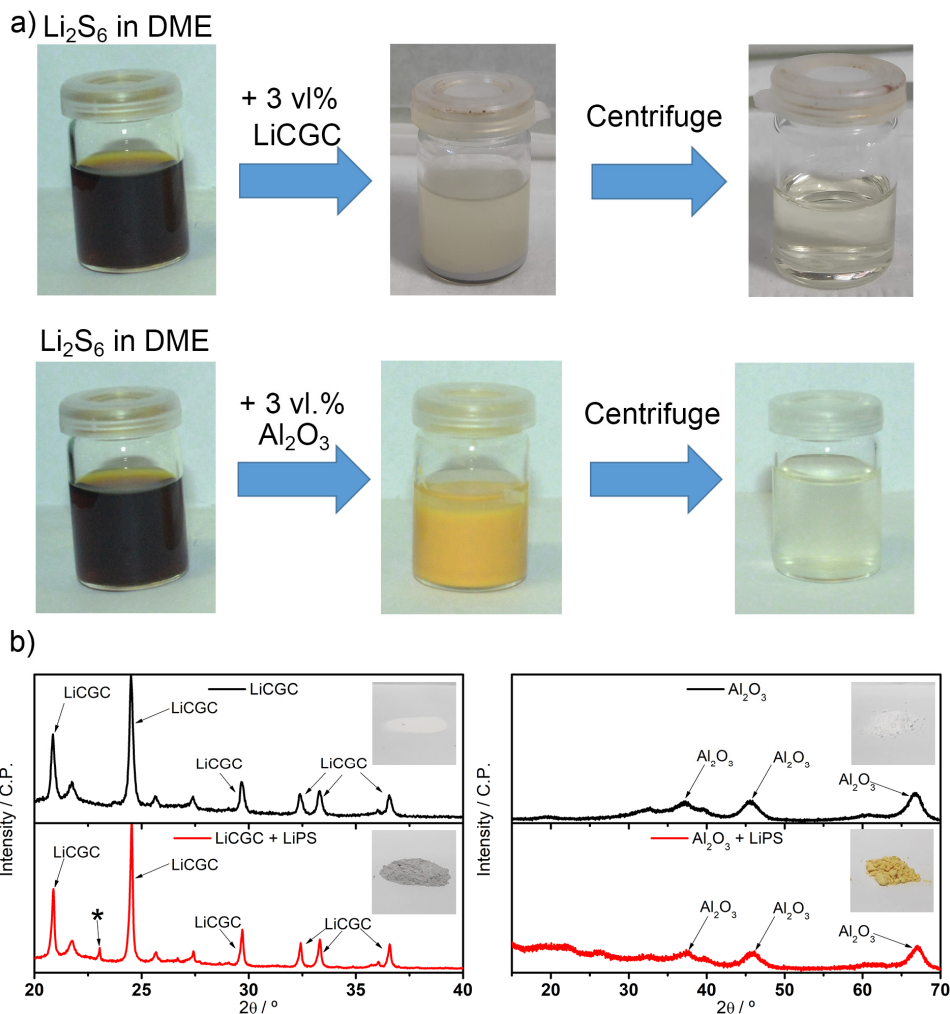


Figure 4.5. a) Compatibility visual tests for 25 Mm Li_2S_6 /DME solution in contact for 1 h with 3 v.l.% of either LiCGC or Al_2O_3 . b) XRD patterns and photos (inset) of the pristine ceramic particles and the particles after the contact with LiPS solution.

4.4 ELECTROCHEMICAL PERFORMANCE

The prepared SCE were tested as electrolytes for ASSLSBs. **Figure 4.6a** presents the cycling performance of $\text{Li}^0 | \text{SCE} | \text{S}$ full cells at 70 °C. The performance of the reference system $\text{Li}^0 | \text{SPE} | \text{S}$ is also included. For LiCGC containing LSB, the cell behavior in terms of Coulombic efficiency is as low as that of the bare LiTFSI/PEO reference, and in terms of capacity the obtained values are lower in general. **Figure 4.6b** shows discharge/charge profiles for the first cycle of each rate of LiCGC

containing cells, where overcharge is clearly observed. After all the characterization of LiCGC-based SCEs, it can be concluded that LiCGC is not a good choice for our configuration of ASSLSBs due to its high reactivity towards LiPS and instability in contact with Li^0 negative electrode. Although LATP, and specially LAGP, have been already successfully implemented in LSBs, it has been done in different configurations, that included physical separators to avoid direct contact with the metallic anode and were the main role of the ceramic material was to act as LiPS barrier.^{30,31,39,40}

In contrast, the cells with Al_2O_3 containing SCE delivered Coulombic efficiency values close to 100% at any discharge rate (**Figure 4.6a**), with the absence of overcharge in the discharge/charge profiles (**Figure 4.6c**). The cell only shows critically drop of Coulombic efficiency values after 25 cycles. However, the cells containing this filler features decreased discharge capacity values in comparison with the filler-free reference. This demonstrates that the presence of this filler improves remarkably the cycling stability of the cell, but has a negative effect on delivered cell capacity. With these results and the previous compatibility studies, we can conclude that on the one hand, the presence of Al_2O_3 is contributing to the stabilization of the Li^0 /electrolyte interface by promoting a robust and high quality SEI layer. On the other hand, and based on strong LiPS/ Al_2O_3 interaction, we can hypothesize that during the discharge the LiPSs are being formed in the positive electrode and diffuse to the electrolyte. Once in the electrolyte, those LiPS will be absorbed and strongly attached to the filler surface. The filler will act as a LiPS barrier and will prevent their further reaction on the negative electrode, *i.e.*, shuttle effect and related overcharge. However, those LiPSs will remain strongly attached to the ceramic filler in the electrolyte, and will hardly diffuse back to the positive electrode. This retention of LiPS away from the positive electrode will result in a lack of contact between electronic conductive carbon and electroactive species, preventing electron flow to these species and thus, their subsequent reduction reaction, leading to a critical active material loss in the positive electrode. This is in agreement with discharge/charge profiles of the cells in **Figure 4.6c**, where the cell shows well developed upper plateau and slope region, *i.e.*, the region where S_8 is reduced to high order LiPS, Li_2S_x , $x=4, 6, 8$; but a clearly reduced discharge capacity in the lower plateau region, where soluble Li_2S_4 should be further reduced to low order LiPS. This indicates that high order LiPS are properly generated, but later they diffuse and stay strongly anchored on the filler particles in the electrolyte, hindering its complete reduction reactions. This problematic is schematically represented in **Figure 4.6d**.

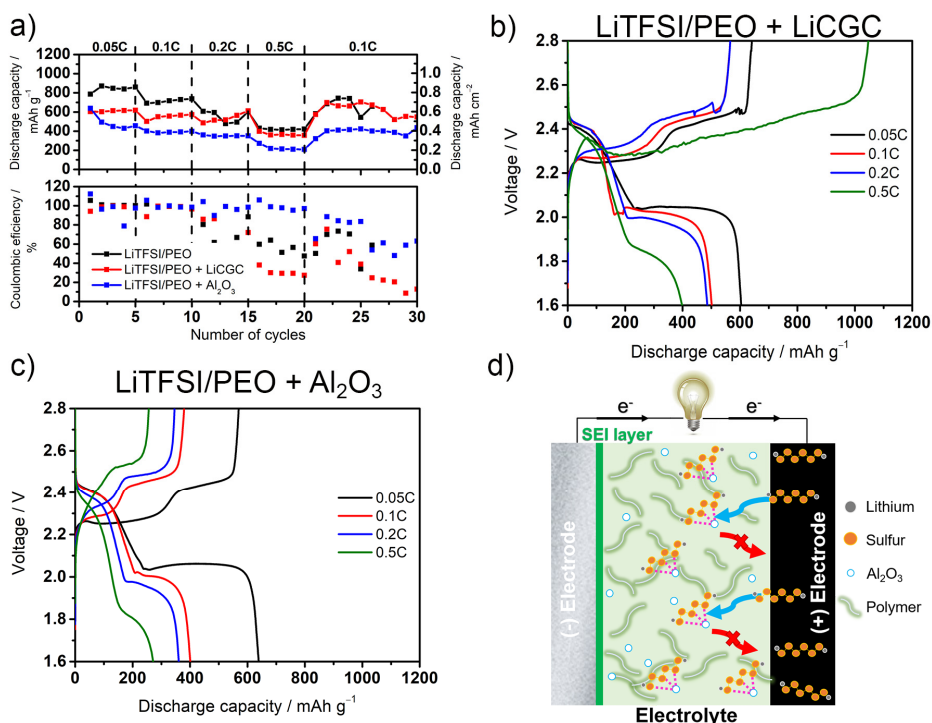


Figure 4.6. a) Discharge capacity and Coulombic efficiency of $\text{Li}^0|\text{SPE}$ or $\text{SCE}|\text{S}$ electrode cells at different C-rates. Discharge/charge profiles during the first cycle at each rate for b) $\text{LiTFSI/PEO} + \text{LiCGC}$ and c) $\text{LiTFSI/PEO} + \text{Al}_2\text{O}_3$ cells. d) Schematic representation of the working mechanism in $\text{Li}^0|\text{LiTFSI/PEO} + \text{Al}_2\text{O}_3|\text{S}$ electrode cell. All the measurements were done at 70°C .

In conclusion, the use of LiCGC as a filler in ASSLSBs is not appropriate due to its compatibility issues with LSB components, so its further study was discarded. In the case of Al_2O_3 , the results are not satisfactory yet, but the cell presents an outstanding stability improvement after the addition of the filler. Furthermore, the working mechanism of this electrolyte has been clearly depicted, and this paves the way for new cell configurations where the benefits of Al_2O_3 , in terms of strong interaction with LiPS and Li^0 electrode stabilizer, could be exploited. This new cell configuration will be described in the following point.

4.5 NOVEL CELL DESIGN

On the one hand, previous sections proved that the addition of Al_2O_3 to the reference SPE to obtain a SCE has clear benefits in terms of $\text{Li}^0/\text{electrolyte}$ compatibility. On the other hand, Al_2O_3 has been demonstrated to strongly interact

with LiPS by dipole-dipole interaction. Furthermore, many publications have already reported the use of Al_2O_3 and several other metal oxides as positive electrode additives in the positive electrode in LSBs due to their strong LiPS anchoring properties, which can avoid their undesired diffusion.^{36,41-43} Some studies reported, after calculations by Density Functional Theory, that metal oxides have much favorable absorption energy over LiPS than other positive electrode components such as graphite.^{38,44}

On the basis of above-mentioned properties of the Al_2O_3 and Al_2O_3 containing SCEs, a novel cell configuration was conceived in order to benefit from Li^0 stabilizing properties, but avoid an irreversible mass loss in the positive electrode. For that purpose, the cell shown in **Figure 4.7a** was built, comprising a modified positive electrode and a bilayer electrolyte. 3 vol.% Al_2O_3 was included in the catholyte as positive electrode additive, in order to act as LiPS reservoir and avoid its undesired diffusion. For the bilayer electrolyte, a Al_2O_3 containing SCEs of the minimum viable thickness, *c.a.* 25 μm , was included in contact with Li^0 to stabilize Li^0 /electrolyte interphase; and a filler-free 50 μm SPE membrane was included in contact with positive electrode to allow the small remnant of diffused LiPS to move in an irreversible-anchoring-free area close to the positive electrode, allowing them to diffuse back and facilitate their further reaction.

The feasibility of this strategy is demonstrated by the excellent performance of the tested cell in **Figure 4.7b**, with a delivered capacity as high as reference SPE containing cell, but a higher Coulombic efficiency even at high rates for 30 cycles. Remarkably, discharge/charge profiles in **Figure 4.7c** show absence of overcharge and well developed lower plateau on discharge, indicating a high utilization of active material. The cell delivers similar capacity values compared to LiTFSI/PEO reference, and an unprecedented value of 755 mAh g^{-1} and 0.85 mAh cm^{-2} at 0.1C after 30 cycles, with a capacity retention of almost 100% back to 0.1C, after cycling at fast rates.

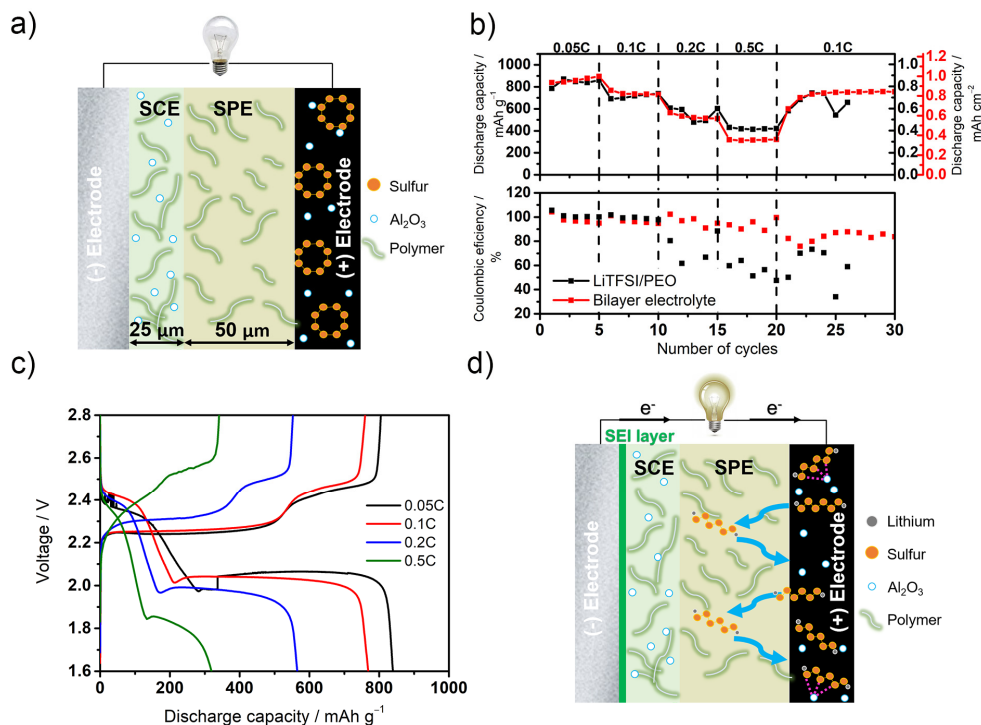


Figure 4.7. a) Schematic representation of the assembled cell before cycling. b) Discharge capacity and Coulombic efficiency of Li⁰|SCE+SPE|modified S electrode cells at different C-rates. c) discharge/charge profiles during the first cycle at each rate. d) Schematic representation of assembled cell during the cycling. All the measurements were done at 70 °C.

This demonstrates that the SCEs creates a robust SEI layer that protects Li⁰ electrode from both dendrite/mossy lithium growth and LiPS attack, while Al₂O₃ in the positive electrode hinders active material loss and enables high capacity retention. Furthermore, the filler free SPE layer close to the positive electrode enables the reutilization of the small remnant of diffused LiPS. The schematic representation of this novel configuration is shown in **Figure 4.7d**. This work was published.⁴⁵

4.6 DISCUSSION

The fillers were successfully incorporated and homogeneous self-standing membranes were obtained. The incorporation of the fillers did not have a remarkable effect on physicochemical or electrochemical properties. The incorporation of neither active or inactive fillers did not improve conductivity

values, which could be related to their non-optimized composition, shape, orientation, *etc.* However, the selectivity to Li^+ increased after the addition of the fillers, so the total Li^+ conductivity was finally compensated. Furthermore, the fillers had strong effect on Li^0/SPE stability, which was negative for LiCGC fillers (the filler was prone to reduce in contact with Li^0) and remarkably positive for Al_2O_3 . In the same vein, LiCGC was demonstrated to be highly susceptible to reduction in contact with LiPS, while Al_2O_3 was found to be stable and to interact strongly with these reaction intermediates by dipole-dipole interactions.

The ASSLSBs results show that while LiCGC did not bring any positive effect in cell performance, the Al_2O_3 -based SCE helped to improve cell stability and rate response. The direct implementation of Al_2O_3 containing SCEs brought stable cell cycling but a decreased discharge capacity due to LiPS immobilization far from positive electrode area. After understanding Al_2O_3 -based SCE interaction with other cell components, initial cell design was modified. On the one hand, Al_2O_3 was added as positive electrode additive for LiPS anchoring. On the other hand, bilayer electrolyte allowed the stabilization of the negative electrode, but enabled free movement of LiPS in the positive electrode area, increasing their electrochemical utilization. This novel cell design enabled a stable cell cycling without affecting the obtained capacity values.

This study sets a precedent in SPE and SCE-based ASSLSBs performance in terms of delivered cell capacity (gravimetric and areal) and capacity retention combination (**Table 4.1**). It also sets a precedent in the understanding of the role and optimum exploitation of Al_2O_3 filler. Furthermore, this work deepens in the understanding and development of bilayer electrolytes, first proposed by our group in a previous work.⁴⁶

Table 4.1. Comparison of the results of the present chapter and the previous works. The reference number refers to State of Art section. HNT and MIL-53(Al) refers to halloysite nanotubes and aluminum containing metal-organic framework

Ref.	Electrolyte recipe	Initial cap. / mAh g ⁻¹ , (mAh cm ⁻²)	End of life cap. / mAh g ⁻¹ , (mAh cm ⁻²)	Cap. loss / % cycle ⁻¹
S23	LiTFSI/PEO	450 (0.45)	450 (0.5)	0%
S24	LiTFSI/PEO	1350 (1.08)	600 (0.48)	1.38%
S24	LiTFSI/PEO + HNT	800 (0.64)	745 (0.6)	0.07%
S29	LiTFSI/PEO + MIL-53(Al)	640 (0.51)	558 (0.45)	0.016%
S31	LiTFSI/PEO + Li ₇ La ₃ Zr ₂ O ₁₃	900 (0.54)	900 (0.54)	0%
This work	LiTFSI/PEO / LiTFSI/PEO + Al ₂ O ₃	768 (0.86)	755 (<u>0.85</u>)	<u>0.14%</u>

4.7 CONCLUSIVE REMARKS

The addition of two different electrolyte fillers, active LiCGC and inactive Al₂O₃, to reference LiTFSI/PEO SPE have been studied, with the aim of obtaining SCEs. The addition of the fillers did not have a remarkable effect in physicochemical and electrochemical properties of the membranes. In contrast, they strongly interacted with cell components, *i.e.*, Li⁰ and LiPS.

The studied active filler, LiCGC, did not have bring any benefit in conductivity terms, and was proven to be unstable and to get reduced in direct contact with Li⁰ or LiPS. Therefore, its use as electrolyte filler in ASSLSBs did not bring any positive effect. In contrast, Al₂O₃ filler brought remarkable effects in terms of Li⁰/electrolyte interface stabilization, and demonstrated strong LiPS adsorption capability through dipole-dipole interaction. Furthermore, a novel cell configuration was proposed, based on a bilayer electrolyte, with unprecedented results in terms of in terms delivered capacity at excellent capacity retention.

The integration of Al₂O₃ has been demonstrated to be a low-cost and effective strategy to reinforce and improve the electrochemical performance of the conventional LiTFSI/PEO electrolyte in ASSLSBs.

4.8 REFERENCES

- (1) Weston, J. E.; Steele, B. C. H. Effects of Inert Fillers on the Mechanical and Electrochemical Properties of Lithium Salt-Poly(Ethylene Oxide) Polymer Electrolytes. *Solid State Ionics* **1982**, *7* (1), 75–79.
- (2) Yang, T.; Zheng, J.; Cheng, Q.; Hu, Y.-Y.; Chan, C. K. Composite Polymer Electrolytes with Li₇La₃Zr₂O₁₂ Garnet-Type Nanowires as Ceramic Fillers: Mechanism of Conductivity Enhancement and Role of Doping and Morphology. *ACS Appl. Mater. Interfaces* **2017**, *9* (26), 21773–21780.
- (3) Liu, W.; Liu, N.; Sun, J.; Hsu, P.-C.; Li, Y.; Lee, H.-W.; Cui, Y. Ionic Conductivity Enhancement of Polymer Electrolytes with Ceramic Nanowire Fillers. *Nano Lett.* **2015**, *15* (4), 2740–2745.
- (4) Lin, D.; Liu, W.; Liu, Y.; Lee, H. R.; Hsu, P.-C.; Liu, K.; Cui, Y. High Ionic Conductivity of Composite Solid Polymer Electrolyte via In Situ Synthesis of Monodispersed SiO₂ Nanospheres in Poly(Ethylene Oxide). *Nano Lett.* **2016**, *16* (1), 459–465.
- (5) Dissanayake, M. A. K. L.; Jayathilaka, P. A. R. D.; Bokalawala, R. S. P.; Albinsson, I.; Mellander, B.-E. Effect of Concentration and Grain Size of Alumina Filler on the Ionic Conductivity Enhancement of the (PEO)₉LiCF₃SO₃:Al₂O₃ Composite Polymer Electrolyte. *J. Power Sources* **2003**, *119–121*, 409–414.
- (6) Jayathilaka, P. A. R. ; Dissanayake, M. A. K. ; Albinsson, I.; Mellander, B.-E. Effect of Nano-Porous Al₂O₃ on Thermal, Dielectric and Transport Properties of the (PEO)₉LiTFSI Polymer Electrolyte System. *Electrochim. Acta* **2002**, *47* (20), 3257–3268.
- (7) Shin, J. H.; Passerini, S. PEO-LiN(SO₂CF₂CF₃)₂ Polymer Electrolytes. *J. Electrochem. Soc.* **2004**, *151* (2), A238.
- (8) Syzdek, J.; Armand, M.; Marcinek, M.; Zalewska, A.; Żukowska, G.; Wieczorek, W. Detailed Studies on the Fillers Modification and Their Influence on Composite, Poly(Oxyethylene)-Based Polymeric Electrolytes. *Electrochim. Acta* **2010**, *55* (4), 1314–1322.
- (9) Keller, M.; Appetecchi, G. B.; Kim, G.-T.; Sharova, V.; Schneider, M.; Schuhmacher, J.; Roters, A.; Passerini, S. Electrochemical Performance of a Solvent-Free Hybrid Ceramic-Polymer Electrolyte Based on Li₇La₃Zr₂O₁₂ in P(EO)₁₅LiTFSI. *J. Power Sources* **2017**, *353*, 287–297.
- (10) Croce, F.; Appetecchi, G. B.; Persi, L.; Scrosati, B. Nanocomposite Polymer Electrolytes for Lithium Batteries. *Nature* **1998**, *394* (6692), 456–458.
- (11) Kumar, B.; Scanlon, L. G. Polymer-Ceramic Composite Electrolytes. *J. Power Sources* **1994**, *52* (2), 261–268.
- (12) Zagórski, J.; López del Amo, J. M.; Cordill, M. J.; Aguesse, F.; Buannic, L.; Lordés, A. Garnet-Polymer Composite Electrolytes: New Insights on Local Li-Ion Dynamics and Electrodeposition Stability with Li Metal Anodes. *ACS Appl. Energy Mater.* **2019**, *2* (3), 1734–1746.
- (13) Judez, X.; Piszcz, M.; Coya, E.; Li, C.; Aldalur, I.; Oteo, U.; Zhang, Y.; Zhang, W.; Rodriguez-Martinez, L. M.; Zhang, H.; et al. Stable Cycling of Lithium Metal Electrode in Nanocomposite Solid Polymer Electrolytes with Lithium Bis(Fluorosulfonyl)Imide. *Solid State Ionics* **2018**, *318* (July 2017), 95–101.

- (14) Jeong, S. S.; Lim, Y. T.; Choi, Y. J.; Cho, G. B.; Kim, K. W.; Ahn, H. J.; Cho, K. K. Electrochemical Properties of Lithium Sulfur Cells Using PEO Polymer Electrolytes Prepared under Three Different Mixing Conditions. *J. Power Sources* **2007**, *174* (2), 745–750.
- (15) Lin, Y.; Wang, X.; Liu, J.; Miller, J. D. Natural Halloysite Nano-Clay Electrolyte for Advanced All-Solid-State Lithium-Sulfur Batteries. *Nano Energy* **2017**, *31* (October 2016), 478–485.
- (16) Tao, X.; Liu, Y.; Liu, W.; Zhou, G.; Zhao, J.; Lin, D.; Zu, C.; Sheng, O.; Zhang, W.; Lee, H.-W.; et al. Solid-State Lithium–Sulfur Batteries Operated at 37 °C with Composites of Nanostructured $\text{Li}_7\text{La}_3\text{Zr}_2\text{O}_{12}$ /Carbon Foam and Polymer. *Nano Lett.* **2017**, *17* (5), 2967–2972.
- (17) Zhu, P.; Yan, C.; Zhu, J.; Zang, J.; Li, Y.; Jia, H.; Dong, X.; Du, Z.; Zhang, C.; Wu, N.; et al. Flexible Electrolyte-Cathode Bilayer Framework with Stabilized Interface for Room-Temperature All-Solid-State Lithium-Sulfur Batteries. *Energy Storage Mater.* **2019**, *17*, 220–225.
- (18) Liang, J.; Sun, Q.; Zhao, Y.; Sun, Y.; Wang, C.; Li, W.; Li, M.; Wang, D.; Li, X.; Liu, Y.; et al. Stabilization of All-Solid-State Li–S Batteries with a Polymer–Ceramic Sandwich Electrolyte by Atomic Layer Deposition. *J. Mater. Chem. A* **2018**, *6* (46), 23712–23719.
- (19) Zhang, C.; Lin, Y.; Liu, J. Sulfur Double Locked by a Macro-Structural Cathode and a Solid Polymer Electrolyte for Lithium-Sulfur Batteries. *J. Mater. Chem. A* **2015**, *3* (20), 10760–10766.
- (20) Hassoun, J.; Scrosati, B. Moving to a Solid-State Configuration: A Valid Approach to Making Lithium-Sulfur Batteries Viable for Practical Applications. *Adv. Mater.* **2010**, *22* (45), 5198–5201.
- (21) Zhu, X.; Wen, Z.; Gu, Z.; Lin, Z. Electrochemical Characterization and Performance Improvement of Lithium/Sulfur Polymer Batteries. *J. Power Sources* **2005**, *139* (1–2), 269–273.
- (22) Liang, X.; Wen, Z.; Liu, Y.; Zhang, H.; Huang, L.; Jin, J. Highly Dispersed Sulfur in Ordered Mesoporous Carbon Sphere as a Composite Cathode for Rechargeable Polymer Li/S Battery. *J. Power Sources* **2011**, *196* (7), 3655–3658.
- (23) Nakajima, K.; Katoh, T.; Inada, Y. Lithium Ion Conductive Glass Ceramics: Properties and Application in Lithium Metal Batteries. In *Symposium on Energy Storage Beyond Lithium Ion*; 2010.
- (24) Gao, R.; Wang, H.; Zhu, Q.; Li, B.; Hellmut, E.; Zhang, X.; Xu, S. Effect of Y_2O_3 on Structure and Mechanical Properties of SiO_2 - Al_2O_3 - MgO Glasses. *Kuei Suan Jen Hsueh Pao/Journal Chinese Ceram. Soc.* **2016**, *44* (10), 1465–1470.
- (25) Golodnitsky, D.; Strauss, E.; Peled, E.; Greenbaum, S. Review—On Order and Disorder in Polymer Electrolytes. *J. Electrochem. Soc.* **2015**, *162* (14), A2551–A2566.
- (26) Lin, C. W.; Hung, C. L.; Venkateswarlu, M.; Hwang, B. J. Influence of TiO_2 Nano-Particles on the Transport Properties of Composite Polymer Electrolyte for Lithium-Ion Batteries. *J. Power Sources* **2005**, *146* (1–2), 397–401.
- (27) Zhang, H.; Li, C.; Piszcz, M.; Coya, E.; Rojo, T.; Rodriguez-Martinez, L. M.; Armand, M.; Zhou, Z. Single Lithium-Ion Conducting Solid Polymer Electrolytes: Advances and Perspectives. *Chem. Soc. Rev.* **2017**, *46* (3), 797–815.
- (28) Manthiram, A.; Yu, X.; Wang, S. Lithium Battery Chemistries Enabled by Solid-

- State Electrolytes. *Nat. Rev. Mater.* **2017**, 2 (4), 16103.
- (29) Wang, S.; Ding, Y.; Zhou, G.; Yu, G.; Manthiram, A. Durability of the $\text{Li}_{1+x}\text{Ti}_{2-x}\text{Al}_x(\text{PO}_4)_3$ Solid Electrolyte in Lithium–Sulfur Batteries. *ACS Energy Lett.* **2016**, 1 (6), 1080–1085.
- (30) Xu, H.; Wang, S.; Manthiram, A. Hybrid Lithium–Sulfur Batteries with an Advanced Gel Cathode and Stabilized Lithium–Metal Anode. *Adv. Energy Mater.* **2018**, 8 (23), 1800813.
- (31) Gu, S.; Huang, X.; Wang, Q.; Jin, J.; Wang, Q.; Wen, Z.; Qian, R. A Hybrid Electrolyte for Long-Life Semi-Solid-State Lithium Sulfur Batteries. *J. Mater. Chem. A* **2017**, 5 (27), 13971–13975.
- (32) Nunes-Pereira, J.; Costa, C. M.; Lanceros-Méndez, S. Polymer Composites and Blends for Battery Separators: State of the Art, Challenges and Future Trends. *J. Power Sources* **2015**, 281, 378–398.
- (33) Croce, F.; Persi, L.; Ronci, F.; Scrosati, B. Nanocomposite Polymer Electrolytes and Their Impact on the Lithium Battery Technology. *Solid State Ionics* **2000**, 135 (1–4), 47–52.
- (34) Yu, X.; Bi, Z.; Zhao, F.; Manthiram, A. Polysulfide-Shuttle Control in Lithium–Sulfur Batteries with a Chemically/Electrochemically Compatible NaSICON-Type Solid Electrolyte. *Adv. Energy Mater.* **2016**, 6 (24), 1601392.
- (35) Liang, X.; Hart, C.; Pang, Q.; Garsuch, A.; Weiss, T.; Nazar, L. F. A Highly Efficient Polysulfide Mediator for Lithium–Sulfur Batteries. *Nat. Commun.* **2015**, 6 (1), 5682.
- (36) Kim, M.-S.; Shin, E. S.; Kim, J.-S.; Cho, W. Il; Oh, S. H. The Effect of $\text{V}_2\text{O}_5/\text{C}$ Additive on the Suppression of Polysulfide Dissolution in Li–Sulfur Batteries. *J. Electroceramics* **2014**, 33 (3–4), 142–148.
- (37) Tao, Y.; Wei, Y.; Liu, Y.; Wang, J.; Qiao, W.; Ling, L.; Long, D. Kinetically-Enhanced Polysulfide Redox Reactions by Nb_2O_5 Nanocrystals for High-Rate Lithium–Sulfur Battery. *Energy Environ. Sci.* **2016**, 9 (10), 3230–3239.
- (38) Ding, N.; Zhou, L.; Zhou, C.; Geng, D.; Yang, J.; Chien, S. W.; Liu, Z.; Ng, M.-F.; Yu, A.; Hor, T. S. A.; et al. Building Better Lithium–Sulfur Batteries: From LiNO_3 to Solid Oxide Catalyst. *Sci. Rep.* **2016**, 6 (1), 33154.
- (39) Yu, X.; Manthiram, A. Enhanced Interfacial Stability of Hybrid-Electrolyte Lithium–Sulfur Batteries with a Layer of Multifunctional Polymer with Intrinsic Nanoporosity. *Adv. Funct. Mater.* **2019**, 29 (3), 1805996.
- (40) Wang, Q.; Wen, Z.; Jin, J.; Guo, J.; Huang, X.; Yang, J.; Chen, C. A Gel-Ceramic Multi-Layer Electrolyte for Long-Life Lithium Sulfur Batteries. *Chem. Commun.* **2016**, 52 (8), 1637–1640.
- (41) Liang, X.; Hart, C.; Pang, Q.; Garsuch, A.; Weiss, T.; Nazar, L. F. A Highly Efficient Polysulfide Mediator for Lithium–Sulfur Batteries. *Nat. Commun.* **2015**, 6 (1), 5682.
- (42) Zhao, T.; Ye, Y.; Peng, X.; Divitini, G.; Kim, H.-K.; Lao, C.-Y.; Coxon, P. R.; Xi, K.; Liu, Y.; Ducati, C.; et al. Advanced Lithium–Sulfur Batteries Enabled by a Bio-Inspired Polysulfide Adsorptive Brush. *Adv. Funct. Mater.* **2016**, 26 (46), 8418–8426.
- (43) Ding, B.; Shen, L.; Xu, G.; Nie, P.; Zhang, X. Encapsulating Sulfur into Mesoporous TiO_2 Host as a High Performance Cathode for Lithium–Sulfur Battery. *Electrochim. Acta* **2013**, 107, 78–84.
- (44) Gu, X.; Tong, C. J.; Wen, B.; Liu, L. M.; Lai, C.; Zhang, S. Ball-Milling

- Synthesis of ZnO@sulphur/Carbon Nanotubes and Ni(OH)₂@sulphur/Carbon Nanotubes Composites for High-Performance Lithium-Sulphur Batteries. *Electrochim. Acta* **2016**, *196*, 369–376.
- (45) Judez, X.; Eshetu, G. G.; Gracia, I.; López-Aranguren, P.; González-Marcos, J. A.; Armand, M.; Rodriguez-Martinez, L. M.; Zhang, H.; Li, C. Understanding the Role of Nano-Aluminum Oxide in All-Solid-State Lithium-Sulfur Batteries. *ChemElectroChem* **2019**, *6* (2), 326–330.
- (46) Judez, X.; Zhang, H.; Li, C.; Eshetu, G. G.; Zhang, Y.; González-Marcos, J. A.; Armand, M.; Rodriguez-Martinez, L. M. Polymer-Rich Composite Electrolytes for All-Solid-State Li–S Cells. *J. Phys. Chem. Lett.* **2017**, *8*, 3473–3477.

Chapter 5:

Alternative imide-containing salts

The present chapter studies the substitution of conventional LiTFSI electrolyte salt by alternative imide-containing salts with different structural properties. LiFSI is initially demonstrated to allow an unprecedented cell stability, by the generation of a LiF-based protective layer on metallic lithium. However, the high reactivity of the salt towards cell component reduces cell capacity values and hinders its response at fast cycling. For that reason, the LiFTFSI salt is ultimately proposed, which combines the functionalities of LiTFSI and LiFSI salts in a single structure, enabling a synergistic effect that allows stable cell cycling, high capacity and good rate response.

INDEX

5	ALTERNATIVE IMIDE-CONTAINING SALTS..	119
5.1	LITHIUM BIS(FLUOROSULFONYL)IMIDE BASED ELECTROLYTE	121
5.1.1	Physicochemical and electrochemical properties	121
5.1.2	Electrochemical behavior with the Li ⁰ electrode.....	124
5.1.3	Anion stability against LiPSs.....	127
5.1.4	Electrochemical performance.....	129
5.2	LITHIUM (FLUOROSULFONYL) (TRIFLUOROMETHANESULFONYL) IMIDE BASED ELECTROLYTE	131
5.2.1	Physicochemical and electrochemical properties	131
5.2.2	Electrochemical behavior with the Li ⁰ electrode.....	134
5.2.3	Anion stability against LiPS	136
5.2.4	Electrochemical performance.....	138
5.3	DISCUSSION	140
5.4	CONCLUSIONS	142
5.5	REFERENCES	142

5 ALTERNATIVE IMIDE-CONTAINING SALTS

After studying the suitability of the addition of electrolyte additives and electrolyte fillers, this chapter will focus in a completely different approach: the substitution of the lithium bis(trifluoromethanesulfonyl) imide (LiTFSI) electrolyte salt by novel alternative imide-containing salts, yet unexplored in this field. The aim of this modification is the improvement of metallic lithium (Li^0) stability, in order to improve cycling stability of all-solid-state lithium-sulfur batteries (ASSLSBs), without the necessity of adding external electrolyte components, such as additives or fillers.

Although it may seem a simple approach, the proper selection of lithium salts is not an easy task. For lithium salts applied so far in solid polymer electrolyte (SPE)-based ASSLSBs, previous works included the ones based on tetrafluoroborate (BF_4^-),¹ triflate (CF_3SO_3^-),^{2,3} bis(trifluoromethanesulfonyl)imide ($[\text{N}(\text{SO}_2\text{CF}_3)_2]^-$, TFSI⁻),^{4,5} and perchlorate (ClO_4^-)⁶ anions. As previously mentioned in the Introduction chapter, none of these works feature satisfactory performance in ASSLSBs, showing abrupt capacity decays and very limited cycle life. This has been mainly attributed to the unstable operation of the Li^0 negative electrode, as a result of the poor quality of the generated solid-electrolyte interphase (SEI) layer during salt/polymer reduction on the metallic surface. As previously depicted, SEI layer plays a critical role in the Li^0 protection, and must be compact, homogeneous, flexible and lithium ion (Li^+) conductive enough to ensure a proper cycling during several charge/discharge cycles.⁷

With the aim at improving the interfacial compatibility of SPE and Li^0 , Zhou *et al.*⁸ studied the effect of the novel lithium (trifluoromethanesulfonyl)(n-nonafluorobutanesulfonyl) imide salt (LiTNFSI) addition in a poly(ethylene oxide) PEO-based SPEs. The novel LiTNFSI imide-containing salt featured a remarkable Li^0 /SPE compatibility improvement in comparison to the reference LiTFSI. Accordingly, good cycling performance on SPE-based ASSLSBs was reported. The improvement was ascribed to the role of the C_4F_9 -group in forming stable SEI on the Li^0 . **Figure 5.1** compares the chemical structure of both LiTNFSI and LiTFSI salts and shows schematic illustration of the effect of the salt in the quality of the SEI films formed on the electrodes.

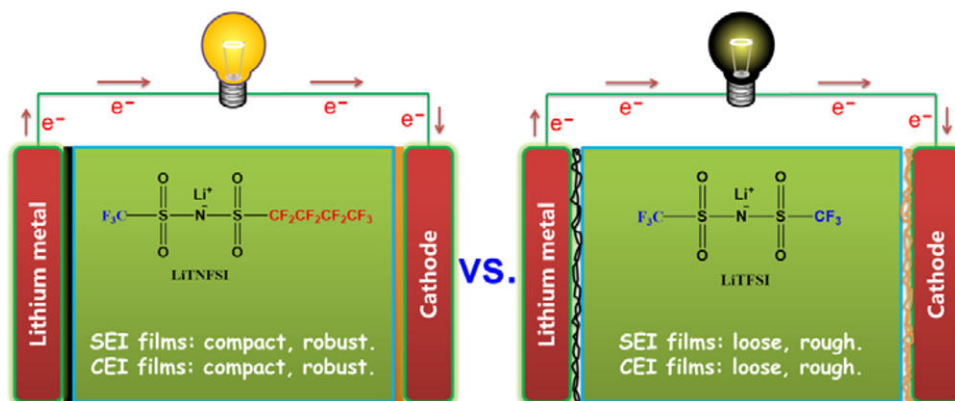


Figure 5.1. Schematic illustration of the formed interfacial films on the electrodes in the presence of LiTNFSI/PEO and LiTFSI/PEO electrolytes. CEI abbreviates cathode/electrolyte interphase. Reprinted with permission from Ref. 8 with permission. Copyright 2019 Americal Chemical Society.

This work demonstrated the suitability of the use of alternative imide-containing salts, rather than conventional LiTFSI, to obtain a proper protection of Li^0 that allows adequate cycling performance of SPE-based ASSLSBs. This work also demonstrated that anion chemistry can dictate the nature and quality of both SEI layers on negative and positive electrodes.

Therefore, this chapter will explore, in two individual sections, the possibility of applying two alternative imide-containing salts in SPE-based ASSLSBs, *i.e.*, lithium bis(fluorosulfonyl)imide (LiFSI) and lithium (fluorosulfonyl)(trifluoromethanesulfonyl) imide (LiFTFSI). With the use of these two alternative salts, this work will attempt to overcome the limitations ascribed to LiTFSI, regarding a poor quality SEI formation on Li^0 , which leads to remarkable overcharge associated with LiPS shuttling. LiFSI has been already reported to form a very favorable SEI on Li^0 and has been successfully implemented in Li^0 -based and liquid electrolyte-based lithium-sulfur batteries (LSBs),^{9–13} but never tried in SPE-based ASSLSBs before. On the other hand, asymmetric LiFTFSI is a rather less explored salt that combines $-\text{CF}_3$ and S–F terminations in its structure, which may allow to synergistically combine the beneficial features of FSI⁻ and TFSI⁻ anions. The chemical structures of LiTFSI, LiFSI, and LiFTFSI are shown in **Figure 5.2**.

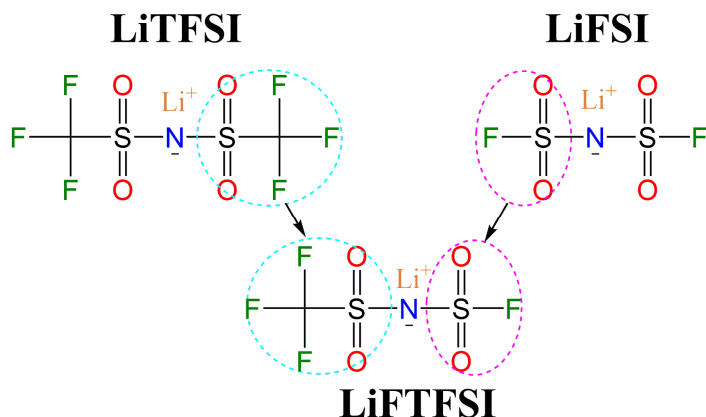


Figure 5.2. Comparison of the chemical structures of LiTFSI, LiFSI, and LiFTFSI salts.

5.1 LITHIUM BIS(FLUOROSULFONYL)IMIDE BASED ELECTROLYTE

For a decade now, LiFSI has been intensively investigated as next-generation salt for Li-based batteries due to its high ionic conductivity (related to the weak interaction of solvated Li⁺ cations and FSI⁻ anions), acceptable chemical stability, and capability on forming stable Li⁺ permeable SEI films on various electrodes.^{9,13–16} Its beneficial properties have been explored not only to develop superior performance liquid electrolytes (both as main salt,⁹ and co-salt¹¹) and ionic liquids,¹⁶ but also SPEs.^{12,17} These features make LiFSI salt an appealing choice in the search of suitable lithium salts that may help to stabilize Li⁰ negative electrode, and thus, enable the development of SPE-based ASSLSBs with satisfactory performance.

The following sections will focus on the physicochemical and electrochemical characterization of the prepared LiFSI-based SPEs, the electrochemical behavior with Li⁰, and the study of anion stability against LiPS. Finally, the suitability of the new electrolytes will be tested in ASSLSBs. The obtained results will be always compared with the reference cell developed in the Chapter 2.

5.1.1 Physicochemical and electrochemical properties

LiFSI containing PEO-based SPEs (1:20 LiFSI:PEO molar ratio) were prepared by solvent casting method. The physicochemical properties of the membrane are characterized in **Figure 5.3**. At the outset, **Figure 5.3a** shows a self-standing and translucent 16 mm diameter SPE membrane, with an indistinguishable appearance compared to the reference LiTFSI/PEO membrane. In order to determine the

solubility of the salt in the PEO membrane, the X-ray diffraction (XRD) patterns of the bare PEO, pristine LiFSI salt and LiFSI/PEO membrane are shown in **Figure 5.3b**. LiFSI/PEO membrane shows only the characteristic diffraction peaks that belongs to the pure crystalline phase of the PEO at $2\Theta = 19^\circ$ and 23° , and shows no peak from pristine LiFSI. This indicates the excellent solubility and complete solvation of the lithium salt in PEO. Regarding, anodic stability, **Figure 5.3c** shows that LiFSI/PEO membrane features similar electrochemical stability than the reference. The linear sweep voltammetry shows a low anodic current of $< 10 \mu\text{A cm}^{-2}$ starting at 3.8 V vs. Li/Li⁺, which can be ascribed to PEO matrix oxidation. Then, at > 5 V vs. Li/Li⁺, pronounced increase of current generated by anion oxidation are observed. However, the oxidation starts well above our upper limit of the working potential, *i.e.*, 2.8 V vs. Li/Li⁺, thus, the membrane is stable to oxidation in our working potential range. Regarding the thermal stability, thermogravimetric analysis (TGA) in **Figure 5.3d** shows that LiFSI/PEO has significantly lower degradation temperature than LiTFSI/PEO, which can be ascribed to the lower stability of the FSI⁻ anion in comparison to TFSI⁻. This can be related to the lower stability of S–F terminal bond in LiFSI in comparison to the stable C–F₃ termination in LiTFSI. However, there is no LiFSI/PEO mass loss at the working temperature of 70 °C, so the membrane is thermally stable enough for operation at the set of conventional conditions.

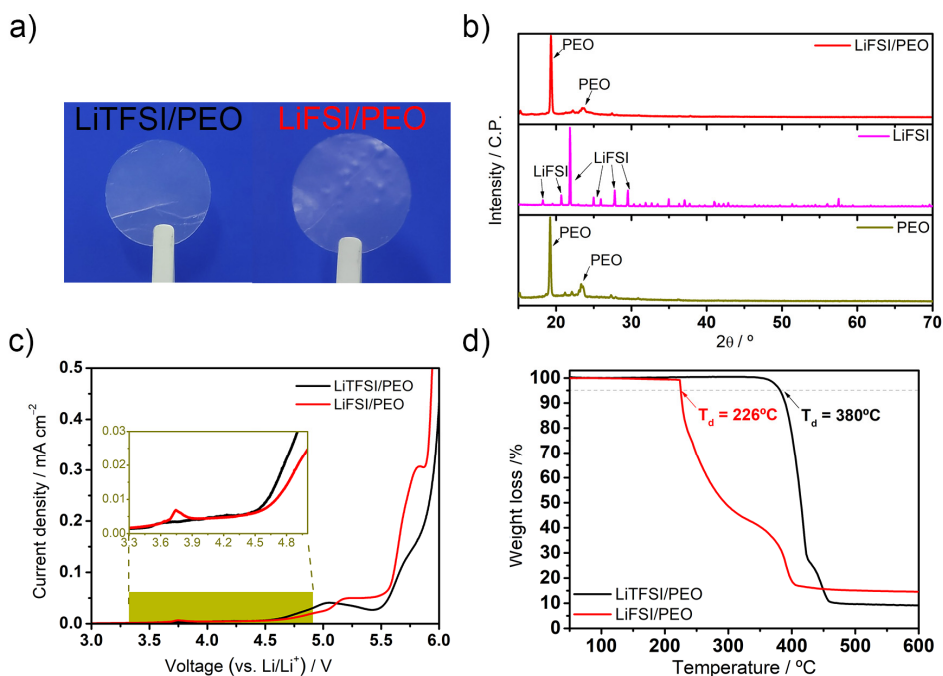


Figure 5.3. Physicochemical and electrochemical properties of LiFSI/PEO and reference LiTFSI/PEO membranes. a) Optical images, b) XRD patterns, c) anodic stabilities at 70 °C, and d) TGA traces.

Figure 5.4a shows differential scanning calorimetry (DSC) traces of both membranes, with the aim of studying the effect of the salt variation in the thermal properties of the membrane, which are closely related with the conductivity. Even if LiFSI containing membrane shows slightly lower glass transition temperature, T_g , compared to LiTFSI/PEO reference, it has higher melting point, T_m , and higher melting enthalpy, ΔH_m . Thus, higher crystallinity, χ_c . This is attributed to the lower plasticizing effect of FSI⁻ anion in comparison to TFSI⁻. This is in agreement with conductivity values in **Figure 5.4b**, where LiTFSI/PEO shows a flatter profile and a less sharp transition around the T_m area, due to the sluggish kinetic of crystallization in the presence of the $-\text{SO}_2\text{CF}_3$ moiety. Nevertheless, even if LiFSI/PEO features remarkably lower conductivities below T_m , its conductivity at operating temperature, *i.e.*, 70 °C, and above are comparable to reference membrane. Regarding lithium transference number, t_{Li^+} , (**Figure 5.4c**) LiFSI/PEO displays slightly lower value than LiTFSI/PEO, 0.12 vs. 0.15. The lowest selectivity to Li⁺ is related to the smaller size of FSI⁻ anion, thus, its higher mobility. As a result, LiFSI/PEO shows lower Li⁺ conductivity at 70 °C (**Figure 5.4c**). However, the conductivity value still remains in the order of 10⁻⁴ S cm⁻¹, which is considered enough for battery performance.

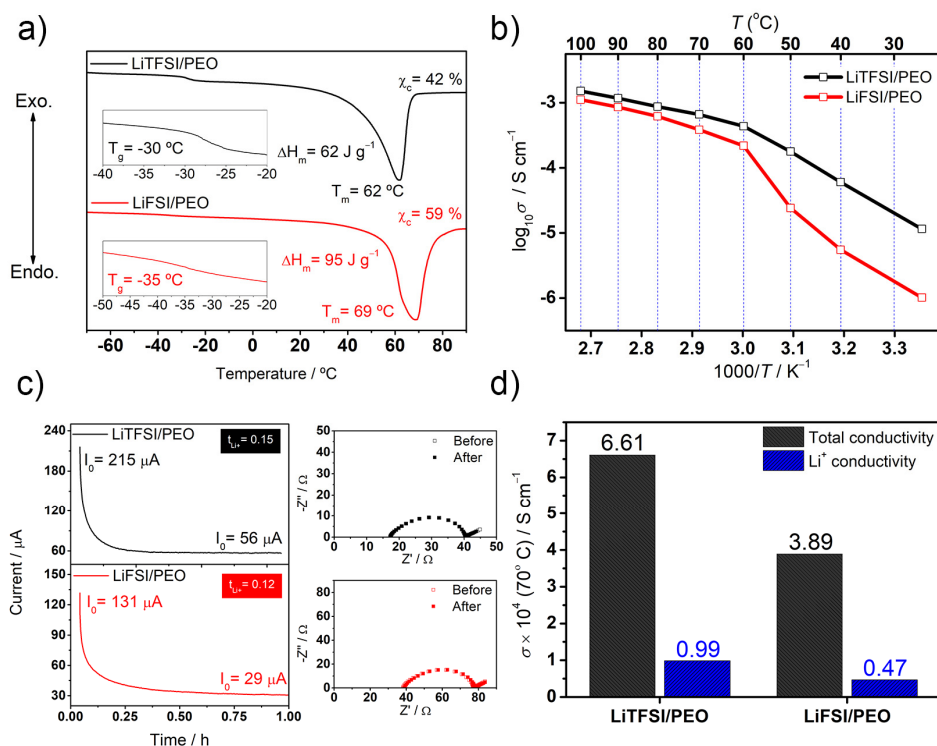


Figure 5.4. Physicochemical and electrochemical properties of LiFSI/PEO and reference LiTFSI/PEO membranes. a) DSC traces b) Arrhenius plots of ionic conductivity; c) chronoamperometry test under 10 mV polarization at 70 °C, and electrochemical impedance spectroscopy measurements before and after the test for t_{Li^+} measurement; and d) Li⁺ conductivity at 70 °C.

In conclusion, even if in comparison with the reference LiTFSI/PEO membrane, the LiFSI/PEO membrane shows more limited properties in certain aspects, such as lower thermal stability and conductivity, it shows yet adequate properties for ASSLSB operation and its full characterization was completed.

5.1.2 Electrochemical behavior with the Li⁰ electrode

LiFSI salt has been previously studied for battery application due to its ability to form high quality SEI films on electrodes. In order to complete the study of the LiFSI/PEO electrolyte, **Figure 5.5** studies the electrochemical behavior of the LiFSI/PEO membrane in contact with the Li⁰ electrode. **Figure 5.5a** shows galvanostatic cycling of Li⁰ | SPE | Li⁰ symmetric cells at 0.1 mA cm⁻² and 2 h semicycles at 70 °C. The voltage response with time and current direction shows stable voltage profiles in the first few cycles due to the formation of SEI layers on

the surface of Li^0 . However, while the reference LiTFSI/PEO faces a dendrite induced short circuit after less than 200 h of operation, LiFSI/PEO can last for more than 500 h, which is a clear indicative of the better compatibility of the PEO membrane in presence of LiFSI.

LiFSI/PEO membranes show again sticky properties after cycling, so the direct the *post-mortem* analysis of the cell components is neither possible in this case. Therefore, 1,2-dimethoxyethane was again selected to study the effect of the salt anion on Li^0 deposits. To check the validity of this archetype solvent, the same galvanostatic cycling ($\text{Li}^0 \mid \text{salt/DME} \mid \text{Li}^0$) was repeated at room temperature (RT) and the same tendency regarding cycling life was verified (**Figure 5.5b**).

Upper part of **Figure 5.5c** shows scanning electron microscopy (SEM) pictures of the abovementioned Li^0 deposits onto Cu foil in the presence of either LiTFSI or LiFSI salts. Those deposits were obtained by galvanostatic cycling of $\text{Li}^0 \mid \text{DME+SALT} \mid \text{Cu foil}$ symmetric cells at 0.1 mA cm^{-2} and 20 h at $25 \text{ }^\circ\text{C}$. While the deposits in presence of LiTFSI/DME shows unevenly plated and more dendritic structures, for LiFSI/DME electrolytes flake-like Li^0 deposits with a relatively homogeneous distribution over substrate are observed. This indicates that the nature of the salt can strongly affect the quality of the surface of the Li^0 deposits.

To shed some more light on the role of salt anions in the electrochemical compatibility between the Li^0 electrode and the electrolytes, the Li^0 deposits were analyzed by X-ray photoelectron spectroscopy (XPS). Bottom part of **Figure 5.5c** shows the C1s and F1s spectra of the samples. Compared to the LiTFSI/DME electrolyte, LiFSI/DME C1s spectra shows less DME reduction derived products, *e.g.*, $\text{H}_2\text{C}=\text{HC}-\text{O}-\text{CH}_3$, CH_3OLi , (R2 and R1 respectively). F1s spectra shows favored highly protective LiF formation in presence of LiFSI salt. LiF is a salt reduction derived product and is one of the predominant SEI species in the DME/LiFSI electrolyte system, while only shows trace amounts in LiTFSI/DME based system. The differences into salt reduction products can be ascribed to the weaker and more reactive S–F bond in FSI^- compared to C–F bond in TFSI^- .¹⁸ While in LiTFSI system, the salt is resistant to reduction and the SEI is mainly formed by DME reduction products; in the LiFSI system, the salt is prone to reaction and the SEI layer is mainly formed by its reduction products. This clearly suggests that FSO_2^- functional group from LiFSI salt can regulate morphology, composition and mechanical stability of SEI layer, thus stabilizing Li^0 anode and mitigating the growth of dendrites.

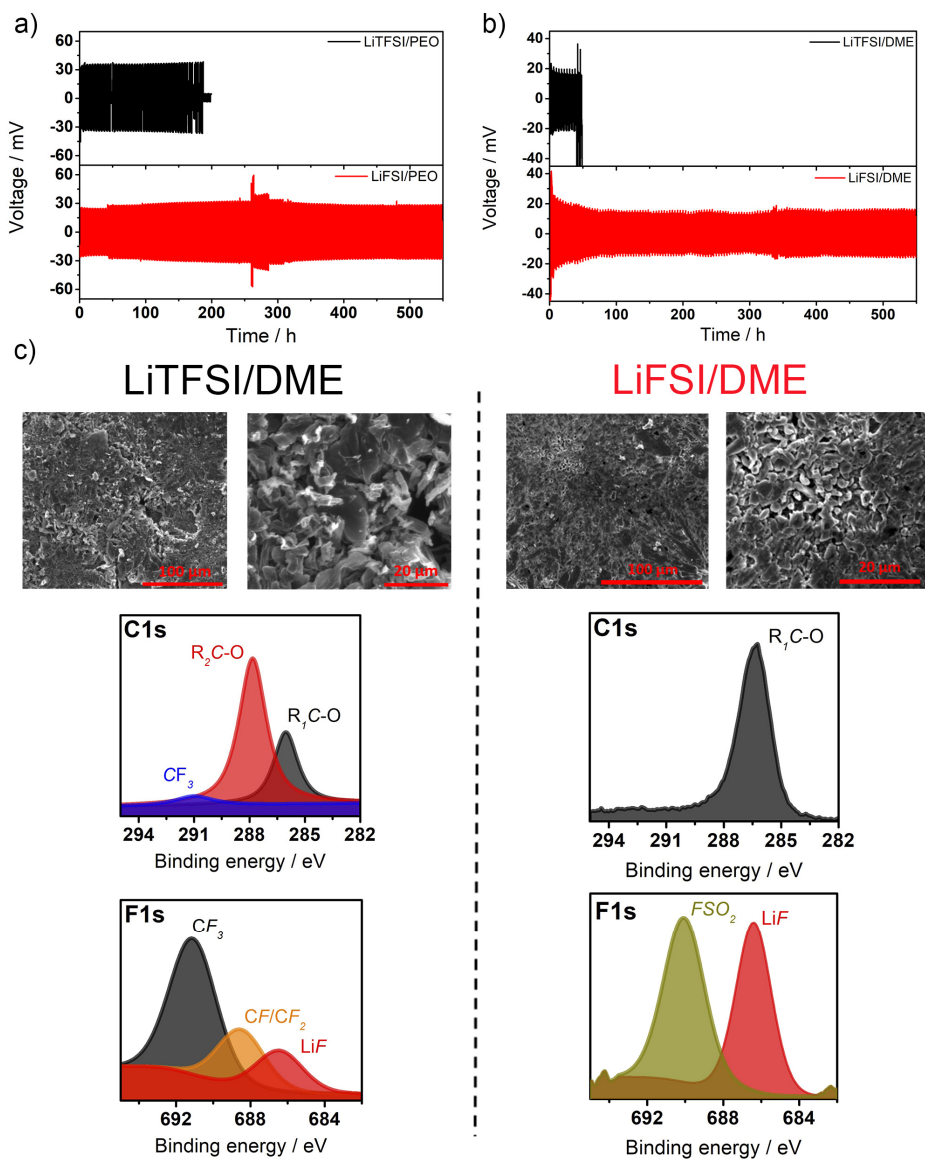


Figure 5.5. Electrochemical behavior of Li^0 electrode in the as-prepared electrolytes. a) Galvanostatic cycling of $\text{Li}^0|\text{SPE}|\text{Li}^0$ symmetric cells at 0.1 mA cm^{-2} and 2 h semicycles at $70 \text{ }^\circ\text{C}$. b) Galvanostatic cycling of $\text{Li}^0|\text{DME}+\text{SALT}|\text{Li}^0$ symmetric cells at 0.1 mA cm^{-2} and 2 h semicycles at $25 \text{ }^\circ\text{C}$. c) SEM images and XPS spectra of Li^0 deposited onto Cu substrates ($\text{Li}^0|\text{DME}+\text{SALT}|\text{Cu}$ cells) at 0.1 mA cm^{-2} during 20 h at $25 \text{ }^\circ\text{C}$. $\text{R}_1\text{C-O}$ and $\text{R}_2\text{C-O}$ refer to $\text{CH}_3\text{O-}$ and $\text{H}_2\text{C=HC-O-CH}_3$, respectively.

All these measurements evidence that the presence of the LiFSI salt generates more favorable SEI in contact with Li^0 and forms a less dendritic, more dense and compact deposits, resulting in better performance of the Li^0 symmetric cells. In summary, it can be concluded that LiFSI containing electrolyte generates a salt-derived inorganic species-containing SEI, a prerequisite for a mechanically and electrochemically stable SEI layer. This, in contrast to the organic rich SEI layer on LiTFSI based electrolyte, paves the way for and high quality interfacial layer and improved Li^0/SPE compatibility. This results are in line with previously mentioned studies, where high quality SEI layers were obtained in presence of LiFSI.

To complement previous results, a chemical simulation was carried out by Dr. Eshetu. These results proved that while TFSI^- anion can only be reduced at very low potentials, close to that of metallic Li^0 with the biphenyl radical anion, FSI^- easily gets reduced starting at 1.0-1.1 V vs. Li/Li^+ by the biphenyl radical monoanion. This confirms that FSI^- anion will be always more prone to reaction with the negative electrode surface.

5.1.3 Anion stability against LiPSs

The chemical reaction between dissolved lithium polysulfides (LiPS) and salt anion may result in i) deteriorated capacity retention due to active material loss, and ii) declined ionic conductivity in the electrolytes. Thus, salt anion resistance towards aggressive LiPS is a desirable property for the development of LSBs.

The direct observation of LiPS/anion interaction in PEO is not possible in this case neither, but the reactivity can be easily observed in liquid media. For that purpose, **Figure 5.6a** compares the appearance of blank DME and 1 M LiTFSI/DME solution before and after the addition of LiPS solution. In contrast to the almost unchanged color of DME/LiTFSI, the greenish color turns to dark orangish in DME/LiFSI electrolyte in presence of LiPS. The color change is objectively confirmed by ultraviolet visible (UV-vis) absorbance spectra in **Figure 5.6b**, which shows an additional peak around 580-640 nm. The change of color confirms the existence of chemical reaction between LiPS and FSI^- anion. In the view of the labile S-F bond, reaction intermediates were proposed and computed by density functional theory (DFT) by Dr. Zhang. The nucleophilic reaction of FSI^- with Li_2S_6 (reference high order LiPS) may lead to the substitution of S-F link by S-S_n linkage, reaching a corresponding reaction energy reaches -654 KJ mol^{-1} , in contrast a less exothermic S-C cleavage in TFSI^- structure, with a remarkably less favorable reaction energy of -221 KJ mol^{-1} . Furthermore, the substitution of both S-F bonds in FSI^- gives an unstable trivalent anion which may have a low solubility in PEO, irreversibly consuming LiPSs.

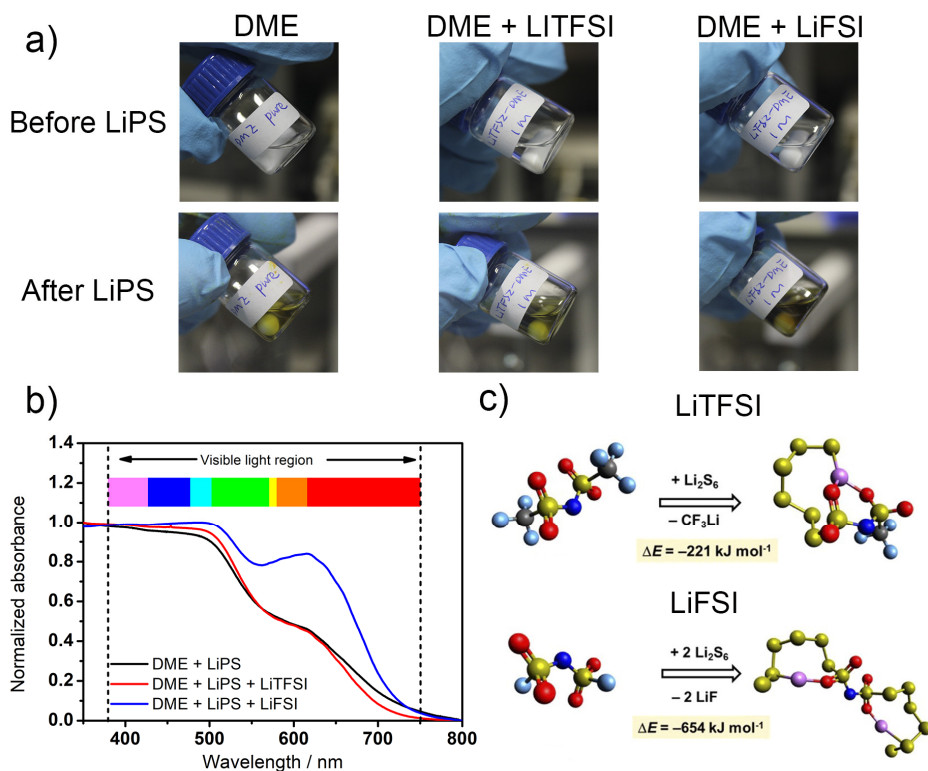


Figure 5.6. Stability of salt anion against LiPS species. a) Appearance of and blank DME and 1 M salt/DME solution before and after the addition of LiPS solution (200:1, salt:LiPS molar ratio) at RT. b) Normalized UV-vis absorption spectra of the LiPS-added solutions after 60 h of contact. c) DFT calculations for the proposed intermediates. Red, yellow, light blue, dark blue, gray and pink balls stand for O, S, F, N, C, and Li atoms, respectively.

In conclusion, it is confirmed that while TFSI⁻ anion is stable in presence of LiPS; the reactions are very likely to take place for FSI⁻, which may lead to irreversible LiPS consumption to some extent. This is an undesirable property for a salt anion, but electrochemical performance test in the following point will confirm until which extent this may affect the performance of the LiFSI/PEO based cell.

5.1.4 Electrochemical performance

Previous two sections have pointed out that the high reactivity of FSI^- anion will have two effects. This significant reactivity will lead to an excellent passivation of the metallic electrode by LiF rich SEI layer, but will probably generate LiPS consumption. For that reason, it is interesting to study the role of LiFSI/PEO membranes in the full ASSLSBs system.

Figure 5.7 presents the cycling performance of $\text{Li}^0|\text{SPE}$ (PEO + LiTFSI or LiFSI)|S cells at 70 °C. Rate capability test in **Figure 5.7a** shows that even if the LiFSI/PEO system delivers lower discharge capacity (*c.a.*, 550 mAh g^{-1} vs. 700 mAh g^{-1} at 0.1C for LiTFSI) and worse rate response (*c.a.*, 170 mAh g^{-1} vs. 400 mAh g^{-1} at 0.5C), a Coulombic efficiency close to 100% is obtained even at the higher rates, indicating the absence of overcharge related to the shuttle effect. According to our studies, the lower discharge capacity and worse rate response of LiFSI/PEO cells in comparison to LiTFSI/PEO cells can be ascribed to two phenomena: i) the high reactivity of FSI^- with LiPS, which may irreversibly consume LiPS; ii) more resistant SEI on Li^0 for LiFSI containing systems, as discharge/charge profiles of the cells shows an increased polarization (voltage difference between charge and discharge) with cycling rate in LiFSI system (**Figure 5.7b**). The reduction products of LiFSI salt lead to a better Li^0 protection, but the thickness of this layer can be excessive and hinder Li^+ conduction, increasing interfacial resistance and decreasing cell capacity.

Focusing on discharge/charge profiles, at high rates LiTFSI/PEO based cells (**Figure 5.7c**) show overcharge, with an extended charge plateau at 2.4–2.5 V vs. Li/Li^+ , related to e^- consumption during LiPS attack to Li^0 negative electrode. However, LiFSI/PEO cell shows no extended charge plateau. Most remarkably, **Figure 5.7d** shows 1000 discharge cycles at constant rate of 0.1C for LiFSI/PEO with no Coulombic efficiency decay, indicating the excellent stability of the prepared ASSLSBs. The capacity decay of this cell may be ascribed to degradation of the positive electrode or to the active material loss, but the absence of overcharge indicates stable Li^0 operation for an unprecedented lifespan in SPE-based ASSLSBs. The previously mentioned studies in the State of Art section in the Introduction chapter reported 200 cycles at most, which means a 5-fold improvement in this work.

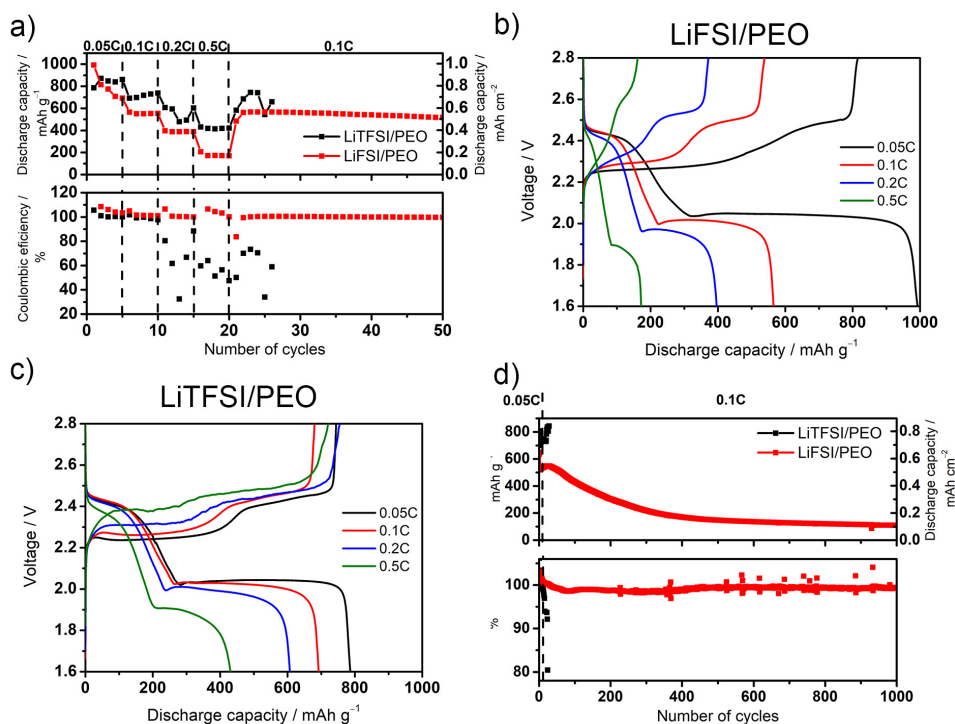


Figure 5.7. a) Discharge capacity and Coulombic efficiency of Li⁰|SPE (PEO + LiTFSI or LiFSI)|S electrode cells at different C-rates. Discharge/charge profiles during the first cycle at each rate for b) LiTFSI/PEO and c) LiFSI/PEO cells. d) Discharge capacity and Coulombic efficiency of Li⁰|SPE (PEO + LiTFSI or LiFSI)|S electrode cells at constant rate of 0.1C, after two initial cycles at 0.05C. All the measurements were done at 70 °C.

At this point, this work sets a precedent in the stability of pure SPE-based ASSLSBs, allowing a proper battery performance in filler/additive free systems by tuning the electrolyte salt. The lower discharge capacity and worse rate response is a problem that needed to be tackled urgently, but it is undoubtedly demonstrated that anion can dictate that the quality of the Li⁰/electrolyte interface, and this has a significant impact on LSB performance. This work was partially published.¹⁹

5.2 LITHIUM (FLUOROSULFONYL) (TRIFLUOROMETHANESULFONYL) IMIDE BASED ELECTROLYTE

Even if the substitution of reference LiTFSI salt by LiFSI salts in PEO-based SPE have brought benefits in terms of cycling stability, the loss in capacity and rate performance is not acceptable for its technical viability. LiTFSI-based electrolytes suffer from poor stability and a prompt cell failure, but the delivered discharge capacity before cell failure is among the highest that have been reported for SPE-based ASSLSBs thus far (refer to State of Art section). Accordingly, the use of asymmetric LiFTFSI salt is proposed, which could, in principle, combine the beneficial features of both FSI⁻ and TFSI⁻ anions and enable the building of a robust SEI, and allow high Coulombic efficiency and long term cycling but with a competitive cell capacity. In contrast to the more studied LiFSI salt, only few research activity in battery field including LiFTFSI have been reported,^{20–25} with only one example in solid electrolyte application.²² Therefore, the following sections will evaluate this novel approach and its suitability for ASSLSBs.

5.2.1 Physicochemical and electrochemical properties

Figure 5.8 includes physicochemical and electrochemical characterization of the prepared LiFTFSI/PEO membrane. Optical images in **Figure 5.8a** show a self-standing membrane with no visible difference with LiTFSI/PEO and LiFSI/PEO ones. XRD spectra (**Figure 5.8b**) shows no presence salt peak in the LiFTFSI/PEO membrane, indicating its full solvation in PEO. Anodic stability in **Figure 5.8c** shows similar response, with an initial peak related to PEO oxidation and a following one related to anion oxidation. Finally, the thermal stability is slightly improved in comparison to LiFSI/PEO as observed by TGA traces (**Figure 5.8d**), but is still lower than reference LiTFSI/PEO. Therefore, the thermal stability is again dictated by the salt. However, no mass loss is observed at 70 °C, indicating its suitability for operation at that temperature.

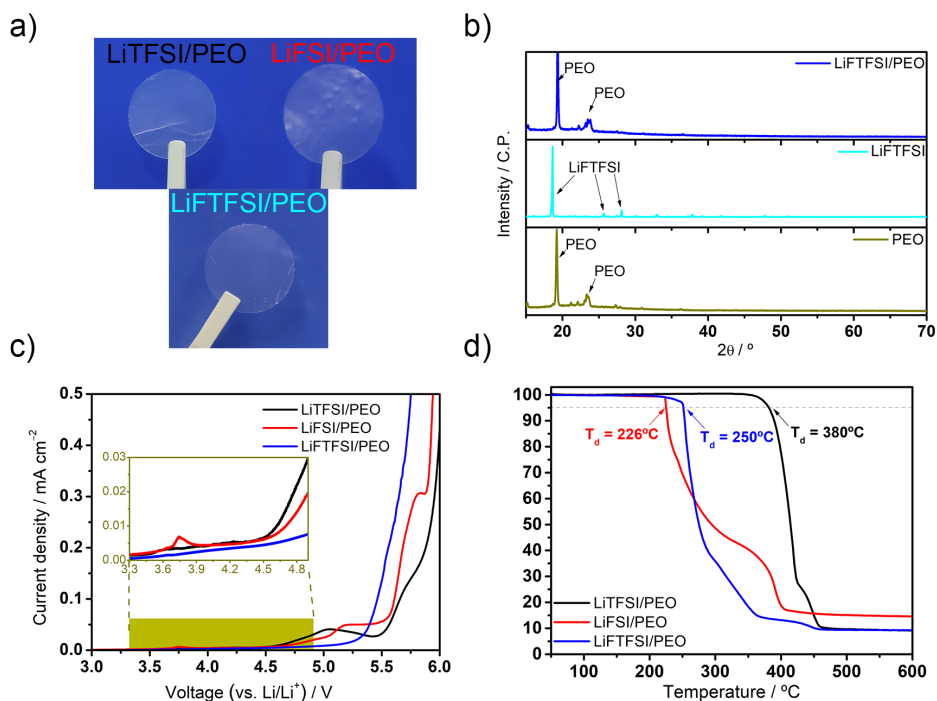


Figure 5.8. Physicochemical and electrochemical properties of LiFSI/PEO compared to reference LiTFSI/PEO and LiFSI/PEO membranes. a) Optical images, b) XRD patterns, c) anodic stabilities at 70 °C, and d) TGA traces.

DSC traces of LiFTFSI/PEO in **Figure 5.9a** display an intermediate phase transition behavior, *i.e.*, melting point and crystallinity, between LiTFSI/PEO and LiFSI/PEO membranes. So does Arrhenius plot for conductivity (**Figure 5.9b**), which shows a decreased conductivity for LiFTFSI/PEO membrane in comparison to reference LiTFSI-containing one, but a softer transition around the T_m compared to LiFSI/PEO membrane. At operation temperature (70 °C) LiFTFSI-based membrane shows a conductivity total of $6.31 \times 10^{-4} \text{ S cm}^{-1}$ and a t_{Li^+} of 0.19 (**Figure 5.9c**), which results in a Li^+ conductivity of $1.19 \times 10^{-4} \text{ S cm}^{-1}$ (**Figure 5.9d**). The increased t_{Li^+} of LiFTFSI containing membrane may be related to the lower anion mobility due to its asymmetric structure.

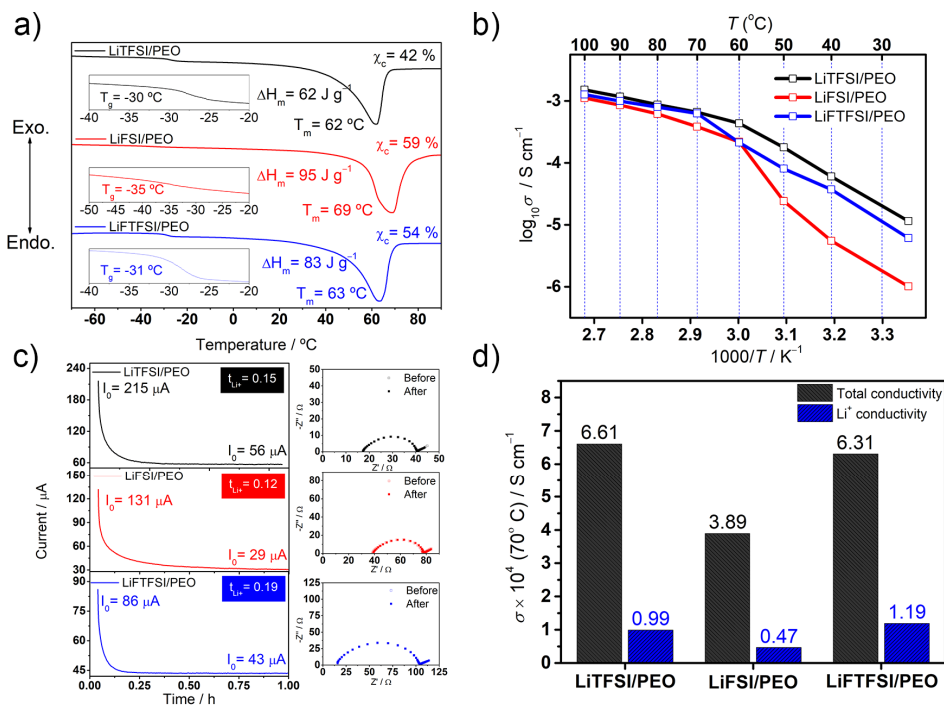


Figure 5.9. Physicochemical and electrochemical properties of LiTFFSI/PEO compared LiTFSI/PEO reference and LiFSI/PEO membranes. a) DSC traces, b) Arrhenius plots of ionic conductivity; c) Chronoamperometry test under 10 mV polarization at 70 °C, and electrochemical impedance spectroscopy measurements before and after the test for t_{Li^+} measurement; and d) Li^+ conductivity at 70 °C.

In conclusion, LiTFFSI-based SPE membranes have been successfully prepared. The membranes feature, in general, intermediate properties between LiTFSI and LiFSI salts in terms of thermal stability, thermal transition properties and conductivity. This can be related to the presence of both $-SO_2CF_3$ and $-FSO_2$ ending in the structure of the salt.

5.2.2 Electrochemical behavior with the Li^0 electrode

Regarding the interfacial stability of LiFTFSI electrolytes with Li^0 , electrochemical response of the SPE studies are summarized in **Figure 5.10**. Galvanostatic cycling of $\text{Li}^0 \mid \text{LiFTFSI/PEO} \mid \text{Li}^0$ symmetric cell (**Figure 5.10a**) shows improved operation time with respect to LiTFSI/PEO reference, and features a cycle life as stable as the one for LiFSI/PEO-based cell. Again, the same tendency is verified for in DME in **Figure 5.10b**.

The SEM images on the Li^0 deposits on Cu foil in presence of LiFTFSI salt (**Figure 5.10c**) show, in contrast to LiTFSI/DME system, flake-like deposits with homogeneous distribution, and no dendritic structures, neither big agglomerates. The C1s spectra from the surface of Li^0 deposits in the presence of LiFTFSI/DME electrolyte shows, as for reference LiTFSI/DME, solvent derived products, but in a less extent. For example, the presence of the DME derived $\text{H}_2\text{C}=\text{HC}-\text{O}-\text{CH}_3$ (R_2) is remarkably minimized. Regarding the F1s spectra, even in a lesser extent than LiFSI/DME, normalized atomic percentage of F-containing species shows a favored LiF formation for LiFTFSI system (23 at.%) in comparison to LiTFSI system (18 at.%).

Therefore, LiFTFSI shows an intermediate tendency between LiTFSI and LiFSI in forming less desirable organic species and more desirable LiF, which is in line with its structure where it is endowed with half $-\text{CF}_3$ and half S-F bond functionality. However, as seen in the galvanostatic cycling in both **Figure 5.10a** and **Figure 5.10b**, the generated SEI on the Li^0 is enough for a proper protection of the negative electrode over cycling. These results confirm the importance of the $-\text{FSO}_2$ group in the regulation, composition and mechanical stability of the SEI layer. Chemical simulations test showed that, similar to LiFSI, LiFTFSI can easily get reduced at higher voltages than those necessary for the LiTFSI reduction, which is again an indicative of its reactivity through the reduction of the $-\text{FSO}_2$ moiety.

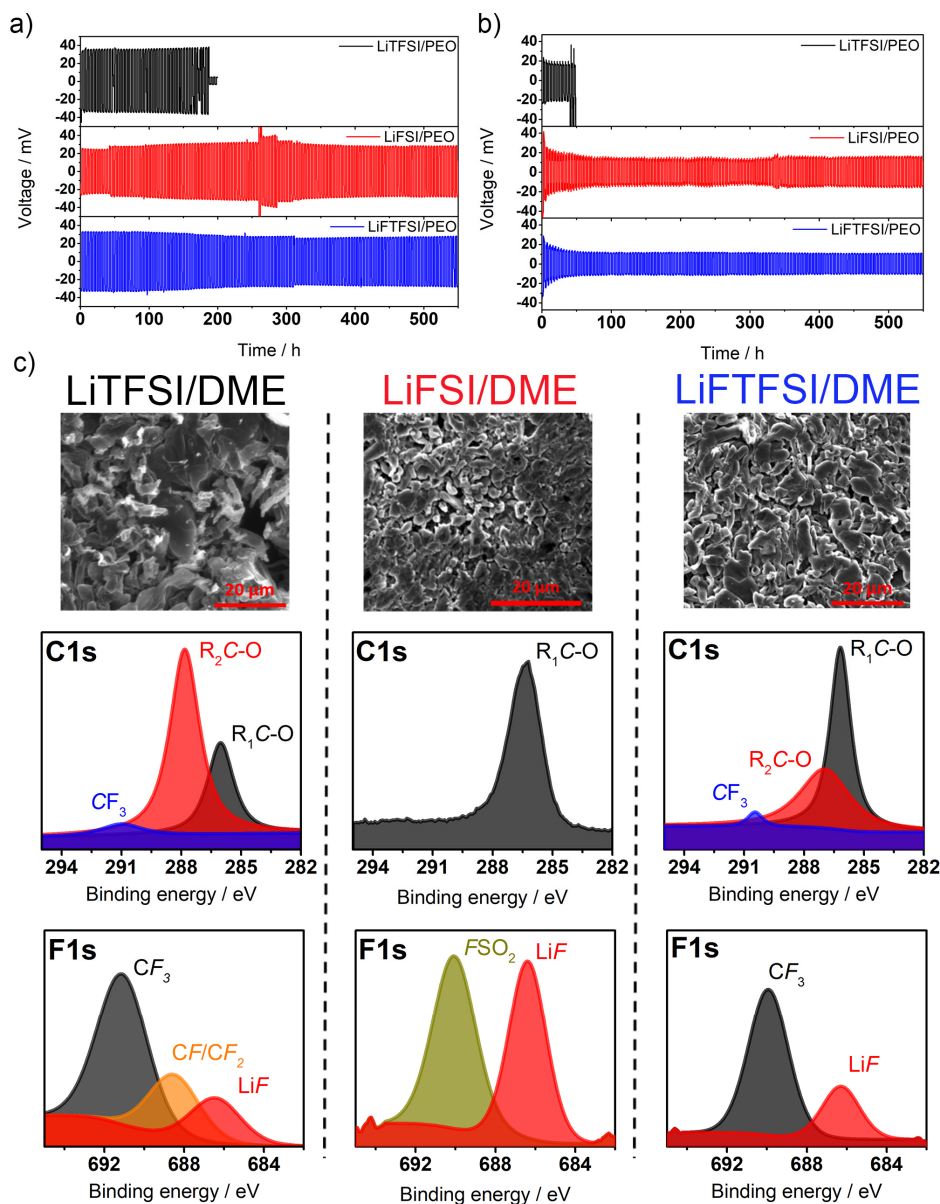


Figure 5.10. Electrochemical behavior of Li^0 electrode in the as-prepared electrolytes. a) Galvanostatic cycling of $\text{Li}^0|\text{SPE}|\text{Li}^0$ symmetric cells at 0.1 mA cm^{-2} and 2 h semicycles at 70°C . b) Galvanostatic cycling of $\text{Li}^0|\text{DME}+\text{SALT}|\text{Li}^0$ symmetric cells at 0.1 mA cm^{-2} and 2 h semicycles at 25°C . c) SEM images and XPS spectra of the Li^0 deposited onto Cu substrates ($\text{Li}^0|\text{DME}+\text{SALT}|\text{Cu}$ cells) at 0.1 mA cm^{-2} during 20 h at 25°C . $\text{R}_1\text{C-O}$ and $\text{R}_2\text{C-O}$ refer to $\text{CH}_3\text{O-}$ and $\text{H}_2\text{C=HC-O-CH}_3$, respectively.

In conclusion, these promising results prove the slightly lower tendency to electrochemical reduction for FTFSI⁻ vs. FSI⁻, but still its higher liability compared to TFSI⁻. This results in an effective enough passivation layer that allows negative electrode protections, enabling its prolonged stable cycling.

5.2.3 Anion stability against LiPS

As for the LiFSI salt study, the stability of FTFSI⁻ anion stability against LiPS was studied by mixing both in DME and the further UV-vis analysis of the sample. **Figure 5.11a** shows that after the addition of LiPS to DME/LiFTFSI solution, the color of the mixture varies from the reference DME+LiPS. This is an indicative of LiPS reaction with the salt anion. UV-vis spectra in **Figure 5.11a** confirms the color change, but also shows that the shift is less intense than in LiFSI/DME system. This suggests that there is a reaction between FTFSI⁻ anion and LiPS, but less dramatic than with FSI⁻ anion. DFT calculations confirm that hypothesis. While the reaction of FTFSI⁻ anion with LiPS by substitution of its single S–F bond is more favorable than S–C substitution in TFSI⁻ anion (-359 KJ mol^{-1} vs. -221 KJ mol^{-1}), it is not as exothermic as for FSI⁻ anion (-654 KJ mol^{-1}). Furthermore, in comparison to FSI⁻, the resulting $\text{CF}_3\text{SO}_2\text{N}^{(-)}\text{SO}_2\text{-S}_6^{(-)}$ intermediate divalent anion may be electrochemically reversible and sufficiently soluble in PEO due to its asymmetrical structure, thereby allowing its reversible utilization.

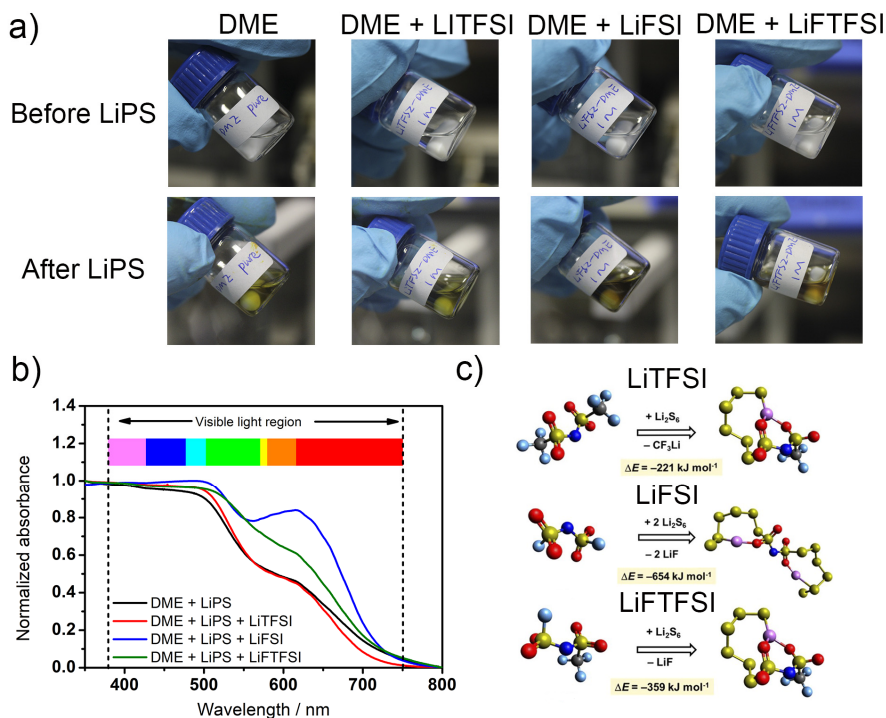


Figure 5.11. Stability of salt anion against LiPS species. a) Appearance of and blank DME and 1 M salt/DME solution before and after the addition of LiPS solution (200:1, salt:LiPS molar ratio) at RT. b) Normalized UV-vis absorption spectra of the LiPS-added solutions after 60 h of contact. c) DFT calculations for the proposed intermediates. Red, yellow, light blue, dark blue, gray and pink balls stand for O, S, F, N, C, and Li atoms, respectively.

To sum up, FTFSI⁻ anion yet shows reactivity against LiPS. Nonetheless, the reaction is less favorable than for the FSI⁻ anion, which is observed by a less dramatic UV-Vis signal shift, and can be ascribed due to the single S-F bond in its structure. Furthermore, the reaction products may be soluble and could be further utilized, reducing the active material consumption.

5.2.4 Electrochemical performance

The previous points revealed that while LiFTFSI containing electrolytes will generate a protective enough SEI layer, they present less reactivity against reaction intermediates, which makes it an interesting candidate for the development of SPE-based on ASSLSBs. Therefore, the influence of LiFTFSI on cell performance was studied in this section and presented in **Figure 5.12**. Rate capability test in **Figure 5.12a** shows that while LiFTFSI containing system can deliver similar capacities in comparison with LiTFSI based reference, it can feature Coulombic efficiencies close to 100 % at any rate. **Figure 5.12b** shows discharge/charge profiles of the assembled cell, which do not show any sign of overcharge with well-defined charge curves in all the tested rates. Remarkably the cell features an initial discharge capacity as high as 1168 mAh g⁻¹ at 0.05C (1.17 m mAh cm⁻²) and a yet considerable capacity of *ca.* 600 mAh g⁻¹ at 0.5C (0.6 m mAh cm⁻²).

This means that LiFTFSI-based electrolyte, thanks to the combination of both -CF₃ and S-F functionalities, can exhibit at the same time a high discharge capacity and high cycling stability. This is ascribed to: i) higher stability of the anion against reaction intermediates, limiting its irreversible consumption; and ii) the protective enough generated SEI after anion reduction. Furthermore, we can hypothesize that while LiFSI-based electrolyte could generate an excessively thick SEI, LiFTFSI-based electrolyte generates a protective enough SEI, but thinner, that allows faster Li⁺ conduction and enables a better rate response.

Aiming to analyze whether the same benefits from molecular lever salt tailoring, *i.e.*, LiFTFSI, can be obtained by the equimolar mixture at macromolecular level of LiTFSI and LiFSI, *i.e.*, a mixture of 50 wt.% of each salt (LiTFSI₅₀LiFSI₅₀), **Figure 5.12c** compares the performance of both types electrolytes. The test proves that the simple physical mixture of LiTFSI and LiFSI (LiTFSI₅₀LiFSI₅₀/PEO) delivers lower capacity and causes poorer Coulombic efficiencies, with a dramatic cell failure after 30 cycles. This fact proves that the high performance and stability of LiFTFSI-based electrolyte is associated to a synergistic effect that combines optimally the features of both TFSI⁻ and FSI⁻ anions, resulting from its unique molecular structure. Finally, at a constant cycling rate of 0.1C, LiFTFSI-based cell can stably operate during 50 cycles with a superior discharge capacity compared to LiFSI-based cell (**Figure 5.12d**). This work was published.²⁶

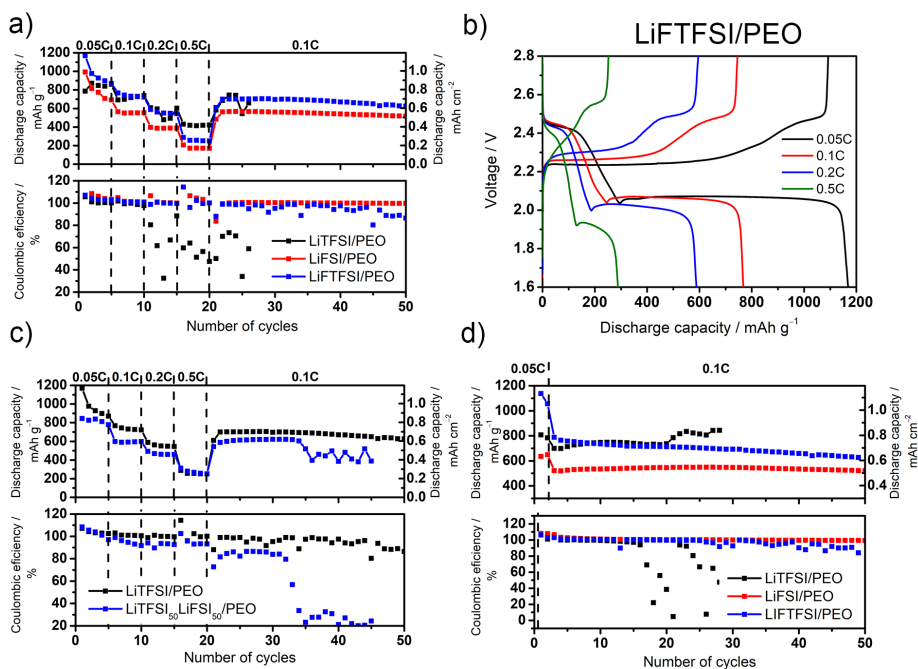


Figure 5.12. a) Discharge capacity and Coulombic efficiency of the different $\text{Li}^0|\text{SPE}|\text{S}$ electrode cells at different C-rates. b) Discharge/charge profiles during the first cycle at each rate for LiFTFSI/PEO cells. c) Discharge capacity and Coulombic efficiency of the LiFTFSI-based cell in comparison with LiTFSI₅₀LiFSI₅₀ containing cell. d) Discharge capacity and Coulombic efficiency of the different $\text{Li}^0|\text{SPE}|\text{S}$ electrode cells at constant rate of 0.1C, after two initial cycles at 0.05C. All the measurements were done at 70 °C.

5.3 DISCUSSION

Initially, LiFSI/PEO membranes were successfully prepared and characterized. Although these LiFSI-based membranes feature in certain aspects some less desirable properties compared to LiTFSI/PEO ones, such as lower thermal stability and lower conductivity, those properties are still in an acceptable range for ASSLSB operation and are compensated by their excellent stability upon cycling.

In the other hand, the presence of FSI⁻ anion in contact with Li⁰ generates a high quality, compact and mechanically robust LiF rich SEI layer that enables an improved Li⁰ negative electrode operation. Regarding, anion stability against LiPS, reaction among is highly likely to take place. Both high reactivity in contact with Li⁰ and with LiPS, which is positive in the former case and negative in the later, is related to the weakness of the terminal S-F group in FSI⁻ anion.

An effective Li⁰ protection enables stable SPE-based ASSLSB operation for an extraordinary number of cycles, which sets a precedent is SPE based ASSLSBs (see **Table 5.1**). The lowest capacity and worst capability of the LiFSI/PEO system in comparison to reference LiTFSI/PEO can be ascribed to irreversible LiPS consumption and to more resistive SEI.

Table 5.1. Comparison of the results of the present chapter and the previous works. The reference number refers to State of Art section. LiTf and LiTNFSI refer to lithium trifluoromethanesulfonate and lithium (trifluoromethanesulfonyl)(n-nonafluorobutanesulfonyl) imide.

Ref.	Electrolyte recipe	Cycle life
S19	LiTFSI/PEO	20
S20	LiTf/PEO	10
S21	LiTf/PEO	10
S22	LiBF ₄ /PEO	10
S23	LiTNFSI	200
S24	LiTFSI/PEO	40
S25	LiClO ₄ /PEO	30
This work	LiFSI/PEO	<u>1000</u>

This study demonstrated that LiTFSI and LiFSI can hardly be used as single electrolyte salts in ASSLSBs, due to stability or low capacity issues. For that reason, the synergistic combination at molecular level of both anions, *i.e.*, FTFSI⁻ was studied and proposed. LiFTFSI/PEO electrolyte featured intermediate physicochemical and electrochemical properties between LiTFSI/PEO and LiFSI/PEO, which can be related to the presence of -SO₂CF₃ and -FSO₂ endings in the structure of the salt. However, those intermediate properties are optimum with regard to electrochemical behavior with Li⁰ electrode and reactivity with LiPSs, allowing stable enough Li⁰/SPE compatibility and reduced LiPS reactivity.

This synergetic combination of both functionalities allow the LiFTFSI/PEO based ASSLSBs to feature high discharge capacity, good rate capability with the absence of overcharge during 50 cycles. In comparison to previous studies, this cell provides the highest reported areal capacity (at the initial cycle at 0.05C) and good end of life capacity (**Table 5.2**). Interestingly, this behavior is not obtained with the simple equimolar mixture of LiTFSI and LiFSI salts, which highlights the importance of combining both functionalities at molecular level.

Table 5.2. Comparison of the results of the present chapter and the previous works. The reference number refers to State of Art section. LiTNFSI refers to lithium lithium (trifluoromethanesulfonyl)(n-nonafluorobutanesulfonyl) imide.

Ref.	Electrolyte recipe	Cycle life	Initial capacity / mAh g ⁻¹ (mAh cm ⁻²)	End of life capacity / mAh g ⁻¹ (mAh cm ⁻²)
S23	LiTNFSI/PEO	200	450 (0.45)	450 (0.45)
S24	LiTFSI/PEO	40	1350 (1.08)	600 (0.48)
S25	LiClO ₄ /PEO	30	600 (0.48)	600 (0.48)
This work	LiFTFSI/PEO	50	<u>1168 (1.17)</u>	<u>626 (0.63)</u>

5.4 CONCLUSIONS

TFSI⁻ reference anion shows several desirable properties, such as good thermal and chemical stability. However, its reduction products on Li⁰ generate a low quality SEI layer that limits its application in SPE-based ASSLSBs. FSI⁻ alternative anion is a high-quality SEI builder, but its high reactivity towards LiPS consumes active materials and results in too low cell capacity.

The synergistic combination of both anions by molecular tailoring gives a novel LiFTFSI salt that brings beneficial features, with sufficient SEI quality and lowered reactivity towards LiPSs, obtaining optimized discharge capacity and long-term cyclability.

This chapter proves the suitability of alternative LiFSI and LiFTFSI imide salts for the development of highly stable ASSLSBs. However, it is also indirectly demonstrated that the salt anion not only affects the SEI quality, but also can have a great impact on the active material utilization and rate response of ASSLSBs, by dictating the internal cell resistance or limiting the undesired consumption of active material.

In the same vein, this and the previous chapter confirm a commonly accepted fact in LSBs studies, *i.e.*, it is very challenging to obtain batteries with both high capacity and long life cycling. For that reason, LSB-related studies usually focus in either performance improvement or cell lifespan improvement, while both are rarely obtained simultaneously.

5.5 REFERENCES

- (1) Jeong, S. S.; Lim, Y. T.; Choi, Y. J.; Cho, G. B.; Kim, K. W.; Ahn, H. J.; Cho, K. K. Electrochemical Properties of Lithium Sulfur Cells Using PEO Polymer Electrolytes Prepared under Three Different Mixing Conditions. *J. Power Sources* **2007**, *174* (2), 745–750.
- (2) Shin, J. H.; Kim, K. W.; Ahn, H. J.; Ahn, J. H. Electrochemical Properties and Interfacial Stability of (PEO)₁₀LiCF₃SO₃ÀTi n O 2n (1 Composite Polymer Electrolytes for Lithium / Sulfur Battery. *Mat. Sci. Eng. B* **2002**, *95*, 148–156.
- (3) Park, C. W.; Ryu, H. S.; Kim, K. W.; Hur, B. Y.; Cho, K. K.; Ahn, J. H.; Lee, J. Y.; Ahn, H. J. Effect of Sulfur Electrode Composition on the Electrochemical Property of Lithium/PEO/Sulfur Battery. *Met. Mater. Int.* **2004**, *10* (4), 375–379.
- (4) Marmorstein, D.; Yu, T. .; Striebel, K. .; McLarnon, F. .; Hou, J.; Cairns, E. . Electrochemical Performance of Lithium/Sulfur Cells with Three Different Polymer Electrolytes. *J. Power Sources* **2000**, *89* (2), 219–226.
- (5) Lin, Y.; Wang, X.; Liu, J.; Miller, J. D. Natural Halloysite Nano-Clay Electrolyte for Advanced All-Solid-State Lithium-Sulfur Batteries. *Nano Energy* **2017**, *31*

- (July 2016), 478–485.
- (6) Liang, J.; Sun, Q.; Zhao, Y.; Sun, Y.; Wang, C.; Li, W.; Li, M.; Wang, D.; Li, X.; Liu, Y.; et al. Stabilization of All-Solid-State Li–S Batteries with a Polymer–Ceramic Sandwich Electrolyte by Atomic Layer Deposition. *J. Mater. Chem. A* **2018**, *6* (46), 23712–23719.
 - (7) Lin, D.; Liu, Y.; Cui, Y. Reviving the Lithium Metal Anode for High-Energy Batteries. *Nat. Nanotechnol.* **2017**, *12* (3), 194–206.
 - (8) Ma, Q.; Qi, X.; Tong, B.; Zheng, Y.; Feng, W.; Nie, J.; Hu, Y. S.; Li, H.; Huang, X.; Chen, L.; et al. Novel Li[(CF₃SO₂)(n-C₄F₉SO₂)N]-Based Polymer Electrolytes for Solid-State Lithium Batteries with Superior Electrochemical Performance. *ACS Appl. Mater. Interfaces* **2016**, *8* (43), 29705–29712.
 - (9) Qian, J.; Henderson, W. A.; Xu, W.; Bhattacharya, P.; Engelhard, M.; Borodin, O.; Zhang, J.-G. High Rate and Stable Cycling of Lithium Metal Anode. *Nat. Commun.* **2015**, *6* (1), 6362.
 - (10) Hu, J. J.; Long, G. K.; Liu, S.; Li, G. R.; Gao, X. P. A LiFSI–LiTFSI Binary-Salt Electrolyte to Achieve High Capacity and Cycle Stability for a Li–S Battery. *Chem. Commun.* **2014**, *50* (93), 14647–14650.
 - (11) Miao, R.; Yang, J.; Feng, X.; Jia, H.; Wang, J.; Nuli, Y. Novel Dual-Salts Electrolyte Solution for Dendrite-Free Lithium-Metal Based Rechargeable Batteries with High Cycle Reversibility. *J. Power Sources* **2014**, *271*, 291–297.
 - (12) Zhang, H.; Liu, C.; Zheng, L.; Xu, F.; Feng, W.; Li, H.; Huang, X.; Armand, M.; Nie, J.; Zhou, Z. Lithium Bis(Fluorosulfonyl)Imide/Poly(Ethylene Oxide) Polymer Electrolyte. *Electrochim. Acta* **2014**, *133*, 529–538.
 - (13) Kim, H.; Wu, F.; Lee, J. T.; Nitta, N.; Lin, H.-T.; Oschatz, M.; Cho, W. Il; Kaskel, S.; Borodin, O.; Yushin, G. In Situ Formation of Protective Coatings on Sulfur Cathodes in Lithium Batteries with LiFSI-Based Organic Electrolytes. *Adv. Energy Mater.* **2015**, *5* (6), 1401792.
 - (14) Shkrob, I. A.; Marin, T. W.; Zhu, Y.; Abraham, D. P. Why Bis(Fluorosulfonyl)Imide Is a “Magic Anion” for Electrochemistry. *J. Phys. Chem. C* **2014**, *118* (34), 19661–19671.
 - (15) Zhang, H.; Feng, W.; Nie, J.; Zhou, Z. Recent Progresses on Electrolytes of Fluorosulfonimide Anions for Improving the Performances of Rechargeable Li and Li-Ion Battery. *J. Fluor. Chem.* **2015**, *174*, 49–61.
 - (16) Zhang, H.; Li, L.; Feng, W.; Zhou, Z.; Nie, J. Polymeric Ionic Liquids Based on Ether Functionalized Ammoniums and Perfluorinated Sulfonimides. *Polymer (Guildf)*. **2014**, *55* (16), 3339–3348.
 - (17) Kimura, K.; Yajima, M.; Tominaga, Y. A Highly-Concentrated Poly(Ethylene Carbonate)-Based Electrolyte for All-Solid-State Li Battery Working at Room Temperature. *Electrochem. commun.* **2016**, *66*, 46–48.
 - (18) Eshetu, G. G.; Diemant, T.; Grugeon, S.; Behm, R. J.; Laruelle, S.; Armand, M.; Passerini, S. In-Depth Interfacial Chemistry and Reactivity Focused Investigation of Lithium–Imide- and Lithium–Imidazole-Based Electrolytes. *ACS Appl. Mater. Interfaces* **2016**, *8* (25), 16087–16100.
 - (19) Judez, X.; Zhang, H.; Li, C.; González-Marcos, J. A.; Zhou, Z.; Armand, M.; Rodríguez-Martinez, L. M. Lithium Bis(Fluorosulfonyl)Imide/Poly(Ethylene Oxide) Polymer Electrolyte for All Solid-State Li–S Cell. *J. Phys. Chem. Lett.* **2017**, *8* (9), 1956–1960.
 - (20) Meister, P.; Siozios, V.; Reiter, J.; Klamor, S.; Rothermel, S.; Fromm, O.; Meyer,

- H.-W.; Winter, M.; Placke, T. Dual-Ion Cells Based on the Electrochemical Intercalation of Asymmetric Fluorosulfonyl-(Trifluoromethanesulfonyl) Imide Anions into Graphite. *Electrochim. Acta* **2014**, *130*, 625–633.
- (21) Beltrop, K.; Meister, P.; Klein, S.; Heckmann, A.; Grünebaum, M.; Wiemhöfer, H.-D.; Winter, M.; Placke, T. Does Size Really Matter? New Insights into the Intercalation Behavior of Anions into a Graphite-Based Positive Electrode for Dual-Ion Batteries. *Electrochim. Acta* **2016**, *209*, 44–55.
- (22) Di Lecce, D.; Sharova, V.; Jeong, S.; Moretti, A.; Passerini, S. A Multiple Electrolyte Concept for Lithium-Metal Batteries. *Solid State Ionics* **2018**, *316* (September 2017), 66–74.
- (23) Fan, X.; Chen, L.; Ji, X.; Deng, T.; Hou, S.; Chen, J.; Zheng, J.; Wang, F.; Jiang, J.; Xu, K.; et al. Highly Fluorinated Interphases Enable High-Voltage Li-Metal Batteries. *Chem* **2018**, *4* (1), 174–185.
- (24) Moretti, A.; Jeong, S.; Giffin, G. A.; Jeremias, S.; Passerini, S. Li-Doped N-Methoxyethyl-N-Methylpyrrolidinium Fluorosulfonyl-(Trifluoromethanesulfonyl)Imide as Electrolyte for Reliable Lithium Ion Batteries. *J. Power Sources* **2014**, *269*, 645–650.
- (25) Sharova, V.; Moretti, A.; Diemant, T.; Varzi, A.; Behm, R. J.; Passerini, S. Comparative Study of Imide-Based Li Salts as Electrolyte Additives for Li-Ion Batteries. *J. Power Sources* **2018**, *375* (September 2017), 43–52.
- (26) Eshetu, G. G.; Judez, X.; Li, C.; Martinez-Ibañez, M.; Gracia, I.; Bondarchuk, O.; Carrasco, J.; Rodriguez-Martinez, L. M.; Zhang, H.; Armand, M. Ultrahigh Performance All Solid-State Lithium Sulfur Batteries: Salt Anion's Chemistry-Induced Anomalous Synergistic Effect. *J. Am. Chem. Soc.* **2018**, *140* (31), 9921–9933.

Chapter 6:

Fluorine-free salts

This chapter explores the substitution of the conventional F-containing LiTFSI salt by a F-free alternative, with the aim of reducing battery cost, environmental impact, and the presence of low conductive fluorine species. In this regard, LiTCM salt is explored for the first time for battery application, with excellent results in performance, especially in terms of delivered capacity and rate response. Furthermore, the novel F-free chemistry of the generated passivation layer on lithium electrode is depicted in detail. Finally, these promising results are upscaled and tested at pouch cell level for the first time.

INDEX

6	FLUORINE-FREE SALTS	149
6.1	PHYSICOCHEMICAL AND ELETROCHEMICAL PROPERTIES	150
6.2	ELECTROCHEMICAL BEHAVIOR WITH Li^0	153
6.3	ANION STABILITY AGAINST LIPS	158
6.4	ELECTROCHEMICAL PERFORMANCE	159
6.5	UPSCALING TO POUCH CELL	161
6.6	DISCUSSION	164
6.7	CONCLUSIONS	166
6.8	REFERENCES	166

6 FLUORINE-FREE SALTS

The previous chapters showed that one of the approaches to overcome interlinking challenges in all-solid-state lithium-sulfur batteries (ASSLSBs) lies in the proper selection of the electrolyte and the in-depth understanding of the mechanism dictating its performance. In particular, the preceding chapter demonstrated that the salt anion chemistry plays a critical role in dictating overall electrochemical performance. In that chapter, the effect of two alternative fluorinated salts, *i.e.*, lithium bis(fluorosulfonyl)imide (LiFSI) and lithium (fluorosulfonyl)(trifluoromethanesulfonyl) imide (LiFTFSI), in poly(ethylene oxide) (PEO)-based electrolytes were studied in ASSLSBs.

Being the most extended and successful salts, the fluorinated salts can lead to robust solid/electrolyte interface (SEI) layer on metallic lithium (Li^0), based on LiF film-builder, after anion reduction. However, fluorine chemistry presents intrinsic problems, such as, i) costly and environmental harmful synthesis processes, ii) high density of F-containing species, and iii) high resistivity of the SEI films when becoming a thick layer [related to poor lithium ion (Li^+) conductivity of LiF, *c.a.* $10^{-31} \text{ S cm}^{-1}$].¹

Thus, the challenging exploration of alternative non-fluorine salt anions, which lead to alternative effective SEI forming products, and at the same time enable a cost-effective green chemistry is of utmost importance. In this regard, lithium tricyanomethanide (LiTCM) is proposed for the first time as an electrolyte salt complying with the above-mentioned properties yet to be proven in battery application. This salt was selected for its commercial availability, the weak coordination of salt anion (which can lead to high solubility PEO), and due to the presence of three nitrile groups in its structure, which can lead to highly conductive nitrogen containing reduction products.

From the synthesis point of view, LiTCM can be obtained via one-pot reaction using cheap malononitrile and cyanogen chloride starting materials. Malononitrile is an active methylene reagent for condensation reactions, for preparing synthetic intermediates and for the synthesis of heterocycles, and cyanogen chloride is produced in large quantities in dedicated sites.^{2,3} In contrast, the introduction of the C-F is energy and resources intensive, for example by electrochemical fluorination or by Halex process.⁴⁻⁶

This chapter will initially focus on the preparation of LiTCM/PEO membranes and the characterization of their physicochemical and electrochemical properties. Later, the compatibility between LiTCM and the cell components will be studied, with the special attention to the completely different chemistry of the SEI formed on Li^0 in the absence of fluorine. Finally, the membrane will be applied in

ASSLSBs coin cells. Thanks to the promising results that will be described within this chapter, the defined coin cell will be upscaled to larger format pouch cells, in order to explore one step further in the technology development value chain.

6.1 PHYSICOCHEMICAL AND ELECTROCHEMICAL PROPERTIES

Membranes were obtained by solvent casting method, and the Li salt:(EO) ratio was fixed in 1:20, as in previous studies. The structure of the LiTCM salt is presented along with the structure of LiTFSI salt for comparison in **Figure 6.1a**. Optical images in **Figure 6.1b** presents 16 mm diameter translucent and self-standing LiTCM/PEO membranes. No crystallized salt is visible in the image, and it is confirmed by X-ray diffraction (XRD) spectra in **Figure 6.1c**. The XRD data of the final membrane only features the typical diffraction peaks related to crystalline PEO phase at room temperature (RT). The absence of salt related peaks indicates its full solvation. Regarding the thermal stability of the membrane, thermogravimetric analysis (TGA) traces in **Figure 6.1d** demonstrate a similar degradation temperature, T_d , for LiTCM/PEO in comparison with the reference LiTFSI/PEO. The degradation temperature of LiTCM was reported to be higher than 600 °C by Dai *et al.*,⁷ which can be related to its high structural integrity. Thus, the stability of LiTCM membrane is dictated by PEO. In any case, the membrane shows excellent thermal stability at the operating temperature of 70 °C.

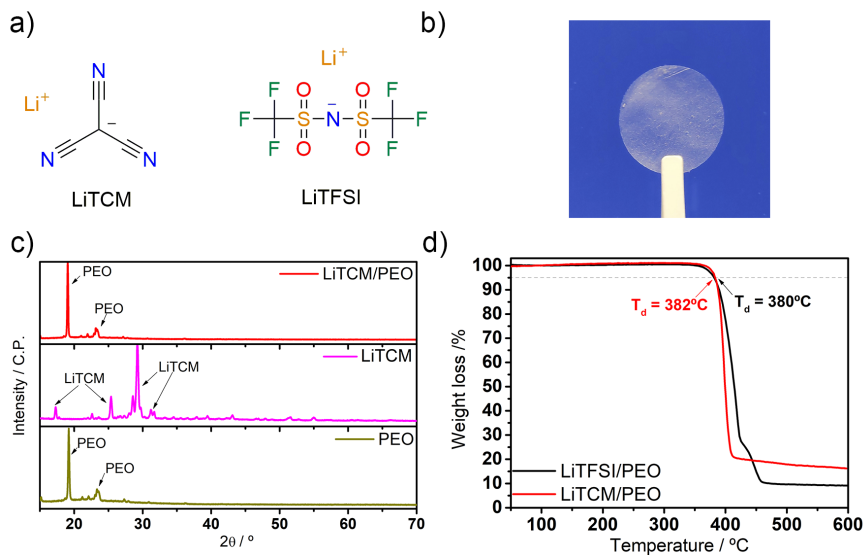


Figure 6.1. Physicochemical and electrochemical properties of the LiTCM/PEO membrane. a) Molecular structure of LiTCM and LiTFSI salts. b) Optical image, c) XRD patterns, and d) TGA traces of LiTCM/PEO membrane.

Regarding anodic stabilities, the **Figure 6.2a** demonstrates that the LiTCM/PEO membrane features a completely different response to oxidation compared to the LiTFSI/PEO membrane and other membranes based on fluorine containing salts. The linear sweep voltammetry (LSV) test shows that the LiTCM/PEO membrane presents lower electrochemical stability to oxidation than the LiTFSI-based one, due to the absence of strong electron withdrawing F-based groups. Comparison among membranes with various LiTCM/PEO ratios in **Figure 6.2b** evidences that the peak intensity is increasing with salt concentration. Therefore, the oxidation phenomena that starts about 4 V vs. Li/Li^+ must be undoubtedly related with the anion oxidation.

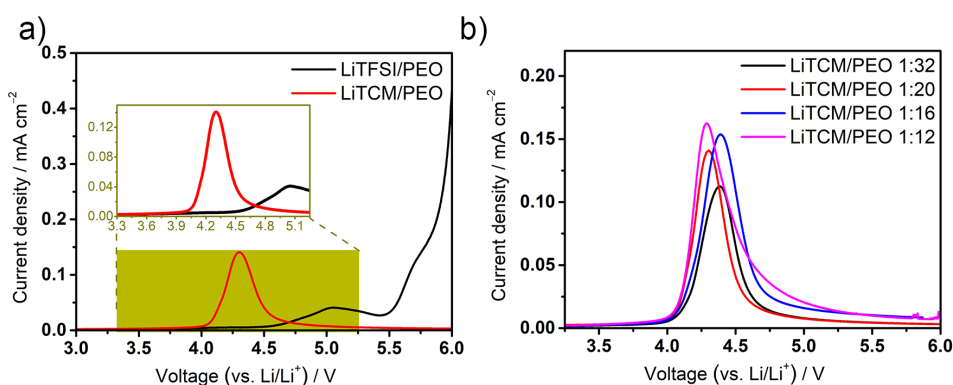


Figure 6.2. Anodic stability study of a) LiTCM/PEO and LiTFSI/PEO membranes, and b) LiTCM/PEO membranes with different Li salt:polymer ratios. All the measurements were done at 70 °C.

The use of LiTCM will be limited by anodic stability in several active materials, *e.g.*, $\text{LiNi}_x\text{Mn}_y\text{Co}_z\text{O}_2$ or $\text{LiNi}_{0.5}\text{Mn}_{1.5}\text{O}_4$. However, it is suitable for lower voltage active materials, such as LiFePO_4 or sulfur.

Finally, the phase transition properties and the conductivity were measured and are displayed in **Figure 6.3**. The differential scanning calorimetry (DSC) in **Figure 6.3a** indicates that the glass transition and melting temperatures, T_g and T_m , of the LiTCM/PEO membrane are similar to the ones of the reference LiTFSI/PEO. In contrast, it shows higher melting enthalpy, ΔH_m , and thus, higher crystallinity, χ_c . This evidences the lower plasticizing effect of the salt, which is related to the lower degree of the structural flexibility of cyanomethanide anion center ($\text{C}-\text{C}\equiv\text{N}$) in LiTCM in comparison to sulfonamide anion center ($-\text{SO}_2\text{NSO}_2-$) in LiTFSI. This fact is confirmed by the sharper transition of conductivity around the T_m in Arrhenius plot of conductivity (**Figure 6.3b**), showing LiTCM-based membrane lower conductivity values below it. However, above the T_m the conductivity of the studied membrane comparable with the value of the reference LiTFSI/PEO.

Regarding Li^+ transport selectivity, *i.e.*, transference number (t_{Li^+}), the LiTCM based membrane shows a value of 0.31, which is considerably higher than the value of 0.15 for the LiTFSI/PEO reference (**Figure 6.3c**). This improvement can be related to the interaction between anion and polymer matrix in the presence of the $\text{C}-\text{C}\equiv\text{N}$ moiety, which decreases the mobility of anions with respect to that of Li^+ . After all, the LiTCM/PEO membrane presents a Li^+ conductivity of $1.69 \times 10^{-4} \text{ S cm}^{-1}$ at 70°C (**Figure 6.3d**), which is higher than reference LiTFSI/PEO and is adequate for battery cycling.

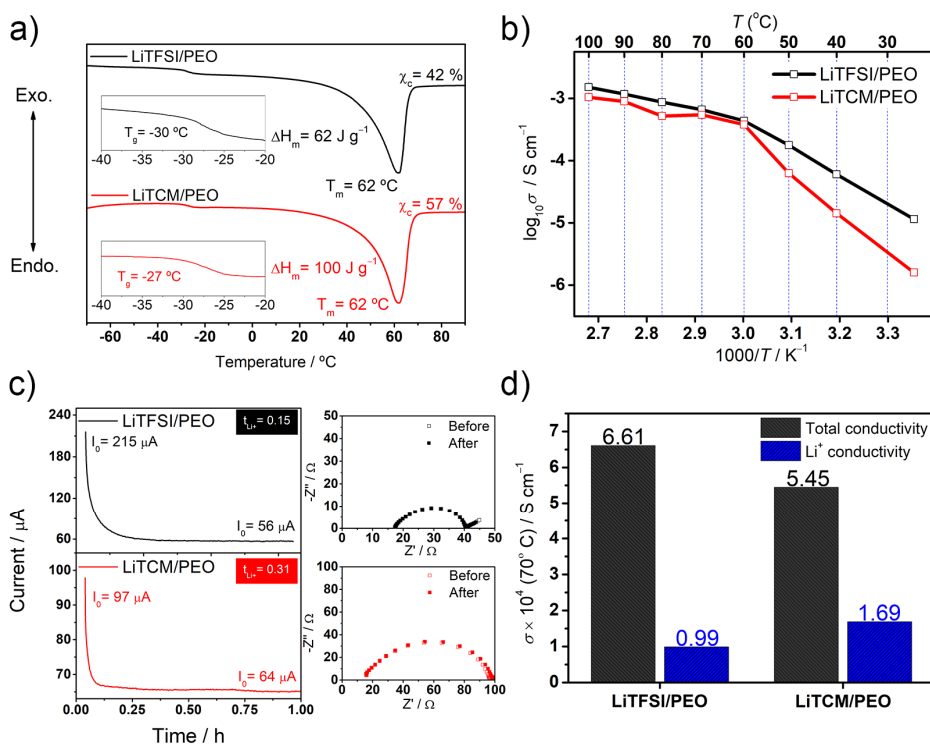


Figure 6.3. Thermal transition and conductivity properties of the LiTCM/PEO membrane in comparison with LiTFSI/PEO membrane. a) DSC traces; b) Arrhenius plot of conductivity; c) chronoamperometry test under 10 mV polarization at 70°C , and electrochemical impedance spectroscopy measurements before and after the test for t_{Li^+} measurement; and d) Li^+ conductivity at 70°C .

All in all, the LiTCM/PEO membrane has been successfully prepared and presents similar properties compared to reference LiTFSI/PEO. The most noticeable limitation is the decreased anodic stability. However, the salt is stable in the voltage range of lithium-sulfur battery chemistry. The improvement in conductivity and Li^+ selectivity are the most salient features.

6.2 ELECTROCHEMICAL BEHAVIOR WITH Li^0

In comparison with the previously studied anions, the TCM^- anion presents a completely different fluorine free structure, so we can expect a singular behavior of the LiTCM/PEO membrane in contact with Li^0 . The galvanostatic cycling of $\text{Li}^0 | \text{LiTCM/PEO} | \text{Li}^0$ membrane shows improved operation time of *ca.* 250 h before the start of a erratic cycling (**Figure 6.4a**). Most remarkably, the cell shows a current induced overpotential as low as ≈ 10 mV, in contrast to > 30 mV for LiTFSI system, which is an indicative of a reduced cell resistance to Li^+ movement. This can be related to a more Li^+ conductive SEI layer on Li^0 , inferring differences in the nature of the SEI building materials. This phenomenon has been observed before in the additives chapter, in which highly conductive Li_3N was one of the SEI forming species. For that reason, even if it needs to be confirmed by X-ray photoelectron spectroscopy (XPS) measurements in Li^0 deposits, we can expect that LiTCM reduction generates Li_3N or similar products while contacting the metallic electrode.

The upper part of **Figure 6.4b** presents optical and SEM images of the Li^0 deposits on Cu foils in presence 1,2-dimethoxyethane (DME) and corresponding salts. In the optical image, the deposits in presence of non-fluorinated LiTCM anion feature black color and more homogeneous and smooth structures, unlike the greyish color of the scattered Li^0 deposits in the F-containing LiTFSI. SEM pictures of those deposits show that the structures are smaller and present a more homogeneous particle size and morphology in presence of LiTCM. To find out the composition of the surface of the deposits, XPS analysis (done by Dr. Zhang) is seen bottom part of **Figure 6.4b**. N1s spectra shows four characteristic peaks in LiTCM containing systems, in contrast to a single peak related to incompletely reduced salt anion in LiTFSI system. Among the salt derived products, the C=N bond is an indicative of the presence of decomposition products with carbon atoms that have one double bond with nitrogen and two single bond with nitrogen and carbon atoms, *i.e.*, C-C(C)=N or C-C(N)=N. The conjugated C=N bond presence are also testified by the observed π -excitation which appears at slightly higher binding energy. The small peak at 398 eV is related to the existence of highly Li^+ conductive Li_3N ($6 \times 10^{-3} \text{ S cm}^{-1}$)⁸, confirming its presence as hypothesized before.

C1s spectra in both LiTFSI and LiTCM systems shows the presence of solvent reduction derived products, *i.e.*, $\text{H}_2\text{C}=\text{HC}-\text{O}-\text{CH}_3$, CH_3OLi , ($\text{R}_2\text{C}-\text{O}$ and R_1-O respectively). However, in the case of LiTCM, apart from confirming the presence of previously mentioned C=N and C=N (π^*) bonds, the existence of C-C bond is certified. All this results suggest the formation of a SEI based on conjugated C=N groups, which endows the black color of the deposits and the good coating integrity and mechanical strength.

Finally, to deepen in the XPS observations and study the composition of the inner SEI, an additional XPS analysis was done after treating the surface of the sample using Ar^+ sputtering during 540 s (C1s spectra in **Figure 6.4b**). The Ar^+ sputtering allows to remove the outermost surface of the sample and make the XPS analysis in more inner areas of the sample. In both cases the products originating from the reduction of salts become more prominent over the ones from solvent reduction with etching time, *e.g.*, $\text{C}=\text{N}$ increases from 8 to 23 at.% in LiTCM system and CF_3 groups from 8 to 22 at.% in LiTFSI system. This testifies that the reduction of the salt occurs more prominently in the inner part of the SEI, in the proximity of the highly reducing Li^0 . Remarkably, in LiTCM/DME derived sample, the presence of C–C bond becomes more prominent. This trend indicates that in the inner part of the SEI, where the potential is close to that of Li^0 , LiTCM reduction can finally yield C–C bond containing groups, *e.g.*, graphene.

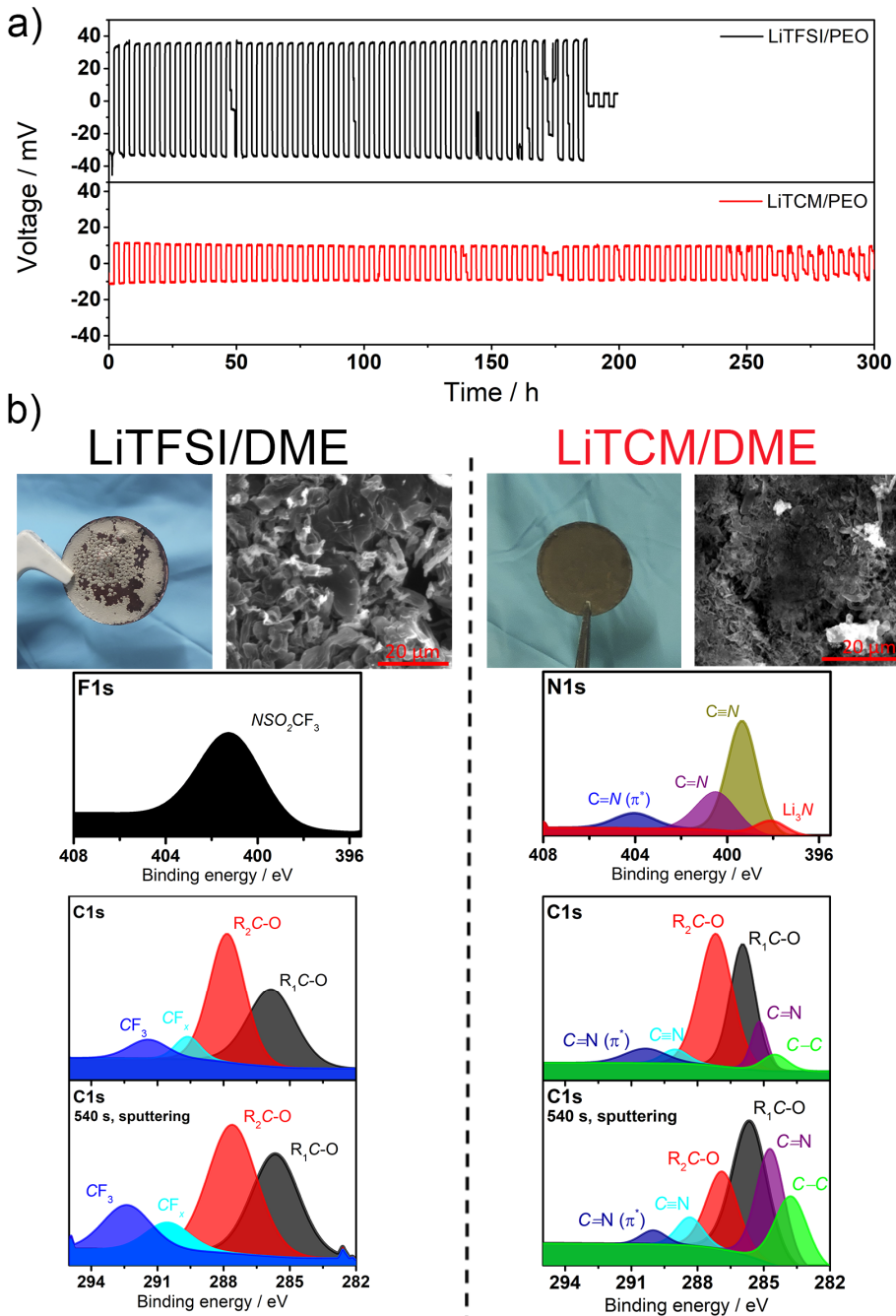
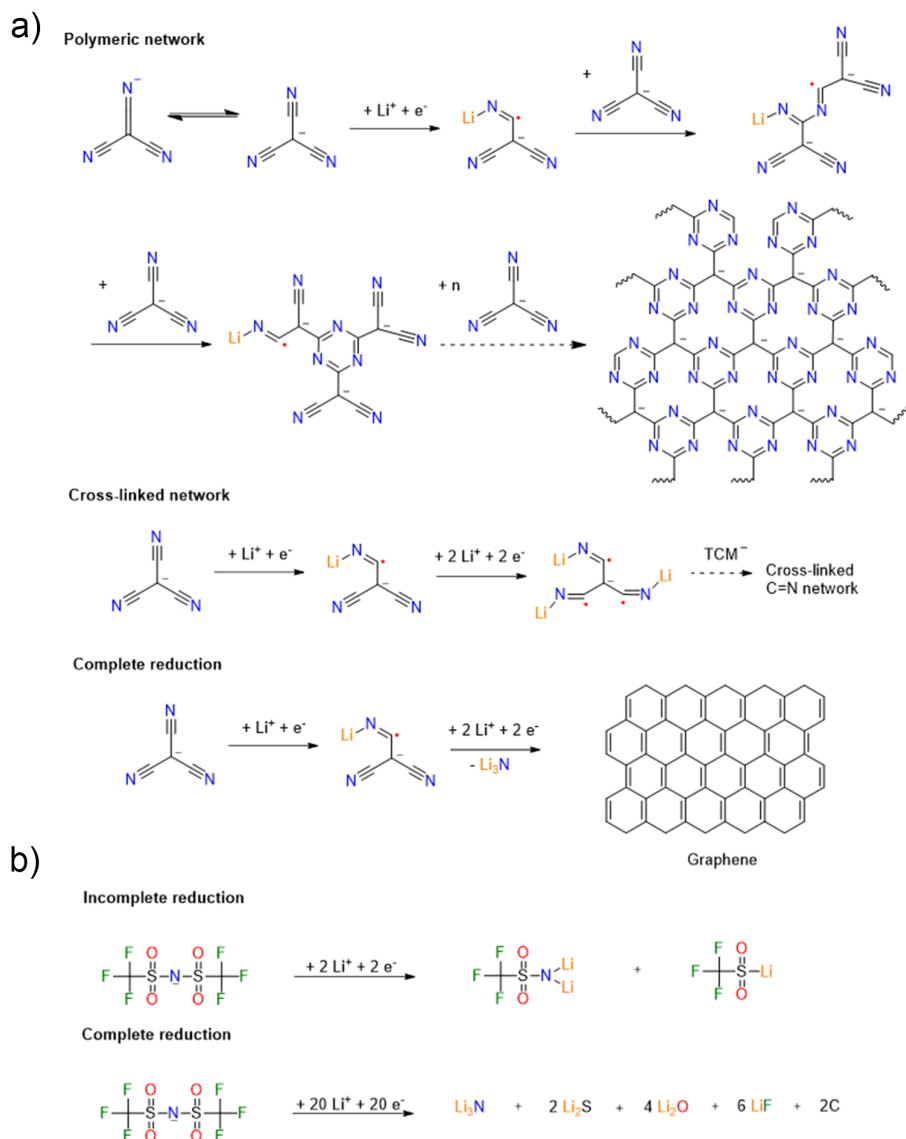


Figure 6.4. Electrochemical behavior of Li^0 electrode in the as-prepared electrolytes. a) Galvanostatic cycling of $\text{Li}^0|\text{SPE}|\text{Li}^0$ symmetric cells at 0.1 mA cm^{-2} and 2 h semicycles at 70°C . b) c) Optical and SEM images, and XPS spectra (outermost surface and after

540 s of sputtering with Ar^+ for the C1s spectra) of Li^0 deposited onto Cu substrates ($\text{Li}^0|\text{DME}+\text{SALT}|\text{Cu}$ cells) at 0.1 mA cm^{-2} during 20 h at 25°C . $\text{R}_1\text{C}-\text{O}$ and $\text{R}_2\text{C}-\text{O}$ refer to $\text{CH}_3\text{O}-$ and $\text{H}_2\text{C}=\text{HC}-\text{O}-\text{CH}_3$, respectively.

Chemical simulations by biphenyl tests confirmed that the electrochemical reductions of both anions was only feasible at extremely low potentials of $0.15 \text{ V vs. Li/Li}^+$ or below. This corroborates well XPS results where the decomposition products of the salt increase from the outermost surface to the inner part, due to the heightened reducing ability close to metallic Li^0 .

On the basis of the analysis studied before, the reduction mechanism of LiTCM salt is proposed in **Scheme 6.1a**. These results clearly suggest the formation of a conjugated $\text{C}=\text{N}$ groups. The trimerization of TCM-based ionic liquids and alkali metal salts have been reported in previous work for synthesizing nitrogen-enriched carbons,^{7,9,10} where a $\text{C}=\text{N}$ network was obtained via heating. The exhaustive reduction reaction of LiTCM can also lead finally to the formation of graphene and Li_3N , confirmed by the presence of both $\text{C}-\text{C}$ bonds and Li_3N in XPS. On the other hand, based on the tests on this and previous chapters, we can propose a 2 e^- reduction reaction of LiTFSI leading to $\text{CF}_3\text{SO}_2\text{NLi}$ and $\text{CF}_3\text{SO}_2\text{Li}$. The complete and more improbable 20 e^- reduction will lead to the generation of lower molecular weight products, such as LiF, whose existence in small quantities was confirmed by XPS.



Scheme 6.1. The proposed reduction mechanism for the reduction of the LiTCM and LiTFSI salts.

In conclusion, the morphological and chemical composition of the SEI formed in LiTFSI and LiTCM electrolytes is summarized in **Figure 6.5**. The organic species resulting from solvent decomposition are dominant in the outermost surface while the ones resulting from salt reduction are dominant in the inner part. The reduction of LiTFSI leads to small amount of LiF, Li₂S and Li₃N molecules, but the SEI is

mainly formed by bigger and less desirable high molecular weight salt reduction products, *i.e.*, $\text{CF}_3\text{SO}_2\text{NLi}$ and $\text{CF}_3\text{SO}_2\text{Li}$, and solvent derived products. In contrast, the reduction of LiTCM leads to the formation of C=N network and Li_3N , which form a high mechanically stable and highly Li^+ conducting SEI layer.

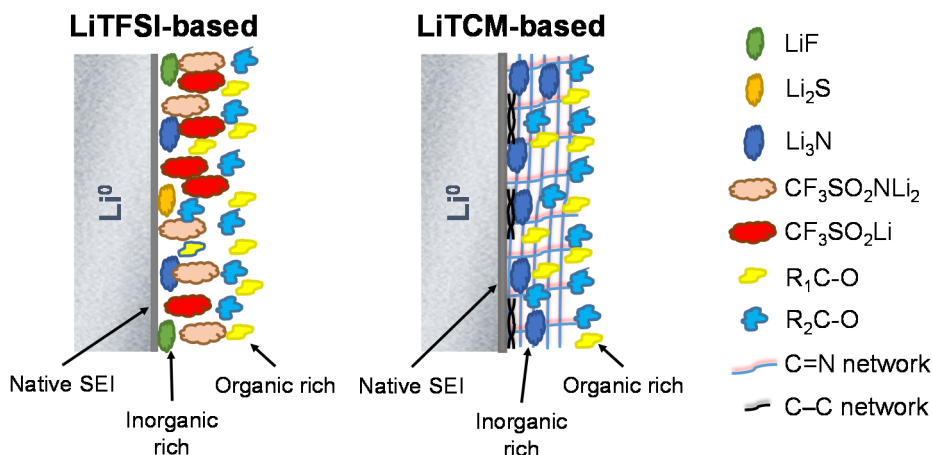


Figure 6.5. Schematic illustration of the SEI formed on Li^0 electrode in the LiTFSI- and LiTCM-based electrolytes.

6.3 ANION STABILITY AGAINST LIPS

The presence of highly soluble lithium polysulfides (LiPSs) in both catholyte and in the electrolyte media, may lead to compatibility issues with the salt anion in terms of anion decomposition and active material consumption. Therefore, the effect of the addition of LiTCM salt (200:1 salt:polysulfide molar ratio) in a 0.1 M $\text{Li}_2\text{S}_6/\text{DME}$ solution was studied by means of color change and Density Functional Theory (DFT). The study of ultraviolet visible (UV-vis) absorbance spectra of the solution in **Figure 6.6a** before and after the addition of the salt. In contrast to LiTFSI added solution, where no color change was observed, LiTCM added solution shows some color intensification at long wavelengths. This indicates that the LiTCM may react to some extent with LiPSs and thus result in an extra conjugation of the S_6 group. Some different reactions between the TCM^- anion and Li_2S_6 were proposed and the reaction heat (ΔE) was computed with DFT by Dr. Zhang (**Figure 6.6b**). The addition reaction of Li_2S_6 onto TCM^- $[(\text{NC})_2\text{C}^-(\text{C}=\text{NLi})\text{S}_6^{(-)}]$ is more energetically favorable than the nucleophilic substitution of the one cyano group with Li_2S_6 $[(\text{NC})_2\text{C}^-\text{S}_6^{(-)}]$, *i.e.*, -336 kJ mol^{-1} vs. -190 kJ mol^{-1} . In comparison with previously computed values, the addition reaction of the TCM^- is less favorable than the nucleophilic substitution reaction

for LiTFSI (-221 kJ mol^{-1}), as calculated in the previous chapter, but close to that of LiFTFSI (-359 kJ mol^{-1}). Moreover, the reaction intermediates of the reaction between LiTCM and LiPS may be sufficiently electrochemically reversible and could be sufficiently soluble in PEO, due to its asymmetrical structure.

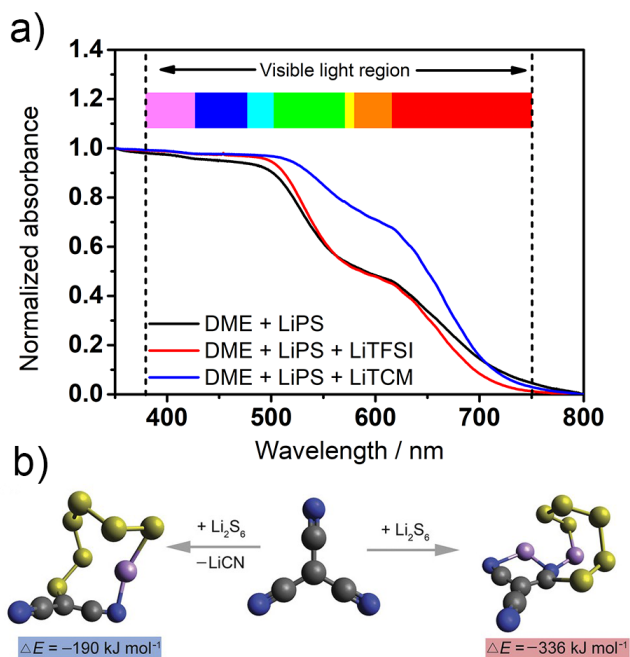


Figure 6.6. Stability of salt anion against LiPS species. a) Normalized UV-vis absorption spectra of the LiPS-added solutions after 60 h of contact. c) DFT calculations for the proposed intermediates. Yellow, dark blue, gray and pink balls stand for S, N, C, and Li atoms, respectively.

6.4 ELECTROCHEMICAL PERFORMANCE

The fluorine-free LiTCM salt behaves completely different in terms of SEI chemistry and reactivity towards LiPS in comparison with the fluorine salts studied before. However, up to now, its features seem also perfectly compatible with lithium-sulfur battery chemistry. For that reason, knowing the good SEI-forming ability of TCM^- anion and its relatively good stability against LiPSs, the viability of using the LiTCM/PEO membrane in ASSLSBs will be studied for the first time.

Note that i) the charge cut-off voltage of the cell was limited to 2.6 V vs. Li/Li^+ (2.8 V vs. Li/Li^+ was used before), so LiTFSI-based reference cell with the same cutoff voltage was repeated accordingly with similar results; and that ii) LiTCM

based positive electrode shows *ca.* 15% lower sulfur areal loading due to the modified viscosity of the electrode slurry as a result of the remarkably lower molecular weight of the salt (97 g mol^{-1} vs. 287 g mol^{-1} for LiTFSI).

Figure 6.7a presents the electrochemical performance of the LiTCM/PEO based ASSLSBs, showing excellent discharge capacity, rate capability and stability. After few activation cycles, a discharge capacity of 780 mAh g^{-1} (0.66 mAh cm^{-2}) is obtained at 0.1C, which is comparable to the reference LiTFSI-based system. Most, remarkably, when comparing the discharge capacity with the initial values at 0.1C, the cell capacity only decreases 9% and 35% when doubling (0.2C) and quintupling (0.5C) cycling rate. The maximum achieved capacity for LiTCM/PEO system is 0.76 mAh cm^{-2} , which is just slightly lower than the value of 0.81 mAh cm^{-2} for the reference LiTFSI/PEO. Moreover, after about 25 cycles the Coulombic efficiency of the cell starts decreasing gradually, but without a dramatic drop in contrast to LiTFSI/PEO-based system.

The discharge and charge profiles of the LiTCM/PEO cell in **Figure 6.7b** shows the typical plateau/slope/plateau profile for multistep S_8 reduction to Li_2S . It also demonstrates stable charge plateaus, with just some mild overcharge at 0.5C.

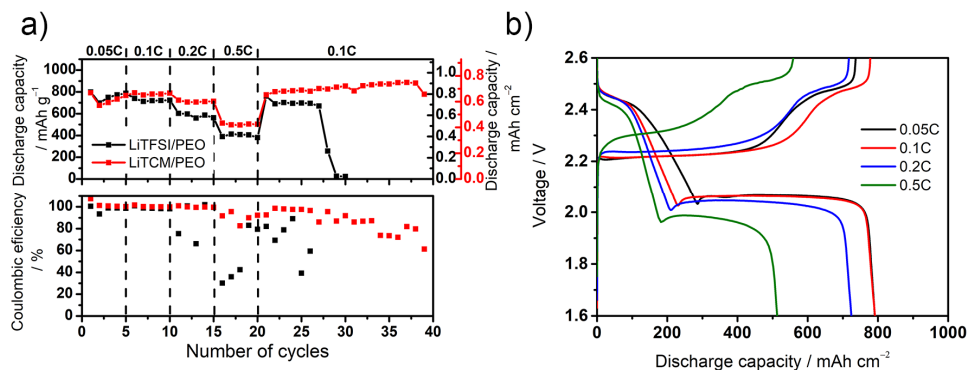


Figure 6.7. a) Discharge capacity and Coulombic efficiency of $\text{Li}^0|\text{SPE}$ (PEO + LiTFSI or LiTCM)|S cells at different C-rates. b) Discharge/charge profiles during the first cycle at each rate for LiTCM/PEO cells. All the measurements were done at 70°C .

In conclusion, the LiTCM salt has been demonstrated to work stably in the highly challenging lithium-sulfur cell environment, featuring excellent gravimetric capacity and rate capability, comparable to that of the reference LiTFSI/PEO electrolyte, but with an improved cell stability. This can be related to the combination of different properties, such as the improvement in Li^+ conduction selectivity, the high mechanical strength and conductivity of the generated SEI layer, or the limited reactivity against LiPS.

Based on this promising results, the first trials for the upscaling of the system were performed. Pouch cells preparation and testing will be presented in the following point.

6.5 UPSCALING TO POUCH CELL

The study of materials at pouch cell level requires considerably higher amount of materials and time. This means a higher cost of demonstration but the performance and operating conditions are closer to those of real batteries, so the obtained results will be more representative of real application. The results with this non-fluorine salt are promising enough in terms of performance and materials viability to consider system evaluation at pouch cell level.

For that purpose, the methodology for the preparation of a single layer ASSLSB pouch cell assembly was set and systems with a 20 cm² size positive electrode (*vs.* 1.3 cm² for coin cell) were prepared (see details in section 3 of the Appendix). **Figure 6.8a** shows an optical picture of both coin cell and pouch cell along with a scale for size comparison. **Figure 6.8b** presents discharge capacity and Coulombic efficiency of the pouch cell during 6 cycles. In terms of capacity, pouch cell shows no activation and a capacity of 835 mAh g⁻¹ (0.69 mAh cm⁻²) at 0.1C, which is similar to that of the coin cell. However, regarding Coulombic efficiency, the pouch cell features lower values from the initial cycles. The discharge/charge profiles of the cell in **Figure 6.8c** demonstrates remarkably higher charge capacities in comparison to discharge even at the early cycles, *i.e.*, overcharge.

Thus, the cycling at pouch cell level shows similar discharge capacities can be obtained, but the cycling stability seems much worse than in coin cell. For a more clear comparison, a discharge/charge cycle at 0.1C of a pouch cell and a coin cell have been plotted in cyclic way (inverting the discharge) in **Figure 6.8d**. The discharge and charge profiles of the coin cell are well defined and the equivalent state of charge and discharge can be easily identified due to the exact fitting of the plateaus. In contrast, for pouch cell, the charge profile is clearly shifted and the slope and upper plateau regions of the charge do not fit the ones of the discharge. Remarkably, in the low plateau the polarization related overpotential is similar in both pouch and coin cell, indicating a similar value of cell resistance. For that reason, the shift in charge cannot be ascribed to increased resistance but to undesired electrochemical processes at high voltages.

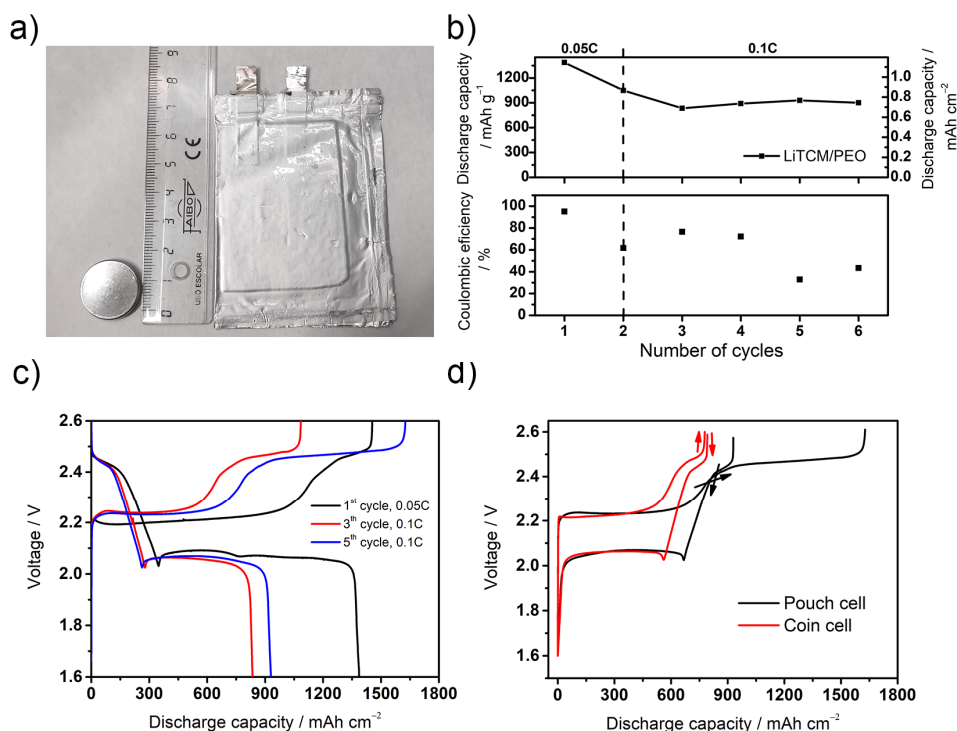


Figure 6.8. a) Optical images of a coin cell and a pouch cell along with a ruler for size comparison. b) Discharge capacity and Coulombic efficiency of the $\text{Li}^0|\text{LiTCM}/\text{PEO}|\text{S}$ pouch cells at 0.05C for 2 cycles and 0.1C for the remaining. c) Discharge/charge profiles of the 1st, 3th and 5th cycle of LiTCM/PEO pouch cells. d) Centered 5th cycle discharge/charge profile of the pouch cell in comparison to a cycle of the coin cell. The downward and upward arrows indicate discharge and charge, respectively. All the measurements were done at 70 °C.

Some alternative test were carried out in order to identify the critical issues during the upscaling step. Even if the absence of polarization initially discards the high resistance problem in **Figure 6.8d**, electrochemical impedance spectroscopy measurements were done hourly in fresh assembled $\text{Li}^0|\text{LiTCM}/\text{PEO}|\text{S}$ pouch and coin cells during the thermal pretreatment at 70 °C (**Figure 6.9a**). The obtained impedance curves were fitted to the equivalent circuit displayed in the inset of the figure, and the bulk resistance (R_b) and the sum of the interfacial (R_i) and charge transfer (R_{ct}) resistance evolution are plotted with time. The remaining abbreviations correspond to interfacial capacitance (Q_i), double layer capacitance (Q_{dl}) and diffusion capacitance (Q_{dif}). In both coin and pouch cell the R_b , related to electrolyte, remains constant from the first measurement, indicating fast polymer membrane heating and melting. The main difference between the two systems is that while in coin cell the $R_i + R_{ct}$ term needs around 16 hours of heat treatment to

stabilize, similar values can be obtained at pouch cell in only 6 hours. This does not only discard the contact problem in pouch cell, but reveals that the contact in pouch cell configuration seems more favorable than in coin cell. In contrast to pressure sealing in coin cell, the pouch cells are closed by strong vacuum, which seems to considerably improve the contact. However, both configurations reach similar resistance values at the end of the 24h, so differences in contact among them after the pretreatment can be discarded.

During a State of Art research around lithium sulfur pouch cell development, in order to find the root cause for the instability, a work from Zhang *et al.*¹¹ was found to be very inspiring. This research asserted that, in contrast to the most challenging shuttle effect in coin cells, Li^0 induced polarization is the most common cause responsible for pouch cell failure. To study sizing effect of the metallic electrode, symmetric $\text{Li}^0 | \text{LiTCM/PEO} | \text{Li}^0$ cells were assembled in pouch cell size ($20 \text{ cm}^{-2} \text{ Li}^0$) and compared with the previous results in coin cell in **Figure 6.9b**. During the first 150 h of the test, erratic and instable cycling is occurs much earlier for pouch cell les, in contrast to stable and flat voltage profiles in coin cells system. Furthermore, after *ca.* 45 h the cell voltage progressively decreased reaching soon values as low as 5 mV, which is indicative of dendrite growth.

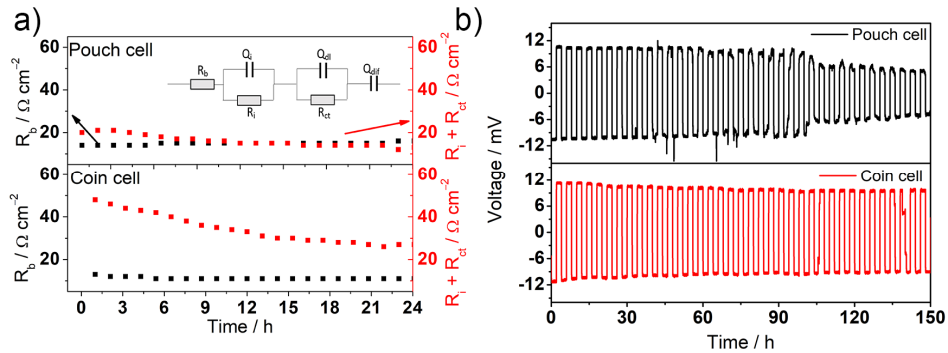


Figure 6.9. a) Bulk, interfacial and charge transfer resistance evolution during the 24 h of heat pretreatment at 70 °C for both $\text{Li}^0 | \text{LiTCM/PEO} | \text{S}$ pouch and coin cell. Results were measured by EIS and fitted to the equivalent circuit on the inset figure. a) Galvanostatic cycling of $\text{Li}^0 | \text{LiTCM/PEO} | \text{Li}^0$ symmetric pouch and coin cells at 0.1 mA cm^{-2} and 2 h semicycles at 70 °C.

Our results confirm that the performance of the Li^0 in pouch cell size for our system is not as stable as in coin cell level. Zhang *et al.*¹¹, in the above-mentioned work, claimed that even the current per surface unit in pouch cell is the same as in coin cell, the total applied current is much higher in the pouch cell. If this current cannot be uniformly distributed on the negative electrode, it may result much higher charge depositing at nucleation points, and thus, easier dendritic or mossy lithium

generation. This will lead to higher polarization and a decrease in the reversibility of the electrochemical reactions, hence, early instability and cell death.

Therefore, the stability of the Li^0 electrode is identified as the most challenging step for upscaling. Even if the stability of Li^0/SPE interface may be well enough for cycling at coin cell level, more attention should be paid to the quality of the SEI layer for pouch cell preparation.

6.6 DISCUSSION

LiTCM was proposed as a novel fluorine free for battery application. Self-standing membranes were obtained, which featured similar properties in comparison with LiTFSI/PEO membrane. The decreased anodic stability due to prompt anion oxidation was the most remarkable limitation. However, that phenomenon occurs well-above the cut-off voltage of ASSLSBs, so will not be a limitation in our cell chemistry. The improvement of Li^+ conductivity and transport selectivity are the most salient features.

In comparison to LiTFSI salt, the reduction of LiTCM salt on Li^0 leads to a more protective and conductive SEI layer containing $\text{C}=\text{N}$ and Li_3N , which allows a longer operation time of Li^0 symmetric cells and decreased interfacial resistance. Furthermore, even if the anion reactivity towards LiPS was found to be higher than the case of LiTFSI, it is still moderate and may be sufficiently reversible.

Regarding LiTCM/PEO membrane application in ASSLSBs, the results were found to be excellent, with high discharge capacities and, especially, excellent rate response. Remarkably, the capacity only decreased 9% and 35% after doubling a quintupling cycling rate. A comparison in **Table 6.1** demonstrates that LiTCM/PEO features the best reported rate response in comparison with two recent works (S30 and S32), and with our reference LiTFSI/PEO (in gravimetric capacity terms). The comparison of the rate response with more State of Art studies is challenging due to the absence of rate capability test or the use of different rates. Regarding stability, even if Coulombic efficiency values of the LiTCM/PEO cell started decreasing after 25 cycles, the descent was gradual, in contrast to drastic drops in LiTFSI/PEO system, indicating a higher cell stability.

Table 6.1. Comparison of the results of the present chapter and the previous works. The reference number refers to State of Art section. MIL-53(Al) refers to aluminum containing metal organic framework.

Ref.	Electrolyte recipe	Capacity / mAh g ⁻¹ (mAh cm ⁻²)			
		0.05C	0.1C	0.5C	0.2C
S30	LiTFSI/PEO + MIL-53(Al)+ carbon	N.A.	907 (0.63)	627 (0.44)	N.A.
S32	PEO + Li _{0.33} La _{0.557} TiO ₃	384 (0.49)	358 (0.45)	N.A	262 (0.33)
Our reference	LiTFSI/PEO	794 (0.81)	720 (0.73)	560 (0.57), unstable	410 (0.41), unstable
<u>This work</u>	LiTCM/PEO	790 (0.67)	780 (0.66)	<u>710</u> (0.60)	<u>498</u> (0.42)

Finally, regarding initial upscaling studies, first pouch cells were successfully assembled. Here, similar discharge capacities could be obtained but cycling stability was clearly penalized. The characterization studies discarded any internal resistance increase issues, but the unstable cycling of Li⁰ was identified as the main limitation. Thus, future steps must focus on deepening in the stability of Li⁰/SPE compatibility in order to allow longer cycle life at prototype level. For that purpose, several strategies are being studied, including i) the addition of LiFSI as co-salts in order to generate SEI containing an optimum combination of Li₃N and LiF; or ii) the addition of thin Al₂O₃-containing layer on the Li⁰ side in order to benefit from the excellent SEI generated in the presence of this filler.

6.7 CONCLUSIONS

This work opens the avenue toward the study of new fluorine-free anions as promising candidates for lithium-sulfur batteries. LiTCM salt has been demonstrated to be an excellent choice for ASSLSBs due to its excellent physicochemical and electrochemical properties and its good stability with cell components, added to the environmental and cost effective features. Remarkably, the novel chemistry of the generated SEI on Li^0 in presence of LiTCM has been described in detail, discovering that anion reduction will lead to the formation of a highly stable and conductive SEI with combination of C=N networks and Li_3N . The cells based on LiTCM/PEO electrolyte feature excellent discharge capacity and rate capability with improved stability in comparison with the reference LiTFSI/PEO electrolyte. Furthermore, the anion chemistry has been demonstrated once more to be critical in ASSLSB performance in terms of stability, delivered capacity and rate performance. This work was partially published.¹²

The promising results of LiTCM/PEO based ASSLSBs at coin cell level led to upscaling to pouch cell level. The methodology for pouch cell assembly and characterization has been set. The results show similar gravimetric and areal capacities but worse stability. The root cause of this issue has been identified to be related to the bigger size of the Li^0 electrode. Therefore, the future work will focus on the reinforcement of this critical interface by the use of co-salts or electrolyte fillers, in order to form a robust SEI formation, based on the learning attained during this Thesis

6.8 REFERENCES

- (1) Pan, J.; Cheng, Y.-T.; Qi, Y. General Method to Predict Voltage-Dependent Ionic Conduction in a Solid Electrolyte Coating on Electrodes. *Phys. Rev. B* **2015**, *91* (13), 134116.
- (2) Freeman, F. Chemistry of Malononitrile. *Chem. Rev.* **1969**, *69* (5), 591–624.
- (3) Täschler, C.; Breuer, A. Process for Preparing Alkal Metal or Alkaline Earth Metal Tricyanomethanes, 2011.
- (4) Zhang, H.; Feng, W.; Nie, J.; Zhou, Z. Recent Progresses on Electrolytes of Fluorosulfonimide Anions for Improving the Performances of Rechargeable Li and Li-Ion Battery. *J. Fluor. Chem.* **2015**, *174*, 49–61.
- (5) Conte, L.; Gambaretto, G.; Caporiccio, G.; Alessandrini, F.; Passerini, S. Perfluoroalkanesulfonylimides and Their Lithium Salts: Synthesis and Characterisation of Intermediates and Target Compounds. *J. Fluor. Chem.* **2004**, *125* (2), 243–252.
- (6) Siegemund, G.; Schwertfeger, W.; Feiring, A.; Smart, B.; Behr, F.; Vogel, H.; McKusick, B.; Kirsch, P. Fluorine Compounds, Organic. In *Ullmann's Encyclopedia of Industrial Chemistry*; Wiley-VCH Verlag GmbH & Co. KGaA: Weinheim, Germany, 2016; pp 1–56.

- (7) Guo, B.; Sun, X.-G.; Veith, G. M.; Bi, Z.; Mahurin, S. M.; Liao, C.; Bridges, C.; Paranthaman, M. P.; Dai, S. Nitrogen-Enriched Carbons from Alkali Salts with High Coulombic Efficiency for Energy Storage Applications. *Adv. Energy Mater.* **2013**, *3* (6), 708–712.
- (8) Zhu, Y.; He, X.; Mo, Y. Strategies Based on Nitride Materials Chemistry to Stabilize Li Metal Anode. *Adv. Sci.* **2017**, *4* (8), 1600517.
- (9) Fulvio, P. F.; Lee, J. S.; Mayes, R. T.; Wang, X.; Mahurin, S. M.; Dai, S. Boron and Nitrogen-Rich Carbons from Ionic Liquid Precursors with Tailorable Surface Properties. *Phys. Chem. Chem. Phys.* **2011**, *13* (30), 13486.
- (10) Lee, J. S.; Wang, X.; Luo, H.; Dai, S. Fluidic Carbon Precursors for Formation of Functional Carbon under Ambient Pressure Based on Ionic Liquids. *Adv. Mater.* **2010**, *22* (9), 1004–1007.
- (11) Cheng, X.-B.; Yan, C.; Huang, J.-Q.; Li, P.; Zhu, L.; Zhao, L.; Zhang, Y.; Zhu, W.; Yang, S.-T.; Zhang, Q. The Gap between Long Lifespan Li-S Coin and Pouch Cells: The Importance of Lithium Metal Anode Protection. *Energy Storage Mater.* **2017**, *6*, 18–25.
- (12) Zhang, H.; Judez, X.; Santiago, A.; Martinez-Ibañez, M.; Muñoz-Márquez, M. Á.; Carrasco, J.; Li, C.; Eshetu, G. G.; Armand, M. Fluorine-Free Noble Salt Anion for High-Performance All-Solid-State Lithium–Sulfur Batteries. *Adv. Energy Mater.* **2019**, *9* (25), 1900763.

Chapter 7:

General overview

The aim of this chapter is to present an overview of the results obtained during this Thesis and in context with literature. The main focus is to identify main advances in the research topic and examine possible future strategies.

7 GENERAL OVERVIEW

Among the several strategies developed to solve the intrinsic issues of lithium sulfur batteries (LSBs), the use of solid electrolytes has been proven to be one of the most straightforward strategies, allowing to simultaneously overcome several limitations. Furthermore, this option is still a quite unexplored choice in comparison with others, such as positive electrode tuning.

Apart from allowing to overcome some of the most challenging limitations, the use of solid electrolytes can, according to our calculations, allow to improve achievable gravimetric energy densities in the cells. This is related to the minimization of inert elements in solid cells, and it is further accentuated with the use of lightweight solid polymer electrolytes (SPEs) or low filler containing solid composite electrolytes (SCEs) (**Figure 7.1**).

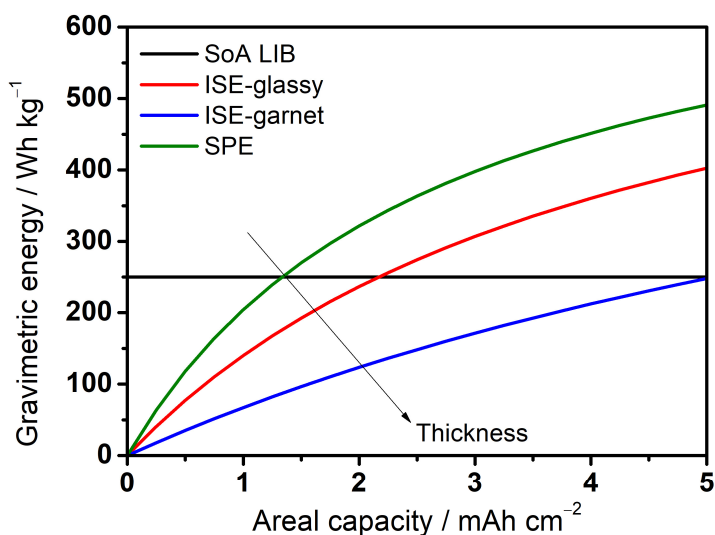


Figure 7.1. Estimated gravimetric energy density of LSBs based on different 50 μm thickness electrolytes. Values for State of Art lithium ion batteries (SoA LIB) are included as reference. ISE refers to inorganic solid electrolytes.

This calculations also allowed to fix cell properties and a targeted performance of 1.2 mAh cm⁻². When the first reference SPE-based all-solid-state lithium-sulfur battery (ASSLSB) was assembled based on bis(trifluorosulfonyl)imide (LiTFSI)/poly(ethylene oxide) electrolyte, the cell response was not stable due to overcharge (**Figure 7.2a**). However, the failure was ascribed to the unstable metallic lithium (Li⁰)/SPE interface (**Figure 7.2b**), which could not protect the

metallic electrode from the lithium polysulfides (LiPSs) present in the electrolyte (**Figure 7.2c**).

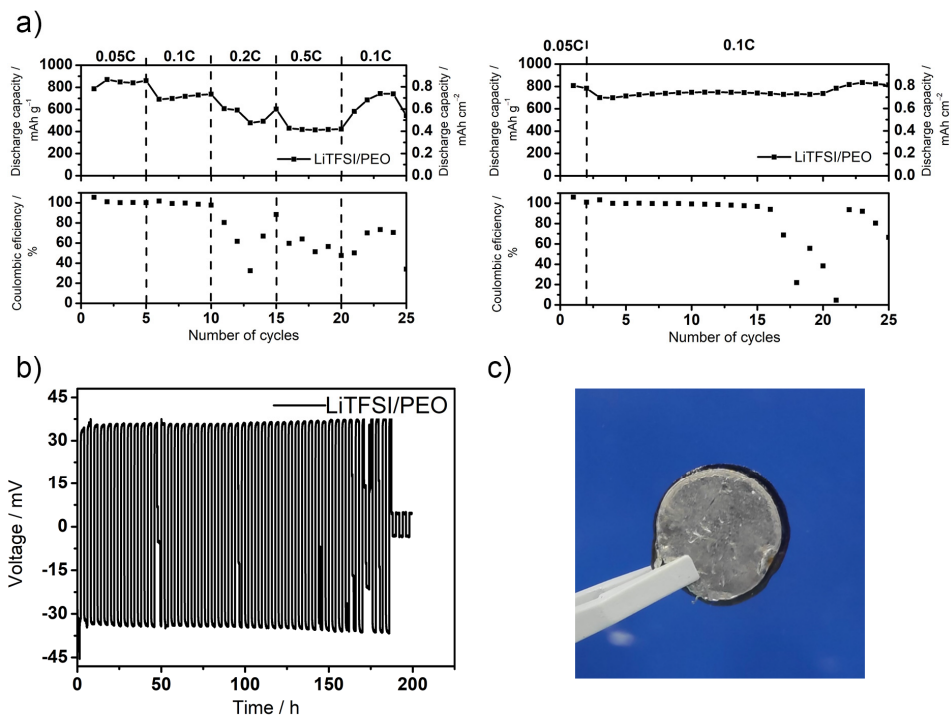


Figure 7.2. a) LiTFSI/PEO-based ASSLSBs cell cycling at various (left) and constant (right) rates. b) Galvanostatic cycling of Li⁰ | LiTFSI/PEO | Li⁰ symmetric cells at 0.1 mA cm⁻² and 2 h semicycles. c) Optical image of the ASSLSBs cell after failure. All the cells were tested at 70 °C.

Based on this, different strategies were designed based on modified electrolyte configurations. Initially, the use of two electrolyte additives, conventional LiNO₃ and newly proposed LiN₃, was studied. Both additives demonstrated to have a great influence in the Li⁰/SPE interfacial compatibility by means of generation of a robust solid/electrolyte interface (SEI) layer. This work demonstrated the benefits of the highly conductive Li₃N SEI forming product. Both additives featured similar performance at ASSLSB level, but the novel LiN₃ was found by X-ray photoelectron spectroscopy (XPS) to get reduced exclusively to Li₃N, while LiNO₃ can also get reduced to other oxygen containing low conductive species. The most remarkable properties of the electrolytes are summarized in **Table 7.1**, which confirm, at the same time, the importance of Li⁰ protection to allow a longer life ASSLSB performance.

Table 7.1. Comparison of the most remarkable properties of the additive-free and the additive containing electrolytes.

Additive	Main SEI products	Li ⁰ SPE Li ⁰ cell		ASSLSBs lifespan / cycle number
		Life / h	Overpotential / ΔV	
Additive free	Organic products, unreacted salt	< 200	>30	15
LiNO ₃	Li ₃ N, LiF, Li ₂ O, LiNO ₂	< <u>300</u>	> 15	<u>30</u>
LiN ₃	Li ₃ N	<u>500</u>	< 12	<u>30</u>

Even if the use of additives enabled to double the cycle life of the cell, the discharge capacity was decreased by 20%. In order to improve the cell performance without any sacrifice in capacity, the use of low amount of ceramic fillers was studied as alternative.

The addition of 3 vol.% of the active Li⁺ conducting glass ceramic (LiCGC) filler and inactive Al₂O₃ did not bring any beneficial effect in the conductivity of the electrolytes. However, it was demonstrated that small amount of this fillers could have a great effect of Li⁰/SPE interfacial stability. LiCGC was proven to have a negative effect in contact with Li⁰ and LiPS due to its tendency to get reduced. In contrast, Al₂O₃ was found to outstandingly enhance SEI quality and to strongly immobilize LiPSs.

The direct implementation of Al₂O₃ containing SCEs brought stable cell cycling but a decreased discharge capacity. After understanding the role of Al₂O₃ in ASSLSBs, initial cell design was modified. This novel cell design (**Figure 7.3a**) enabled a stable cell cycling without affecting the obtained capacity values (**Figure 7.3b**). This cell delivered a maximum of 0.99 mAh cm⁻² at 0.05C in the initial cycles and 0.85 mAh cm⁻² at 0.1C at the end of the 30th cycle.

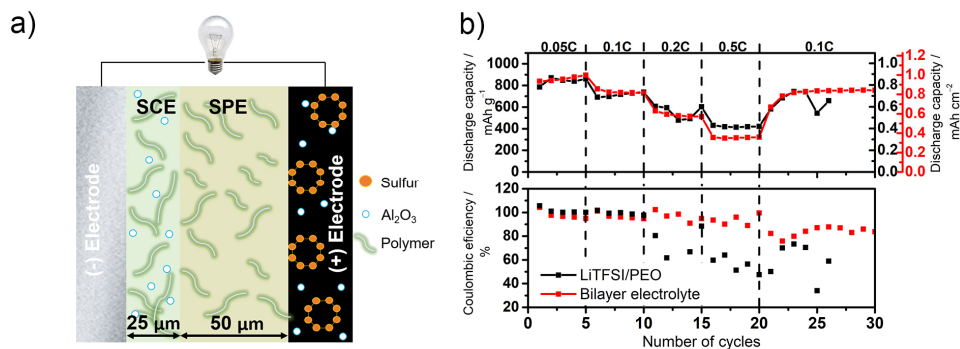


Figure 7.3. Schematic representation of the assembled cell before cycling. b) Discharge capacity and Coulombic efficiency of $\text{Li}^0|\text{SCE}+\text{SPE}|\text{modified S}$ electrode cells at different C-rates and $70\text{ }^\circ\text{C}$.

This values did not yet achieve our targeted performance, but set a precedent in terms of delivered capacity among the reported studies and reported an excellent capacity retention, as summarized in **Table 7.2**.

Table 7.2. Comparison of the results of the present Thesis and the previous works. The reference number refers to State of Art section. HNT and MIL-53(Al) refers to halloysite nanotubes and aluminum containing metal-organic framework.

Ref.	Electrolyte recipe	Initial cap. / mAh g^{-1} , (mAh cm^{-2})	End of life cap. / mAh g^{-1} , (mAh cm^{-2})	Cap. loss / $\% \text{ cycle}^{-1}$
S23	LiTFSI/PEO	450 (0.45)	450 (0.5)	0%
S24	LiTFSI/PEO	1350 (1.08)	600 (0.48)	1.38%
S24	LiTFSI/PEO + HNT	800 (0.64)	745 (0.6)	0.07%
S29	LiTFSI/PEO + MIL-53(Al)	640 (0.51)	558 (0.45)	0.016%
S31	LiTFSI/PEO + $\text{Li}_7\text{La}_3\text{Zr}_2\text{O}_{13}$	900 (0.54)	900 (0.54)	0%
This work	LiTFSI/PEO / LiTFSI/PEO + Al_2O_3	768 (0.86)	755 (0.85)	0.14%

The integration of Al_2O_3 was demonstrated to be a low-cost and effective strategy to reinforce and improve the electrochemical performance of the conventional LiTFSI/PEO electrolyte in ASSLSBs. Deepening in this question, we can observe that the filler interacts in the Li^0/SPE interface, and to an extent, in SPE/positive electrode interface, to prevent LiPS loss. For this reason, the direct coating of these interfaces by Al_2O_3 nanolayers could bring the same benefits as the one observed in this work. The interfacial coating, *e.g.*, by sputtering, could improve surface coverage, and thus, improve cell performance. Therefore, this strategy will be studied in the future.

In a novel approach, the LiTFSI salt was substituted by alternative imide-containing salts, in order to allow acceptable cell performances without adding extra components. For that purpose, the reference salt was initially substituted by the well-known SEI former lithium bis(fluorosulfonyl)imide (LiFSI) salt. The reduction of this salt generated a LiF rich SEI layer that allowed extended Li^0 symmetric cell life, highlighting the mechanically stable SEI-forming properties of this product. An effective Li^0 protection enabled the stable SPE-based ASSLSB operation for an extraordinary number of 1000 cycles, quintupling the lifespan of the previously reported longest life cell. However, the liability of the S–F bond generated excessive anion reactivity towards LiPSs and excessively thick SEI layer, which decreased overmuch the discharge capacity and rate response of the cell.

Therefore, this study demonstrated that LiTFSI and LiFSI can hardly be used as single electrolyte salts in ASSLSBs, due to low stability or low capacity issues. For that reason, lithium (fluorosulfonyl)(trifluoromethanesulfonyl) imide (LiFTFSI) intermediate solution was proposed. The LiFTFSI/PEO electrolyte featured intermediate physicochemical and electrochemical properties between LiTFSI/PEO and LiFSI/PEO, but those intermediate properties were found to be optimum with regard to cell performance. This synergetic combination of both functionalities allow the LiFTFSI/PEO based ASSLSBs to obtain a high discharge capacity, good rate capability and acceptable stability, with the absence of overcharge during 50 cycles (**Figure 7.4**). Remarkably, the first discharge of the cell reached 1.17 mAh cm^{-2} , very close to the targeted value.

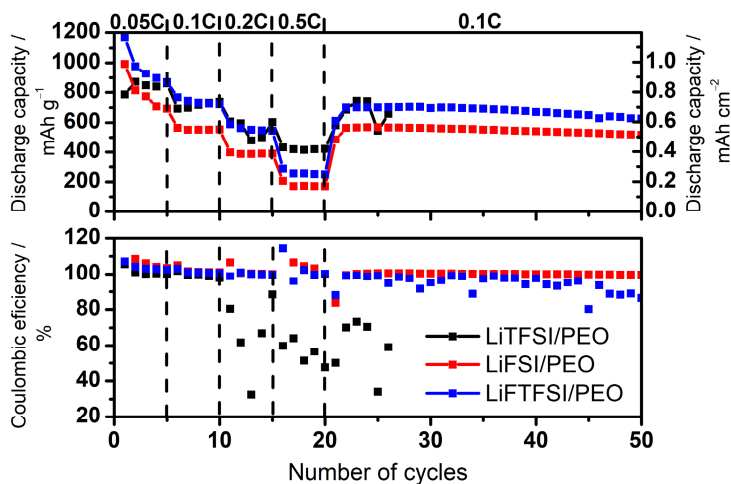


Figure 7.4. Discharge capacity and Coulombic efficiency of the different $\text{Li}^0|\text{SPE}|S$ electrode cells at different C-rates. All the measurements were done at 70°C .

This chapter also demonstrated the determining effect of the anion chemistry in the cell performance, not only by means of SEI quality tuner, but also by affecting active material utilization and rate response. In order to explore another performance improving salts, but at the same time trying to search options with reduced environmental impact and cost, a F-free alternative salt was explored.

In this regard, lithium tricyanomethanide (LiTCM) was proposed for the first time as an electrolyte salt. In comparison to LiTFSI salt, the reduction of LiTCM salt on Li^0 led to a more protective and conductive SEI layer, which allows a longer operation time of Li^0 symmetric cells and decreased interfacial resistance. It was concluded that the reduction of the salt leads to a highly stable SEI based on C=N network and Li_3N . This confirmed the excellent properties of Li_3N as SEI building material. The properties of the LiTCM/PEO membrane allowed an excellent cell performance, with high discharge capacity and, especially, the best reported rate response, as reported in **Table 7.3**.

Table 7.3. Comparison of the results of the present Thesis and the previous works. The reference number refers to State of Art section. MIL-53(Al) refers to aluminum containing metal organic framework.

Ref.	Electrolyte recipe	Capacity / mAh g ⁻¹ (mAh cm ⁻²)			
		0.05C	0.1C	0.5C	0.2C
S30	LiTFSI/PEO + MIL-53(Al)+ carbon	N.A.	907 (0.63)	627 (0.44)	N.A.
S32	PEO + Li _{0.33} La _{0.557} TiO ₃	384 (0.49)	358 (0.45)	N.A	262 (0.33)
Our reference	LiTFSI/PEO	794 (0.81)	720 (0.73)	560 (0.57), unstable	410 (0.41), unstable
<u>This work</u>	LiTCM/PEO	790 (0.67)	780 (0.66)	<u>710</u> (0.60)	<u>498</u> (0.42)

If we compare in **Figure 7.5** the cell capacities and the cycle life obtained in the different previous studies and over the course of this Thesis, two main conclusions can be drawn. First, as stated before, the systems developed in the course of this Thesis report the highest areal capacity values at good cycle life. In this regard, both LiTFSI/PEO-based, and specially LiTCM/PEO-based cells feature optimum properties in terms of the combination of cell capacity and cycle life.

Second, a general tendency can be observed (indicated by the discontinuous arrow): those cells that provide higher discharge capacities can cycle steadily for shorter number of cycles. On the contrary, the cells that can sustain longer stable cycling usually perform lower capacity values. This is a commonly accepted fact in LSBs battery research, and obtaining systems with both high capacity and stability is a major challenge.

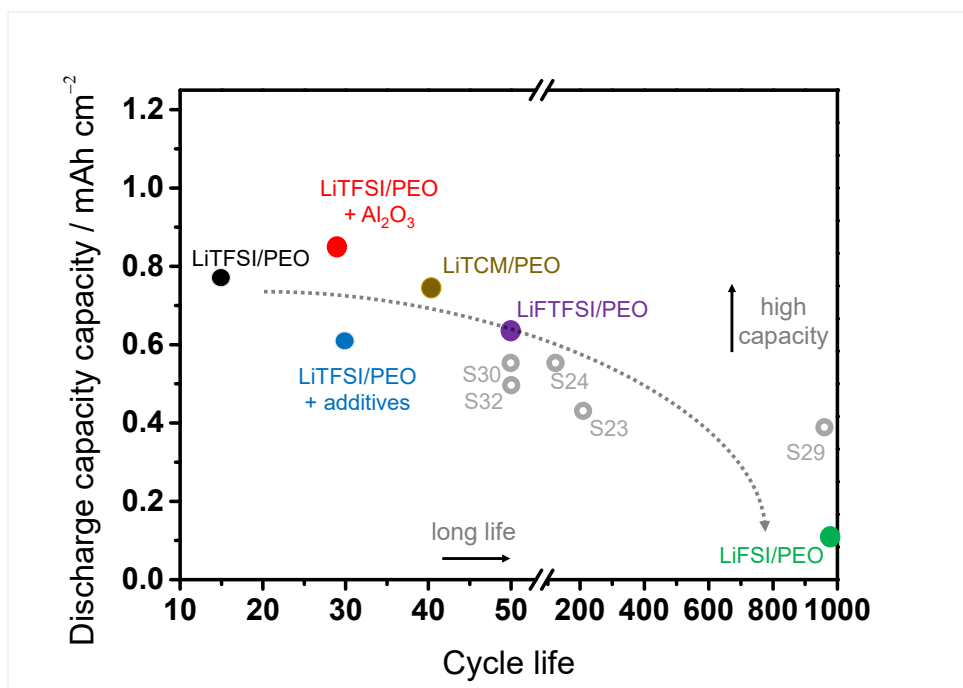


Figure 7.5. Representation of discharge capacity vs. cycle life for the different systems studied in this Thesis work. Numbers refer to the references in State of Art section.

Finally, the upscaling of the LiTCM/PEO results to the first prototypes of pouch cells revealed that the sizing of Li⁰ would be the most limiting step. Therefore, yet more attention should be paid in the stabilization of this electrode. In this regard, identification of the excellent SEI forming properties of the mechanically stable LiF and the highly conductive Li₃N opens an avenue to the study of their combination. For that purpose, the use of small amounts of LiFSI as co-salt in LiTCM-based system will be studied in the future. Furthermore, we are also exploring electrolyte salts that contain molecular structures that can finally lead to the presence of both products in the SEI.

In conclusion, even if the targeted performance of 1.2 mAh cm⁻² has not yet been achieved, close values have been obtained, and the highest values in literature so far have been reported in this work. Moreover, great advances have been obtained in SPE-based ASSLSBs performance, and the role of the electrolytes in battery performance has been depicted in detail. The gained knowledge and the use of optimized positive electrodes will allow SPE-based ASSLSBs to achieve superior energy density values in the near future.

Chapter 8:

Conclusive remarks

In this final chapter the main conclusions from this Thesis work are collected and summarized, along with some possible future steps, based on the gained knowledge. The contributions of this work to the field of polymer -based all-solid-state lithium-sulfur batteries are also pointed out.

8 CONCLUSIVE REMARKS

Several conclusions can be drawn from this PhD work:

- Among different “beyond Li-ion” batteries, lithium sulfur batteries (LSBs) are one of the most attractive alternatives, especially due to their high achievable gravimetric energy density. However, the deployment of this technology is still hindered by several challenges related to its complex chemistry.
- The use of solid electrolytes in lithium-sulfur batteries, especially light-weight solid polymer electrolytes (SPEs), can simultaneously help to face several challenges while, according to our models, allow the increase of the achievable energy density values.
- The all-solid-state lithium-sulfur batteries (ASSLSBs) based on state of art lithium bis(trifluoromethanesulfonyl)imide (LiTFSI)/poly(ethylene oxide) electrolyte present limitations in terms of stability. This is related to the presence of reaction intermediates, *i.e.*, lithium polysulfides (LiPSs), in the electrolyte, and to the poor generated solid/electrolyte interface (SEI) layer on the metallic lithium (Li^0) electrode.
- The use of both, the widely-explored lithium nitrate (LiNO_3) and novel lithium azide (LiN_3) additives has been demonstrated to be a simple, viable, and effective approach to circumvent the stability problems of the cells LiTFSI/PEO based cells. This improvement was ascribed to the effect of the additives in the SEI composition. Especially, the reduction of LiN_3 led to highly protective and conductive Li_3N .
- Two different fillers have been explored for the preparation of solid composite electrolytes (SCEs). The studied Li-ion conductive glassy ceramic did not bring any beneficial effect to the cell performance due to its instability, both electrochemical and chemical, with Li^0 and LiPSs. In contrast, Al_2O_3 brought remarkably positive effect in terms of SEI quality and demonstrated strong LiPSs adsorption capability. However, the direct implementation of Al_2O_3 containing SCEs led to a decreased cell capacity. In a different approach, its use in bilayer SCE/SPE electrolyte, and in the positive electrode as LiPS anchoring sites, enabled stable cell cycling with no sacrifice in discharge capacity.
- In a different approach, LiTFSI was substituted by the alternative imide containing lithium bis(fluorosulfonyl)imide (LiFSI) salt. LiFSI was proven to improve the Li^0 electrode stability by means of LiF-rich SEI layer generation by salt anion reduction. However, even if the cell stability was remarkably improved, this anion is highly reactive with LiPSs, consuming reaction intermediates and decreasing cell capacity. In contrast, the synergistic

combination of both FSI⁻ and TFSI⁻ functionalities in the asymmetric lithium (fluorosulfonyl)(trifluoromethanesulfonyl) imide (LiFTFSI) was found to be an optimum solution, by means of sufficient SEI quality and lowered reactivity towards LiPSs. The use of LiFTFSI/PEO electrolytes allowed optimum discharge capacities and stable cycling. In this chapter, it was demonstrated that the salt anion chemistry plays a vital role in cell performance, not only affecting the SEI layer composition, but also having a great impact on the active material utilization and rate response.

- Finally, the use of lithium tricyanomethanide (LiTCM) as alternative fluorine-free salt resulted in membranes with excellent properties and good compatibility with cell components. The novel SEI chemistry, after LiTCM reduction on Li⁰, was proven to be based on a combination of C=N structure and Li₃N. The cells delivered excellent discharge capacity, rate capability and improved stability, in comparison to reference LiTFSI salt based cells.
- The first steps of the upscaling to pouch cell were set and the characterization helped to identify Li⁰ upscaling as the limiting stage. Thus, future work will take advantage of the gained knowledge during this Thesis in order to design novel electrolyte recipes. Those strategies can be based on the combination of different studied approaches, *e.g.*, by the combined use of LiTCM and LiFSI in order to obtain a Li₃N and LiF combining SEI protecting layer; or by the improvement of the applied strategies, *e.g.*, by the generation of Al_xO_y nanolayers on Li⁰ electrodes by sputtering.
- Regarding the scope of this thesis, even if this work has not finally achieved the targeted performance of 1.2 mAh cm⁻², it has set various precedents in the development of SPE-based ASSLSBs. Those include, the understanding of LiTFSI/PEO failure mechanism, the addition of electrolyte additives, the use of bilayer electrolytes, the substitution on LiTFSI by alternative LiFSI and LiFTFSI imide containing salts, and finally, the use of the novel fluorine-free LiTCM salt as electrolyte salt for battery application, and the achievement of the highest reported values in terms of areal capacity and rate performance.

The obtained results and conclusions are well in alignment with the objectives defined at the beginning of this thesis. The quality indicators of this work are included in the section 4 of the Appendix section, and detail the contributions of this work in form of publications and works presented in international conferences.

Appendix

INDEX

1 LIST OF REFERENCES FOR THE STATE OF ART STUDY.....	187
2 SCILAB CODE FOR ENERGY DENSITY CALCULATION.....	190
3 EXPERIMENTAL DETAILS.....	194
3.1 MATERIALS	194
3.2 PREPARATION OF CELL COMPONENTS.....	195
3.2.1 Solvent casting preparation of polymer membranes	
195	
3.2.2 Ball milling preparation of polymer membranes	195
3.2.3 Preparation of positive electrodes.....	195
3.2.4 Coin cell assembly	196
3.2.5 Pouch cell assembly	196
3.3 CHARACTERIZATION TECHNIQUES.....	197
3.3.1 X-ray diffraction.....	197
3.3.2 Scanning electron microscopy	197
3.3.3 Electrochemical stability test.....	197
3.3.4 Thermogravimetric analysis.....	197
3.3.5 Differential scanning calorimetry	198
3.3.6 Conductivity test.....	198
3.3.7 Lithium transference number measurement	199
3.3.8 Galvanostatic cycling	200
3.3.9 Lithium metal deposit generation	200
3.3.10 X-ray photoelectron spectroscopy.....	201
3.3.11 Polysulfide reactivity test	201
3.3.12 Chemical simulation test.....	201
3.3.13 Lithium sulfur cell cycling	201

4	QUALITY INDICATORS	203
4.1	PUBLICATIONS.....	203
4.2	WORKS PRESENTED IN CONFERENCES	205
4.3	CO-AUTHOR CONFERENCES	205
5	REFERENCES IN THE APPENDIX.....	207

APPENDIX**1 LIST OF REFERENCES FOR THE STATE OF ART STUDY**

- (S1) Hayashi, A.; Ohtomo, T.; Mizuno, F.; Tadanaga, K.; Tatsumisago, M. All-Solid-State Li/S Batteries with Highly Conductive Glass–Ceramic Electrolytes. *Electrochem. commun.* 2003, 5 (8), 701–705.
- (S2) MACHIDA, N. Electrochemical Properties of Sulfur as Cathode Materials in a Solid-State Lithium Battery with Inorganic Solid Electrolytes. *Solid State Ionics* 2004, 175 (1–4), 247–250.
- (S3) Hayashi, A.; Ohtsubo, R.; Ohtomo, T.; Mizuno, F.; Tatsumisago, M. All-Solid-State Rechargeable Lithium Batteries with Li₂S as a Positive Electrode Material. *J. Power Sources* 2008, 183 (1), 422–426.
- (S4) Kobayashi, T.; Imade, Y.; Shishihara, D.; Homma, K.; Nagao, M.; Watanabe, R.; Yokoi, T.; Yamada, A.; Kanno, R.; Tatsumi, T. All Solid-State Battery with Sulfur Electrode and Thio-LISICON Electrolyte. *J. Power Sources* 2008, 182 (2), 621–625.
- (S5) Takeuchi, T.; Kageyama, H.; Nakanishi, K.; Tabuchi, M.; Sakaebe, H.; Ohta, T.; Senoh, H.; Sakai, T.; Tatsumi, K. All-Solid-State Lithium Secondary Battery with Li[Sub 2]S–C Composite Positive Electrode Prepared by Spark-Plasma-Sintering Process. *J. Electrochem. Soc.* 2010, 157 (11), A1196.
- (S6) Nagao, M.; Hayashi, A.; Tatsumisago, M. Sulfur–Carbon Composite Electrode for All-Solid-State Li/S Battery with Li₂S–P₂S₅ Solid Electrolyte. *Electrochim. Acta* 2011, 56 (17), 6055–6059.
- (S7) Lin, Z.; Liu, Z.; Fu, W.; Dudney, N. J.; Liang, C. Lithium Polysulfidophosphates: A Family of Lithium-Conducting Sulfur-Rich Compounds for Lithium-Sulfur Batteries. *Angew. Chemie Int. Ed.* 2013, 52 (29), 7460–7463.
- (S8) Nagao, M.; Imade, Y.; Narisawa, H.; Kobayashi, T.; Watanabe, R.; Yokoi, T.; Tatsumi, T.; Kanno, R. All-Solid-State Li-Sulfur Batteries with Mesoporous Electrode and Thio-LISICON Solid Electrolyte. *J. Power Sources* 2013, 222, 237–242.
- (S9) Nagata, H.; Chikusa, Y. Activation of Sulfur Active Material in an All-Solid-State Lithium–Sulfur Battery. *J. Power Sources* 2014, 263, 141–144.
- (S10) Unemoto, A.; Yasaku, S.; Nogami, G.; Tazawa, M.; Taniguchi, M.; Matsuo, M.; Ikeshoji, T.; Orimo, S. I. Development of Bulk-Type All-Solid-State Lithium-Sulfur Battery Using LiBH₄ Electrolyte. *Appl. Phys. Lett.* 2014, 105 (8).
- (S11) Yamada, T.; Ito, S.; Omoda, R.; Watanabe, T.; Aihara, Y.; Agostini, M.; Ulissi, U.; Hassoun, J.; Scrosati, B. All Solid-State Lithium–Sulfur Battery Using a Glass-Type P₂S₅–Li₂S Electrolyte: Benefits on Anode Kinetics. *J. Electrochem. Soc.* 2015, 162 (4), A646–A651.
- (S12) Han, F.; Yue, J.; Fan, X.; Gao, T.; Luo, C.; Ma, Z.; Suo, L.; Wang, C. High-Performance All-Solid-State Lithium-Sulfur Battery Enabled by a Mixed-Conductive Li₂S Nanocomposite. *Nano Lett.* 2016, 16 (7), 4521–4527.
- (S13) Yao, X.; Huang, N.; Han, F.; Zhang, Q.; Wan, H.; Mwizerwa, J. P.; Wang, C.; Xu, X. High-Performance All-Solid-State Lithium–Sulfur Batteries Enabled by

- Amorphous Sulfur-Coated Reduced Graphene Oxide Cathodes. *Adv. Energy Mater.* 2017, 7 (17), 1–9.
- (S14) Suzuki, K.; Mashimo, N.; Ikeda, Y.; Yokoi, T.; Hirayama, M.; Kanno, R. High Cycle Capability of All-Solid-State Lithium–Sulfur Batteries Using Composite Electrodes by Liquid-Phase and Mechanical Mixing. *ACS Appl. Energy Mater.* 2018, 1 (6), 2373–2377.
- (S15) Zhang, Y.; Liu, T.; Zhang, Q.; Zhang, X.; Wang, S.; Wang, X.; Li, L.; Fan, L. Z.; Nan, C. W.; Shen, Y. High-Performance All-Solid-State Lithium-Sulfur Batteries with Sulfur/Carbon Nano-Hybrids in a Composite Cathode. *J. Mater. Chem. A* 2018, 6 (46), 23345–23356.
- (S16) Ge, Q.; Zhou, L.; Lian, Y. meng; Zhang, X.; Chen, R.; Yang, W. Metal-Phosphide-Doped Li₇P₃S₁₁ Glass-Ceramic Electrolyte with High Ionic Conductivity for All-Solid-State Lithium-Sulfur Batteries. *Electrochem. commun.* 2018, 97 (October), 100–104.
- (S17) Ulissi, U.; Ito, S.; Hosseini, S. M.; Varzi, A.; Aihara, Y.; Passerini, S. High Capacity All-Solid-State Lithium Batteries Enabled by Pyrite-Sulfur Composites. *Adv. Energy Mater.* 2018, 8 (26), 1801462.
- (S18) Li, X.; Liang, J.; Luo, J.; Wang, C.; Li, X.; Sun, Q.; Li, R.; Zhang, L.; Yang, R.; Lu, S.; Huang, H.; Sun, X. High-Performance Li–SeS_x All-Solid-State Lithium Batteries. *Adv. Mater.* 2019, 1808100, 1808100.
- (S19) Marmorstein, D.; Yu, T. .; Striebel, K. .; McLarnon, F. .; Hou, J.; Cairns, E. . Electrochemical Performance of Lithium/Sulfur Cells with Three Different Polymer Electrolytes. *J. Power Sources* 2000, 89 (2), 219–226.
- (S20) Shin, J. H.; Kim, K. W.; Ahn, H. J.; Ahn, J. H. Electrochemical Properties and Interfacial Stability of (PEO)₁₀LiCF₃SO₃ÁTi n O 2n (1 Composite Polymer Electrolytes for Lithium / Sulfur Battery. *Mat. Sci. Eng. B* 2002, 95, 148–156.
- (S21) Park, C. W.; Ryu, H. S.; Kim, K. W.; Hur, B. Y.; Cho, K. K.; Ahn, J. H.; Lee, J. Y.; Ahn, H. J. Effect of Sulfur Electrode Composition on the Electrochemical Property of Lithium/PEO/Sulfur Battery. *Met. Mater. Int.* 2004, 10 (4), 375–379.
- (S22) Jeong, S. S.; Lim, Y. T.; Choi, Y. J.; Cho, G. B.; Kim, K. W.; Ahn, H. J.; Cho, K. K. Electrochemical Properties of Lithium Sulfur Cells Using PEO Polymer Electrolytes Prepared under Three Different Mixing Conditions. *J. Power Sources* 2007, 174 (2), 745–750.
- (S23) Ma, Q.; Qi, X.; Tong, B.; Zheng, Y.; Feng, W.; Nie, J.; Hu, Y. S.; Li, H.; Huang, X.; Chen, L.; Zhou, Z. Novel Li[(CF₃SO₂)(n-C₄F₉SO₂)N]-Based Polymer Electrolytes for Solid-State Lithium Batteries with Superior Electrochemical Performance. *ACS Appl. Mater. Interfaces* 2016, 8 (43), 29705–29712.
- (S24) Lin, Y.; Wang, X.; Liu, J.; Miller, J. D. Natural Halloysite Nano-Clay Electrolyte for Advanced All-Solid-State Lithium-Sulfur Batteries. *Nano Energy* 2017, 31 (July 2016), 478–485.
- (S25) Liang, J.; Sun, Q.; Zhao, Y.; Sun, Y.; Wang, C.; Li, W.; Li, M.; Wang, D.; Li, X.; Liu, Y.; Adair, K.; Li, R.; Zhang, L.; Yang, R.; Lu, S.; Huang, H.; Sun, X. Stabilization of All-Solid-State Li–S Batteries with a Polymer–Ceramic Sandwich Electrolyte by Atomic Layer Deposition. *J. Mater. Chem. A* 2018, 6 (46), 23712–23719.
- (S26) Zhu, X.; Wen, Z.; Gu, Z.; Lin, Z. Electrochemical Characterization and Performance Improvement of Lithium/Sulfur Polymer Batteries. *J. Power*

- Sources 2005, 139 (1–2), 269–273.
- (S27) Hassoun, J.; Scrosati, B. Moving to a Solid-State Configuration: A Valid Approach to Making Lithium-Sulfur Batteries Viable for Practical Applications. *Adv. Mater.* 2010, 22 (45), 5198–5201.
- (S28) Liang, X.; Wen, Z.; Liu, Y.; Zhang, H.; Huang, L.; Jin, J. Highly Dispersed Sulfur in Ordered Mesoporous Carbon Sphere as a Composite Cathode for Rechargeable Polymer Li/S Battery. *J. Power Sources* 2011, 196 (7), 3655–3658.
- (S29) Xue, Z.; He, D.; Xie, X. Poly(Ethylene Oxide)-Based Electrolytes for Lithium-Ion Batteries. *J. Mater. Chem. A* 2015, 3 (38), 19218–19253.
- (S30) Zhu, Y.; Li, J.; Liu, J. A Bifunctional Ion-Electron Conducting Interlayer for High Energy Density All-Solid-State Lithium-Sulfur Battery. *J. Power Sources* 2017, 351, 17–25.
- (S31) Tao, X.; Liu, Y.; Liu, W.; Zhou, G.; Zhao, J.; Lin, D.; Zu, C.; Sheng, O.; Zhang, W.; Lee, H.-W.; Cui, Y. Solid-State Lithium–Sulfur Batteries Operated at 37 °C with Composites of Nanostructured $\text{Li}_7\text{La}_3\text{Zr}_2\text{O}_{12}$ /Carbon Foam and Polymer. *Nano Lett.* 2017, 17 (5), 2967–2972.
- (S32) Zhu, P.; Yan, C.; Zhu, J.; Zang, J.; Li, Y.; Jia, H.; Dong, X.; Du, Z.; Zhang, C.; Wu, N.; Dirican, M.; Zhang, X. Flexible Electrolyte-Cathode Bilayer Framework with Stabilized Interface for Room-Temperature All-Solid-State Lithium-Sulfur Batteries. *Energy Storage Mater.* 2019, 17, 220–225.
- (S33) Qiu, Y.; Li, W.; Zhao, W.; Li, G.; Hou, Y.; Liu, M.; Zhou, L.; Ye, F.; Li, H.; Wei, Z.; Yang, S.; Duan, W.; Ye, Y.; Guo, J.; Zhang, Y. High-Rate, Ultralong Cycle-Life Lithium/Sulfur Batteries Enabled by Nitrogen-Doped Graphene. *Nano Lett.* 2014, 14 (8), 4821–4827.
- (S34) Brückner, J.; Thieme, S.; Böttger-Hiller, F.; Bauer, I.; Grossmann, H. T.; Strubel, P.; Althues, H.; Spange, S.; Kaskel, S. Carbon-Based Anodes for Lithium Sulfur Full Cells with High Cycle Stability. *Adv. Funct. Mater.* 2014, 24 (9), 1284–1289.
- (S35) Gomez, I.; Mecerreyes, D.; Blazquez, J. A.; Leonet, O.; Ben Youcef, H.; Li, C.; Gómez-Cámer, J. L.; Bundarchuk, O.; Rodriguez-Martinez, L. Inverse Vulcanization of Sulfur with Divinylbenzene: Stable and Easy Processable Cathode Material for Lithium-Sulfur Batteries. *J. Power Sources* 2016, 329, 72–78.
- (S36) Tan, X.; Lv, P.; Yu, K.; Ni, Y.; Tao, Y.; Zhang, W.; Wei, W. Improving the Cyclability of Lithium-Sulfur Batteries by Coating PPy onto the Graphene Aerogel-Supported Sulfur. *RSC Adv.* 2016, 6 (51), 45562–45568.
- (S37) Zheng, C.; Niu, S.; Lv, W.; Zhou, G.; Li, J.; Fan, S.; Deng, Y.; Pan, Z.; Li, B.; Kang, F.; Yang, Q. H. Propelling Polysulfides Transformation for High-Rate and Long-Life Lithium–Sulfur Batteries. *Nano Energy* 2017, 33 (January), 306–312.
- (S38) Zhou, G.; Sun, J.; Jin, Y.; Chen, W.; Zu, C.; Zhang, R.; Qiu, Y.; Zhao, J.; Zhuo, D.; Liu, Y.; Tao, X.; Liu, W.; Yan, K.; Lee, H. R.; Cui, Y. Sulfiphilic Nickel Phosphosulfide Enabled Li_2S Impregnation in 3D Graphene Cages for Li-S Batteries. *Adv. Mater.* 2017, 29 (12), 1603366.
- (S39) Liu, W.; Jiang, J.; Yang, K. R.; Mi, Y.; Kumaravadivel, P.; Zhong, Y.; Fan, Q.; Weng, Z.; Wu, Z.; Cha, J. J.; Zhou, H.; Batista, V. S.; Brudvig, G. W.; Wang, H. Ultrathin Dendrimer–Graphene Oxide Composite Film for Stable Cycling Lithium–Sulfur Batteries. *Proc. Natl. Acad. Sci.* 2017, 114 (14), 3578–3583.
- (S40) Zhao, Y.; Tan, R.; Yang, J.; Wang, K.; Gao, R.; Liu, D.; Liu, Y.; Yang, J.; Pan,

- F. 3D-Hybrid Material Design with Electron/Lithium-Ion Dual-Conductivity for High-Performance Li-Sulfur Batteries. *J. Power Sources* 2017, 340, 160–166.
- (S41) Zhou, T.; Lv, W.; Li, J.; Zhou, G.; Zhao, Y.; Fan, S.; Liu, B.; Li, B.; Kang, F.; Yang, Q. H. Twinborn TiO₂-TiN Heterostructures Enabling Smooth Trapping-Diffusion-Conversion of Polysulfides towards Ultralong Life Lithium-Sulfur Batteries. *Energy Environ. Sci.* 2017, 10 (7), 1694–1703.
- (S42) Deng, W.; Zhou, X.; Fang, Q.; Liu, Z. A Bifunctional Hierarchical Porous Carbon Network Integrated with an In Situ Formed Ultrathin Graphene Shell for Stable Lithium-Sulfur Batteries. *J. Mater. Chem. A* 2017, 5 (26), 13674–13682.
- (S43) Zhong, Y.; Xia, X.; Deng, S.; Zhan, J.; Fang, R.; Xia, Y.; Wang, X.; Zhang, Q.; Tu, J. Popcorn Inspired Porous Macrocellular Carbon: Rapid Puffing Fabrication from Rice and Its Applications in Lithium-Sulfur Batteries. *Adv. Energy Mater.* 2018, 8 (1), 1701110.

2 SCILAB CODE FOR ENERGY DENSITY CALCULATION

//Estimation of energy density of Li-S batteries with liquid and solid electrolytes
clc, clear, tic()

//General parameters

Vave= 2.10 *//V. Li-S average voltage*
 mcc= 2.7*10⁻³ *//g/cm2. Current collector mass*
 vcc=10*10⁻⁴ *// cm3/cm2. depends on thickness*
 NP= 3 *//Negative/positive capacity ratio.*
 CLi= 3861 *// mAh/g. Lithium theoretical capacity*
 rhoLi=0.53 *//g/cm3. Lithium density*
 rhoS=1.96 *//g/cm3. Sulfur density*
 rhoC=2.20 *//g/cm3. Carbon density*

////////////////////////////////////
 //////////////////////////////////MAIN FUNCTIONS////////////////////////////////////
 //////////////////////////////////////

//Gravimetric energy

function Eg=GravimetricEnergy(Ca)
 ms=Ca/Cg *//gS/cm2. Sulfur active mass*
 mcatho=ms/Sperc *//g/cm2. Total cathode mass*
 mLi= Ca*NP/CLi *//g/cm2. Lithium mass*
 Wtot=mcc+mcatho+mLi+msep+melec *//g/cm2. Total mass*
 Eg=Vave*Ca/Wtot *//Wh kg-1. Gravimetric energy*
endfunction

///Volumetric Energy

function Ev=VolumetricEnergy(Ca)
 ms=Ca/Cg *//gS/cm2 Sulfur active mass*
 vcatho=(ms/rhoS+ms*Cperc/Sperc/rhoC+ms*Bperc/Sperc/rhoB)/(1-ecatho) *//(sulfur volume+carbon volume+binder volume)*(1-porosity)*
 vLi=Ca*NP/CLi/rhoLi
 vtot=vcc+vcatho+vLi+vsep+velec *//l/cm2*
 Ev=Vave*Ca/vtot

endfunction

//////Performance parameters

Cg=1000 //mAh g-1. Gravimetric capacity

Cavec=(0:0.25:5) //mAh cm-2.

////////////////////////////////////

////////////////////////////////ELECTROLYTE AMOUNT STUDY////////////////////////////////

////////////////////////////////////

//General properties for solid eletrolytes//

Thickvec=[10:10:300] // um. Electrolyte thickness

Sperc=0.50, Cperc= 0.15, Bperc=1-Sperc-Cperc // Sulfur, carbon and binder fraction

msep=0,vsep=0 // g/cm2 , cm3/cm2. Separator mass and volume. No separator

//Glassy-ISE

rhoglassy=1.90 // g/cm3. Membrane density

eglassy=0, ecathoglassy=0 // Glassy membrane and cathode porosity fraction

//Garnet-ISE

rhogarnet=5.15 // g/cm3. Membrane density

egarnet=0, ecathogarnet=0 // Poly membrane and cathode porosity fraction

//SPE

rhopoly=1.20 // g/cm3. Membrane density

epoly=0.20, ecathopoly=0.20 // Poly membrane and cathode porosity fraction

//CSE

ecompo=0.20, ecathocompo=0.20 // Composite membrane and cathode porosity fraction

FillerVperc=0.03 // Filler volume fraction

for i=1:length(Cavec)

Ca=Cavec(i), ms=Ca/Cg // mg cm-2. Sulfur mass in the cathode

for j=1:length(Thickvec)

Thick=Thickvec(j)

//Glassy-ISE

rhoelec=rhoglassy, rhoB=rhoglassy, eelec=eglassy, ecatho=ecathoglassy //Takes specific properties

melec=Thick/10000*rhoelec*(1-eelec) //mg cm-2. Electrolyte mass

velec=Thick/10000 //cm3 cm-2. Electrolyte volume

EgGlassy(i,j)=GravimetricEnergy(Ca) // Wh kg-1. Gravimetric energy. [i,j]=[Ca,Thick]

EvGlassy(i,j)=VolumetricEnergy(Ca) //Wh L-1. Volumetric energy

//Garnet-ISE

rhoelec=rhogarnet, rhoB=rhogarnet, eelec=egarnet, ecatho=ecathogarnet //Takes specific properties

melec=Thick/10000*rhoelec*(1-eelec) //mg cm-2. Electrolyte mass

velec=Thick/10000 //cm3 cm-2. Electrolyte volume

EgGarnet(i,j)=GravimetricEnergy(Ca) // Wh kg-1. Gravimetric energy.

EvGarnet(i,j)=VolumetricEnergy(Ca) //Wh L-1. Volumetric energy

//SPE

rhoelec=rhopoly, rhoB=rhopoly, eelec=epoly, ecatho=ecathopoly //Takes specific properties

melec=Thick/10000*rhoelec*(1-eelec) //mg cm-2. Electrolyte mass

velec=Thick/10000 //cm3 cm-2. Electrolyte volume

EgPoly(i,j)=GravimetricEnergy(Ca) // Wh kg-1. Gravimetric energy.

EvPoly(i,j)=VolumetricEnergy(Ca) //Wh L-1. Volumetric energy

//CPE

Appendix

```

    eelec=ecompo, ecatho=ecathocompo //Takes specific properties
    rhocompo=((1-FillerVperc)*rhopoly)+(FillerVperc*rhogarnet) // g cm-3. Combination of PEO
+ Garnet
    rhoelec=rhocompo, rhoB=rhocompo,
    melec=Thick/10000*rhoelec*(1-eelec) //mg cm-2. Electrolyte mass
    velec=Thick/10000 //cm3 cm-2. Electrolyte volume
    EgCompo(i,j)=GravimetricEnergy(Ca) // Wh kg-1. Gravimetric energy.
    EvCompo(i,j)=VolumetricEnergy(Ca) //Wh L-1. Volumetric energy
end
end
//Li-ion values
LIBgravis=ones(length(Cavec),length(Thickvec))*250 // Wh kg-1. Gravimetric energy.
LIBvolus=ones(length(Cavec),length(Thickvec))*700 //Wh L-1. Volumetric energy

//liquid electrolytes//
EAMvec=[1:1:20] // um. Electrolyte thickness
Sperc=0.60, Cperc= 0.30, Bperc=1-Sperc-Cperc // Sulfur, carbon and binder fraction
msep=1.20*10^-3,vsep=25*10^-4 // g/cm2 , cm3/cm2. Separator mass and volume
rhoelec=1.13, rhoB=1.76 // g/cm3. Electrolyte and binder density
ecatho=0.10 // Cathode porosity fraction

for i=1:length(Cavec)
    Ca=Cavec(i), ms=Ca/Cg // mg cm-2. Sulfur mass in the cathode
    for j=1:length(EAMvec)
        EAM=EAMvec(j)
        melec=ms*1000*EAM/1000*rhoelec //g/cm2 //mg cm-2. Electrolyte mass
        velec=0 //cm3 cm-2. Electrolyte volume
        EgLiq(i,j)=GravimetricEnergy(Ca) // Wh kg-1. Gravimetric energy. [i,j]=[Ca,Thick]
        EvLiq(i,j)=VolumetricEnergy(Ca) //Wh L-1. Volumetric energy
    end
end
end
//Li-ion values
LIBgravil=ones(length(Cavec),length(EAMvec))*250 // Wh kg-1. Gravimetric energy.
LIBvolul=ones(length(Cavec),length(EAMvec))*700 //Wh L-1. Volumetric energy

////////////////////////////////////
////////////////////////////////////FILLER CONTENT STUDY////////////////////////////////////
////////////////////////////////////

//General properties for solid eletrolytes//
Thick=50 // um. Electrolyte thickness
Sperc=0.50, Cperc= 0.15, Bperc=1-Sperc-Cperc, msep=0,vsep=0 // Sulfur, carbon and binder
fraction and separator mass and volume
ecompo=0.20, ecathocompo=0.20 // Composite membrane and cathode porosity fraction
FillerVpercvec=[0 0.01 0.03 0.05 0.10 0.20 0.50]

for k=1:length(Cavec)
    Ca=Cavec(k), ms=Ca/Cg // mg cm-2. Sulfur mass in the cathode
    for l=1:length(FillerVpercvec)
        FillerVperc=FillerVpercvec(l)
        //CPE
        eelec=ecompo, ecatho=ecathocompo //Takes specific properties

```

```

rho_compo = ((1 - FillerVperc) * rho_poly) + (FillerVperc * rho_garnet) // g cm-3. Combination of PEO
+ Garnet
rho_elec = rho_compo, rho_B = rho_compo,
melec = Thick / 10000 * rho_elec * (1 - eelec) // mg cm-2. Electrolyte mass
velec = Thick / 10000 // cm3 cm-2. Electrolyte volume
Eg_Comp_Filler_amount(k,l) = GravimetricEnergy(Ca) // Wh kg-1. Gravimetric energy.
Ev_Comp_Filler_amount(k,l) = VolumetricEnergy(Ca) // Wh L-1. Volumetric energy
end
end

t = toc(), disp(t, 'Calculation time was (s):')

```

3 EXPERIMENTAL DETAILS

The following section describes the experimental details for the material preparation and characterization through this Thesis work. For materials characterization and testing at cell level the experiments were at least triplicated. For the materials characterization the average values were calculated and plotted. For the tests involving coin cells, the values corresponding to the median sample were plotted. The characterization of reference samples and blanks was repeated every few months in order to identify possible variations in raw materials or equipments.

3.1 MATERIALS

Poly(ethylene oxide) (PEO) (molecular weight of 5×10^6 g mol⁻¹, Sigma Aldrich) was used as received. Lithium bis(trifluoromethanesulfonyl)imide (LiTFSI) salt (99.95%, Sigma-Aldrich), lithium bis(fluorosulfonyl)imide (LiFSI) salt (battery grade, Suzhou Fluolyte), and lithium (fluorosulfonyl)(trifluoromethanesulfonyl) imide (LiFTFSI) salt (98%, Provisco) were introduced as received to an argon filled glove box (GB) and manipulated always under dry atmosphere. Lithium tricyanomethanide (LiTCM) (98% Provisco) was dried at 155 °C and vacuum in order to remove acetonitrile (ACN) solvent before its storage in the GB.

Lithium azide additive (LiN₃) (20 wt.% in water, Sigma-Aldrich) was received and dried under vacuum at 50 °C before its storage in GB. Lithium nitrate (LiNO₃) (99.99%, Sigma-Aldrich) was directly transferred to the GB as received.

Al₂O₃ (5 nm γ -Al₂O₃, US Nano) and lithium ion conducting glass ceramic (LiCGC) (400 nm powder, Ohara Inc.) for their use as fillers were received and dried under vacuum at 50 °C before their storage in GB.

Sulfur (powder 99.98%, Sigma Aldrich) and Ketjen-black conductive carbon (EC-600JD, AkzoNobel) were stored as received in close containers. Both were regularly dried under vacuum at 50 °C. Li₂S (99.98%, Sigma Aldrich) and biphenyl (analytical standard, Sigma Aldrich) were stored in the GB as received.

1,2-dimethoxyethane (Anhydrous, 99.5%, Sigma Aldrich) and tetrahydrofuran (anhydrous, >99.9%, Sigma-Aldrich) were transferred to the GB as received. Acetonitrile (>99.8%, Fisher chemical) was used as received and stored in a chemicals storage cabinet.

Lithium discs (14×0.05 mm chips, China Energy Lithium Co., Ltd.) and lithium foil ($10 \text{ cm} \times 10 \text{ m} \times 0.05$ mm foil, China Energy Lithium Co., Ltd.) were directly transferred to the GB as received.

3.2 PREPARATION OF CELL COMPONENTS

3.2.1 Solvent casting preparation of polymer membranes

For preparing solid polymer electrolytes (SPE) membranes by solvent casting method, the corresponding lithium salt was initially dissolved in ACN with the help of magnetic stirring. Later, the PEO was added to the slurry and the mixture was magnetically stirred at 300 rpm for at least 5 h. The molar ratio Li salt:(EO) units was fixed to 1/20 and solvent/electrolyte amount was fixed to $50 \text{ ml}_{\text{ACN}} \text{ g}_{\text{PEO}}^{-1}$.

Finally, the membrane slurry was poured into a Teflon dish and dried overnight in the desiccator. The following day the membrane was dried at $50 \text{ }^\circ\text{C}$ and vacuum for 10 min to remove remaining solvent. Afterwards, membrane was hot pressed at $100 \text{ }^\circ\text{C}$ and 3 T pressure for about 1 min to decrease porosity and regulate membrane thickness to $50 \text{ }\mu\text{m}$. Finally, 16 mm diameter membranes were punched dried at $50 \text{ }^\circ\text{C}$ and vacuum for 6 h before being stored in an argon-filled glove box.

3.2.2 Ball milling preparation of polymer membranes

SPEs were prepared by ball milling only in the case where ceramic particles needed to be dispersed. For this purpose lithium salt was initially dissolved in ACN (solvent amount was reduced to obtain a final ratio of $30 \text{ ml}_{\text{ACN}} \text{ g}_{\text{PEO}}^{-1}$). Later, the corresponding amount of ceramic particles were added and magnetically dispersed for 30 min. Afterwards, PEO was added and magnetically stirred for 3 h. The slurry was introduced in the ball milling jars (Pulverisette 7, Fritsch) and the balls (5 mm diameter):slurry mass ratio was fixed in 30. The slurry was mixed in two 10 min steps at 250 rpm and another four 10 min steps at 400 rpm, with 10 min rest between steps. Finally, the slurry was recovered and poured in Teflon dish. The following hot pressing, punching and drying steps are equal to the ones in solvent casting method.

3.2.3 Preparation of positive electrodes

Composite sulfur cathode was prepared by the mixture of 40 wt.% sulfur, 15 wt.% Ketjen Black conductive carbon and 45 wt.% catholyte, *i.e.*, binder. The catholyte was prepared following the same procedure as in membrane preparation, where

the polymer and the salt were dissolved in ACN and stirred for 6 h to get the so-called catholyte slurry. Afterwards, dry sulfur and carbon mixture was added to the wet catholyte slurry and dispersed by a high-performance dispersing instrument (Ultra Turrax, IKA) at 16000 rpm for 20 min.

The slurry obtained was degassed for 30 min (roller mixer, Stuart) and later casted with a wet thickness of 500 μm (Micrometer adjustable film applicator, IKA) and dried under vacuum at 50 $^{\circ}\text{C}$ for 1 h. Cathodes were later punched to 13 mm discs, and the obtained sulfur loading was about 1 $\text{mg}_\text{S} \text{cm}^{-2}$, unless specified. Cathodes were finally vacuum dried at 50 $^{\circ}\text{C}$ for 6 h and transferred to the glove box for permanent storage.

3.2.4 Coin cell assembly

Different coin cell configurations were prepared. For Stainless steel (SS)|SPE|SS coin cell, the SPE electrolyte was placed between two SS spacers. In those cases where the area of the SPE wanted to be minimized, the SPE was placed in the inner space of a 50 μm thickness and 16 mm diameter Kapton film. The diameter of the inert space was adjusted according to the desired contact area.

For Li^0 |SPE|SS coin cell, the SPE electrolyte was placed between one lithium disc and one SS electrode. In this case, 3 mm diameter and 250 μm SS disc were used, which were placed in the middle of a 16 mm and 250 μm thickness Teflon rings, with an inner 3 mm diameter ring.

For symmetric Li^0 |SPE| Li^0 coin cell, SPE electrolyte was placed between two Li^0 discs. An additional spacer, in contact with coin cell case, was added to ensure enough inert pressure.

Finally, for Li^0 |SPE|S electrode coin cell, SPE electrolyte was placed between one lithium disc and a sulfur cathode. An additional spacer, in contact with coin cell case, was added to ensure enough inert pressure.

In all these systems analyzed, CR2032 coin cell parts were used and the cells were assembled in an argon filled glove box. Cells were heated at 70 $^{\circ}\text{C}$ during 24 h before cycling.

3.2.5 Pouch cell assembly

For pouch cells assembly, the positive electrode was cut with a 54 x 37.5 mm mold in a press (0.1 T). The positive electrode was placed on the top of a larger SPE, and the leftover edges were trimmed with scissors. Li^0 electrode with sufficient

size was cut by scissors from a lithium foil belt. All the parts were packed together inside a pouch bag and aluminum and nickel taps were connected to positive and negative electrodes, respectively. Cells were closed under vacuum and thermally sealed. Pouch cells were assembled in the glove box and the cells were heated at 70 °C during 24 h before cycling.

3.3 CHARACTERIZATION TECHNIQUES

3.3.1 X-ray diffraction

X-ray diffraction (XRD) patterns were recorded on a Bruker D8 Discover X-ray diffractometer, using $\lambda_{\text{Cu-K}\alpha} = 1.54056 \text{ \AA}$ radiation in the 2θ range from 15 ° to 80 ° with a step width of 0.0198°.

3.3.2 Scanning electron microscopy

Surface morphology images of the prepared samples were examined by a field emission Quanta 200 FEG (FEI) scanning electron microscope, operated up to 30 kV. The air sensitive samples were transferred directly from the GB with the help of an air-tight holder.

3.3.3 Electrochemical stability test

The electrochemical stability to oxidation of the polymeric membranes was measured by linear sweep voltamperometry (LSV) in $\text{Li}^0|\text{SPE}|\text{SS}$ cells, with a 3 mm diameter SS electrode to improve the quality of the signal. The LSV measurements were carried out between the open circuit potential and 6.0 V vs. Li/Li^+ at a scan rate of 1 mV s^{-1} and a temperature of 70 °C. Before testing, the cells were thermally treated at 70 °C for 24 h.

3.3.4 Thermogravimetric analysis

Thermogravimetric analysis (TGA) was performed on a STA 449 F3 system connected to QMS 403 Aëolos (Netzsch). Around 5-10 mg of the prepared electrolyte samples were placed in an aluminum pan. The samples were heated from room temperature to 600 °C at a heating rate of 10 °C min^{-1} under the argon flow.

3.3.5 Differential scanning calorimetry

The differential scanning calorimetry measurements were done in a Q2000 (TA Instruments) equipment. Around 5-10 mg of the prepared electrolyte sample were sealed in an aluminum crucible in an argon-filled glove box. The sample was measured for two consecutive scans at a cooling and heating rate of $10\text{ }^{\circ}\text{C min}^{-1}$ in the temperature range of -80 to $100\text{ }^{\circ}\text{C}$. The glass transition temperature (T_g) was taken at the onset of the heat capacity change, while the melting (T_m) point was taken at the peak of the heat capacity change. The melting enthalpy (ΔH_m) was calculated by the integration of the heat in the melting peak.

No salt melting is expected in the temperature range of the measurement, thus, the crystallinity of the membrane, χ_c , can be directly obtained by comparison of the obtained ΔH_m with the theoretical ΔH_m of the pure crystalline PEO, 196 J g^{-1} , according to the following formula:

$$\chi_c = \frac{\Delta H_m^{\text{sample}}}{\Delta H_m^{\text{PEO}} \cdot x_{\text{PEO}}} \quad (\text{A.1})$$

x_{PEO} refers to the mass fraction of PEO in the membrane:

3.3.6 Conductivity test

The ionic conductivity of the electrolyte was measured by alternating current electrochemical impedance spectroscopy (EIS) using a VMP3 potentiostat (Bio-Logic Science Instruments) with frequency range of 10^{-2} - 10^6 Hz and a signal amplitude of 10 mV in a SS|SPE|SS coin cells. The membrane diameter was limited to 8 mm by kapton film. The variable temperature was controlled by Vötsch VT 7004 oven. Before testing, the cells were thermally treated at $70\text{ }^{\circ}\text{C}$ for 24h. The obtained EIS spectra were fitted to the following circuit to obtain the bulk resistance, R_b , of the electrolyte:

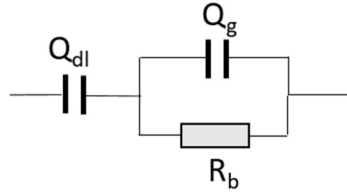


Figure A.1. Equivalent circuit for EIS spectra fitting in SS|SPE|SS cells.² Q_{dl} , Q_g and R_b abbreviate double layer capacitance, geometric capacitance and bulk resistance.

The obtained R_b value was converted to conductivity, σ , as follows:

$$\sigma = R_b \frac{t_{elec}}{A_{elec}} \quad (\text{A.2})$$

t_{elec} and A_{elec} abbreviate electrolyte thickness and area, respectively. Membrane thickness was determined after cell testing and opening, by direct measurement with the help of a micrometer (Digimatic Micrometer, Mitutoyo).

3.3.7 Lithium transference number measurement

Lithium transference number of the polymer electrolyte, t_{Li^+} , was determined at 70 °C by a combination of alternating current EIS and direct current polarization using a symmetric $Li^0 | SPE | Li^0$ cell. Before testing, the cells were thermally treated at 70 °C for 24 h. For the measurement, a 10 mV DC voltage step (ΔV) was applied, using a VMP3 potentiostat (Bio-Logic Science Instruments), until a steady current was obtained (usually 2–3 h in this study). The initial (I^0) and steady (I^s) currents were measured. The impedance spectra of the cell were recorded in the frequency range of 10^{-2} - 10^6 Hz and voltage oscillation of 10 mV, before and after the polarization to obtain the initial (R_b^0) and final (R_b^s) bulk resistances of the electrolyte, and the initial (R_i^0) and final (R_i^s) interfacial resistances. In this case, the impedances were fitted according to the following equivalent circuit.

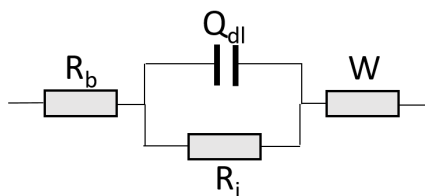


Figure A.2. Equivalent circuit for EIS spectra fitting in SS|SPE|SS cells. Q_{dl} and W abbreviate double layer capacitance and Warburg diffusion coefficient, respectively.

Based on these values for the parameters above, the t_{Li^+} was then calculated by the following equation as described by Evans *et al.*³:

$$t_{Li^+} = \frac{I^s R_b^s (\Delta V - I^0 R_i^0)}{I^0 R_b^0 (\Delta V - I^s R_i^s)} \quad (\text{A.3})$$

3.3.8 Galvanostatic cycling

The galvanostatic cycling of the $Li^0|SPE|Li^0$ cells were evaluated using a Maccor Tester (Series 4000). Only in this case, the membrane thickness was adjusted to 100 μm to compensate the higher cell pressure. The symmetric cells were cycled galvanostatically at 70 $^\circ\text{C}$ with a current density of 0.1 mA cm^{-1} and a half-cycle duration of 2 h. Before testing, the cells were thermally treated at 70 $^\circ\text{C}$ for 24 h.

3.3.9 Lithium metal deposit generation

The cell for the generation of the Li^0 deposits differs from the previous ones. In this case $Li^0|\text{liquid electrolyte}|Cu$ foil cells were assembled. To prepare liquid electrolytes, 1 M of the studied salt was previously dissolved in DME and stirred magnetically for at least 1 h. Later a Celgard[®] separator of 16 mm diameter and an approximate thickness of 25 μm was placed between electrodes and soaked with 80 μl of the electrolyte solution. The cells were mounted and sealed in the GB, and later tested in a Maccor Tester at room temperature with a current density of 0.1 mA cm^{-1} in a single direction for 20 h. Finally, cells were transferred back to the GB and opened to recover Li^0 deposits on the Cu foil for further analysis. The samples were gently rinsed with DME and dried thoroughly under vacuum.

3.3.10 X-ray photoelectron spectroscopy

The X-ray photoelectron spectroscopy (XPS) spectra were recorded were measured by a Phoibos 150 XPS with a non-monochromatic Mg K_{α} source ($h\nu = 1253.6$ eV). The spectra were recorded with high resolution scans at low power (100 W, 20 eV pass energy, and 0.1 eV energy step). The samples were directly transferred from the GB to the equipment with the help of a home designed air-tight setup. The peak assignment was done based on the data of the work by Passerini *et al.*⁴

3.3.11 Polysulfide reactivity test

Initially 0.1 M Li_2S_6 solution were prepared in DME by mixing Li_2S and sulfur in a mole ratio of 1:5, followed by magnetic stirring for one week at room temperature. Later, a predetermined amount of $\text{Li}_2\text{S}_6/\text{DME}$ solution was added to a stirred solution of 1 M of interest salt in DME to obtain a final salt: Li_2S_6 ratio of 1:200. The mixture stirred for 60 h before further analysis.

Finally, the ultraviolet-visible (UV-vis) spectroscopy measurements were carried out, without further dilution, on a Cary 500 UV-vis spectrophotometer (Varian)

3.3.12 Chemical simulation test

Low potential chemical, *i.e.*, biphenyl, was dissolved in ultrapure and dry tetrahydrofuran (THF) for about 30 min. Later, grounded Li° was added to the solution in a 1:1 mole ratio (biphenyl: Li°). The reaction mixture was stirred for about 5h at RT using a special glass-coated magnetic stirring in order to avoid any sort of chemical etching. Afterward, a dark blue color, characteristic of the biphenyl radical monoanion was observed. For the two electrons extraction, biphenyl: Li° molar ratio of 1:2 was used, resulting in the formation of a deep dark blue biphenyl radical dianion. After the complete formation of the radical anions, different anions were added in the corresponding ratio in order to study reduction reactions involving different amounts of electrons. Monitoring the changes in color was then employed as a mean to evaluate the stability of the salt anions toward electrochemical reduction.

3.3.13 Lithium sulfur cell cycling

The cycling performance of the assembled $\text{Li}^0|\text{SPE}|\text{S}$ electrode cells was tested by galvanostatic cycling at different discharge and charge rates between 2.8-1.6 V vs. Li/Li^+ at 70 °C using a Maccor Series 4000 battery tester. Before testing, the cells were thermally treated at 70 °C for 24 h.

The cycling performances of the cells were characterized at different discharge/charge rates between 2.8 and 1.6 V at 70°C using a Maccor Battery Tester (Series 4000).

In the case the EIS data wanted to be harvested, the cell was cycled using a VMP3 potentiostat (Bio-Logic Science Instruments). The EIS measurements were done with frequency range of 10^{-2} - 10^6 Hz and a signal amplitude of 10 mV. The following equivalent circuit was used in that case:

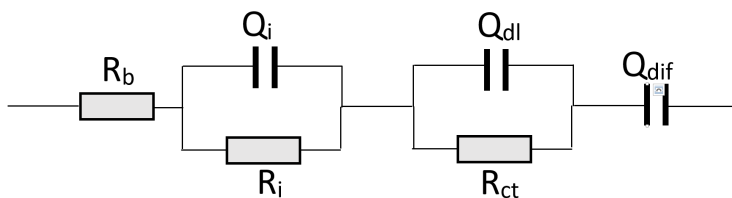


Figure A.3. Equivalent circuit for EIS spectra fitting in $\text{Li}^0|\text{SPE}|\text{S}$ electrode cells.⁵ R_b , R_i , R_{ct} , Q_i , Q_{dl} , and Q_{dif} abbreviate bulk, interfacial and charge transfer resistances, and interfacial, double layer and diffusion capacitances.

4 QUALITY INDICATORS

4.1 PUBLICATIONS

The following articles were published in indexed journals during this PhD work. Impact factor (IF) of the journal and number of citations (NC) were updated in October of 2019 with the data extracted from Google Scholar.

- (1) Judez, X.; Martinez-Ibañez, M.; Santiago, A.; Armand, M.; Zhang, H.; Li, C. Quasi-Solid-State Electrolytes for Lithium Sulfur Batteries: Advances and Perspectives. *J. Power Sources* **2019**, 438 (July), 226985. (IF= 7.5, NC= N/A.).
- (2) Eshetu, G. G.; Judez, X.; Li, C.; Martinez-Ibañez, M.; Sánchez-Diez, E.; Rodriguez-Martinez, L. M.; Zhang, H.; Armand, M. CHAPTER 4. Solid Electrolytes for Lithium Metal and Future Lithium-Ion Batteries. In *Future Lithium-ion Batteries*; Royal Society of Chemistry: Cambridge, **2019**; Vol. 2019-January, pp 72–101. (IF= N/A, NC= N/A.).
- (3) Zhang, H.; Oteo, U.; Judez, X.; Eshetu, G. G.; Martinez-Ibañez, M.; Carrasco, J.; Li, C.; Armand, M. Designer Anion Enabling Solid-State Lithium-Sulfur Batteries. *Joule* **2019**, 3 (7), 1689–1702. (IF=N/A , NC=3).
- (4) Zhang, H.; Judez, X.; Santiago, A.; Martinez-Ibañez, M.; Muñoz-Márquez, M. Á.; Carrasco, J.; Li, C.; Eshetu, G. G.; Armand, M. Fluorine-Free Noble Salt Anion for High-Performance All-Solid-State Lithium–Sulfur Batteries. *Adv. Energy Mater.* **2019**, 9 (25), 1900763. (IF=24.9, NC=1).
- (5) Judez, X.; Qiao, L.; Armand, M.; Zhang, H. Energy Density Assessment of Organic Batteries. *ACS Appl. Energy Mater.* **2019**, 2 (6), 4008–4015. (IF=N/A, NC=N/A).
- (6) Judez, X.; Eshetu, G. G.; Gracia, I.; López-Aranguren, P.; González-Marcos, J. A.; Armand, M.; Rodriguez-Martinez, L. M.; Zhang, H.; Li, C. Understanding the Role of Nano-Aluminum Oxide in All-Solid-State Lithium-Sulfur Batteries. *ChemElectroChem* **2019**, 6 (2), 326–330. (IF=4.0, NC=3).
- (7) Zhang, H.; Oteo, U.; Zhu, H.; Judez, X.; Martinez-Ibañez, M.; Aldalur, I.; Sanchez-Diez, E.; Li, C.; Carrasco, J.; Forsyth, M.; Armand, M. Enhanced Lithium-Ion Conductivity of Polymer Electrolytes by Selective Introduction of Hydrogen into the Anion. *Angew. Chemie Int. Ed.* **2019**, 58 (23), 7829–7834. (IF=12.3, NC=4).
- (8) Zhang, H.; Eshetu, G. G.; Judez, X.; Li, C.; Rodriguez-Martínez, L. M.; Armand, M. Electrolyte Additives for Lithium Metal Anodes and

- Rechargeable Lithium Metal Batteries: Progress and Perspectives. *Angew. Chemie Int. Ed.* **2018**, *57* (46), 15002–15027. (IF=12.3, NC=75).
- (9) Judez, X.; Eshetu, G. G.; Li, C.; Rodriguez-Martinez, L. M.; Zhang, H.; Armand, M. Opportunities for Rechargeable Solid-State Batteries Based on Li-Intercalation Cathodes. *Joule* **2018**, *2* (11), 2208–2224. (IF=N/A, NC=13).
- (10) Eshetu, G. G.; Judez, X.; Li, C.; Martinez-Ibañez, M.; Gracia, I.; Bondarchuk, O.; Carrasco, J.; Rodriguez-Martinez, L. M.; Zhang, H.; Armand, M. Ultrahigh Performance All Solid-State Lithium Sulfur Batteries: Salt Anion's Chemistry-Induced Anomalous Synergistic Effect. *J. Am. Chem. Soc.* **2018**, *140* (31), 9921–9933. (IF=14.7, NC=30).
- (11) Gracia, I.; Benyoucef, H.; Judez, X.; Oteo, U.; Zhang, H.; Li, C.; Rodriguez-Martinez, L. M.; Armand, M. S-Containing Copolymer as Cathode Material in Poly (Ethylene Oxide) -Based All-Solid-State Li-S Batteries. *J. Power Sources* **2018**, *390* (April), 148–152. (IF=7.5, NC=11).
- (12) Judez, X.; Zhang, H.; Li, C.; Eshetu, G. G.; González-Marcos, J. A.; Armand, M.; Rodriguez-Martinez, L. M. Review—Solid Electrolytes for Safe and High Energy Density Lithium-Sulfur Batteries: Promises and Challenges. *J. Electrochem. Soc.* **2018**, *165* (1), A6008–A6016. (IF=3.1, NC=40).
- (13) Eshetu, G. G.; Judez, X.; Li, C.; Bondarchuk, O.; Rodriguez-Martinez, L. M.; Zhang, H.; Armand, M. Lithium Azide as an Electrolyte Additive for All-Solid-State Lithium-Sulfur Batteries. *Angew. Chemie Int. Ed.* **2017**, *56* (48), 15368–15372. (IF=12.3, NC=57).
- (14) Judez, X.; Piszcz, M.; Coxa, E.; Li, C.; Aldalur, I.; Oteo, U.; Zhang, Y.; Zhang, W.; Rodriguez-Martinez, L. M.; Zhang, H.; Armand, M. Stable Cycling of Lithium Metal Electrode in Nanocomposite Solid Polymer Electrolytes with Lithium Bis(Fluorosulfonyl)Imide. *Solid State Ionics* **2017**, *318* (2018), 95–101. (IF=2.9, NC=13).
- (15) Judez, X.; Zhang, H.; Li, C.; Eshetu, G. G.; Zhang, Y.; González-Marcos, J. A.; Armand, M.; Rodriguez-Martinez, L. M. Polymer-Rich Composite Electrolytes for All-Solid-State Li–S Cells. *J. Phys. Chem. Lett.* **2017**, *8*, 3473–3477. (IF=7.3, NC=33).
- (16) Judez, X.; Zhang, H.; Li, C.; González-Marcos, J. A.; Zhou, Z.; Armand, M.; Rodriguez-Martinez, L. M. Lithium Bis(Fluorosulfonyl)Imide/Poly(Ethylene Oxide) Polymer Electrolyte for All Solid-State Li-S Cell. *J. Phys. Chem. Lett.* **2017**, *8* (9), 1956–1960. (IF=7.3, NC=52).

This results in a total amount of citations of 339 and an h-index of 9.

4.2 WORKS PRESENTED IN CONFERENCES

The following works were presented in conferences by the PhD candidate:

- (1) **Oral contribution:** Judez, X.; Eshetu, G. G.; Santiago, A.; Martinez-Ibañez, M.; Rodriguez-Martinez, L. M.; Armand, M.; González-Marcos, J. A.; Zhang, H.; Li, C. Polymer-based electrolytes for all-solid-state Li-S batteries. Power our Future 2019. 2019, Vitoria-Gasteiz, Spain.
- (2) **Poster:** Judez, X.; Eshetu, G. G.; Gracia, I.; López-Aranguren, P.; González-Marcos, J. A.; Armand, M.; Rodriguez-Martinez, L. M.; Zhang, H.; Li, C. Understanding the Role of Nano-Aluminum Oxide in All-Solid-State Lithium-Sulfur Batteries. 7th Workshop “Lithium-Sulfur batteries”. 2018. Dresden, Germany.

4.3 CO-AUTHOR CONFERENCES

The following works with participation of the PhD candidate were presented in conferences:

- (1) **Oral contribution:** Judez, X.; Zhang, H.; Eshetu, G. G.; Aldalur, I.; Martinez-Ibañez, M.A.; Otaegui, L.; Zagorski, J.; Armand, M.; Li, C.; Rodriguez-Martinez, L. M. Towards Competitive Lithium Sulfur Batteries. IDTechEX. 2018. Berlin, Germany.
- (2) **Poster:** Judez, X.; Martinez-Ibañez, M.A.; Sanchez-Diez, E.; Gracia, I.; Zhang, H.; Eshetu, G. G.; Li, C.; Aldalur, I.; Oteo, U.; Shanmukaraj, D.; Rodriguez-Martinez, L. M.; Armand, M. Solid polymer electrolytes for safe and high energy density lithium batteries. VI Jornadas de Investigación de la Facultad de Ciencia y Tecnología. 2018. Leioa, Spain.
- (3) **Oral contribution:** Judez, X.; Zhang, H.; Aldalur, I.; Piszcz, M.; Li, C.; Otaegi, L.; Zagorski, J.; Lucienne, B.; Llordes, A.; Rojo, T.; Kilner, J.; M.; Armand, M.; Rodriguez-Martinez, L.M. Evaluation of polymer-rich composite electrolytes for all solid state Li-S batteries. Power our Future 2017. 2017. Vitoria-Gasteiz, Spain.
- (4) **Poster:** Judez, X.; Piszcz, M.; Coya, E.; Li, C.; Aldalur, I.; Oteo, U.; Zhang, Y.; Zhang, W.; Rodriguez-Martinez, L. M.; Armand, M.; Zhang, H. Stable cycling of lithium metal electrode in nanocomposite solid polymer electrolytes with lithium bis(fluorosulfonyl)imide. 21st Internacional Conference on Solid State Ionics. 2018. Padua, Italy.
- (5) **Oral contribution:** Judez, X.; Zhang, H.; Aldalur, I.; Piszcz, M.; Li, C.; Otaegi, L.; Zagorski, J.; Lucienne, B.; Llordes, A.; Rojo, T.; Kilner, J.; M.;

Armand, M.; Rodriguez-Martinez, L. M. Evaluation of solid electrolytes for all solid state Li-S batteries. *Lithium Sulfur: Mechanisms, Modelling & Materials*. 2017. London, United Kingdom.

5 REFERENCES IN THE APPENDIX

- (1) Zardalidis, G.; Mars, J.; Allgaier, J.; Mezger, M.; Richter, D.; Floudas, G. Influence of Chain Topology on Polymer Crystallization: Poly(Ethylene Oxide) (PEO) Rings vs. Linear Chains. *Soft Matter* **2016**, *12* (39), 8124–8134.
- (2) Sequeira, C. A. C.; Plancha, M. J. C.; Araújo, L. P. S. Conductivity Studies on Solid Polymer Electrolytes. *Le J. Phys. IV* **1994**, *04* (C1), C1-17-C1-35.
- (3) Evans, J.; Vincent, C. A.; Bruce, P. G. Electrochemical Measurement of Transference Numbers in Polymer Electrolytes. *Polymer (Guildf)*. **1987**, *28* (13), 2324–2328.
- (4) Eshetu, G. G.; Diemant, T.; Grugeon, S.; Behm, R. J.; Laruelle, S.; Armand, M.; Passerini, S. In-Depth Interfacial Chemistry and Reactivity Focused Investigation of Lithium–Imide- and Lithium–Imidazole-Based Electrolytes. *ACS Appl. Mater. Interfaces* **2016**, *8* (25), 16087–16100.
- (5) Deng, Z.; Zhang, Z.; Lai, Y.; Liu, J.; Li, J.; Liu, Y. Electrochemical Impedance Spectroscopy Study of a Lithium/Sulfur Battery: Modeling and Analysis of Capacity Fading. *J. Electrochem. Soc.* **2013**, *160* (4), A553–A558.

The development of more efficient and competitive batteries is crucial for a complete transition to more sustainable energy models. In this regard, all-solid-state lithium-sulfur batteries, especially those based on lightweight solid polymer electrolytes, present several benefits in comparison with conventional lithium-ion batteries. However, the performance of these batteries is not satisfactory yet due to challenges related to lithium/polymer compatibility. This work aims to understand the failure mechanism behind that poor performance, and propose different strategies to overcome those limitations. Those strategies include the use of electrolyte additives, electrolyte fillers, alternative imide salts, and fluorine-free salts.